TECHNISCHE UNIVERSITÄT MÜNCHEN

Fakultät Wissenschaftszentrum Weihenstephan
für Ernährung, Landnutzung und Umwelt

Lehrstuhl für Mikrobiologie

Bacteria-phage interactions: Insights into quorum sensing-induced anti-phage defense, phage therapy and the pulmonary human virome composition

Judith Susanne Feichtmayer

Vollständiger Abdruck der von der Fakultät Wissenschaftszentrum Weihenstephan für Ernährung, Landnutzung und Umwelt der Technischen Universität München zur Erlangung des akademischen Grades eines

Doktors der Naturwissenschaften (Dr. rer. nat.)

genehmigten Dissertation.

Vorsitzender:	Prof. Dr. Siegfried Scherer
Prüfer der Dissertation:	1. Priv.-Doz. Dr. Christian Griebler
	2. Prof. Dr. Wolfgang Liebl

Diese Dissertation wurde am 06.12.2018 bei der Technischen Universität München eingereicht und durch die Fakultät Wissenschaftszentrum Weihenstephan für Ernährung, Landnutzung und Umwelt am 24.04.2019 angenommen.

Für meinen Vater, ohne den ich diesen Weg nie gegangen wäre.

Für meine Mutter, die mich in schweren Zeiten immer wieder aufgebaut hat.

„Ich bin immer noch verwirrt, aber auf einem höheren Niveau.“

Enrico Fermi

TABLE OF CONTENTS

SUMMARY

Viruses are the most abundant biological entity on Earth. Bacteriophages (viruses that predate solely on prokaryotes) have a major impact on microbial communities. Phages shape and influence bacterial diversity as well as expand the microbial genetic reservoir *via* host-specific replication. Thus, phages drive the adaptation of bacteria to a changing environment. In this thesis, the ecology of bacteria and phage interactions is elucidated. The evaluation of currently available methods for the quantification of viral particles from pure isolates as well as complex environmental samples is the focus of the first chapter. Low viral concentrations and lack of virus-specific enumeration methods are common problems when working with environmental samples. In a cross-comparison of five different methods and two different staining protocols, nanoparticle-tracking analysis produced the most reliable results, but was also of limited use with very small virus particles. Here, the purpose of the quantification has to be taken into account when choosing the right technique.

The second chapter concerns the application of phages to control *Pseudomonas aeruginosa.* Thereto, specific viruses were isolated from environmental and human-related sources, tested and characterized on their ability to be used as bacteria controlling agents. Thirteen lytic phages could be isolated from human-associated samples and 17 phages arose from wastewater. The characterization includes temperature and pH preference and tolerance, the lytic potential at different virus-to-bacteria ratios, the lytic potential against attached bacteria, and some molecular and genetic features of the isolates. Most isolates favored moderate temperatures and neutral pH. Initially, the isolates were able to reduce planktonic cells, but bacteria developed resistance soon after encounter. Cells grown in biofilms, however, were not affected by the phages. Genetically, all isolates showed a high similarity to each other, and to the already described phage vB_PaeM_CEB_DP1.

The third chapter focuses on the potential impact of phages on microbial communication. Quorum sensing has been shown to be involved in the anti-phage defense strategy of some bacteria. The model strain *Pseudomonas putida* was exposed to several lytic phages. The collected data on population dynamics and signal molecules were not only analyzed but also used for a mathematical model-based testing of hypothetical interaction scenarios between phages and the bacterial quorum sensing system. The results provided strong evidence that quorum sensing contributes to bacterial anti-phage resistance in *P. putida*; however, none of the applied models could fully reproduce the experimental data.

Compared to the single interaction of viruses with bacteria in a well-defined environment, metagenomic analysis from more complex systems such as the human lung can provide

additional information on their interplay. The last chapter reports on the role of the virome in a healthy or a chronically diseased lung. The extremely low content of viral DNA in the pulmonary lavage samples, respectively the overall low sample volumes that were provided, impeded metagenomic sequencing and complicated the analysis of the sequencing data. In the few samples that could be successfully sequenced, a core virome which was present in all samples independent of the disease pattern and a flexible virome related to the progress of the disease were identified.

In summary, this thesis contributes to a better understanding of the ongoing struggle between phages and their bacterial hosts. Further, the evaluated and optimized methods can be used to increase the yield and depth of information in virus-related studies. By that, an in-depth understanding of the role viruses and especially bacteriophages might play in complex ecosystems can be achieved.

ZUSAMMENFASSUNG

Bakteriophagen, also Viren, die sich ausschließlich in Prokaryoten vermehren, haben einen enormen Einfluss auf bakterielle Gemeinschaften. Durch ihre Wirts-spezifische Replikation formen und beeinflussen Phagen nicht nur die bakterielle Diversität, sondern erweitern auch das genetische Reservoir ihrer Wirte. Damit tragen die Phagen erheblich zur Anpassung von Bakterien an sich verändernde Umgebungen bei. In dieser Doktorarbeit wird die Ökologie der Interaktionen zwischen Bakterien und Viren beleuchtet. In dem ersten Kapitel werden unterschiedliche aktuelle Methoden zur Virenquantifizierung reiner Virenisolate als auch komplexerer Umweltproben miteinander verglichen. Gerade Letztere bereiten oft Schwierigkeiten bei der Quantifizierung, da diese Proben oft niedrig konzentriert sind und Viren-spezifische Methoden nicht anwendbar sind. Fünf verschiedene Methoden zur Quantifizierung, sowie zwei verschiedene Verfahren zum Anfärben der Viren wurden vergleichend gegenübergestellt. Die Nanopartikel-Tracking Analyse in Kombination mit einer Partikelfärbung bei niedrigerer Temperatur erzielte die verlässlichsten Werte, jedoch mit Einschränkung bei zu geringen Partikelgrößen. Wie sich durch diesen Vergleich zeigte, muss bei der Wahl der richtigen Methode das angestrebte Ziel der Quantifizierung bereits berücksichtigt werden.

Im zweiten Kapitel wird eine mögliche Verwendung von Phagen zur Kontrolle des opportunistischen Keims *Pseudomonas aeruginosa* beleuchtet. Dazu wurden spezifische lytische Viren sowohl aus Umweltproben als auch aus menschlichen Proben isoliert, und auf ihre antimikrobielle Fähigkeit getestet. Aus den humanen Proben konnten 13 lytische Viren isoliert werden und aus den Abwasserproben 17 Viren. Die Charakterisierung der Viren umfasste die Temperatur und pH Präferenz sowie Toleranz, die Erfassung des lytischen Potentials bei verschiedenen Viren-Bakterien Verhältnissen und gegen Bakterien, die in einem Biofilm organisiert sind. Zusätzlich wurden molekulare und genetische Eigenschaften der Isolate untersucht. Die meisten Isolate favorisierten moderate Temperaturen und einen neutralen pH. Planktonische Zellen wurden anfänglich stark reduziert, allerdings entwickelten die Bakterien nach Aufeinandertreffen relativ schnell eine gewisse Resistenz. Im Gegensatz dazu wurden die adhärenten Zellen von den Phagen nicht beeinflusst. Die Isolate zeigten eine hohe genetische Übereinstimmung untereinander, sowie zu dem bereits beschriebenen Phagen vB_PaeM_CEB_DP1.

Das dritte Kapitel behandelt einen möglichen Einfluss von Phagen auf die bakterielle Kommunikation. Es konnte bereits bei einzelnen Bakterien gezeigt werden, dass Quorum Sensing an der Phagenabwehr beteiligt ist. Das Modellbakterium *Pseudomonas putida* wurde einer Mischung von verschiedenen lytischen Phagen ausgesetzt. Die erhobenen Messdaten

bezüglich der Populationsdynamiken und Konzentrationen der Signalmoleküle wurden nicht nur analysiert, sondern auch dazu verwendet, verschiedene Szenarien einer hypothetischen Interaktion von Phagen mit dem bakteriellem Quorum Sensing System mit Hilfe von mathematischer Modellierung zu überprüfen. Obwohl keine der verwendeten Modellierungen die experimentellen Daten vollständig abbilden konnte, weisen die Modellierungsergebnisse durchaus daraufhin, dass auch in *P. putida* Quorum Sensing an der bakteriellen Phagenabwehr und –resistenz beteiligt ist.

Verglichen mit der Analyse der Interaktionen einzelner Viren mit Bakterien in einer definierten Umgebung, kann eine Metagenomanalyse von Proben, die aus einer komplexen Umgebung wie der menschlichen Lunge stammen, zusätzliche und detailliertere Informationen generieren. In dem letzten Kapitel wird die Rolle des Viroms in einer gesunden oder chronisch erkrankten Lunge, am Beispiel der chronischen obstruktiven Lungenerkrankung analysiert. Der geringe Anteil an viraler DNA in den Lavage Proben der Lunge, sowie das generelle geringe Probenvolume das zur Analyse zur Verfügung gestellt wurde, erschwerten die Metagenomsequenzierung und die anschließende Analyse der Daten. In den wenigen erfolgreich sequenzierten Proben konnte jedoch ein Kernvirom identifiziert werden, welches in allen Proben vorhanden war, unabhängig von einer Erkrankung. Zusätzlich konnte ein flexibles Virom festgestellt werden, welches den Krankheitsverlauf widerspiegelte.

Durch die unterschiedliche Methodik, die in dieser Arbeit angewandt wurde, konnte ein besseres Verständnis der komplexen Beziehungen zwischen Viren und Bakterien erlangt werden. Des Weiteren trägt die Evaluierung und Optimierung der Methoden bei, die Quantität und Aussagefähigkeit der gewonnenen Informationen aus virenbezogenen Studien zu erhöhen. Gerade die Rolle der Viren und besonders der Bakteriophagen in komplexen Ökosystemen kann dadurch besser analysiert und beurteilt werden.

LIST OF PUBLICATIONS

Parts of the presented work have already been published or have been submitted to a journal and will soon be published:

Section 1.2:

Feichtmayer, J., Deng, L. & Griebler, C. Antagonistic microbial interactions: Contributions and potential applications for controlling pathogens in the aquatic systems. *Frontiers in Microbiology* **8,** (2017).

Section 3.1:

Feichtmayer, J., Pickl, C., Griebler, C., Klingl, A., Kurmeyer, R. & Deng, L. Virus enumeration under the microscope: a rigorous assessment and comparison of enumeration methods for environmental viruses. Submitted.

Section 3.3: Shared first-authorship*

Ghorai, A.*, **Feichtmayer, J.***, Pérez-Velázquez, J., Rothballer, M., Kuttler, C., Griebler, C., Deng, L. & Hense, B. A. Do lytic bacteriophages interact with quorum sensing in *Pseudomonas putida*? Modelling evaluation of batch experiments. Submitted.

Section 3.4:

Elbehery, A. H. A., **Feichtmayer, J.**, Singh, D., Griebler, C. & Deng, L. The Human Virome Protein Cluster Database (HVPC): A Human Viral Metagenomic Database for Diversity and Function Annotation. *Front. Microbiol.* **9,** 1110 (2018).

Presentations at conferences:

Feichtmayer, J., Ghorai, A., Kuttler, C., Cerit, J., Deng, L., Griebler, C. & Hense, B. A. Bacteria - Phage Interaction and the impact of Quorum Sensing. Poster presentation at 5th Joint Conference of the DGHM & VAAM 2017 in Würzburg.

Feichtmayer, J., Griebler, C. & Deng, L. Towards viral metagenomics of ultra-low concentrated DNA samples in the human lung. Oral presentation durch the Environmental Virology 2015 Polony Workshop in Haifa, Israel.

LIST OF ABBREVIATIONS

Abi	Abortive infection system
AHL	N-acyl homoserine lactone
AIP	Autoinducing peptides
Amp	Ampicillin
ANOVA	Analysis of variance
BAL	Bronchoalveolar lavage
bp	Base pairs
Cas	CRISPR associated sequence
cDNA	Complementary DNA
CF	Cystic fibrosis
CFU	Colony forming units
Cipro	Ciprofloxacin
COPD	Chronic obstructive pulmonary disease
CRISPR	Clustered regularly interspersed palindromic repeats
crRNA	CRISPR RNA
DNA	Deoxyribonucleic acid
dNTP	Deoxynucleoside triphosphate
EPI	Epifluorescence microscopy
EPS	Extracellular polymeric substances
FCM	Flow cytometry
FCM30	FCM measurement result with 30 °C staining procedure
FCM80	FCM measurement result with 80 °C staining procedure
GW	Groundwater
HGT	Horizontal gene transfer
hr	Hours
HS	Homoserine
HSL	Homoserine lactone (here: 3-oxo-C10-HSL)
LPS	Lipopolysaccharides
LuxI	AHL synthase LuxI
LuxR	AHL receptor LuxR
LW	Lake water
MDA	Multiple displacement amplification

MID	Minimal infectious dose
min	Minutes
MOI	Multiplicity of infection
mQ H_2O	Milli-Q purified water
MTase	Cognate methyltransferase
NTA	Nanoparticle-tracking analysis
NTA30	NTA measurement result with 30 °C staining procedure
NTA80	NTA measurement result with 80 °C staining procedure
OD	Optical density
ODE	Ordinary differential equation
OTU	Operational taxonomic unit
PA	Plaque assay
PAMP	Pathogen-associated molecular patterns
PCoA	Principal coordinate analysis
PEG	Polyethyleneglycol
PFU	Plaque forming units
PRR	Pattern recognition receptors
qPCR	Quantitative real-time PCR
QS	Quorum sensing
R-M	Restriction modification system
RBP	Receptor binding protein
REase	Restriction endonucleases
RNA	Ribonucleic acid
RNase	Ribonuclease
rpm	Rounds per minute
RW	River water
sd	Standard deviation
sec	Seconds
SIE	Superinfection exclusion systems
SRA	Sequence read archive
TA	Toxin-anti-toxin system
TAE	Tris-Acetat-EDTA-buffer
TE	Tris-EDTA-buffer
TEM	Transmission electron microscopy

UV	Ultraviolet light
VBR	Virus-to-bacteria ratio
VFDB	Virulence Factor Database
VLP	Virus-like particle
WW	Wastewater

LIST OF FIGURES

LIST OF TABLES

1 INTRODUCTION

1.1 Viruses in the environment

Viruses are small particles that range in size between 16 nm to 750 nm [1,2]. They are obligate intracellular parasites and therefore rely for their own replication on a viable host metabolism. Because of their millions of years lasting evolution, they are well adapted to their host organisms. Generally, the genetic material of viruses can be single- or double-stranded, linear, circular or segmented DNA or RNA that even may possess different polarities, ranging from few kbp to Mbp [3]. Their genome is surrounded by a protein capsid that can have a spherical (i.e. icosahedral) or helical symmetry. In some cases, the genome is complexed with cellular histones (e.g. papillomavirus) or viral proteins (e.g. adenovirus). Some viruses may be additionally enveloped by a lipid double layer that derived from cellular membrane systems of their hosts and may carry additional viral glycoproteins, albeit having an envelope also reduces the survivability of a virus in the environment [1].

1.1.1 Bacteriophages

In this thesis, the focus lies on bacteriophages, which are viruses that solely replicate in prokaryotes. With an estimation of 10^{30} microbes on Earth [4] and an average of 10 viruses per prokaryotic cell, viruses are with 10^{31} particles the most abundant biological entity on the planet [5]. Most bacteriophages are tailed dsDNA viruses belonging to the order auf *Caudovirales*, consisting of the three families *Myoviridae*, *Siphoviridae* and *Podoviridae*, although also polyhedral, filamentous or pleomorphic ssRNA and ssDNA phages are known as well [6].

The viral abundance in an ecosystem varies with nutrient availability, as this has an influence on the total number of hosts; thus the more oligotrophic an environment is, the less viral particles are present. Generally, viral numbers range between 10^7 to 10^{11} particles L^{-1} or g^{-1} dry weight in soil, ground or surface water [7–9]. Especially in surface waters, viral particles may underlie seasonal changes, resulting in higher concentrations during summer and lower concentrations during winter, thus also following the dynamics of their microbial hosts [10–12].

1.1.2 Viral replication

The replication of phages follows some common steps that are also valid for the replication of eukaryotic viruses: Adsorption to the surface receptors of a suitable host cell, separation of nucleic acid from the protein capsid, replication and expression of nucleic acid, protein synthesis, virion assembly and release of the progeny virus particles [5]. Bacteriophages can express different types of life cycles (**Figure 1-1**). When a virulent phage infects a bacterial cell,

the viral DNA is injected into the cytoplasm, where it redirects the host metabolism and starts viral gene expression, genome replication and morphogenesis. As a result, genomes, capsids and tails (where necessary) are synthesized and assembled. After a complete packaging of the progeny into virions, the lysis of the bacterial host is induced by viral holins, leading to the formation of pores within the cytoplasmic membrane and by phage-encoded endolysins (peptidoglycan hydrolases), leading finally to the hydrolyzation of the peptidoglycan layer. Upon the bacterial burst, dozens to thousands of new virulent particles are released into the environment, ready to infect surrounding bacteria [13]. Some phages are also released by budding or extrusion; both not necessarily leading to the death of the infected cell. This is the case during a chronic infection [6]. Another prevalent life cycle is the lysogenic cycle (**Figure 1-1**). Here, the nucleic acid of a temperate phage does not initiate the reproduction of progeny immediately upon injection, but rather integrates into the bacterial genome where it maintains as prophage and replicates along with the host. This condition may be stable for thousands of generations and affects the phenotype of the bacterium, as viral genes might be expressed, which are during the usual course of an infection not expressed (lysogenic conversion) [14]. At some time, however, a trigger induces the switch from the lysogenic to the lytic cycle. This trigger is generally a result from increasing stress for the host cell (e.g., lack of nutrients, exposure to chemicals, temperature or UV-light) [15]. In the pseudolysogenic life cycle, phages show neither a lytic behavior, nor a lysogenic one. Thus, the virus enters the cell without initiating the multiplication of the genome or integrating as prophage and maintaining in the cell line, however, the viral nucleic acid is not degraded. This form of life cycle is usually caused by e.g. starving host cells and is terminated with the initiation of either the lytic or lysogenic cycle [16,17].

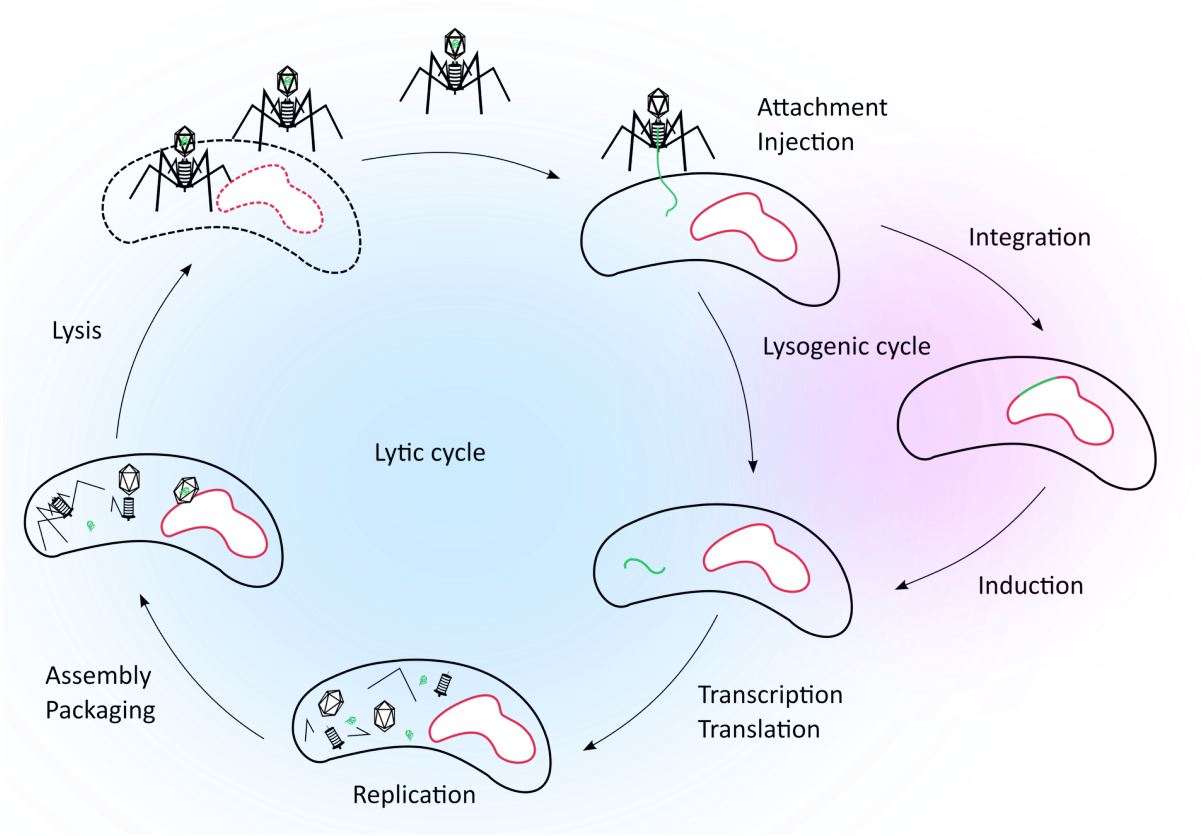

Figure 1-1: Replication cycles of bacteriophages. Lytic cycle results in the death of the infected host cell. With the lysogenic replication cycle, viral nucleic acid gets incorporated into the bacterial genome and stays there until some induction takes places, which is the signal for the phage to switch to a lytic life cycle.

1.2 Impact of bacteriophages on the microbial world

Generally, viruses are very host-specific and have a rather narrow host range. Some phages however are capable of infecting also a broader host range [18,19]. It has been shown that the morphology can provide an indication of the host range and the form of viral replication. For example, myoviruses are typically lytic and have a broader host range, thus can quickly take advantage of increasing host populations, which is consistent with r-selection (short generation times with high rates of reproduction) [20,21]. *Siphoviridae* display an intermediate host range and prefer a lysogenic lifestyle, indicating that these viruses are more K-selected, showing longer generation times and lower reproductive rates [22].

Although bacteriophage ecology and interplay with microbes has been studied best and longest in the marine environment, the genetic richness that has been found was to 60–80 % not similar to any sequences in known databases. Additionally, the most abundant genotypes make up less than 5 % of the viral communities, whereas the majority of genotypes comprises less than

0.01 % of the communities [23,24]. These numbers clearly indicate, that our knowledge about phages and their interaction with bacteria is still in the early stages.

1.2.1 Effects of virus – induced cell lysis

Estimates of the viral-induced bacterial mortality rates are highly variable (numbers range from 5–72 % of the marine bacterial population) and poorly constrained [25–30]. On the other hand, viral abundances are relatively constant over time, indicating that viral progeny is continuously produced with a significant proportion of their hosts being lysed [31]. Less is known about the effect of virus-induced lysis on photosynthetic eukaryotes, but it is assumed that the daily impact of viruses on eukaryotic phytoplankton accounts for several percent [21,32].

Lytic phages have an enormous influence on biogeochemical cycles due to the chemical and physical effects of the cell debris which is released through the virus-induced lysis of the bacterial host, as well as on the diversity of the microbial community, as the rate of viral infection largely depends on the host density. Generalizing, the more abundant a bacterial host is, the more likely an infection will be [7,15,22].

Lysed cells will release protein debris, nucleic acids, organic nitrogen and phosphorous compounds found in the cytoplasm, along with virus progeny [15]. The liberation of carbon and nutrients is thus an important support for other autotrophic and heterotrophic microorganisms [33,34]. Indeed, the presence of lytic viruses in an experimental study led to an increase in bacterial production and carbon mineralization rates of 27 % and a recycling rate of photosynthetically fixed organic carbon to dissolved organic material of 6–26 % [31,35]. A model developed by Proctor and Fuhrman suggested that viral lysis liberates approximately 1 µg L^{-1} dissolved organic carbon per bacterial generation in a marine system, leading to a carbon release ranging from 0.1–0.6 µg L^{-1} d^{-1} offshore and 0.7–5.2 µg L^{-1} d^{-1} nearshore [36]. For freshwater systems, carbon release rates have been estimated to 0.36 µg L^{-1} d^{-1} in the epilimnion, to 5.92 µg L^{-1} d^{-1} and 8.08 µg L^{-1} d^{-1} in the metalimnion and the anoxic hypolimnion, respectively [37].

With the lysis of host cells, phages contribute not only to bacterial mortality but also to bacterial diversity. The released cell debris may serve as nutritional source for surrounding bacteria and the partial niche emptying allows other bacterial species to fill in. This relationship is often also described as “Kill the winner hypothesis”, which is elaborated in section 1.4.3 and **Figure 1-7**. Thus, virus-induced bacterial lysis is a powerful procedure to impede the overgrowth of certain species, finally allowing for a co-existence of prokaryotes [17].

1.2.2 Effects of phage – induced gene transfer

Proportions of bacteria that carry a least one inducible temperate phage in its genome vary between 43 and 71 %, suggesting that the majority of marine phage-host systems are lysogenic [38–41]. Despite of the major effect, the lytic 'lifestyle' might be unfavorable in environments with low host densities [15]. In the cases where the likelihood for progeny phages to find new hosts upon release is low, lysogeny is favorable [42]. The ability of temperate phages to establish a stable relationship with their hosts can have profound ramifications on the lifestyle, fitness, immunity, virulence, distribution and evolution of prokaryotes (**Figure 1-2**) [43–47]. This involves the transduction of genes, a phenomenon named horizontal gene transfer (HGT) or lysogenic conversion. Phage genomes that harbor these genes become a part of the bacterial genome, where they may confer resistance to antibiotics, detoxification of heavy metals, acquisition and utilization of certain nutrients, evasion of predators or colonization of specific environments [48]. For the marine environment, the annual rate of gene transfer from virus to host has been extrapolated to 10^{24} genes [42]. Given the frequency of recombination that occurs between phage and host genes, phage populations likely serve as genetic reservoirs which are able to extend the ecological niches of the host [49].

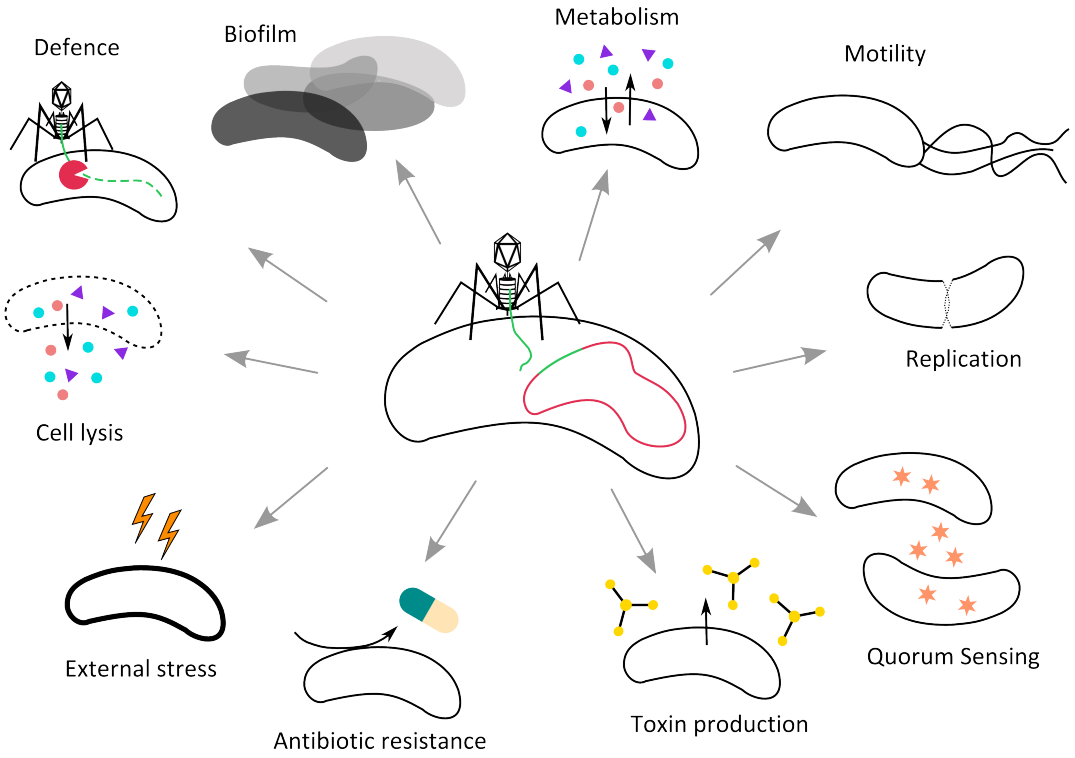

Figure 1-2: Influence of phages on bacterial behavior. Bacteriophages may have profound effects on the bacterial behavior. They may induce the bacterial cell lysis with the release of nutrients, the organization in biofilms, bacterial motility or replication. Phage-mediated horizontal gene transfer helps bacteria to cope better with external stress, enhances their metabolism or their ability to develop resistance against antibiotics or produce toxins. Bacterial quorum sensing may be affected through the presence of phages. For the prevention of an infection or lysis of the bacterial cells, bacteria may evolve different resistance strategies. Excellent review providing more details and further examples: [13].

A classic example of lysogenic conversion is the phage-mediated transfer of extracellular toxin genes, such as the botulinum neurotoxin type C1 encoded by phage CEβ [50], toxin CT, the principal virulence factor of *Vibrio cholerae*, encoded by phage CTX (in addition, the phage genome contains high numbers of virulence genes involved in antibiotic resistance, host adhesion and host invasion [51]), or the diphteria toxin of *Corynebacterium diphteriae* encoded by phage β [52]. Also other bacteria such as *Escherichia coli* [53,54], *Streptococcus pyogenes* [45,55,56], *Salmonella enterica* [57–60], or *Staphylococcus aureus* [61–63] increase their virulence through virus-encoded extracellular toxins, effector proteins participating in invasion, enzymes such as superoxide dismutase, staphylokinase, phospholipase or DNase as well as proteins affecting resistance to serum and altering antigenicity, superantigens, adhesion factors, proteinases, or mitogenic factors [43,64]. However, the production of some of these toxins are linked to an induction of the prophage. For example, the transcription of Shiga toxin genes,

carried by the prophages H-19B and 933W of *E.coli* O157:H7, is initiated upon prophage induction, resulting in a subsequent phage-induced cell lysis, accompanied by a release of Shiga toxin into the environment [65–67]. Noteworthy, antibiotic treatment of bacteria might serve as trigger, which leads to the induction of the prophage, thus, the treatment of this particular *E.coli* strain O157:H7 with the antibiotic ciprofloxacin resulted in the expression and secretion of Shiga toxins [68,69].

Another very prominent example of the contribution of viral-encoded genes is the enhancement of bacterial metabolism by expressing genes actively involved in photosynthesis, although this is more linked to lytic phages and therefore called lytic conversion. Hallmark of a lytic infection is the phage-induced shut-down of the host's metabolism. However, to secure the viral reproduction, cyanophages infecting *Prochlorococcus* or *Synechococcus* encode proteins, that become part of the host's photosynthesis apparatus or replace already degraded (host) photosynthesis proteins. Cyanophage S-PM2 for example carries the genes *psbA* and *psbD*, which encode for the photosystem II reaction center core polypeptides D1 and D2 [70–72]. Besides this enhancement for the host photosynthesis, viral genes analogous to the cyanobacterial *hli* (high-light inducible protein), *petE* (plastocyanin) and *petF* (ferredoxin) have been found to protect the host from photobleaching [73].

As last topic, the phage-supported survival of bacteria facing detrimental exposures shall be shortly elaborated. In *E.coli*, several prophage genes enhance the bacterial resistance towards environmental stressors (such as oxidative, acidic or osmotic stress, which are parts of the hosts' immune response triggered through a bacterial infection) or towards antibiotics (upon treatment of a bacterial infection or naturally produced by e.g. *Streptomycetes*), such as quinolones or β-lactams [74]. Modi and colleagues could observe that the phage metagenomes from ciprofloxacin and/or ampicillin treated mice were not only enriched in microbial functions that contribute to host metabolism and provide selective growth advantage by broadening the spectrum utilizable nutrients, but were also enriched in genes for resistance to the administered drug class. Upon treatment with ciprofloxacin (which targets bacterial DNA replication), resistance to DNA-synthesis inhibitors was increased, whereas in ampicillin treatments (which inhibits the cell wall synthesis) the resistance to cell-wall-synthesis inhibitors was enhanced. Besides, new resistance genes were found as well, which encode functions such as quinolone efflux pumps, drug-specific inactivators or multidrug-resistance exporters resulting in a general increase of antibiotic resistant bacterial colonies. These findings suggest that the phageome may serve as an adaptive repository for functions important for the host commensal relationship, which can contribute relevant functional advantages to their microbial hosts [75].

1.3 Bacteria-virus arms race

Phages fuel the genetic reservoir of bacteria, however, not every viral infection is beneficial for bacteria. Bacteria have therefore evolved a number of mechanisms to evade phage infection. The next section presents and describes evading strategies that bacteria can apply to prevent a phage infection. Consecutively, viral counteractive measures are discussed.

1.3.1 Bacterial evading mechanisms

The initial step of phage infection is the adsorption to specific bacterial surface receptors, mainly represented by surface proteins, polysaccharides and lipopolysaccharides; hence, the first measure to impede an infection lies in preventing phage attachment (**Figure 1-3**). This can be achieved by decreasing the receptor availability through structural adaptation of cell surface receptors or downregulation of receptors [76] (**Figure 1-3 B**). Excessive production of structured extracellular polymers (EPS; such as exopolysaccharides, alginates or hyaluronic acids) deteriorates the accessibility of surface receptors [77] (**Figure 1-3 D**). In addition to hiding receptors, bacteria may produce decoys such as outer membrane vesicles that irreversible bind phages, thus significantly reduce the efficiency of phage infection [78] (**Figure 1-3 F**).

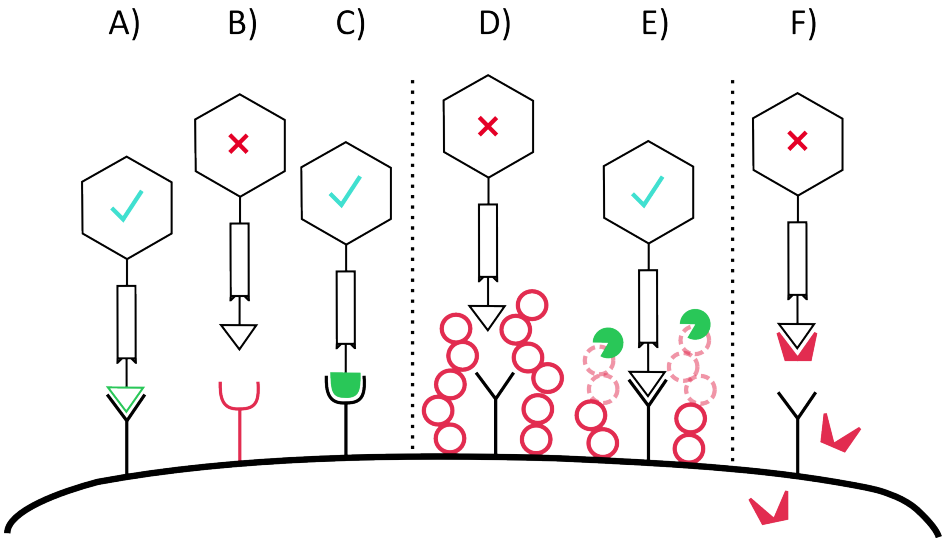

Figure 1-3: Bacterial defense mechanism: Preventing phage adsorption. A: Phage recognizes a suitable cell surface receptor and binds to it, which initiates further steps of viral infections. B: By modification of the receptor structure, the viral receptor binding protein (RBP) is not able to recognize its receptor anymore, thus no infection takes place. C: Phages can react by adapting their RBP, so that it recognizes the modified receptor again. D: Bacteria may also reduce the accessibility of the receptors by secreting EPS (red circles), which ultimately prevent an adsorption. E: Phages on the other hand may have EPS degrading enzymes attached to their fibers, which degrade the EPS layer and expose the receptors. F: Bacterial cells may also produce decoy molecules, which are secreted into the cell's environment and are able to bind to the viral RBP. Thereby, the viruses are not able to infect anymore, as their RBP are irreversibly blocked.

Following a successful adsorption, the injection of phage DNA may be blocked by superinfection exclusion (SIE) systems. Known SIE systems are membrane-anchored or membrane-associated proteins, that do not only protect the infected cell but also the surrounding population, as the infecting phage is rendered non-infectious following DNA ejection [79]. SIE proteins are often encoded in prophages, suggesting that SIE systems are more important for phage-phage interactions than for phage-host interactions [76].

Upon successful DNA injection, the bacterial immune system is mobilized and able to distinguish the host (self) genome from viral (non-self) genomes and inactivate the latter while protecting the former. The immune system can be divided into the innate and the adaptive or acquired immune system [80]. Very well characterized innate immune systems are the extremely diverse restriction-modification (R-M) modules, that employ methylation *via* cognate methyltransferases (MTase) to label and thus protect the self-DNA (**Figure 1-4 A**), while cleaving

any unmodified non-self-DNA through the action of restriction endonucleases (REase) [81,82] (**Figure 1-4 B**). Analogously, the DND system degrades foreign-DNA, while protecting phosphorothioated self-DNA [83]. Usually, the restriction enzyme is more active than the MTase, consequently, the incoming phage DNA is quickly cleaved [76]. In contrast, the adaptive immune system, which is represented by clustered regularly interspaced short palindromic repeats (CRISPR) and CRISPR-associated genes (Cas), memorizes previous encounters with phages and attacks invaders specifically upon re-infection [84] (**Figure 1-4 D**). Short viral DNA sequences are incorporated as protospacers in the CRISPR locus. Upon re-infection, the CRISPR locus is transcribed into a single transcript, which is then cleaved by the Cas proteins into crRNA units containing one targeting spacer. Cas-crRNA complexes interfere with the in-coming phage DNA by complementary base pairing, finally resulting in the degradation of the viral DNA through the Cas enzymes [85–87].

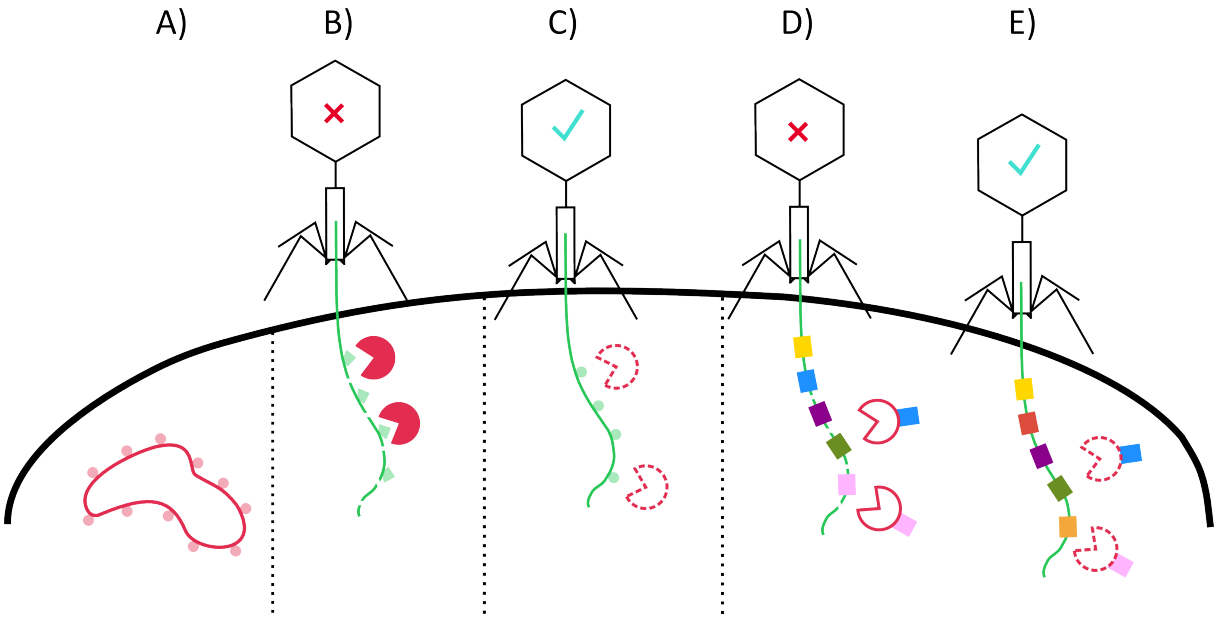

Figure 1-4: Bacterial defense mechanism: Degrading viral DNA. A: Naturally, bacterial DNA is protected from degradation by modification, e.g. methylation. B: Viral DNA, that lacks this methylation patter however is recognized by the restriction endonucleases (REase) and degraded. C: Viruses may prevent their DNA degradation by imitating the methylation pattern of their host DNA or modifying their DNA pattern, thus being not recognizable for the REase anymore. D: The CRISPR-Cas system is a more specific measure, based on the recognition of a specific viral DNA segment, finally also resulting in the degradation of the viral DNA. E: The induction of a single point mutation in this viral DNA segment is however already sufficient, to prevent any recognition by the CRISPR-Cas system.

A more radical measure of protection is the abortive infection (Abi) system. Here, cell death is induced by e.g. loss of the membrane potential upon successful viral infection as an altruistic behavior to protect the surrounding bacterial population from predation [79,88,89]. One mediator of Abi is the toxin-anti-toxin (TA) system. In general terms, a bacterial cell constantly produces a toxin molecule, which is neutralized by an anti-toxin (**Figure 1-5 A**). The expression of both is tightly controlled but, as soon as imbalances in the regulation occur, such as for example a successful phage infection, the anti-toxin production is abrogated, the toxins accumulate in the cell and as consequence the bacterium will undergo a programmed cell death [76,90] (**Figure 1-5 B**).

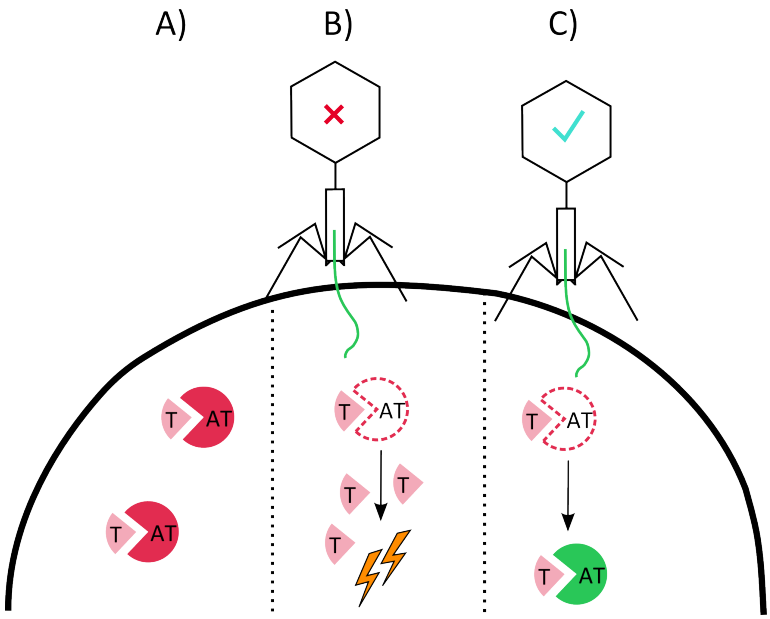

Figure 1-5: Bacterial defense mechanisms: Inducing cell death. A: In a bacterial cell, toxins (T) and neutralizing anti-toxins (AT) are constantly produced. B: Has a viral infection taken place, the anti-toxin is degraded and the now accumulating toxin induces at some point the death of the infected host. As a consequence, this virus infection will not result in viral progeny. C: The host's death may be prevented by the expression of compensating anti-toxins of viral origin, which neutralizes the toxin instead.

Intriguingly, not only bacteria carry anti-phage defense systems, also phages themselves have been found to be in the possession of such anti-phage systems. In the genome of *Haeomphilus influenzae* for example, a cryptic prophage carrying a *HindIII* R-M gene complex is located [91]. The reason might be the prevention of a superinfection, that is preventing other (similar) phages from infecting an already infected cell [92,93].

1.3.2 Viral resistance strategies

Phages on the other hand have in return evolved myriads of counteractive measures that allow them to infect nonetheless. Thus, phages have the potential to circumvent every bacterial defense strategy. They quickly adapt to new receptors by modification of their receptor binding proteins (RBP) [94] or by stochastic recognition of variable host receptors [95] (**Figure 1-3 C**). Phages can gain access to receptors that are masked by surface components, such as capsules or EPS, by hydrolyzing these barriers. These EPS-degrading enzymes (hydrolyses or lyases) are connected to the RBP complex [96,97] (**Figure 1-3 E**). Indeed, studies could show that phage genes involved in host recognition are amongst the fastest evolving genes [88,98,99]. Bacterial restriction modification systems can be dodged by passive or active mechanisms. Passive mechanisms are for example the reduction of restriction sites present in a phage genome or their orientation [81,100], as well as the incorporation of modified bases, such as uracil or hydroxymethyl uracil instead of thymine [101,102] (**Figure 1-4 C**). Co-injection of masking proteins, which bind to the viral DNA and render the restriction site inaccessible or mimic the phosphate backbone of DNA interfere actively with the R-M system [103–105]. Bacterial CRISPR-Cas system may easily be annulled by mutations in the protospacer region (mutation in one single nucleotide is already sufficient) [106] (**Figure 1-4 E**), by the presence of anti-CRISPR proteins that presumably interfere with the formation or action of the ribonucleoprotein CRISPR-Cas surveillance complexes [107], or by the action of a phage-encoded CRISPR-Cas system, that targets and inactivates specifically the host anti-viral defense system [108,109]. An abortive infection or a toxin-anti-toxin system may be by-passed by preventing the anti-toxin degradation [110] or expressing a phage-encoded protein that functionally replaces the unstable anti-toxin and neutralizes the toxin [111,112] (**Figure 1-5 C**).

1.3.3 Bacteria – virus interdependency

A common feature of bacterial anti-phage defense systems is the high genetic alterability, which results from the co-evolutionary arms-race with phages [113]. Evidences can be seen in the plethora of different R-M systems [81,114], CRISPR-Cas variations [115,116], or toxin-anti-toxin systems [90], that display additionally high evolutionary rates [85,117–119].

These variabilities in defense and offence systems of bacteria and phages are by-products of a host-pathogen relationship, which can be better described as an ongoing arms-race, ultimately having an impact on global nutrient cycles, ecosystems, climate [7,120], the evolution of the biosphere [121], as well as on the evolution of virulence in human pathogens [43]. This multifaceted process is a dynamic equilibrium locking both, phages and bacteria in a continuous state of co-evolution [122], thus mainly driving genetic novelty and shaping genotypic,

phenotypic and community-level diversity [123–126]. Hence, the costs for carrying and expressing anti-phage resistance mechanisms serve as a key factor in shaping the evolutionary dynamics between a phage and its host.

An important factor that vastly shapes the interdependency is the associated cost of genetically encoding a certain defense strategy. One example may be the increasing energy costs associated with carrying the additional genetic load and indeed, only a small portion of a bacterial population holds a plasmid or a prophage, encoding for a certain defense mechanism [85]. Likewise linked to increasing energy costs is the (constant) downregulation of surface receptors used for viral recognition and adsorption, as those receptors may have important functions in e.g. nutrient uptake [127]. The constant expression of defense systems bears also the risk of autoimmunity. Especially in R-M systems, the restriction enzyme is often more stable than the DNA-protecting bacterial methylase, thus having detrimental consequences if constantly active [128]. Also the CRISPR-Cas system bears the potential of incorporating self-genetic material in the spacer region, thus resulting in autoimmunity as well [129]. The lethal nature of abortive infection mechanisms may only serve as a last resort for individual bacteria to protect self-sacrificingly their population.

1.3.4 Economization of anti – phage response: bacterial quorum sensing

Phages lack the ability for an active movement therefore the abundance of a bacterial strain influences the infection success. The more abundant and the more metabolic active a certain host is, the more likely it will be infected by its phages [7,30,36]. Thus, the predatory pressure phages impose on a bacterial population increases with growing cell densities as consequently also the probability for a phage to meet its host increases. However, bacteria have evolved the ability to record the abundance of surrounding clonal cells and react in a cell density-dependent manner. The production and export of small cell-to-cell signaling molecules by bacteria, so called autoinducers, are known to regulate a wide range of bacterial behaviors [130]. With increasing cell density, the released signal molecules accumulate in the extracellular milieu. Once a certain threshold concentration of the molecule is reached and by that, also a critical population density, a coordinated change in bacterial behavior is initiated [131]. This effective and widely-used form of bacterial communication and regulation system has been termed ‘quorum sensing’ (QS) [132]. The number of individuals in a quorate population is not appointed, but rather depends on the relative rates of synthesis and turnover or loss of QS signal molecules [133,134]. These signal molecules are manifold in structure and most bacteria produce more than one type. In gram-negative bacteria, different molecule classes, such as N-acyl homoserine lactones (AHL),

4-quinolones, fatty acids or fatty acid methyl esters have been identified as QS signal molecules, with AHLs being the best studied and understood system. Most AHL producing bacteria synthesize several structurally different AHLs, characterised by a homoserine lactone (HSL) ring with a N-acylated fatty acyl group at the α-position and unsubstituted in the β- and γ- positions. The acyl chain varies in length, saturation level and oxidation state, and has in most cases an even number of carbon atoms (C4–C18) [131,135]. While gram-negative bacteria employ hydrophobic, low molecular weight signal molecules, gram-positive bacteria engage post-translationally modified and occasionally quite complex peptides as QS signaling molecules. These autoinducing peptides (AIPs) range from 5 to 34 amino acids in length and typically contain unusual chemical architectures. Examples are oligopeptide lantibiotics [136], thiolactone peptides [137] or isoprenylated tryptophan peptides [138,139]. Up to date, autoinducer-2, a collective term for a family of interconvertible furanone compounds, is the only signal molecule, that is utilized by both, gram-negative and gram-positive bacteria [131].

The principle mode of action of a QS response system will be expounded exemplarily by the AHL-mediated signal synthesis and transduction (**Figure 1-6**). The low basal production of AHL by the AHL synthase LuxI is not enough by itself to activate the cytoplasmic AHL receptor LuxR. The rapid diffusion of the small molecule out of the bacterial cell ensures, that it will not accumulate without input from other cells. LuxR is the cytoplasmic receptor for AHL, as well as a transcription factor initiating gene expression. Without the AHL, the LuxR protein is unstable and is rapidly being degraded. However, with increasing cell density, more and more AHLs are accumulating in the surrounding medium and now, AHL molecules diffuse back into the cell and bind to LuxR. The LuxR-AHL complex activates the expression of more LuxI (positive feedback-loop), as well as the gene expression of adjacent genes. Prominent examples are the cell density controlled expression of secondary metabolites (e.g. antibiotics), bioluminescence, swarming, virulence or biofilm formation [131].

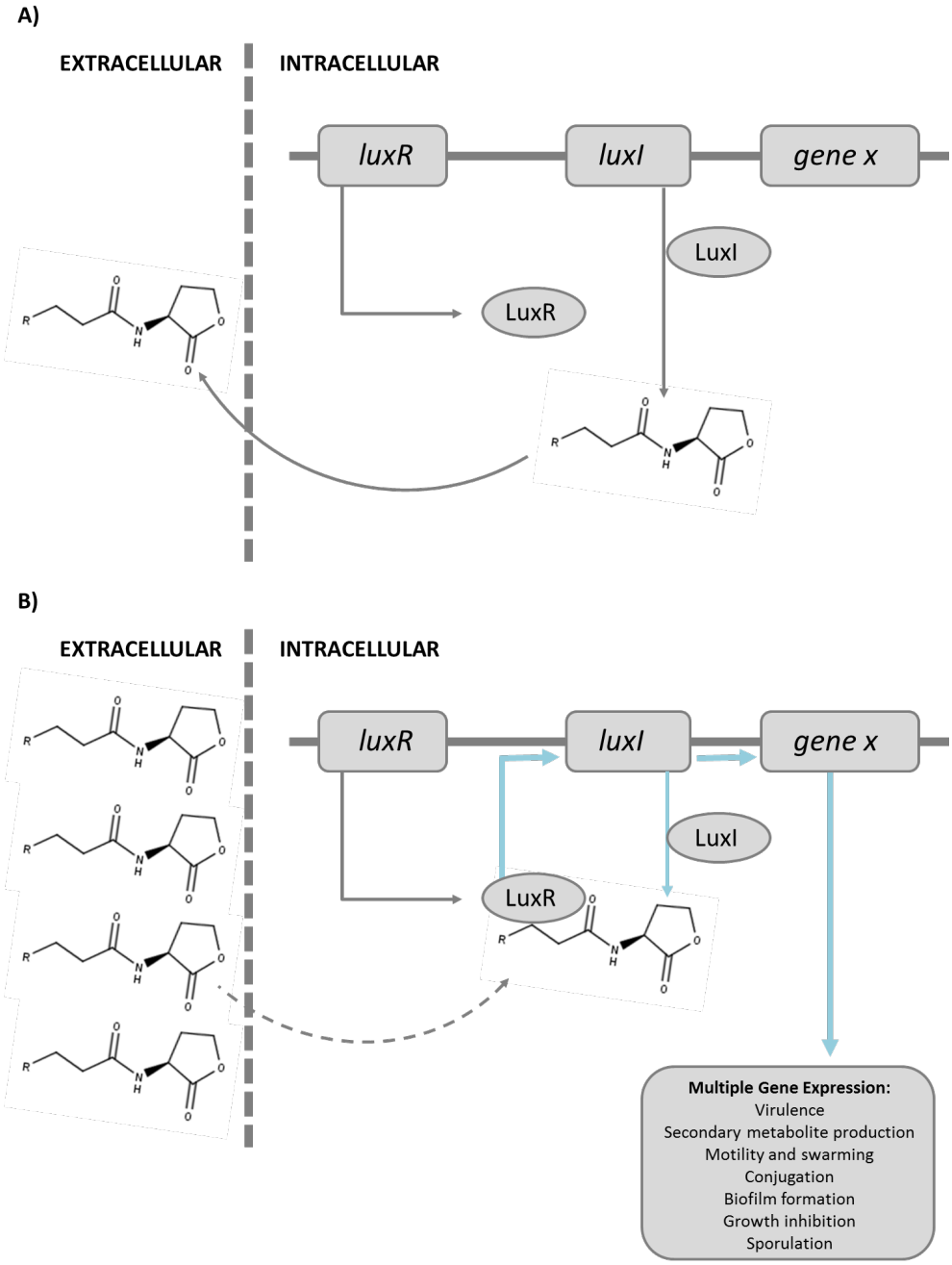

Figure 1-6: Schematic of a general AHL mediated quorum sensing system. A: Constantly produced AHL molecules diffuse out of the bacterial cells and accumulate in the surrounding milieu. B: Once a sufficient AHL concentration has been reached, AHL diffuses back into the cells and activates members of the LuxR transcriptional regulator protein family. The LuxR/AHL complex is responsible for activating or repressing multiple target structural genes. Mostly, *luxI* is one of these target genes, resulting in a positive autoinduction circuit in which the AHL signal molecule also controls its own synthesis (positive feedback-loop).

Besides the mentioned cell density dependent gene expression, there are some evidences, that also phage defense strategies could be modulated according to cell density and thus according to the potential threat of a phage infection. For example, QS triggers the surface receptor downregulation in *Escherichia coli* (LamB is essential for phage λ adsorption) and in *Vibrio anguillarum* (OmpK is used by phage KVP40) [140,141]. A down-regulation of these receptors renders the bacteria at high cell densities almost fully resistant to their respective phages, however, not only surface receptors are altered by the QS system. For *Pseudomonas aeruginosa* and *Serratia* sp. it has been shown that QS mediates the expression of the antiviral CRISPR-Cas system as well [142,143].

1.4 Bacteria – phage interactions affecting human health and disease

As already indicated in a previous section, through their ability to modulate bacteria, phages may also have an influence on higher trophic levels and by that might affect or even contribute to dysbiosis.

1.4.1 The role of the microbiome in health and disease

Microbes colonize every surface of the human body that comes into contact with the external environment like the skin, mouth, gastrointestinal tract and even the lung [144–146]. It is therefore not surprising, that the human body holds 10-fold more bacterial cells than own cells [147].

The human microbiome is a unique polymicrobial community protecting the human host on the one hand from pathogenic assault by competing for sites of attachments and nutrients, as well as producing antimicrobial substances [148], and on the other hand altering the host's metabolism by modulating lipid metabolism and glucose homeostasis, absorbing lipid-soluble vitamins, or activate respectively inactivate drugs [149]. The composition of the microbiota thus affects metabolic, regulatory and morphogenetic networks.

During the establishment of a (chronic) disease, the microenvironment in the affected organ changes. Consequently, the microbiota present for example in diseased lungs (e.g., patients suffering from asthma, cystic fibrosis (CF) or chronic obstructive pulmonary disease (COPD)) differs from the microbiota in healthy lungs [150–153]. On the other hand, many studies revealed, that changes in the abundance of bacterial species, or imbalances of the dynamic equilibrium in the bacterial composition are linked to several human disorders. Thus, a reduced or altered bacterial diversity is often accompanied by a diseased state (e.g., [150,154,155]. One well studied environment hereby is the human gut. The gut microbiome interacts with the

mucus layer and epithelial cells, as well as with the underlying lamina propria immune cells, thus contributing to the health or disease of the human host [156]. This emphasizes that the gut microbiome is closely linked to the human metabolism and therefore also to metabolic disorders like obesity or diabetes [154,157]. For the human lungs, *Prevotella* and *Veillonella* spp. have been identified as a distinctive component of the healthy microbiome. The reduction of these strains in COPD or in asthmatic patients, together with an increasing presence of *Haemophilus* or *Neisseria* (both human-pathogenic bacteria) may co-occur during the progress of the disease [150]. However, it is still unclear whether the presence or absence of a certain bacterium as part of the microbiota is the condition for the development of a (chronic) disease or the result of a successful disease establishment.

1.4.2 Human – associated virome studies

The virome comprises all viruses in and on an organism. It consists of prokaryotic, archaeal and eukaryotic viruses, as well as exogenous viral elements in the host chromosomes (e.g., prophages or endogenous retroviruses). Members of the virome influence the phenotype of the host in a combinatorial manner by interacting with other members of the microbiome (such as other members of the virome itself, the bacterial microbiome or the mycobiome) and by interacting with individual variations in host genetics. Together these interactions may influence a range of phenotypes, which may be important for health and disease [158].

The gut virome has been intensively studied in the last decades. Indeed, it is the best studied human-associated virome. In contrast to studies in the marine environment, viral ratios to bacterial numbers were 10-fold less, equalizing bacteria and virus numbers in the gut [159,160]. However, phages tend to accumulate on mucosal surfaces and within mucosa, giving rise to bacteria:phage ratios as high as 1:20 within the intestinal mucosa [161]. The healthy gut virome is dominated by bacteriophages, although eukaryotic viruses such as members of the families *Picobirnaviridae*, *Adenoviridae*, *Anelloviridae*, *Astroviridae* or *Bocaviruses*, *Enteroviruses*, *Rotaviruses*, and *Sapoviruses* have been identified as well [162,163]. The gut virome has been characterized by a high degree of inter-personal variation, which was much higher than in the associated gut microbiome. However, the intra-personal variation over a 2.5 years period was with a maintenance of 80 % of virotypes relatively low [159,160,162]. Interestingly, the environment seems to have a more profound influence on the composition, as a similar diet resulted in inter-personal concordance [160]. Also sharing the same household caused similarities in the homologues of the oral viral communities. Nonetheless, viromes from stool samples were distinct from those of the saliva [164]. Surprisingly, the human skin virome is

dominated by eukaryotic DNA viruses (most prominent are *Papillomaviridae*, *Polyomaviridae* and *Circoviridae*), with only few reads identified as phages [165]. In human lungs, the role of phages has mostly been evaluated in the diseased state but by now, no general assessment of the healthy lung virome has been conducted. Lim and colleagues studied the virome in the lungs of CF patients with sputum samples [166]. In the CF viromes, 6 % of the total metagenomics sequences were unique, corresponding to aromatic amino acid biosynthesis, which could not be found in the non-CF viromes [167]. Besides, phages of common CF associated pathogens (e.g., *Pseudomonas* spp., *Burkholderia* spp., *Haemophilus influenza* or *Staphylococcus* spp.) have been found in all pulmonary lobes [168].

1.4.3 Phages as modulators of the microbiome

De Paepe and colleagues have postulated four different mechanisms by which commensal phages may affect the human gut microbiota [169]. The bacterial host population must be above a critical density for a phage to being able to infect. When host numbers are too low, the chance that a phage will get lost is higher, than its chance to infect [170]. Consequently, only if the prey density is high, also the virus will be able to replicate. This concept is also known as “kill the winner” (**Figure 1-7 A**). Therefore, phages quantitatively kill only the dominant commensal bacteria in the intestinal ecosystem, which could be shown in germ-free mice colonized with symbiotic bacteria and fecal phages [171]. Analogously to the classical predator-prey relationship in ecology, also the relationship between viruses and their microbial hosts follows commonly a Lotka-Volterra dynamic, characterised by a top-down control of microbial communities [159]. The oscillations between host and phage populations have been shown for marine environments [172], however, this trend was absent in the gut system of humans [159], horses [173] or pigs [174].

Phage-mediated horizontal gene transfer may transduce survival factors like genes involved in metabolic pathways, functional genes or virulence factors, which can be either offensive, like genes for antibiotic resistance or toxin production or defensive, helping to modify bacterial antigenicity by masking of antigens [43,159,160]. The latter could be shown with enzymes of temperate phages modifying the O-antigen of bacterial lipopolysaccharides (LPS) [175,176]. Viral-encoded toxin genes, either expressed during lytic or lysogenic cycle, like Diphtheria, Cholera or Shiga toxins bear the risk of emerging new pathogenic bacteria (**Figure 1-7 D**) [13,43,48,51,177,178]. Adjacent to toxins, also effector proteins can be directly secreted into eukaryotic cells or biofilms and target not only aktin filaments, microtubules, mitochondria, lysosomes, tight junctions or extracellular polymeric substances, but also disrupt cell signaling

pathways like MAPK, cAMP, GTPases Rho, Rac and Cdc42 [179,180]. Prophages may thus serve as anchor points for genome rearrangements, interrupt genes through insertion, or silence genes by induction of phage repressors. They provide not only immunity to related phage infections, but also lyse closely related competitive strains ("kill the relative", see **Figure 1-7 B**) [43,181]. As bacterial phage receptors expressed on bacterial cells can contribute to the bacterial virulence, the evolution of phage-resistant offspring may lose the aptitude to cause disease [182]. However, the induction of temperate phages upon presence of inducive agents, such as antibiotics at sub-inhibitory concentrations [69], or compounds present in cigarette smoke, may result in host lysis (**Figure 1-7 C**). *Lactobacillus* phage is for example induced by cigarette smoke, thus causing a higher risk for smokers to develop a bacterial vaginosis, as vaginal lactobacilli are reduced as a consequence [183].

In the case of the oral microbiome, it is known that disorders lead to periodontitis. Variations in the oral virome are mirrored by the microbiome, presuming that phages can have an effect on the development of periodontal diseases [184]. The presence of phages of *Aggregatibacter actinomycetemcomitans* was even found to be positively correlated with a rapidly destructive periodontitis [185]. The microenvironment in an organ changes during disease. In CF for example, the airways are distinguished by hypoxia and a low pH. Exudations show accumulated concentrations in amino acids, DNA and phospholipids [186,187]. The adaptations that microorganisms have to face in order to survive under those conditions, are reflected by the metabolic profiles of the CF viromes [188]. On this note, genes involved in aromatic amino acid biosynthesis pathways (quorum sensing), exopolysaccharide biosynthesis (biofilms), virulence (β-lactamases, multi-drug efflux pumps) are abundant in the virome fraction [167]. The diversity of the viral specimen identified in the lung displayed a spatial heterogeneity [168]. The explicit involvement of the human virome with regard to health and dysbiosis is still not fully clarified. Although bacteriophages do not have a direct influence on the human's body, they are essential for human health, as they are able to manipulate the human microbiome, serve as reservoirs of genetic diversity of the microbiota (horizontal transfer of virulence, antibiotic resistance or metabolic genes), and interact with the host immune system through stimulation of innate and adaptive immune responses [169,189–191]. Furthermore, the presence of enteric viruses has been associated with pathogenesis of dysbiosis and intestinal disorders (Inflammatory bowel disease, Crohn's disease or colon cancer) [192,193]. However, it is believed that deciphering the human virome will improve the understanding, prevention, and treatment of currently unexplained or partially understood diseases involving viral and bacterial pathogens, as well as provide insights into the evolution of viral families and cross-species viral transmissions [194].

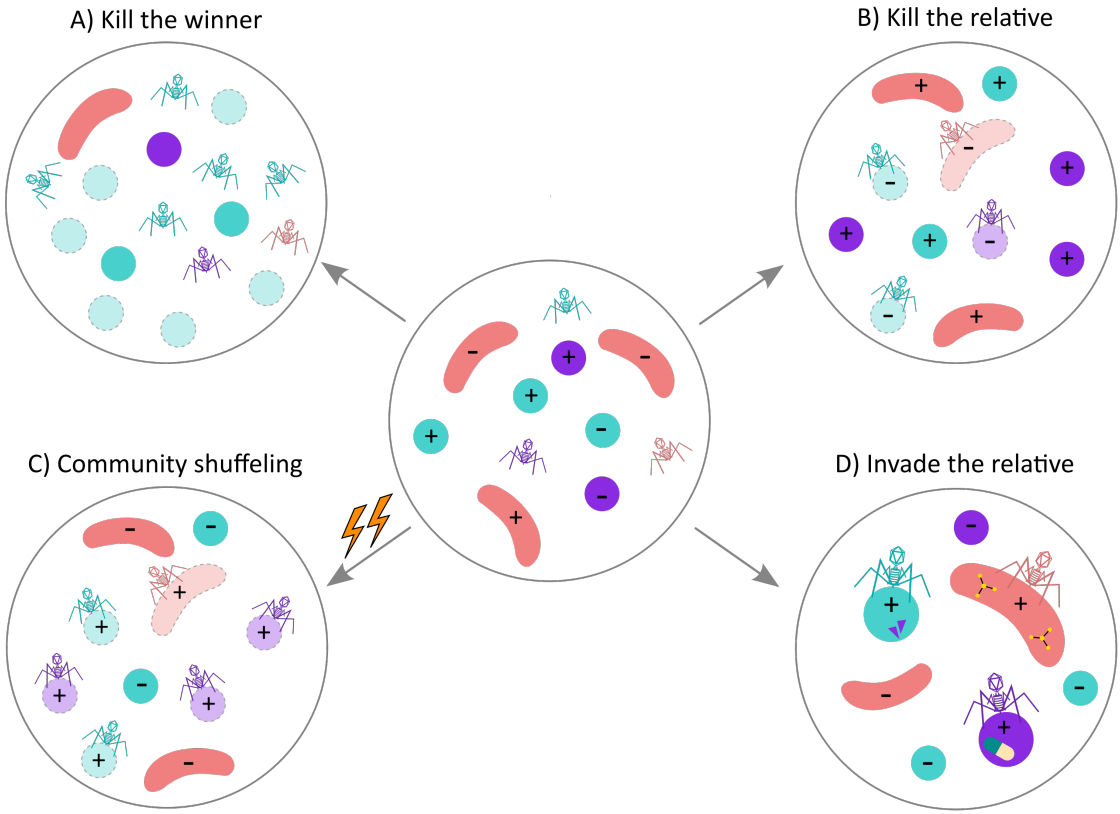

Figure 1-7: Different models of possible bacteria-phage interactions. A: Kill the winner. Bacterial numbers are too low for a viral infection, but proliferating and overgrowing species reach a threshold concentration, at which phages can infect and lyse and therefore restore the initial equilibrium. B: Kill the relative. Lysogenic bacteria that have a prophage integrated are resistant to the respective free lytic phage, leading to advantage of lysogenic populations over non-lysogens. C: Community shuffling. Impact of stress (indicated by orange arrow) on a population leads to the induction of prophages, which switch to their lytic lifecycle and kill their hosts. A positive feed-back loop may take place if the massive lysis leads to a host reaction, such as inflammation. The net result is a global displacement of populations, and possibly dysbiosis. D: Temperate phages infect new hosts and integrate into the host's genome as prophages. Thus, they contribute to the emergence of new bacterial strains that are e.g. able to utilize new substrates, produce toxins or enhance antibiotic resistance. Symbols: + indicates the presence of a prophage, - indicates the absence. Visualized according to the description in [169].

Moreover, in times of increasing development of (multiple) antibiotic resistance with decreasing discoveries of new antimicrobial compounds, the specificity of bacteriophages for problematic (pathogenic) bacteria amongst others, regains more and more interest. **Table 1-1** summarizes potential therapeutic applications of bacteriophages [195]. The usage of phages to control problematic bacteria harbors many advantages compared to antibiotic treatments: phages

exhibit a great specificity and efficiency for their target bacteria consequently avoiding the impairment of the commensal microbiome. Additionally, bacteriophages are unable to replicate in eukaryotic cells, thus they are not pathogenic to humans and they persist only as long as the bacterial host is present in the system [196,197]. However, as the development of anti-phage resistance might appear relatively fast, the administration of single-phage treatments is evited in favor of applying a combination of either different lytic phages at high concentrations, targeting the same host, or a combination of antibiotics and phages. The narrow host range of a single phage may be overcome as well through administering a cocktail of different phages.

Table 1-1: Potential therapeutic applications of bacteriophages in humans. A: The single lytic phage used as an antimicrobial (single phage administration), bears the risk of rapid bacterial resistance development from clonal selection and alterations in phage preparation. B: Multiple phage administration can overcome pathogenic bacteria resistance. C: Further antimicrobial effects can be achieved in a synergistic action with antibiotics. D: Genetical modifications can be used for enhancing the natural antibacterial capacity of phages, for example for the targeted derangement of biofilms. E: Phages might be used for the modulation of the gut microbiota thus enlarging their ability for the utilization of previously non-usable nutrients or enhancing metabolic rates.

Direct antimicrobial effects				**Indirect modulation**
A Application of single lytic phages	B Application of multiple phages	C Phages in combination with antibiotics	D Engineered phages	E Modulation of microbiota
Alterations in phage preparation - Fast development of resistance	Multiple bacterial receptors are targeted + Lower risk of resistance development	Synergistic action + Lower risk of resistance development	Genetic modification e.g. EPS-degrading enzymes linked to viral tail fibers + Enhancement of the natural antibacterial activity	Improvement and enhancement of nutrient degradation + Stabilization of microbiota + Benefit for host/microbiota

Nowadays, phages are widely used for the biocontrol of herbal or foodborne pathogens in agriculture or the decontamination in aquacultures and food industries [198–200]. Besides, phages may serve as diagnostic tools (phage typing) to detect specific bacteria, e.g., methicillin resistant *Staphylococcus aureus*, by fluorescently labelled phages, plaque formation or by the expression of luciferase genes delivered through modified phages [201,202]. Generally, the use of engineered phages gains more and more attention. Phage-encoded or associated enzymes are capable to degrade barriers to phage adsorption, bacterial cell walls (lysins) or EPS structures in a biofilm, which may then be further antagonized [203–205].

To what extent phages will be approved for usage in humans is debatable. Currently, few clinical trials with phage preparations are conducted [206,207]. However, concerns and challenges of e.g., the host range, resistance development, manufacturing processes concerning the removal of endotoxins and pyrogenes released during phage-induced lysis, potential systemic side effects of phage therapy or the delivery of the phages to their destination, remain [208]. The innate immune system plays a major role when clearing a bacterial infection upon administration of antibiotics. Likewise, the efficacy of phages as therapeutic agents is supposed to be enhanced by the activation of the innate immune system through phage-induced cell lysis [209]. Indeed, mathematical modeling suggested that phages alone are not able to remove a certain pathogen completely. This will be only possible in cooperation with the immune system [210,211]. As consequence, immunocompromised patients, which are actually those patients, where opportunistic and multiple antibiotic resistant bacteria cause a lot of problems, would possibly be excluded from phage therapy. Besides the activation of the immune system by phage-induced bacterial lysis, pathogen-associated molecular patterns (PAMPs) presented by phages are recognized by pattern recognition receptors (PRR) and stimulate the immune system as well [209]. In addition, some phages may express proteins that mediate an interaction with mammalian cells and thus promote an immune response [212]. On the other hand, phages may also show anti-inflammatory properties through inhibitory effects on excessive reactive oxygen species production or induction of IL-10 production. IL-10 is an anti-inflammatory cytokine, important for the development of a certain immune tolerance [213]. Here, phage therapy may help to reduce an excessive immune response [214]. Although phages do not infect eukaryotic cells, they do also provoke the adaptive immune systems. The antibodies IgM and IgG have been found to bind to the head and tail of phage T2 [215]. In 81 % of tested human sera, IgG directed at several T4-like phage head proteins could be detected [212]. Both, the activation of the innate and the adaptive immune system by the phages might also impair the success of phage therapy, as the phages might be cleared before pathogens are lysed. This topic was already investigated

in 1987, where 57 patients that received phage therapy were tested on their anti-phage antibody titer before and after the therapy. Anti-phage antibodies could be detected throughout the therapy in all patients, however, only in two patients, this led to a failure of the phage therapy. In all other 55 patients, the infection could be cleared despite the detected anti-phage antibodies [216]. Conclusively, an interference of our immune system with the therapeutic efficiency cannot be excluded, as comprehensive and statistically sound studies are scarce. Nevertheless, concerning the safety risks for patient, the immunogenicity of phages seems not an issue [209].

1.5 Aim and hypotheses

1.5.1 Virus quantification techniques in the spotlight

Nowadays, phages are successfully used for the decontamination of food, plants, fields and livestock, for example to control fish diseases [198], plant pathogens [200] or foodborne pathogens [199]. However, obtaining an approval for the usage of phages as human therapeutics requires meticulous characterization of both, phages and their host organism (in particular with the background of the human system), as well as a precise quantification of the phage preparations. Several quantification techniques are available on the market, holding different advantages but also drawbacks. The gold standard of viral quantification still claims to be the plaque assay technique. It allows a rather inexpensive detection of active (infectious) viral particles related to a particular host strain, but with poor reproducibility rates and time consuming preparations. Quantitative real-time PCR is a molecular technique allowing a quick quantification for a single virus species or group, based on the presence of a specific viral nucleic acid with high reproducibility rates, but also associated with high costs. Additionally, genetic information of the targeted virus is needed in order to being able to design virus-specific primer sequences. In contrast to the plaque assay, the mere presence of nucleic acid does not necessarily prove the presence of an infectious viral particle. Thus, this method quantifies free viral DNA, infectious and non-infectious particles. Epifluorescence microscopy is widely used for determining vial abundances in greater volumes, for example seawater [217]. It uses fluorescent DNA dyes to trace viral particles in a solution with subsequent mounting on a filter or a microscope glass slide for a microscopic enumeration. Another popular method, initially used for the identification, quantification and separation of eukaryotic immune cells and prokaryotes based on individual properties, which has been adapted as a high-throughput method for the quantification of viral particles is flow cytometry [218,219]. Viral DNA is fluorescently labelled and quantified according to fluorescence and scatter signals. These analyses are inexpensive;

however the equipment is rather costly. A fairly new approach to determine viral concentrations is the nanoparticle-tracking analysis using for example, NanoSight instrument. A microscope visualizes the Brownian movement of small particles in a liquid phase in real-time and relates it to the particle size. Additional lasers allow tracking of fluorescently labelled particles. The measurement requires only little preparation time but here as well, the equipment is pricy [220].

Determining exact viral titers in a given sample is essential for many applications. Studying viral ecology, general or medical virology, host-phage interactions and their influence on bacterial communities, or virus-to-bacteria ratios make an accurate estimation of viral particles in a given sample essential. However, the quantification of nano-sized viral particles in a sample of unknown composition is a sophisticated task that remains challenging. The small size of the particle itself and the extremely small viral genomes challenge available quantification techniques. The purpose of the first chapter was the comparison of different widely-used quantification techniques in terms of accuracy and applicability for not only pure viral isolates but also complex environmental samples. Viral isolates with distinct genetic compositions (ss- and dsDNA and RNA) and particles sizes were quantified using traditional and particle-specific methods (plaque assay and quantitative PCR), as well as fluorophore-based methods (epifluorescent microscopy, flow cytometry and nanoparticle-tracking analysis). The same methods were then applied (where possible) to samples collected from different aquatic environments with expected higher and lower viral titers.
This comparison should ultimately result in the identification of one method which is particularly suitable for the quantification of viral particles or, alternatively, providing a measuring strategy based on the specific sample type.

1.5.2 Characterization of bacteria – phage interactions

With regard to the fast development of bacterial antibiotic multi-resistances, lytic bacteriophages might serve as controlling agent for pathogenic bacteria. One of these problematic bacteria is *Pseudomonas aeruginosa*. It is a gram-negative, opportunistic bacterium commonly found in various biotic and abiotic habitats, from water and soil to plants, which is able to infect plants, animals and humans [221,222]. *P. aeruginosa* is a major nosocomial pathogen, causing both acute and chronic infections in humans. It is a leading cause of mortality, particularly in immunocompromised patients suffering from immunosuppression, postoperative or traumatic wounds, burns, cancer or cystic fibrosis [223]. One feature, that makes the bacterium so problematic is its low antibiotic susceptibility, which can be attributed to a collective action of multidrug efflux pumps with further chromosomally-encoded antibiotic

resistance genes and a generally low permeability of the bacterial cellular envelope [197]. Additionally, the excessive use of broad-spectrum antibiotics has accelerated the emergence of multidrug resistant bacteria, rendering most chronic infections with *P. aeruginosa* very difficult to treat [224]. Another aggravating attribute is its ability to adhere to surfaces, thus forming virulent biofilms, which protect the individual cells from eradication by antibiotics and complicate a treatment even more [225].

The aim of the second chapter was firstly the isolation of lytic bacteriophages of two different *P. aeruginosa* strains, PAO1 (biofilm-forming wildtype) and a clinical isolate. Thereby, a better understanding of phage and bacteria interactions and their co-evolutionary dynamics should be generated. The isolates were characterized in order to find the optimal temperature and pH for successful infection. Additionally, the genetic composition was investigated by restriction enzyme digestion and metagenomic sequencing. The viral isolates were then further characterized regarding their ability and efficiency to lyse cells organized in a biofilm with the expectation, that the isolates can be used to control planktonic, as well as attached cells of *P. aeruginosa*. Additionally, their suitability for treating acute *P. aeruginosa* infections in humans was tested in a larger scale experiment, which measured the infectivity after incubating the phages for up to 2 weeks at 36 °C or 40 °C. This setting should mimic the elevated temperature the body has upon struggling with an acute infection. In order to being considered as therapeutic agent, phages have to keep their infectivity also at elevated temperatures.

1.5.3 Viral impact on microbial communication

Here, the interplay between lytic phages, their bacterial hosts and quorum sensing as potential mediator of anti-phage response was examined. As already discussed in the introduction (see 1.3.4), some bacteria use QS to sense the potential threat of a phage infection related to their cell density and express anti-phage strategies accordingly. Examples are the QS-induced downregulation of the surface receptors OmpK for phage KVP40 adsorption in *Vibrio anguillarum* and LamB for phage λ adsorption in *Escherichia coli* [140,141]. As a result, these bacteria are nearly fully resistant to their particular phages at high cell densities. Even more, in *V. anguillarum*, QS determines the choice of anti-phage strategies, as at low cell densities with a still inactive QS system, bacteria are protected by enhanced biofilm formation [140]. Also other defense strategies, such as the CRISPR-Cas system has been found to be activated by QS in *P. aeruginosa* and *Serratia* sp. [142,143]. Especially with regard to the rapid development of multiple antibiotic resistant bacterial strains, making use of alternative treatment strategies such as phages and/or QS inhibitors (quorum quenching) is gaining new interest [226–229]. As

it could be nicely shown by Høyland-Kroghsbo and colleagues, the inhibition of QS may result in an increased susceptibility of the bacterium to its phages [142]. However, for these ideas becoming reality, a fundamental understanding of the underlying mechanisms is crucial, not only with regard to individual isolates in a one strain population, but also in multispecies settings and under different environmental conditions [19].

In this chapter, the interaction between the QS system of *Pseudomonas putida* and a combination of different lytic phages was evaluated. It is known, that *P. putida* utilizes QS for switching into an attached lifestyle (QS-induced biofilm formation) [230,231]. Here, it was hypothesized that QS is also involved in the economization of an anti-phage defense. The collected data were not only analyzed but also used for a mathematical model-based verification of different potential contributions. In the first hypothesis no influence of the presence of phages on the QS system is postulated. Here, it is assumed that phages act only by killing the host cells, independently of the QS state. In the second hypothesis, the addition of phages to the system will lead to increased HSL production rates and consequently will lead to an accelerated QS initiation. Similarly, the third hypothesis postulates a phage-dependent upregulation of the production of the intracellular HSL receptor (PpuR), which has already been shown for *V. anguillarum* or *E. coli* [140,141]. Hypothesis four is the most sophisticated. This hypothesis is based on the idea, that being QS active means at the same time for an individual cell to be more resistant against phage attacks, compared to being QS inactive. As a consequence, QS activated cells develop a temporary resistance against phages.

1.5.4 Virome assessment in the lung

Few studies exist that investigate the virome of the human lung. Mostly, these studies are linked to a certain chronic disease of the lung, such as CF. General capture of the virome present in a healthy lung has so far not been undertaken. The aim of this project was in a first attempt to evaluate the virome as present in the bronchoalveolar lavage (BAL) of healthy individuals. Although the lung is influenced greatly through the surrounding environment, it is hypothesized, that a certain phage community is present in a healthy lung, which is distinctively different from a community found in a chronically diseased lung. This will be evaluated with the analysis of BAL samples from COPD patients. Besides this disease-related flexible virome, there is also a core virome, expected to be always present in the lung, independent of its disease state. The phages present in a healthy and a diseased setting will reflect the bacterial community which dominates this particular environment. As the immune system in patients suffering from chronic lung diseases is frail due to inflammations in the pulmonary tissues, a higher bacterial load is

expected. With that, also an increase in phage numbers is anticipated. Furthermore, not only the bacterial load will be affected, but also the composition of the dominating species, which will be mirrored by the virome. All in all, this knowledge will help to better understand how the bacterial community behaves in an altered environment and to what extent phages contribute to their adaptation. Ultimately, this will support the understanding how chronic diseases such as COPD develop and progress.

2 MATERIALS AND METHODS

2.1 Materials

2.1.1 Equipment and consumables

Table 2-1: List of equipment.

Device	Manufacturer
2100 Electrophoresis Bioanalyzer Instrument	Agilent, Santa Clara, US
Allegra® X-15R	Beckman Coulter, Krefeld, D
Cary 50 Bio UV Visible Spectrophotometer	Varian, Palo Alto, US
E220 Focused-Ultrasonicator	Covaris, Woburn, US
Electrophoresis Power Supply E835	Consort, Turnhout, BE
Gel Jet Imager	Intas, Göttingen, D
Genome Sequencer FLX+ Model 3736	Roche, Basel, CH
Heraeus Brutschrank	Thermo Scientific, Waltham, US
Heraeus Megafuge 1.0 R	Thermo Scientific, Waltham, US
Mastercycler Gradient Thermal Cycler, 120 V, 50/60	Eppendorf, Hamburg, D
Microcentrifuge	Eppendorf, Hamburg, D
Ministar silverline	VWR International, Darmstadt, D
Mx3000P qPCR system FAM/SYBR green I filter (492nm-516nm), OS v7.10	Stratagene, San Diego, US
ND-1000 Spectrophotometer	Thermo Scientific, Waltham, US
Pippin Prep DNA Size Selection System	Sage Science, Beverly, US
Thermomixer Compact	Eppendorf, Hamburg, D
TissueLyser II	Qiagen, Hilden, D
Vortex Mixer PV1	Grant, Wiltshire, UK
Victor2 Microplate Reader Wallac 1420	Perkin Elmer, Waltham, US
FC500 flow cytometer (488 nm Argon ion laser)	Beckman Coulter, Brea, US
Axiolab Fluorescence microscope (488 nm laser)	Carl Zeiss, Oberkochen, D
Zeiss EM 912 (OMEGA filter in zero-loss mode)	Carl Zeiss, Oberkochen, D
Tröndle 2k × 2k slow-scan CCD camera	Tröndle Restlichtverstärker Systeme, Moorenweis, D
NanoSight NS300	Malvern Pananalytical Ltd., Malvern, UK

Table 2-2: List of consumables.

Consumables	Manufacturer
8× strip tubes, 0.2-ml	Agilent, Santa Clara, US
Adhesive Sealing Sheets	Thermo Scientific, Waltham, US
AFA Fiber Pre-Slit Snap-Cap 6×16 mm microTUBEs	Covaris, Woburn, US
Amicon Ultra 15 Centrifugal Filter Units 10k Device	Merck Millipore, Darmstadt, D
Anotop 25 Plus Syringe Filters, 0.02 µm	Whatman, Little Chalfont, UK
Combitips advanced Biopur 1 mL	Eppendorf, Hamburg, D
Einmal Küvetten 1.5 mL	Brand, Wertheim, D
Falcon Centrifuge Tubes 15ml; 50 mL	Becton Dickinson, Franklin Lakes, US
Millex-GV Syringe Filter Unit, 0.22 µm	Merck Millipore, Darmstadt, D
Millex-HP Syringe Filter Unit, 0.45 µm	Merck Millipore, Darmstadt, D
Multipette M4	Eppendorf, Hamburg, D
Nanosep Omega-Membran 10kDa	VWR International, Darmstadt, D
Omnifix Luer-Lock Einwegspritzen, 3ml; 5 mL	B.Braun, Melsungen, D
Petri Dish	Greiner BioOne, Kremsmünster, AT
Safe-Lock Tubes 0.5 mL; 1.5 mL; 2 mL	Eppendorf, Hamburg, D
Tip One Bevelled Filter Tip, 10 µL; 20 µL; 100 µL; 200 µL; 1000 µL	Starlab, Hamburg, D
0.22 µm Corning bottle-top vacuum filter system	Sigma Aldrich, St. Louis, US
microTUBE	Covaris, Woburn, US
0.02 µm Anotop 25 syringe filter	Whatman, Maidstone, UK
Trucount Tubes	Becton Dickinson, Franklin Lakes, US
0.02 µm Anodisc filter	Whatman, Little Chalfont, UK
1 mL sterile syringe	Braun, Melsungen, D

2.1.2 Kits, reagents and chemicals

Table 2-3: List of kits and reagents.

Reagent	Manufacturer
2 % Agarose w/ external markers, 100-600 bp	Sage Science, Beverly,US
Agencourt AMPure XP Kit	Beckman Coulter, Krefeld, D
Brilliant III Ultra-Fast SYBR® green QPCR Master Mix	Agilent, Santa Clara, US
Bioanalyzer DNA 7500 and High Sensitivity Kit	Agilent, Santa Clara, US
DyNAmoTM cDNA Synthesis Kit F470l , Finnzymes	Thermo Scientific, Waltham, US
End-It DNA End-Repair Kit	Epicentre, Madison, US
Fast-Link DNA Ligations Kit	Epicentre, Madison, US
GoTaq Green Master Mix	Promega, Madison, US
GS FLX Titanium MV emPCR Kit (Lib-L)	Roche, Basel, CH
GS FLX Titanium PicoTiterPlate Kit 70×75	Roche, Basel, CH
GS FLX Titanium Rapid Library MID Adaptors Kit	Roche, Basel, CH
GS FLX Titanium Rapid Library Preparation Kit	Roche, Basel, CH
GS FLX Titanium Sequencing Kit XLR70	Roche, Basel, CH
Min Elute PCR Purification Kit	Qiagen, Hilden, D
MinElute Reaction Clean Up	Qiagen, Hilden, D
MolYsis kit basic 5	Molzym, Bremen, D
NucleoSpin Gel and PCR Clean Up	Macherey Nagel, Düren, D
PfuUltra II Hotstart PCR Master Mix	Agilent, Santa Clara, US
pGEM-T Easy Vector System II	Promega, Madison, US
Phusion High-Fidelity DNA Polymerase (2 U μL^{-1})	Thermo Scientific, Waltham, US
PowerViral® Environmental RNA/DNA Isolation Kit	Mobio, Carlsbad, US
QIAamp MinElute Virus Spin Kit	Qiagen, Hilden, D
QIAamp Viral RNA Mini Kit	Qiagen, Hilden, D
QIAquick PCR Purification Kit	Qiagen, Hilden, D
qPCR standard sequences	Integrated DNA Technologies, Skokie, US
Quant-iT PicoGreen dsDNA Assay Kit	Invitrogen, Darmstadt, D
SV Total RNA Isolation System	Promega, Madison, US
Ultra Clear Thinwall Tubes 14 × 95 mm	Beckman Coulter, Krefeld, D

Wizard PCR Preps DNA Purification Minicolumns	Promega, Madison, US
Wizard PCR Preps DNA Purification Resin	Promega, Madison, US

Table 2-4: List of chemicals.

Reagent	Manufacturer
0.5 M EDTA, pH 8.0	Life Technologies, Darmstadt, D
1 kb ladder	Promega, Madison, US
1× SYBR gold nucleic acid stain	Thermo Fisher, Waltham, US
100 bp DNA Ladder	Invitrogen, Darmstadt, D
3-oxo-C10-HSL standard	Cayman Chemical, AnnArbor, US
Agar kobe I	Roth, Karlsruhe, D
Ampicillin Natriumsalz	AppliChem, Darmstadt, D
antifade solution	Thermo Fisher, Waltham, US
Ascorbic Acid	Roth, Karlsruhe, D
Blue/Orange Loading dye 6×	Promega, Madison, US
$CaCl_2$	Roth, Karlsruhe, D
DNase I, Grade II	Roche, Basel, CH
DTT	Life Technologies, Darmstadt, D
Ethanol absolut reinst	Th. Geyer, Renningen, D
Gel Red Nucleic Acid Stain 10000×	Biotium, Fremont, US
Glycerol	Merck, Grafing, D
goat-anti-rat antibody conjugated to horseradish peroxidase (GaR-HRP)	Dianova, Hamburg, D
IPTG Solution, 100mM	Fermentas Life Sciences, Schwerte, D
Isopropanol	Sigma Aldrich, St. Louis, US
ISOTON® II Diluent, 20 L	Beckman Coulter, Krefeld, D
KOH	VWR International, Darmstadt, D
LB broth (Miller)	Fluka, Buchs, CH
LE Agarose 500 g	Biozym, Hessisch Oldendorf, D
$MgCl_2$	Sigma Aldrich, St. Louis, US
$MgSO_4$	Fluka, Buchs, CH
Na_2EDTA dihydrate	Fluka, Buchs, CH
NaCl	Sigma Aldrich, St. Louis, US
NaOH	Roth, Karlsruhe, D

Nuclease free water	Promega, Madison, US
PBS buffer	Sigma Aldrich, St. Louis, US
Polyethylenglycol (PEG) 8000	AppliChem, Darmstadt, D
Proteinase K	Fisher Scientific, Waltham, US
Restriction enzymes: AluI, EcoRI, HhaI , NdeI	Thermo Scientific, Waltham, US
SOC Medium, 5 × 10 mL	Fisher Scientific, Waltham, US
TAE Buffer (50×)	AppliChem, Darmstadt, D
TE Buffer	AppliChem, Darmstadt, D
Tris-Base	Merck, Grafing, D
Tris-HCl	Promega, Madison, US
Ultra-Pure LMP Agarose	Invitrogen, Darmstadt, D
X-Gal Solution	Fermentas Life Sciences, Schwerte, D

2.1.3 Microorganisms

Table 2-5: Bacterial and viral strains.

All strains were obtained from *Leibnitz Institute DSMZ* unless otherwise noted.

Strain ID	DSMZ ID	Notes
Escherichia coli ATCC 11303	DSM 613	Host for phage T4 and T7
E.coli ATCC 12435	DSM 5695	Host for phage MS2
E.coli NCCB PC 0886	DSM 13127	Host for phage ΦX174
Pseudomonas putida IsoF	NA	Dr. Michael Rothballer,
P. putida F117	NA	Institute for Network Biology ,
P. aeruginosa CI	NA	Helmholtz Zentrum München
P. aeruginosa PAO1 ATCC 15692	DSM 22644	
Phage T4 (active culture)	DSM 4505	
Phage T7 (active culture)	DSM 4623	
Phage ΦX174 ATCC 13706-B1	DSM 4497	
Phage MS2 ATCC 15597-B1	DSM 13767	
Phages 0251, 0124, 0125, 3301 and 3404		Isolated during thesis

2.1.4 Oligonucleotides

Table 2-6: List of oligonucleotides. All sequences were obtained from Biomers.

Abbreviation	Genetic sequence	Reference
g20 (T7-like phages)	CPS1.1 A: 5'-GTAGWATWTTYTAYATTGAYGTWGG-3' CPS8.1 B: 5'-ARTAYTTDCCDAYRWAWGGWTC-3'	[232]
g23 (T4-like phages)	MZIA1bis fwd: 5'-GATATTTGIGGIGTTCAGCCIATGA-3' MZIA6 rev: 5'-CGCGGTTGATTTCCAGCATGATTTC-3'	[233]
P. aeruginosa phages	gep5 fwd: 5'-GTGATCACACCCGAACTG-3' gep5 rev 5'-ATGTTGGAGCGCATCG-3' gep5_16G>AC rev: 5'-ATGTTGGAGCGCATCAC-3'	This thesis
	Paer_phag_1kb fwd 5'-GCGTACATCGCGAACTCTGG-3' Paer_phag_1kb rev 5'-CCCAAAGATTCATGATGTTGCTGG-3'	This thesis
M13	M13 (-21) M3: 5'-GTAAAACGACGGCCAG-3' M13 rev: 5'-CAGGAAACAGCTATGAC-3'	[234]
DNApol	DNApol_90Fa: 5'-GAYACIYTIRYIYTITCIMG-3' DNApol_90Fa: 5'-GAYACIYTIRYIYTIAGYMG-3'	[235]
	DNApol_355Ra: 5'-GGIAYYTGIGCIARRTTIGG-3' DNApol_355Rb: 5'-GGIAYRTTIGCIARRTTIGG-3'	[235]
16S rDNA	Ba27 fwd: 5'-AGAGTTTGATCMTGGCTCAG-3' Ba907 rev: 5'-CCGTCAATTCMTTTRAGTTT-3' Ba519 fwd: 5'-GWATTACCGCGGCKGCTG-3' Ba907 rev: 5'-CCGTCAATTCMTTTRAGTTT-3'	[236,237]
T4 specific	T4 fwd: 5'-AAGCGAAAGAAGTCGGTGAA-3' T4 rev: 5'-CGCTGTCATAGCAGCTTCAG-3'	[238]
T7 specific	T7_4453 fwd: 5'-CTGTGTCAATGTTCAACCCG-3' T7_5008 rev: 5'-GTGCCCAGCTTGACTTTCTC-3'	[239]
MS2 specific	MS2_2717 fwd: 5'-CTGGGCAATAGTCAAA-3' MS2_ 3031 rev: 5'-CGTGGATCTGACATAC-3'	[240]
ΦX174 specific	PhiX fwd: 5'- ACAAAGTTTGGATTGCTACTGACC-3' PhiX rev: 5'-CGGCAGCAATAAACTCAACAGG-3'	[241]
Human GAPDH specific	GAPDH_1 fwd: 5'-GACTGAGGCTCCCACCTTTC-3' GAPDH_1 rev: 5'-CTCCCCACATCACCCCTCTA-3'	This thesis
Linker A	Linker A fwd: 5'-P*-GTATGCTTCGTGATCTGTGTGGGTGT-3' Linker A rev: 5'-CCACACAGATCACGAAGCATAC-3'	[242]

Primer with **Barcodes** for pyrosequencing	Primer #1: 5‘-P- **CGACA**CCACACAGATCACGAAGCATAC-3‘ Primer #3: 5‘-P- **CTCTA**CCACACAGATCACGAAGCATAC-3‘ Primer #4: 5‘-P- **CTATG**CCACACAGATCACGAAGCATAC-3‘ Primer #14: 5‘-P-**ATGTA**CCACACAGATCACGAAGCATAC-3‘ Primer #15: 5‘-P-**TGAGT**CCACACAGATCACGAAGCATAC-3‘ Primer #21: 5‘-P- **TATCG**CCACACAGATCACGAAGCATAC-3‘ Primer #23: 5‘-P- **CTCAT**CCACACAGATCACGAAGCATAC--3‘	[242]
*: P = phosphorylated		

2.2 Media

The following setting was used for autoclaving media and glassware: 121 °C for 20 min.

2.2.1 1× LB medium

25 g	LB broth (Miller)
ad. 1L	mQ H_2O

Autoclaved before use.

2.2.2 2× LB medium

50 g	LB broth (Miller)
ad. 1L	mQ H_2O

Autoclaved before use.

2.2.3 ABC medium

The medium was prepared according to [243].

Component A (10×):

2 g	$(NH_4)_2SO_4$
6 g	Na_2HPO_4
3 g	KH_2PO_4
3 g	NaCl
ad. 100 mL	mQ H_2O

The pH was adjusted to 6.8. Autoclaved before use.

Component B (1×):

2 mL	1 M $MgSO_4$
0.2 mL	0.5 M $CaCl_2$
0.3 mL	0.01 M $FeCl_3$
ad. 900 mL	mQ H_2O

All stock solutions were prepared separately and sterile filtered (0.22 µm). The pH was adjusted to 6.8.

Component C (100×):

10 mL	1 M $C_6H_5Na_3O_7$

The pH was adjusted to 6.8. Sterile filtered (0.22 µm).

Components were stored at 4 °C. *Prior to* use, components A and B were mixed (in total 1 L) and 10 mL of C were added.

2.2.4 M9 minimal medium

All stock solutions were prepared separately and autoclaved before use.

M9 salt solution (10×):

75.2 g	$Na_2HPO_4 \bullet 2\ H_2O$
30 g	KH_2PO_4
5 g	NaCl
5 g	NH_4Cl
ad. 1 L	mQ H_2O

M9 minimal medium:

100 mL	M9 (10×)	final : 1×
20 mL	20 % Glucose	final: 0.4 %
1 mL	1M $MgSO_4$	final: 1 mM
0.3 mL	1M $CaCl_2$	final: 0.3 mM
ad. 1 L	mQ H_2O	

2.2.5 Solid agar (for plates)

25 g	LB broth (Miller)
15 g	Agar (Kobe I)
ad. 1 L	mQ H_2O

Autoclaved before use. 20 mL was poured per petri dish. Plates were stored at 4 °C

2.2.6 Soft agar (for plates)

25 g	LB broth (Miller)
7.5 g	Agar (Kobe I)
ad. 1 L	mQ H_2O

Autoclaved before use.

2.2.7 Phage buffer

7 g	Na_2HPO_4 anhydrous
3 g	KH_2PO_4 anhydrous
5 g	NaCl
ad. 1 L	mQ H_2O

Autoclaved before use. Afterwards, 10 mL 0.1 M $MgSO_4$ and 10 mL 0.1 M $CaCl_2$ were added and the buffer was 0.02 µm filtered.

2.2.8 Phage precipitation (PEG)

100 g	PEG (8000)	final: 20%
73 g	NaCl	final: 2.5 M
ad. 1 L	mQ H2O	

Autoclaved before use.

2.2.9 $FeCl_3$ precipitation

The precipitation followed the description in [244].

$FeCl_3$ stock solution:

4.83 g	$FeCl_3 \bullet 6\ H_2O$
100 mL	mQ H_2O

EDTA–ascorbate buffer (1×):

1.51 g	Tris base	final: 0.125 M
3.72 g	Na_2–EDTA • 2 H_2O	final: 0.1 M
4.07 g	$MgCl_2 \bullet 6\ H_2O$	final: 0.2 M
3.52 g	Ascorbic acid	final: 0.2 M
4 mL	5 N NaOH	
ad. 100 mL	mQ H_2O	

This buffer was prepared freshly on the days of use. Tris base was completely dissolved in 80 mL mQ H_2O. After that, Na_2–EDTA • 2 H_2O was added and completely dissolved. Once in solution, $MgCl_2 \bullet 6\ H_2O$ was added. The pH drops to 4–5 and the solution will become cloudy. The addition of 3 mL 5 N NaOH will clear the solution and increase the pH to approximately 8.3. The ascorbic acid was added with the last mL of NaOH. The pH was adjusted to 6.0–6.5 and filled up with mQ H_2O to a total volume of 100 mL.

EDTA–ascorbate buffer (2×):

1.51 g	Tris base	final: 0.125 M
7.44 g	Na_2–EDTA • 2 H_2O	final: 0.2 M
8.14 g	$MgCl_2 \bullet 6\ H_2O$	final: 0.4 M
7.04 g	Ascorbic acid	final: 0.4 M
4 mL	5 N NaOh	
ad. 100 mL	mQ H_2O	

Same preparation as described for the 1× buffer.

2.2.10 Cesium chloride gradient

For the CsCl gradient ultracentrifugation, CsCl solutions with different densities were prepared in baked glass ware and with autoclaved and 0.02 µm filtered TE 1×:

ρ = 1.20	11.19 g CsCl	ad. 50 mL TE 1×
ρ = 1.40	26.94 g CsCl	ad. 50 mL TE 1×
ρ = 1.50	33.74 g CsCl	ad. 50 mL TE 1×
ρ = 1.65	43.78 g CsCl	ad. 50 mL TE 1×

2.2.11 DNase I storage buffer

100 µL	1 M Tris–HCl, pH 7.5	autoclaved
20 µL	1 M $CaCl_2$	0.22 µm filtered
10 mL	50 % Glycerol	autoclaved

2.2.12 10× DNase I reaction buffer

1 mL	1 M Tris–HCl, pH 7.5	autoclaved
250 µL	1 M $MgCl_2$	0.22 µm filtered
50 µL	1 M $CaCl_2$	0.22 µm filtered
8.7 mL	mQ H_2O	

2.2.13 DNA extraction buffer

Lysis buffer (pH 12):

700 µL	KOH stock:	0.43 g KOH per 10 mL mQ H_2O
430 µL	DTT stock:	0.8 g DTT per 10 mL mQ H_2O
370 µL	mQ H_2O	

Stop buffer (pH 8.5):

5 g	Tris–HCl
10 mL	mQ H_2O

2.3 Methods

2.3.1 Bacteria cultivation conditions

All bacteria used in this thesis were cultivated in 1× LB medium at 37 °C and with agitation (160 rpm), if not stated otherwise. Each bacterial strain was plated on a LB agar plate, incubated at 37 °C for overnight, and a single colony was then picked and inoculated in fresh 1× LB. This culture was mixed with 20 % glycerol and aliquots (denoting the bacterial stock) were kept frozen at –80 °C.

2.3.2 Bacterial biofilm quantification: Microtiter dish assay

Cells grown in a biofilm were quantified using a crystal violet staining. 100 µL of *P. aeruginosa* PAO1, inoculated in M9 minimal medium until the exponential phase was reached, were pipetted into the wells of a 96 well plate together with 100 µL fresh M9 minimal medium (2.2.4). Plates were incubated at 37 °C without shaking. Staining was performed according to [245]. Briefly, the medium was removed by inverting the plate and washing twice by putting the plate in a tray filled with water. Remaining liquid was briefly but firmly shaken out. This step helps to remove unattached cells and medium components, which might be stained as well, thus reducing the background noise. To each well 125 µL of a 0.1 % crystal violet solution was added and incubated for 10 min at room temperature. Plate was shaken out to remove excess liquid and washed three times in water. Afterwards, the plate was dried completely at 37 °C for approximately 30 min. The stained biofilm was dissolved in 200 µL ethanol 100 % and the absorbance was measured twice using the Victor Photometer at 540 nm with pre-shaking for 10 sec.

2.3.3 Phage isolation

2.3.3.1 Lytic virus isolation from liquids (host-specific)

Isolation of bacteriophages from liquids was performed with a co-incubation of a suitable liquid sample and the bacterial host. 5–10 mL of 2× LB was mixed with the same amount of liquid sample (0.22 µm filtered or unfiltered), inoculated with 5–10 µL of a bacterial stock solution and incubated at 37 °C and 160 rpm overnight. Next day, co-incubated samples were 0.22 µm filtered and the presence of lytic phages was confirmed with a spot assay (2.3.3.3) and further clonally isolated (2.3.3.4).

2.3.3.2 Total virus isolation from solids (host-unspecific)

2.5 g of the solid sample (sediment or feces) were mixed with 10 mL 0.02 µm filtered 10 mM $Na_4P_2O_7 \bullet 10\ H_2O$ and 10 µL 0.02 µm filtered 5 mM EDTA and vortexed vigorously for 20 min at the highest setting. Samples were centrifuged at 2000 × g at 20 °C for 25 min. The

supernatant was transferred and filtered using a 0.22 µm Corning bottle-top vacuum filter system. Again, 10 mL 0.02 µm filtered 10 mM $Na_4P_2O_7 \bullet 10\ H_2O$ and 10 µL 0.02 µm filtered 5 mM EDTA were added to the remaining solid sample and rotated overnight at room temperature with subsequent filtration of the supernatant using the same Corning bottle-top vacuum systems as before. The filtered supernatant containing viral particles was then further processed for DNA or RNA extraction (2.3.9). The filters (containing bacteria) can be stored at –80 °C for RNA extraction or at –20 °C for DNA extraction.

2.3.3.3 Spot assay

A spot assay allows a quick survey of a bigger sample amount for the presence of lytic phages specific for a certain bacterial host. 0.5 mL of a freshly grown bacterial inoculum (OD600 around 0.3) was mixed with 4 mL melted soft agar (60 °C) and poured onto a solid agar plate. Once the agar layer containing the bacteria is solidified, 3 µL of a virus-containing sample (co-incubations of bacteria and environmental samples, 2.3.3) was applied on the agar. A positive (any phage that is able to lyse this bacterium) and negative control (any non-phage containing sample, such as phage buffer or LB medium) was included as well. The plate was incubated overnight at 37 °C. On the next day, the bacteria form a turbid layer with the presence of a lytic virus appearing as a cleared spot, where the sample has been applied. As the tested sample volume is relatively small, each sample was tested in triplicates.

2.3.3.4 Isolation of clonal viruses

Co-incubated samples that resulted in a positive spot assay result were further processed for an isolation of viral particles as especially environmental samples may contain more than one phage able to replicate in the chosen host. In a first step of the generation of pure isolates, a plaque assay was performed (2.3.7.1). As the particle concentration was unknown, several dilutions of the co-incubated sample were plated. After an overnight incubation at 37 °C, a dilution was chosen where singularized plaques were visible. It is assumed, that each plaque is formed from one phage that clonally replicated in bacterial hosts. Using a sterile tip, a well-isolated plaque was picked and added to 100 µL phage buffer (2.2.7). In a first purification round, for each positive sample 30 plaques were picked. The plaque assay was repeated with 10 µL of each of the 30 plaque solutions and 0.5 mL of the bacterium inoculum in 4 mL melted tempered soft agar. After incubation overnight, five plaques per sample were picked off and added to 100 µL phage buffer, which denominates the second round of purification). This process was repeated with one of the five plaques for each sample until the fifth purification, to ensure a single clonal phage preparation. If one of the five plaques did not work, the other four picked

plaques were tested and used instead. After reaching the fifth purification, high-titer lysates of the isolates were produced (2.3.4.1).

2.3.4 Phage propagation

2.3.4.1 Production of high-titer lysates (solid)

In order to reach higher liquid volumes of the phage isolates (after clonal viruses were produced, 2.3.3.4), 10 plaque assays were produced for each purified phage (2.3.7.1). Here, lower dilutions were preferred, resulting in approximately 3000 plaques per plate ("web" pattern). After incubation on the next day, 5 mL of phage buffer (2.2.7) were added to each plate and placed at 4 °C for overnight. The liquid was collected and 0.22 µm filtered. Starting from this high-titer lysate, further virus stocks were produced according to (2.3.4.2).

2.3.4.2 Virus stock production (liquid)

A working culture of the respective *E.coli* strain (see **Table 2-5**) was inoculated in 50 mL 1× LB medium at 37 °C and 160 rpm until an OD600 between 0.3 and 0.5 was reached. According to the viable cell count the colony forming units (CFU) mL^{-1} corresponding to the measured OD600 value could be calculated and the appropriate amount of phage preparation to reach a virus to bacteria range of 0.1 was added. Subsequently, a further incubation overnight at 37 °C and 120 rpm followed.

In order to increase the phage concentration, an alternative propagation strategy was conducted: Bacteria were inoculated in 25 mL 1× LB to an OD600 between 0.3 and 0.5, and the respective amount of viruses was added. After an incubation of 1–2 hr, 25 mL fresh 1× LB medium was added and incubated at 37 °C and 120 rpm for overnight.

On the next day, both types of preparations were purified according to 2.3.5.1.

2.3.5 Viral particle purification

2.3.5.1 Purification from stock production

One tenth of chloroform was added to an overnight bacteria – phage co – incubation (following 2.3.4.2) in order to induce the lysis of the remaining bacterial cells, and incubated for an hour under the hood. The upper phase containing the phages was transferred to a falcon tube and centrifuged at 4000 × g at 4 °C for 20 min to remove the bacterial cell debris. The virus-containing supernatant was then transferred to new falcon tubes and stored at 4 °C.

In case of chloroform sensitivity, this step can be omitted. In this case, the phage-bacteria mix was centrifuged for 20 min at 4000 × g and 4 °C. The supernatant was then filtered with a 0.22 µm syringe filter and stored at 4 °C.

2.3.5.2 CsCl gradient ultracentrifugation

With this method, pure viral samples void of bacterial DNA, cell debris and other contaminating agents can be generated [246]. However, this method is laid out for sample volumes less than 5 mL, therefore, larger volumes needed to be concentrated (2.3.6.2). A CsCl density gradient (2.2.10) was layered carefully into Ultra-Clear Thinwall Tubes starting with 1.8 mL of the highest density ρ = 1.65, then 2.7 mL of ρ = 1.5, 2.7 mL of ρ = 1.4 and 0.9 mL of ρ = 1.2. As a last, the sample was likewise carefully layered (up to 5 mL). All preparations were carefully balanced and inserted into the tube holders of the SW40Ti swing bucket rotor. The ultracentrifuge was operated at 24000 × g at 4 °C for 4 hr. Fractions were collected afterwards in 0.5 mL volumes. The density of each fraction was weighted and the virus-containing samples (ρ = 1.4–1.5) was collected and further processed. If unfiltered samples were used, the bacterial fraction could be collected in the fraction ρ > 1.5. Everything smaller than ρ < 1.4 represents dirt (cell debris, free DNA, etc.).

Clean-up

This step is only needed, if no further DNA extraction occurs and PCR or qPCR shall be directly applied. 2 volumes of PEG 30 % (PEG 8000, 1.6 MNaCl) were mixed with the sample and centrifuged at maximum speed at 4 °C for 30 min. The supernatant was removed and the pellet was washed with 150 µL ice-cold 70 % ethanol (kept at–20 °C). Again, samples were centrifuged at maximum speed for 5 min. The supernatant was removed and the pellet was eluted in 200 µL EB buffer and incubated in a thermomix for 1 min at 1400 rpm and 30 °C.

2.3.6 Concentrating viral particles

2.3.6.1 PEG precipitation

One volume of PEG 8000 solution was mixed with three volumes of 0.22 µm filtered virus containing sample and stored overnight at 4 °C. On the next day, samples were centrifuged at 4000 × g at 4 °C for 20 min. The supernatant was removed carefully and the virus pellet was suspended in phage buffer.

2.3.6.2 $FeCl_3$ precipitation

The precipitation was conducted according to [244] with minor modifications (2.2.9).

One µL of $FeCl_3$ per 1 mL of 0.22 µm filtered sample was added, vigorously mixed and incubated at room temperature for one hour. Virus:iron particles were collected depending on the initial

sample volume and the aimed reduction volume. Filters can be stored at –20 °C (should be kept moist) and processed at a later time.

For large sample volumes: Virus:iron particles were collected on a 0.22 µm filter using a peristaltic pump. Filters were placed in a 50 mL falcon tube and viral particles were eluted with 1 mL EDTA-ascorbate buffer per one mg $FeCl_3$ by rotating at 4 °C overnight. On the next day, the liquid was removed and the filters were centrifuged at low speed (less than 1000 × g for 3–5 min.) in order to recover more buffer.

For small sample volumes: Two mL sample were centrifuged repeatedly at maximum speed for 30 min in a microcentrifuge, until the complete sample volume is pelleted. Supernatant was discarded and the pellet was dissolved in 1 mL EDTA–ascorbate buffer per one mg $FeCl_3$ (this step was mostly done *prior to* DNA extraction, therefore the elution volume was 100–110 µL EDTA–ascorbate buffer).

2.3.6.3 Centrifugal ultrafiltration concentration

This is an easy method for concentrating greater sample volumes. Through centrifugal forces water is pushed through the membrane of the device, but small particles like viruses cannot pass this membrane. The sample with the reduced volume can then be collected.

Maximal 15 mL sample (which had been 0.22 µm pre-filtered) were added to the upper reservoir of the Amicon Ultra 15 Centrifugal Filter Units, 10 kDa Device. This setup has been centrifuged with maximal 4000 × g at 4 °C. Depending on the concentration of viral particles and other small particles the centrifugation needs about 10–15 min to reduce the sample volume to 1 mL. This volume was transferred to a fresh vial and the centrifugation steps were repeated until the sample was consumed.

2.3.7 Viral particle counting

2.3.7.1 Plaque assay

For estimating the concentration of active viral particles in a solution, a plaque assay can be carried out. A suitable bacterial host is mixed with different concentrations of viral particles and incubated over a distinct time. The formed plaques, cleared areas in the bacterial lawn, are a direct indicator for the viral titer.

One mL of a suitable bacterial host was inoculated in 50 mL LB medium until an OD600 of 0.3–0.5. 1× LB medium was used to prepare a serial dilution of the phages to an appropriate dilution. One mL of an equal mixture of bacteria and phage dilution was mixed with 3 mL liquid agar (tempered at 60 °C) and distributed on a bottom layer plate (2.2.5). The plates were incubated at 37 °C for 16–20 h. The number of formed plaques reflects directly the amount of viral particles

in the used dilution, allowing an extrapolation to the plaque forming units (PFU) mL^{-1}. To ensure a more reliable estimation, this measurement should be repeated at least two times.

2.3.7.2 Flow cytometry

Samples taken for the flow cytometric quantification (FCM) of viral particles were pre-filtered with a 0.22 µm syringe filter, fixed with 0.5 % glutardialdehyde and stored at –80 °C until further analysis. Later, the enumeration was carried out using the FC500 flow cytometer equipped with an air-cooled 488 nm Argon ion laser. Samples were prepared as described previously with only minor modifications [218]. In brief, samples were diluted appropriately with sterile, filtered PBS buffer (0.02 µm Anotop 25 syringe filter) to fulfill the instrument's optimal concentration requirements of approximately 10^6 virus-like particles per mL (VLP mL^{-1}). Fluorescent TRUCOUNT beads were added to each sample as an internal reference. The samples were stained with 1× SYBR gold nucleic acid dye and incubated either for 10 min at 80 °C or for 1 hr at 30 °C *prior to* measurement. All samples were measured with a FC500 flow cytometer equipped with an air-cooled 488 nm Argon ion laser in biological and technical replicates. Analysis and evaluation of the samples was performed using StemCXP Cytometer software (v2.2).

2.3.7.3 Epifluorescence microscopy

Staining of the samples was carried out as described by Patel and colleagues [247]. Briefly, all samples were diluted appropriately with 0.02 µm filtered 1× TE buffer to a concentration of approximately 10^7 particles mL^{-1}.

Then, 1 mL of each diluted sample (10 mL of environmental samples) was passed through a 0.02 µm Anodisc filter in duplicates. After complete desiccation, the filter was stained using a droplet of 2× SYBR gold dye with the virus side up, and incubated at room temperature for 15 min in the dark. Stained filters were mounted on a glass slide with 20 µL of antifade solution. Slides were analyzed using an Axiolab fluorescence microscope equipped with a 488 nm laser. A camera was used to take ten pictures per sample, which were analyzed using ImageJ (v1.50i). Numbers of particles on the whole filter were calculated by multiplying the counts with the quotient of the area of the filter by area of the pictures.

2.3.7.4 Nanosight particle counting

Viral isolate samples were diluted appropriately with sterile phage buffer to obtain the optimal concentration range of 10^7–10^9 VLP mL^{-1}. Afterwards, samples were either untreated or stained with 1× SYBR gold for 10 min at 80 °C or 1 hr at 30 °C. Each sample was prepared four times, injected manually into the machine's specimen chamber with a sterile 1 mL syringe, and measured three times for 20 sec at room temperature. Samples were measured using a

NanoSight NS300 equipped with a B488 nm laser module and a sCMOS camera, following the manufacturer's protocol. Analysis was performed with the NTA 3.1 analytical software (release version build 3.1.45).

2.3.7.5 TEM preparations

Samples were applied to carbon-coated copper grids and washed two times with double-distilled water. After each washing step they were blotted onto a filter paper before negative staining with 2 % uranyl acetate for 20 sec as described previously [248]. Transmission electron microscopy was carried out on a Zeiss EM 912 with an integrated OMEGA filter in zero-loss mode. The acceleration voltage was set to 80 kV and images were recorded using a Tröndle 2k × 2k slow-scan CCD camera.

2.3.8 DNase I treatment

The DNA digestion was conducted according to [246].

DNase I was resuspended in DNase I storage buffer to a concentration of 40000 U mL^{-1} (2.2.11). The DNase I was then diluted 1:40 in the 10× reaction buffer with a final concentration of 1000 U mL^{-1} (2.2.12). The diluted DNase I was then used in a 1:10 dilution (100 U mL^{-1}) and incubated for one hour at 37 °C. The reaction was inactivated by addition of 100 mM EDTA solution.

2.3.9 Nucleic acid extraction

2.3.9.1 DNA: Promega Wizard Kit

This DNA extraction method was adapted according to [249].

Briefly, the sample was mixed with an equal volume of Wizard PCR preps DNA purification resin. This mixture was applied on a Wizard PCR preps DNA purification column with the help of a sterile 3 mL or 5 mL syringe. The column was washed with 2 mL 80 % isopropanol, centrifuged at 10000 × g for 2 min and eluted twice with 50 µL and 25 µL 80 °C warm 1× TE by centrifuging at 10000 × g for 30 sec.

2.3.9.2 DNA: AMPure beads

This DNA extraction method was established by Mária Džunková, Australian Centre for Ecogenomics (personal communication).

110 µL sample were mixed with 77 µL lysis buffer and incubated for 10 min at room temperature, then for 1 hr at –80 °C, and finally for 5 min at 55 °C (2.2.13). 110 µL stop buffer was added followed by 1 µL proteinase K (20 mg mL^{-1}), with subsequent incubation for 30 min at 55 °C. 536 µL AMPure beads were mixed with the sample and incubate for 15 min at room temperature. Samples were put on a magnetic stand and the cleared supernatant was removed.

Two washing steps with 1 mL 80 % ethanol each were conducted. For the removal of residual ethanol, the open tubes were air-dried for 10 min at 37 °C. Elution occurred with 32 µL 10 mM Tris and a short incubation of 2 min at room temperature.

2.3.9.3 RNA: QIAamp Viral RNA Mini Kit

RNA has been extracted using the QIAamp Viral RNA Mini Kit from Qiagen according to the manufacturer's protocol.

2.3.10 DNA quantity and quality assessment

2.3.10.1 Polymerase chain reaction (PCR)

The polymerase chain reaction (PCR) allows fast amplification of even very little amounts of DNA in a sample. All reactions were prepared in a UV box with UV-sterilized consumables and were run in a Mastercycler Gradient Thermal Cycler.

Amplification of g20

The used primer-pair CPS1.1_fdw (5'-GTA-GWA-TWT-TYT-AYA-TTG-AYG-TWG-G-3') and CPS8.1_rev (5'-ART-AYT-TDC-CDA-YRW-AWG-GWT-C-3') encodes the portal-vertex-capsid protein gene g20 of cyanomyovirus (T7-like phages) [232]. The product ranges around 600 bp.
Reaction Mix: 12.5 µL GoTaq Green Master Mix, 9.5 µL H_2O, 1.0 µL primer fwd (10 µm), 1.0 µL primer rev (10 µm), 1 µL DNA (25 µL in total).
Cycling conditions: Initial denaturation at 94 °C, 3 min was followed by a total of 30 cycles of denaturation (94 °C, 15 sec), annealing (38 °C + 0.3 °C per cycle, 1 min) and extension (73 °C, 1 min) and a final elongation step at 73 °C for 10 min.

Amplification of g23

The used primer-pair MZIA1bis_fwd (5'- GAT-ATT-TGI-GGI-GTT-CAG-CCI-ATG-A-3') and MZIA6 1_rev (5'-CGC-GGT-TGA-TTT-CCA-GCA-TGA-TTT-C-3') encodes the major capsid protein gene g23 of *Myoviridae* (T4-like phages) [233]. The product ranges between 450 bp to 650 bp.
Reaction Mix: 12.5 µL GoTaq Green Master Mix, 9.5 µL H_2O, 1.0 µL primer fwd (10 µm), 1.0 µL primer rev (10 µm), 1 µL DNA (25 µL in total).
Cycling conditions: Initial denaturation at 94 °C, 3.5 min was followed by a total of 30 cycles of denaturation (94 °C, 15 sec), annealing (38 °C + 0.3 °C per cycle, 1 min) and extension (72 °C, 45 sec) and a final elongation step at 72 °C for 5 min.

Amplification of DNApol

The DNApol primers amplify the polymerase (T7-like) homologue [235]. The forward primer is an equimolar mixture of the primer DNApol-90Fa (5'-GAY-ACI-YTI-RYI-YTI-TCI-MG-3') and DNApol-90Fb (5'-GAY-ACI-YTI-RYI-YTI-AGY-MG-3'). The reverse primer is constituted of DNApol-355Ra (5'-GGI-AYY-TGI-GCI-ARR-TTI-GG-3') and DNApol-355Rb (5'-GGI-AYR-TTI-GCI-ARR-TTI-GG-3').

Reaction Mix: 12.5 µL GoTaq Green Master Mix, 10.5 µL H_2O, 0.5 µL primer 90Fa + b (10 µm), 0.5 µL primer 366Ra + b (10 µm), 1 µL DNA (25 µL in total).

Cycling conditions: Initial denaturation at 94 °C, 4 min was followed by a total of 35 cycles of denaturation (94 °C, 1 min), annealing (35 °C, 1 min) and extension (72 °C, 1 min) and a final elongation step at 72 °C for 10 min.

Amplification of 16S rDNA

For determining eventual bacterial intrusion or bacterial DNA contamination during nucleic acid extraction, the primers targeting the highly conserved area of the 16S rDNA genes can be used. There are several forward and reverse primers, allowing the replication of the complete 16S rDNA gene or only parts of it. Here, the primer pair Ba27_fwd (5'-AGA-GTT-TGA-TCM-TGG-CTC-AG-3') and Ba907_rev (5'-CCG-TCA-ATT-CMT-TTR-AGT-TT-3') were used for amplifying an approximately 800 bp fragment [236].

Reaction Mix: 25 µL GoTaq Green Master Mix, 23 µL H_2O, 0.5 µL primer fwd (50 µm), 0.5 µL primer rev (50 µm), 1 µL DNA (50 µL in total).

Cycling conditions: Initial denaturation at 94 °C, 5 min was followed by a total of 29 cycles of denaturation (94 °C, 30 sec), annealing (52 °C, 30 sec) and extension (70 °C, 1 min) and a final elongation step at 70 °C for 5 min.

After 17, 20, 24, 26 and 29 cycles the program was stopped and one sample was taken out and stored until the last sample finished at 4 °C.

Amplification for *P. aeruginosa* phage isolates: first run

Primer were designed using the NCBI primer-BLAST online tool [250], based on the sequencing information of an equal mixture of 24 *P. aeruginosa* phage isolates and target the gep5 protein, which showed a similarity of 18 % to gp20. The following primers were used:

gep5_fwd (5'-GTG-ATC-ACA-CCC-GAA-CTG-3') and gep5_rev (5'-ATG-TTG-GAG-CGC-ATC-G-3'). Additionally, a modified reverse primer with a substitution on position 16 from G to AC was used: gep5_rev_16G>AC (5'-ATG-TTG-GAG-CGC-ATC-AC-3'). Both pairs results in a fragment

length of 407 bp. Two different primer concentrations (0.1 µm and 0.2 µm), as well as three different annealing temperatures (48 °C, 50 °C and 52 °C) were tested for optimal PCR conditions.

Reaction Mix: 25 µL GoTaq Green Master Mix, 22 µL H_2O, 1 µL primer fwd (10 µm), 1 µL primer rev (10 µm), 1 µL DNA (50 µL in total).

Cycling conditions: Initial denaturation at 94 °C, 3 min was followed by a total of 30 cycles of denaturation (94 °C, 15 sec), annealing (50 °C, 45 sec) and extension (73 °C, 1 min) and a final elongation step at 73 °C for 10 min.

Amplification for *P. aeruginosa* phage isolates: second run

Primer were designed using the NCBI primer-BLAST online tool [250], based on the sequencing information of an equal mixture of 24 *P. aeruginosa* phage isolates. In the second run, a longer fragment was synthesized in order to identify single differences in the phage genomes. As consequence, the PCR was conducted using Phusion High-Fidelity DNA Polymerase (2 U μL^{-1}) which had a higher accuracy. The primer pair Paer_phag_1kb fwd (5'-GCG-TAC-ATC-GCG-AAC-TCT-GG-3') and Paer_phag_1kb rev (5'-CCC-AAA-GAT-TCA-TGA-TGT-TGC-TGG-3') result in a fragment length of 916 bp.

Reaction Mix: 4 µL GC buffer, 11.8 µL H_2O, 0.4 µL dNTPs, 1.0 µL primer fwd (10 µm), 1.0 µL primer rev (10 µm), 0.6 µL DMSO, 0.2 µL Phusion High Fidelity Polymerase, 1 µL DNA (25 µL in total).

Cycling conditions: Initial denaturation at 98 °C, 30 sec was followed by a total of 30 cycles of denaturation (98 °C, 10 sec), annealing (66.2 °C, 30 sec) and extension (72 °C, 30 sec) and a final elongation step at 72 °C for 5 min and hold at 4 °C.

2.3.10.2 DNA clean-up for sequencing

In order to purify the amplified PCR products, the NucleoSpin Gel and PCR Clean Up kit was used according to the manufacturer's protocol. PCR mixes were filled up with 50 µL water (total volume of 100 µL) and 200 µL NTI buffer was added. Washing was performed twice with 700 µL NT3 buffer and finally eluted in 16 µL EB buffer. As a preparation for sequencing, 2 µL gep5_fwd primer (10 µm) was added to each sample and then sent to Eurofins genomics for TubeSeq DNA sequencing.

2.3.10.3 Gel electrophoresis

For separating the different nucleic acid fragments resulting from the different PCRs by length, the samples were (when using the Go Taq Green Master Mix, as it contains already a loading dye) directly loaded on a 2 % agarose gel in 1× TAE buffer, or previously mixed with 1×

Blue/Orange loading dye. In order to assign the nucleic acid fragments to a distinct length, the GeneRuler 1 kb DNA ladder, respectively 100 bp DNA ladder was applied. After applying an electric field (100 V, 200 mA and 150 W for 35 min) the negatively charged DNA molecules moved according to their size through the gel matrix. The forming bands have been visualized with the Gel Red Nucleic Acid Dye in a 3× dilution and an incubation time of 10 min. The visualization was carried out with the Gel Jet Imager.

2.3.10.4 Restricted enzyme digestion

In order to see differences in the genomic composition of the viruses isolated on *P. aeruginosa*, a digestion with different restriction enzymes was conducted. The enzymes AluI, HhaI, NdeI, and EcoRI were chosen. The reaction mixture contained 2 µL enzyme-specific buffer, 1 µL of the respective enzyme, x µL of DNA for 500 ng and y µL of nuclease-free water for a total volume of 20 µL. The incubation and inactivation protocol for each enzyme is shown on **Table 2-7**. The products of the digestions were analyzed on a 1 % agarose gel electrophoresis according to (2.3.10.3) using the GeneRuler 1 kb DNA ladder.

Table 2-7: Incubation and inactivation conditions for different restriction enzymes.

Restriction enzyme	Incubation	Inactivation
AluI	37 °C for 1 hr	65 °C for 20 min
HhaI		20 µL 0.5 MEDTA
NdeI		65 °C for 20 min
EcoRI		65 °C for 20 min

2.3.10.5 Nanodrop

The Nanodrop instrument uses spectrophotometry for a quick measurement of nucleic acid or protein concentrations. The measurement with the ND 1000 was carried out following the manufacturer's manual using 1 µL of sample. For assessing the quality of the samples, two different absorbance ratios can be taken into account. The ratio of the sample absorbance at 260 and 280 nm is used to assess the purity of DNA or RNA. A ratio of ~1.8 is generally accepted as pure for DNA, a ratio of ~2.0 indicates pure RNA. The ratio between the absorbance at 260 and 230 nm should lay around 1.8–2.2. In the presence of proteins, phenol or other contaminants the ratios may be lowered.

2.3.10.6 Quant-iT Pico Green dsDNA

A 96-well plate was prepared as followed. An appropriate amount of sample was filled up with 1× TE buffer to a total volume of 10 µL. Likewise, several dilutions of the λ phage DNA standard ranging from 0 to 25 ng μL^{-1} in 1× TE buffer were prepared. For minimizing pipetting errors, a second dilution series of the standard DNA with the same concentrations was prepared and applied to the plate. 90 µL of a 1:200 dilution of the Pico Green fluorescent dye was added shortly before the measurement occurred. For quantification, the Mx3000P qPCR system (FAM/SYBR® Green I filter (492nm–516nm) system was used.

2.3.10.7 DNA 7500 and High Sensitivity Chip for Bioanalyzer

The Bioanalyzer is an automated lab on a chip system to perform capillary electrophoresis and uses a fluorescent dye that binds to the DNA to determine both DNA concentration and integrity. The DNA 7500 chip allows minimal DNA concentrations (0.5–50 ng μL^{-1}) but a broad sizing range of the fragments (100–7500 bp). For lower concentrations the High Sensitivity DNA Chip was used allowing yet a concentration of 5–500 pg μL^{-1} with similar fragment range (50–7000 bp). The chips were prepared following the High Sensitivity DNA Quick Start Guide and DNA 7500 Quick Start Guide, respectively.

2.3.10.8 Quantitative Real-Time PCR

A qPCR was conducted to quantify the exact amount of a certain gene fragment or genome, respectively, or to detect the presence or absence of a genetic element. All reactions were prepared in a UV box with UV-sterilized consumables. The reactions were conducted using the Mx3000P qPCR system (FAM/SYBR® green I filter (492nm–516nm), OS v7.10). In order to being able to quantify, a standard dilution series was prepared ranging from approximately 10^1 to 10^8 copies μL^{-1}. Standard sequences were ordered from IDT Genomics and covered the complete primer-flanked sequence plus an additional 10 nucleotides at each side.

Quantification of phage T4:

Phage T4 was quantified through the detection of a 163 bp fragment of the gp18 tail protein [238], which is flanked by the T4-specific primer sequences T4 fwd (5'-AAG-CGA-AAG-AAG-TCG-GTG-AA-3') and T4 rev 5('-CGC-TGT-CAT-AGC-AGC-TTC-AG-3').

Reaction Mix: 10 µL Brilliant III Ultra-Fast SYBR green qPCR Master Mix, 6.7 µL H_2O, 1.0 µL primer fwd (10 µm), 1.0 µL primer rev (10 µm), 0.3 µL ROX Reference dye (1:500), 1 µL DNA.

Cycling conditions: Initial denaturation at 95 °C, 10 min was followed by a total of 40 cycles of denaturation (95 °C, 15 sec), annealing (60 °C, 1 min) and extension (72 °C, 1 min). Afterwards,

a dissociation curve was performed using a ramping function with one cycle at 95 °C for 1 min, 60 °C for 30 sec and 95 °C for 30 sec and collecting all points in time.

Quantification of phage T7:

Phage T7 was quantified through the detection of a 555 bp fragment of gene 1 [239], which is flanked by the T7-specific primer sequences T7_4453 fwd (5'-CTG-TGT-CAA-TGT-TCA-ACC-CG-3') and T7_5008 rev (5'-GTG-CCC-AGC-TTG-ACT-TTC-TC-3').

Reaction Mix: 10 µL Brilliant III Ultra-Fast SYBR green qPCR Master Mix, 7.9 µL H_2O, 0.4 µL primer fwd (10 µm), 0.4 µL primer rev (10 µm), 0.3 µL ROX Reference dye (1:500), 1 µL DNA.

Cycling conditions: Initial denaturation at 95 °C, 12 min was followed by a total of 40 cycles of denaturation (95 °C, 30 sec), annealing (58 °C, 30 sec) and extension (72 °C, 1 min). Afterwards, a dissociation curve was performed using a ramping function with one cycle at 95 °C for 1 min, 55 °C for 30 sec and 95 °C for 30 sec and collecting all points in time.

Quantification of phage MS2:

Phage MS2 was quantified through the detection of a 314 bp fragment [240], which is flanked by the MS2-specific primer sequences MS2_2717 fwd (5'-CTG-GGC-AAT-AGT-CAA-A-3') and MS2_ 3031 rev (5'-CGT-GGA-TCT-GAC-ATA-C-3').

Reaction Mix: 10 µL Brilliant III Ultra-Fast SYBR green qPCR Master Mix, 7.5 µL H_2O, 0.6 µL primer fwd (10 µm), 0.6 µL primer rev (10 µm), 0.3 µL ROX Reference dye (1:500), 1 µL cDNA.

Cycling conditions: Initial denaturation at 95 °C, 10 min was followed by a total of 40 cycles of denaturation (95 °C, 15 sec), annealing (50 °C, 30 sec) and extension (72 °C, 30 sec). Afterwards, a dissociation curve was performed using a ramping function with one cycle at 95 °C for 1 min, 50 °C for 30 sec and 95 °C for 30 sec and collecting all points in time.

Quantification of phage ΦX174

Phage ΦX174 was quantified through the detection of a 123 bp fragment [241], which is flanked by the ΦX174-specific primer sequences ΦX fwd (5'- ACA-AAG-TTT-GGA-TTG-CTA-CTG-ACC-3') and ΦX rev (5'-CGG-CAG-CAA-TAA-ACT-CAA-CAG-G-3')

Reaction Mix: 10 µL Brilliant III Ultra-Fast SYBR green qPCR Master Mix, 6.2 µL H_2O, 1.25 µL primer fwd (10 µm), 1.25 µL primer rev (10 µm), 0.3 µL ROX Reference dye (1:500), 1 µL DNA.

Cycling conditions: Initial denaturation at 94 °C, 3 min was followed by a total of 40 cycles of denaturation (94 °C, 15 sec) and annealing (50 °C, 1 min). Afterwards, a dissociation curve was performed using a ramping function with one cycle at 94 °C for 1 min, 60 °C for 30 sec and 94 °C for 30 sec and collecting all points in time.

Quantification of human GAPDH:

In order to detect human DNA contamination in a sample, primer that recognize a fragment in the human GAPDH gene on chromosome 12 were designed using the NCBI primer-BLAST online tool [250]. The product is located in an intron sequence, flanked by the primer sequences GAPDH_1 fwd (5'-GACTGAGGCTCCCACCTTTC-3') and GAPDH_1 rev: 5'-CTCCCCACATCACCCCTCTA-3' and has a length of 144 bp.

Reaction Mix: 10 µL Brilliant III Ultra-Fast SYBR green qPCR Master Mix, 6.7 µL H_2O, 1.0 µL primer fwd (10 µm), 1.0 µL primer rev (10 µm), 0.3 µL ROX Reference dye (1:500), 1 µL DNA.

Cycling conditions: Initial denaturation at 95 °C, 10 min was followed by a total of 40 cycles of denaturation (95 °C, 45 sec), annealing (56 °C, 30 sec) and extension (73 °C, 45 sec). Afterwards, a dissociation curve was performed using a ramping function with one cycle at 95 °C for 1 min, 50 °C for 30 sec and 95 °C for 30 sec and collecting all points in time.

Quantification of bacterial 16S rDNA:

In order to detect bacterial DNA contamination in a sample, primer targeting the 16S rDNA were used: Ba519 fwd (5'-GWATTACCGCGGCKGCTG-3') and Ba907 rev (5'-CCGTCAATTCMTTTRAGTTT-3') [236,237].

Reaction Mix: 10 µL Brilliant III Ultra-Fast SYBR green qPCR Master Mix, 6.7 µL H_2O, 1.0 µL primer fwd (10 µm), 1.0 µL primer rev (10 µm), 0.3 µL ROX Reference dye (1:500), 1 µL DNA.

Cycling conditions: Initial denaturation at 95 °C, 5 min was followed by a total of 40 cycles of denaturation (95 °C, 30 sec), annealing (52 °C, 30 sec) and extension (68 °C, 30 sec), followed by a final extension step (68 °C, 5 min). Afterwards, a dissociation curve was performed using a ramping function with one cycle at 95 °C for 1 min, 55 °C for 30 sec and 95 °C for 1 min and collecting all points in time.

2.3.11 Linker amplification for 454 pyrosequencing

The preparation for 454 pyrosequencing was performed according to Duhaime and colleagues, who optimized the procedure in order to amplify very low amounts of DNA [242].

2.3.11.1 cDNA synthesis

The cDNA synthesis was performed using the DyNAmo cDNA synthesis kit F470L according to the manufacturer's protocol. Briefly, the following reaction mix was prepared and incubated:

Reaction Mix: 10 µL buffer, 3 µL RNase-free H_2O, 1.0 µL random hexamers, 4.0 µL RNA template, 2 µL M-MuLV RNase H^+ reverse transcriptase.

Incubation conditions: Primer extension at 25 °C, 10 min, followed by the cDNA synthesis at 37 °C, 30 min and finalized at 85 °C, 5 min with a final hold at 4 °C.

2.3.11.2 DNA concentrating and shearing

For reduction of the DNA sample volume, the Nanosep Omega-Membrane 10kDa centrifugation device was used. The devices were previously washed with 0.5 mL 1× TE and spun at 14000 × g for 10 min. Samples were applied and centrifuged at 5000 × g for few minutes until reaching the desired volume of 50 µL. The concentrated DNA was applied into a microTUBE and sheared into 500 bp fragments using the E220 Focused-Ultrasonicator with following settings: peak incident power of 175 W, duty factor of 5 %, 200 cycles per bust, treatment time of 35 sec, water temperature of 7 °C and water level of 6.

2.3.11.3 End repair

The sheared DNA was concentrated again to a volume of 35 µL using the Nanosep Omega-Membrane 10kDa centrifugation device and the DNA ends were repaired using End-It DNA End-Repair Kit. For this, the DNA was mixed with 7.5 µL 10× End Repair Buffer, 7.5 µL 10 mM ATP, 7.5 µL 2.5 mM dNTP mix, 3 µL End-repair enzyme mix and 14.5 µL nuclease-free water (total volume of 75 µL). A Mastercycler Gradient Thermal Cycler was used at the following conditions: 2 min at 4 °C, 45 min at 25 °C and hold at 4 °C.

2.3.11.4 Reaction clean up

Next, the samples were purified using the MinElute Reaction Clean Up according to the manufacturer's manual. The samples were eluted in 33 µL 55°C warmed EB buffer.

2.3.11.5 Adaptor annealing

100 nM of the forward and reverse linker A were purchased according to 2.1.4. Each linker was resuspended 1x TE supplemented with 50 mM NaCl to a concentration of 1.14 mM. Both linkers were then mixed equimolar and annealed using a Mastercycler Gradient Thermal Cycler under the following conditions: 93 °C for 2 min, then ramped down to 4 °C at 0.1 °C per sec. This Adaptor A stock was then diluted to 10 µM and stored at –20 °C.

For ligating the Adaptor A to the prepared DNA, the Fast-Link Ligation Kit was used. 30 µL End-repaired sheared DNA was mixed with 7.5 µL 10 µm Adapter A, 5 µL 10x Fast-Link Ligation buffer, 2.5 µL 10 mM ATP and 5 µL Fast-Link DNA Ligase (2 U μL^{-1}). A Mastercycler Gradient Thermal Cycler was used to run the following program: 2 min at 4 °C, 2 hr at 23.5 °C and hold at 4 °C.

After the end of the program the samples were immediately purified using the MinElute Reaction Clean Up kit as described in 2.3.11.4, but eluting twice with 16 µL 1x TE (pH 7.5, 55 °C).

2.3.11.6 Size fractionation

Only DNA fragment sizes between 520–650 bp were further processed. They were selected using the automated optical electrophoresis system Pippin Prep. The instrument and the 2 % Marker B Agarose Gel Cassette were prepared according to the manufacturer's manual.

2.3.11.7 Small-scale PCR titration

This titration PCR was undertaken to determine the optimal cycle number, at which the highest molecular weight DNA products were formed with the lowest amount primer heteroduplexes. In addition, the applied primers added an unique barcode label to each DNA sample. Primers are listed in 2.1.4.

Reaction Mix: 25 µL PfuUltra II Hotstart PCR Master Mix, 2 µL 10 µm barcode primer, 22 µL nuclease-free water and 2 µL DNA. For each sample, primers with a different barcode were used.

Cycling conditions: Initial denaturation at 95 °C, 2 min, a total of 17, 20, 23, 26 or 28 cycles of denaturation (95 °C, 30 sec), annealing (60 °C, 1 min) and extension (72 °C, 1.5 min) followed by a final extension step (72 °C, 10 min).

2.3.11.8 Large-scale PCR

The PCR was repeated with the previously identified optimal cycling conditions five times for each sample.

2.3.11.9 PCR clean up

PCR products generated with the previous PCR were purified using the MinElute PCR Purification Kit according to the manufacturer's protocol. The samples were eluted twice with 21 µL 55 °C warmed EB buffer.

2.3.11.10 Final analysis

The amplified DNA was quantified using Quant-iT PicoGreen dsDNA Assay Kit. The quality was assessed running the samples on a 1.2 % agarose gel in 1x TAE as well as on a DNA 1000 Bioanalyzer chip.

2.3.11.11 Sequencing

The preparation of the samples for 454 pyrosequencing with the GS FLX+ Instrument followed the provided manuals. Here, the GS FLX Titanium SV emPCR Kit (Lib-L), emPCR Breaking Filters SV, Sequencing Kit XLR70 and the PicoTiterPlate Kit were used. Only three BAL samples could be amplified successfully. Only one of four lanes of the sequencing plate was used for the BAL samples with all samples barcoded and pooled equally. Libraries of the two COPD samples were pooled together and took 2/3 of the lane and the healthy control library took 1/3 of the same lane.

2.3.12 Bioinformatic analysis of the BAL samples

2.3.12.1 Sequence quality control

TagCleaner v0.12 [251] was used to predict and trim tag and/or adapter sequences. In the case of paired- end Illumina sequences, AdapterRemoval v2.1.7 [252] was used, instead. PRINSEQ-lite v0.20.4 [253] was used for quality filtering with following parameters: "-trim_qual_left 15 -trim_qual_right 15 -trim_qual_type mean -trim_qual_window 2 -lc_threshold 50 -lc_method entropy -derep 12345 -noniupac -ns_max_n 2 - min_qual_mean 20 -min_len 50 -max_len 800." Reads with an average Phred score of less than 20 were filtered out. Viromes were decontaminated from human-related sequences using DeconSeq v0.4.3 [254] and human reference genome GRCh38 with default parameters. Deconseq was also used to remove reported spiked viral sequences e.g., ΦX174.

2.3.12.2 Sequence assembly, ORF calling and clustering

Sequences were assembled using Newbler v2.9 (Roche) with default parameters. For Illumina sequences, MEGAHIT v1.0.3 [255] with meta-sensitive preset mode and minimum contig length of 180 was ued. Open reading frames (ORFs) were predicted from both contigs and reads using Prodigal v2.6.3 [256] in its metagenomics mode. Predicted proteins were then filtered to keep only non-redundant sequences of at least 60 amino acids length. ORFs from publicly available sequences were then clustered using CD-HIT v4.6 [257] with 60 % identity, 80 % coverage and the following parameters: "-g 1 -n 4 -d 0".

2.3.12.3 Functional annotation and cross-comparison of BAL samples

A BLAST database was created from the representative ORFs of all clusters, resulting in the HVPC database. BAL ORFs were functionally annotated through alignment to the HVPC blast database using BLASTp [258] with a threshold *e*-value of 1×10^{-3} and a bit-score of at least 50. For comparison, BAL ORFs were also aligned to protein coding sequences from all RefSeq and non-RefSeq complete viral genomes downloaded from NCBI (https://www.ncbi.nlm.nih.gov/ on May 10, 2017) as described by Grazziotin *et al.* [259].

The three BAL viromes were also compared in a reference- independent manner using crAss [260]. All high quality reads from the three samples were cross assembled using Newbler v2.9 (Roche) and used as an input for crAss.

2.3.12.4 Taxonomic assignment of BAL samples

A protein blast database was created from protein coding sequences of all RefSeq and non-RefSeq complete viral genomes downloaded from NCBI (https://www.ncbi.nlm.nih.gov/ on May

10, 2017) as described by Grazziotin *et al.* [259]. Only DNA viruses were selected by asserting that the "molecule type" feature in the genbank record of each genome is equal to DNA. Protein coding sequences from BAL samples were aligned to the created blast database using a threshold *e*-value of not more than 1×10^{-3} and a bit-score of at least 50. Taxonomy ids of best hits were mapped to NCBI taxonomy (downloaded from ftp://ftp.ncbi.nih.gov/pub/taxonomy on June 11, 2017) to obtain the full lineage.

Irrespective of annotation, alignment of BAL samples to the HVPC blast database was used as a measure of functional diversity in a sample. HVPC hit counts were prepared, then diversity indices and rarefaction plots were generated in R v3.4.0 [261] using vegan package v.2.4-4 [262]. Taxonomy rarefaction analysis was similarly performed.

2.3.12.5 Virome-borne virulence factors

A protein BLAST database was created from sequences downloaded from the core Virulence Factor Database (VFDB; http://www.mgc.ac.cn/VFs/download.htm) created by the MOH Key Laboratory of Systems Biology of Pathogens, Institute of Pathogen Biology, the Chinese Academy of Medical Sciences & Peking Union Medical College. This database includes sequences from experimentally verified virulence factors from 74 different genera of bacterial pathogens. All high quality reads from BAL samples were compared to this database using BLASTx (*e*-value ≤ 0.001, % identity ≥ 75 %, alignment length ≥ 25 amino acids) to look for potential virulence factors harbored by each BAL virome. Random subsampling (sample size: 2000 reads) was performed 10000 times; each time looking for and counting VFDB hits for each virome. One-way analysis of variance (ANOVA) was performed followed by Dunnett's *post hoc* test to assess statistical significant difference between the means of virulence factor abundance among all BAL sample pairs.

2.3.13 HSL quantification

Samples were 0.22µm filtered and kept at –20 °C until further analysis. 3-oxo-C10 HSL and HS concentrations were measured using an ELISA assay as described in [263]. The 3-oxo-C10-HSL standard was purchased from Cayman Chemical (AnnArbor, USA). The rat monoclonal antibody HSL1-1A5 was produced in-house (E. Kremmer, Institute of Molecular Immunology, Helmholtz Zentrum München, Neuherberg, Germany), as well as the coating antigen HSL2-BSA-r2 as reported elsewhere [264]. As secondary antibody, a goat-anti-rat antibody conjugated to horseradish peroxidase (GaR-HRP) obtained from Dianova (Hamburg, Germany) was used.

2.3.14 Modelling phage - bacteria interactions

Modelling of the interactions between phages, *P. putida* and their phages was performed using simbTUM (V0.34, Technische Universität München). The applied optimization method was the log-likelihood method. The numerical scheme was a controlled random search. The fitting of the individual models was split into several subproblems in order to achieve an optimal conformance. Initially selected parameter values ranged within biologically plausible ranges and literature values. Corresponding parameters for the *ppu* system of *P. putida* were situated according to previous publications [263,265,266] (**Table 2-8**). During the fitting process, virus burst sizes were kept in a typical range between 4 and 1000, as the exact orders of magnitude largely depend on the bacterial species [267,268].

The modelling process followed two strategies. The first was targeted to describe the dynamics between *P. putida* and its phages (P) (population dynamics). The second aimed to describe the QS system. Generally, bacterial growth was limited by the availability of organic carbon, described as $N(t)$. Dying cells were partially recycled and re-used as nutrients (R_{recy}). The phages in the system were assumed to act only as lytic phages, thus inducing host lysis after a successful replication. The population dynamic was described through a system of ordinary differential equations (ODEs), which divides the bacterial population into subpopulations defined by the way they respond to phages, as not all bacteria may be affected equally. Those subpopulations were resistant (B_R), non-resistant (B_N) and infected (B_I) bacteria. B_R and B_N were initially present, whereas B_I appeared at a later time.

The QS system used time-scale arguments [as e.g., in 234,240,241], assuming an equilibrium state for PpuI and HSL, as well as for internal and external HSL concentrations. HSL was bound to PpuR and formed a complex at the rate α_c, with subsequent breaking down at rate γ_c. Through the nature of the HSL dependent communication, two HSL production rates were considered: the background production rate α, and the positive feedback loop which is induced by the dimerized PpuR:HSL complex, expressed by a Hill function at the rate β. A time-dependent variable was introduced to better describe the PpuR:HSL complex. The lactonase activity was also found to be HSL-dependent, however, a natural decay of the lactonase occurred at a rate γ_L.

Table 2-8: Notations of model variables, their dimensions and initial values as determined by fitting to the experimental data.

Parameter	Meaning and units	Initial value
$N(t)$	Nutrient concentration at time t	1.00
$B_N(t)$	Density of non-resistant bacteria at time t (cells L^{-1})	2.90×10^{10}
$B_R(t)$	Density of resistant bacteria at time t (cells L^{-1})	1.50×10^{9}
$B_I(t)$	Density of infected bacteria at time t (cells L^{-1})	0
$P(t)$	Density of phages virus at time t (cells L^{-1})	0
$A(t)$	HSL concentration at time t (nmol L^{-1})	57.00
$R_A(t)$	PpuR-HSL concentration in one cell at time t (mol L^{-1})	4.90×10^{-8}
$L(t)$	Lactonase concentration at time t	0.41

Hypothesis 1. Here, no influence of the presence of phages on the QS system is assumed. For testing this hypothesis, a basic model was constructed under the presumption that phages target only non-resistant bacteria with an infection rate γ_t. According to the behavioural dynamics of the bacterial populations, resistant bacteria have to be already present in the system. HSL is produced by both bacteria types (resistant and non-resistant), independent of their susceptibility. Bacterial cell death occurred either naturally (rate d), or upon successful phage infection (rate δ). The equations describing this basic model can be found in **Equation 6-1** (supplementary material).

Hypothesis 2. Additionally to the basic model before, it was assumed that phages influence the QS system by augmenting the HSL production. This was implemented by the HSL-associated parameters α and β, which changed once phages were present (**Table 2-9**).

Hypothesis 3. The basic model was again adjusted to simulate an influence of the phages on the HSL receptor PpuR production. This was obtained by varying the parameter R_C before and after the addition of phages.

Hypothesis 4. This hypothesis concerns the idea, that in addition to other QS-induced behaviors, the bacteria become more resistant against phage attacks compared to QS inactive bacteria. A similar model approach was considered in [271,272], assuming that the biofilm production is influenced by the current QS state. In this context, two types of non-infected bacteria were introduced: B_{R1} acquired resistance to some extent through QS activation, whereas B_{R2} was resistant *ab initio*, independent of the QS state (**Table 6-6** and **Equation 6-2**, supplementary material).

For all models, the control group D where no phages were added was used to obtain a satisfactory fitting and to determine most of the parameter values present in the models. Parameters concerning the phages were adapted using group A data. Concerning the QS system, the choice of parameter values was based on the findings and fitted parameter values in [263]. The remaining parameters were calibrated using the specific assumptions of each hypothesis (**Table 6-5** and **Table 6-6,** supplementary material).

Table 2-9: Initial values of α and β before the addition of phages after 6 hr of incubation (group A) for hypothesis 2. These values were then modified by fitting the experimental data of group A, the modification factor between the time ranges before and after adding phages is displayed in the last column.

Parameters	Values before phage addition	Modification factor after phage addition
α	8.00×10^{-19}	1.60×10^{-4}
β	1.50×10^{-17}	1.10

3 RESULTS AND DISCUSSION

3.1 Virus quantification techniques in the spotlight

This chapter has been submitted to the journal *Frontiers in Microbiology* and is currently under review:

Feichtmayer, J., Pickl, C., Griebler, C., Klingl, A. & Deng, L. Virus enumeration under the microscope: a rigorous assessment and comparison of enumeration methods for environmental viruses. *Frontiers in Microbiology* (20xx).

3.1.1 Description of the experiment

In this study five viral quantification techniques were cross-compared in terms of accuracy: (i) plaque assay (PA), (ii) quantitative PCR (qPCR), (iii) epifluorescence microscopy (EPI), (iv) flow cytometry (FCM), and (v) nanoparticle-tracking analysis (NTA). For this purpose, four clonal *Escherichia coli* phage isolations with different structural properties were quantified using each method. These phages were: (i) T4, which is a long-tailed (200 nm length), dsDNA virus with a capsid diameter of 57 nm, (ii) T7, also a dsDNA phage characterized by a smaller genome, a shorter tail (length of 28.5 nm) and a capsid diameter of 55 nm, (iii) ΦX174, a 27 nm small ssDNA virus with an icosahedral capsid structure, lacking a tail and the ssRNA virus and (iv) MS2, also without a tail and a diameter size of 27 nm [273,274]. Different staining procedures were followed where applicable. Staining at 80 °C for 10 min is the standard procedure for FCM sample preparations [218]. However, this is a rather harsh treatment, so another staining procedure conducted under gentler conditions at 30 °C, but with a prolonged incubation time was included. By comparing all measurements against the qPCR results, which are assumed to be the most accurate, the optimal preparation procedure and method for an exact and reliable quantification of viral particles was identified. This knowledge was then transferred and verified on four aquatic samples. One sample each was freshly collected from a wastewater treatment plant from the income water tank (Gut Großlappen, Munich, Germany), an on-site groundwater collection well (48°13'25.8"N 11°35'45.4"E, Munich, Germany), a lake (Feldmochinger See; 48°12'56.0"N 11°30'49.4"E, Munich, Germany) and a river (Isar; 48°32'59.3"N, 12°10'42.4"E, Landshut, Germany). These samples contained mixed viral communities of unknown compositions; consequently, specific techniques such as PA or qPCR could not be applied. The natural abundance of viral particles was then quantified with special attention turned to the most accurate method identified previously. Samples for measurements were prepared freshly

on the day of measurement according to the following sections in material and methods (PA: 2.3.7.1, FCM: 2.3.7.2, EPI: 2.3.7.3, NTA: 2.3.7.4). In addition, two different staining techniques for FCM and NTA were applied. One followed a standard procedure at 80 °C for 10 min and the other applied a gentler incubation at 30 °C for 1 hr. For qPCR, DNA or RNA was first isolated (DNA extraction: 2.3.9.1, RNA extraction 2.3.9.3), and in the case of RNA, a subsequent cDNA synthesis was performed (2.3.11.1). For qPCR the respective primer for each phage was applied (2.3.10.8). Measurements were performed in technical and biological duplicates. Additionally, a mixed water sample (lake and wastewater) with an approximate concentration of 108 virus-like particles per mL (VLP mL^{-1}) was prepared. This sample was spiked with 1.00×10^8, 5.00×10^8 and 1.00×10^9 T4 particles mL^{-1}. Before the addition, T4 has been quantified with qPCR according to the description in section 2.3.10.8. Statistical analysis was carried out in R v3.4.3 [261] and RStudio v1.1.383, using the packages ggplot2 v3.0.0 [275], gridExtra v2.3 [276] and car v3.0-0 [277]. Data were log transformed and analysis of variance (ANOVA) was conducted. Normal distribution of data was confirmed by density plots and quantile-quantile plots; homogeneity of variances was confirmed with Levene's test. Afterwards, multiple pairwise comparisons were calculated with a *post-hoc* Tukey honest significant differences test. In addition, similarities in viral isolate quantification methods were assessed using principal coordinate analysis (PCoA).

3.1.2 Experimental results I: Viral isolates

A comparative overview of all methods for individual samples is depicted in **Figure 3-1**. Left panel shows a boxplot with the qPCR median plotted as grey line. The right panel represents the divergence of each method from the average qPCR result.

Phage T4. For the phage T4, qPCR gave a concentration of 1.52×10^{10} gene copies mL^{-1} (standard deviation [sd] = 1.02×10^8, n = 8, coefficient of determination [R^2] =0.991). However, EPI measurements gave a significantly lower result compared with qPCR ($p < 0.001$). Likewise, concentrations measured with FCM in combination with staining at 30 °C (FCM30) and PA were lower. In both 80 °C staining treatments for FCM and NTA (FCM80 and NTA80), significantly higher particle concentrations were detected compared to qPCR ($p < 0.001$). For NTA measurements following a 30 °C staining procedure (NTA30), no significant difference was observed, despite a slightly elevated particle concentration.

Phage T7. A similar pattern appeared for the phage T7. While qPCR measured 4.24×10^{10} gene copies mL^{-1} (sd = 2.91×10^9, n = 8, R^2 = 0.988). EPI, FCM30, and PA gave significantly lower virus concentrations ($p < 0.001$). Here as well, staining at 80 °C significantly increased concentrations in both NTA and FCM ($p < 0.001$). The difference between the NTA30 and the qPCR result was negligible.

Phage MS2. For phage MS2, qPCR quantification revealed 4.01×10^{10} gene copies mL^{-1} ($sd = 1.26 \times 10^{9}$, $n = 8$, $R^2 = 0.986$). Independent of the staining procedure, FCM significantly underestimated the particle concentrations ($p < 0.001$). Meanwhile, NTA30 measurements showed high imprecision with a general underestimation of particle numbers. With EPI, no concentration could be ascertained, as no particles were visible under the microscope at a magnification of 1000. In contrast to other viral isolates, PA and NTA80 gave concentrations more similar to qPCR, but differences were significant ($p < 0.001$). Especially for NTA80, most of the counted particles were larger than 100 nm, which exceeds the actual MS2 diameter (**Figure 3-2 f**).

Phage ΦX174. According to qPCR, phage ΦX174 had a concentration of 8.69×10^{10} gene copies mL^{-1} ($sd = 9.45 \times 10^{9}$, $n = 8$, $R^2 = 0.999$). For all other measurements, ANOVA tests showed significant differences ($p < 0.001$). For NTA30 significantly higher concentrations were obtained ($p < 0.001$). Results from NTA80 were not included as particle sizes of more than 500 nm were observed, indicating the possibility of a strong aggregate formation (**Figure 3-2 g**).

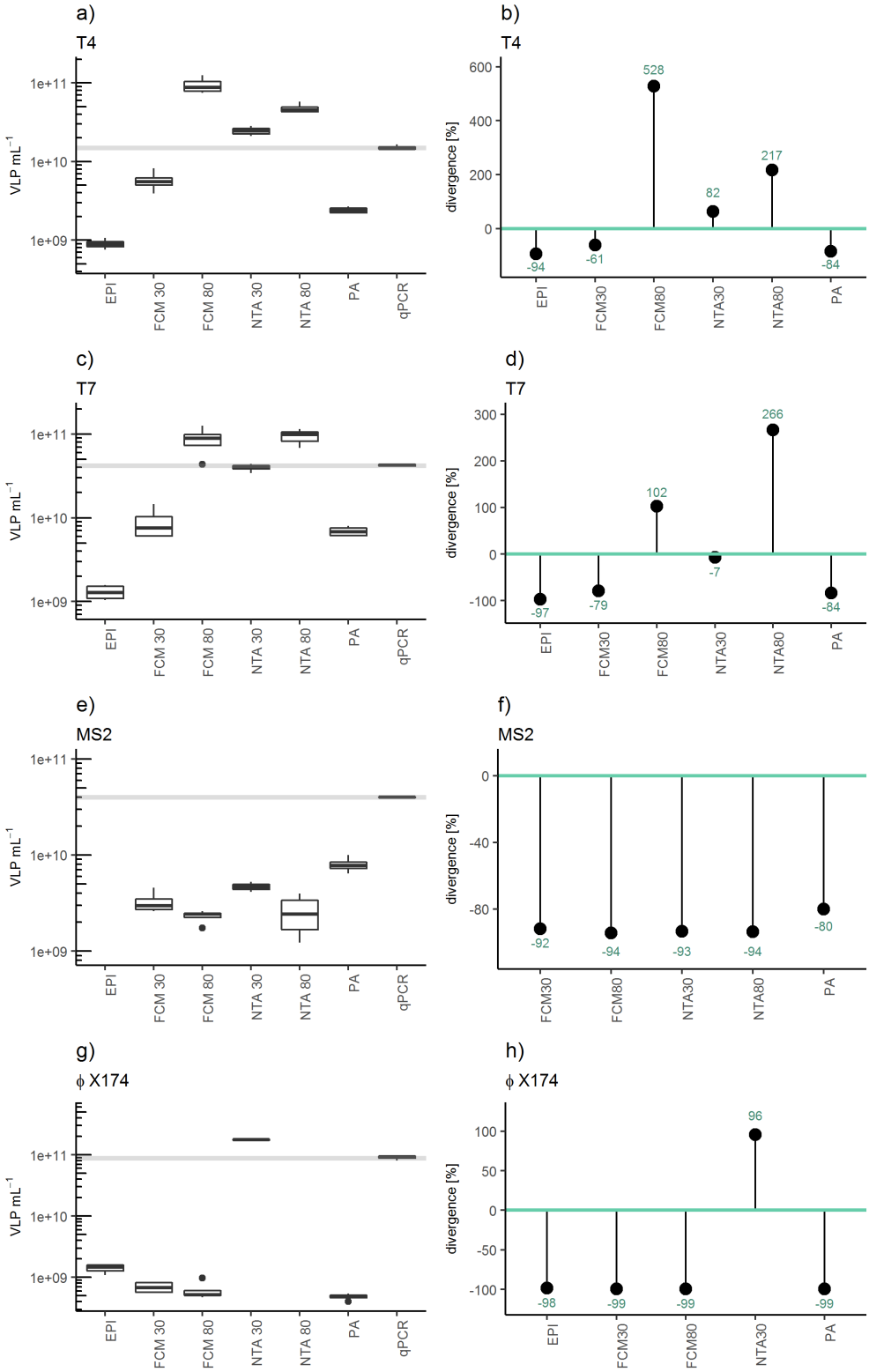

Figure 3-1: Enumeration of clonal viral isolates. a, c, e and g: quantification of phages T4, T7, MS2 and ΦX174, respectively using difference quantification techniques. Grey line represents median concentration measured by qPCR. b, d, f and h: divergence of the different quantification techniques from the qPCR results. Green lines indicate the relative qPCR concentration as 0 % divergence.

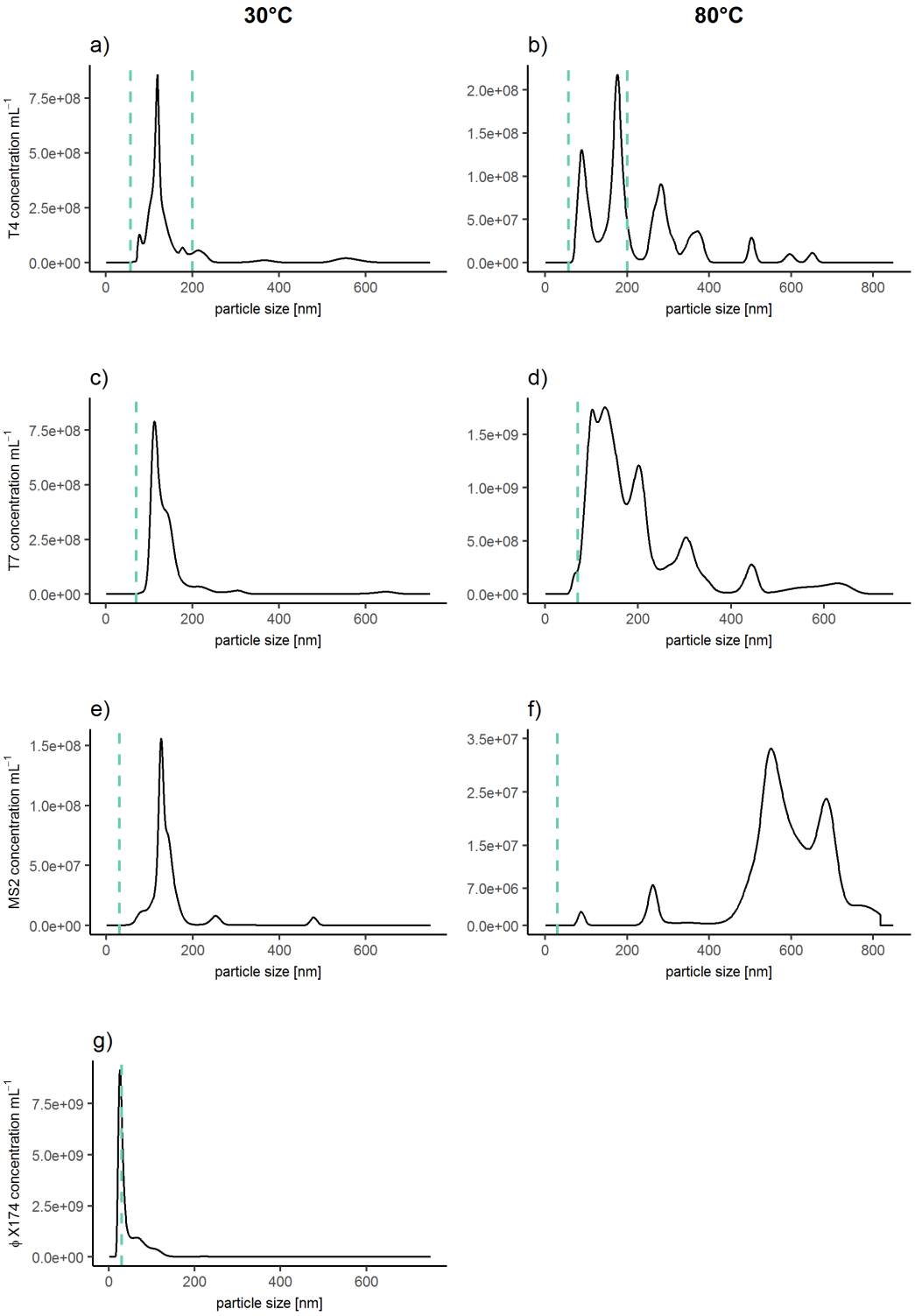

Figure 3-2: Size distribution of viral isolates quantified with NTA method. a, c, e and g: size distribution with 30°C staining of phages T4, T7, MS2 and ΦX174, respectively. b, d, f and h: size distribution with 80°C staining of the respective phages. Dotted green line indicates the actual particle size of the respective virus isolate (T4: range of 57 – 200 nm, T7: 70 nm, MS2: 30 nm, ΦX174: 30 nm). Concentrations represent the average of three measurements of one sample preparation.

Generally, PA consistently underestimated viral concentration compared to qPCR. Divergence of the results was between −80 % and −84 %, with the exception of phage ΦX174 which diverged by −99 % (**Figure 3-1**, right panel). With EPI, a general underestimation between −94 % and −98 % was observed. All 80 °C treatments (for both NTA and FCM) overestimated the T4 and T7 concentrations by more than 100 %. FCM with a staining procedure at 30 °C led to an overall underestimation of particles, varying between −62 % and −99 %. The only method that gave results that did not significantly deviate from the qPCR results for phages T4 and T7 was NTA30, according to ANOVA analysis. This congruency was also confirmed by PCoA analysis, in which a clustering of NTA30 and qPCR was observable (**Figure 3-3**).

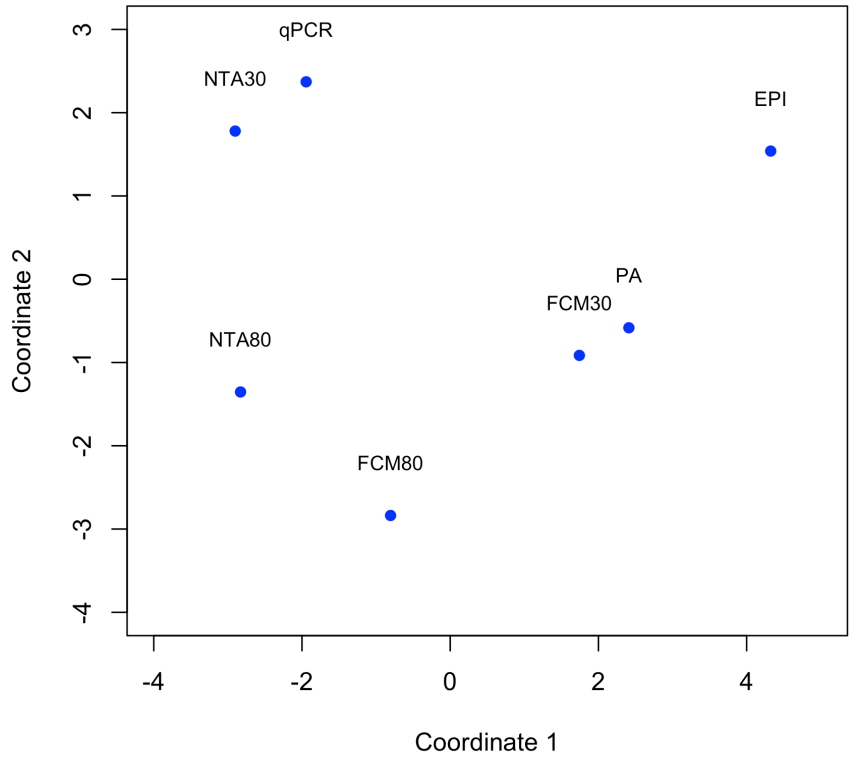

Figure 3-3: PCoA analysis of all viral isolate measurements. A correlation between the quantification methods qPCR and NTA30 is indicated.

3.1.3 Experimental results II: Environmental samples

The complex and heterogeneous nature of environmental water samples, together with a background rather high in abiotic particles, presents challenges to accurate virus quantification. Besides, targeted methods are not applicable if the viral community in its entirety is to be enumerated. However, based on the outcome of the quantification method comparison from the viral isolates, only NTA in combination with an hour-long staining procedure at 30 °C gave concentrations not significantly different from those obtained by qPCR. Accordingly, the NTA30 measurement procedure was identified as the most reliable method.

Groundwater. For groundwater, NTA30, NTA80, and NTA unstained achieved concentrations of approximately 10^7 VLP mL^{-1}. With EPI, no concentration could be ascertained, as the particles showed a fluorescence signal too weak to be visible. Both FCM30 and FCM80 gave lower particle numbers of around 10^5 VLP mL^{-1} (**Figure 3-4 a**).

River water. The river water sample was quantified with NTA30 to a concentration of 10^7 VLP mL^{-1} (**Figure 3-4 b**). A similar result was obtained with FCM80. Both NTA80 and NTA unstained measurements gave ten-fold higher concentrations. EPI and FCM30 accounted for the ten-fold lower concentrations around 10^6 VLP mL^{-1}.

Lake water. For the lake water sample, viral concentrations were similar to the river water (**Figure 3-4 c**). The lowest viral concentration (10^6 VLP mL^{-1}) was determined by EPI, whereas NTA unstained gave the highest virus concentration (10^8 VLP mL^{-1}).

Wastewater. The virus concentration for the wastewater measured with NTA30 was 10^8 VLP mL^{-1} (**Figure 3-4 d**). Higher concentrations were indicated by NTA80 and NTA unstained. The lowest concentration of 10^6 VLP mL^{-1} was obtained by EPI. Neither FCM30 nor FCM80 showed considerable differences from NTA30 (10^8 VLP mL^{-1}).

Across all environmental samples, EPI, FCM30 and FCM80 generally tended to underestimate the viral particle concentration, whereas NTA30 and NTA80 gave concentrations more similar to those of qPCR.

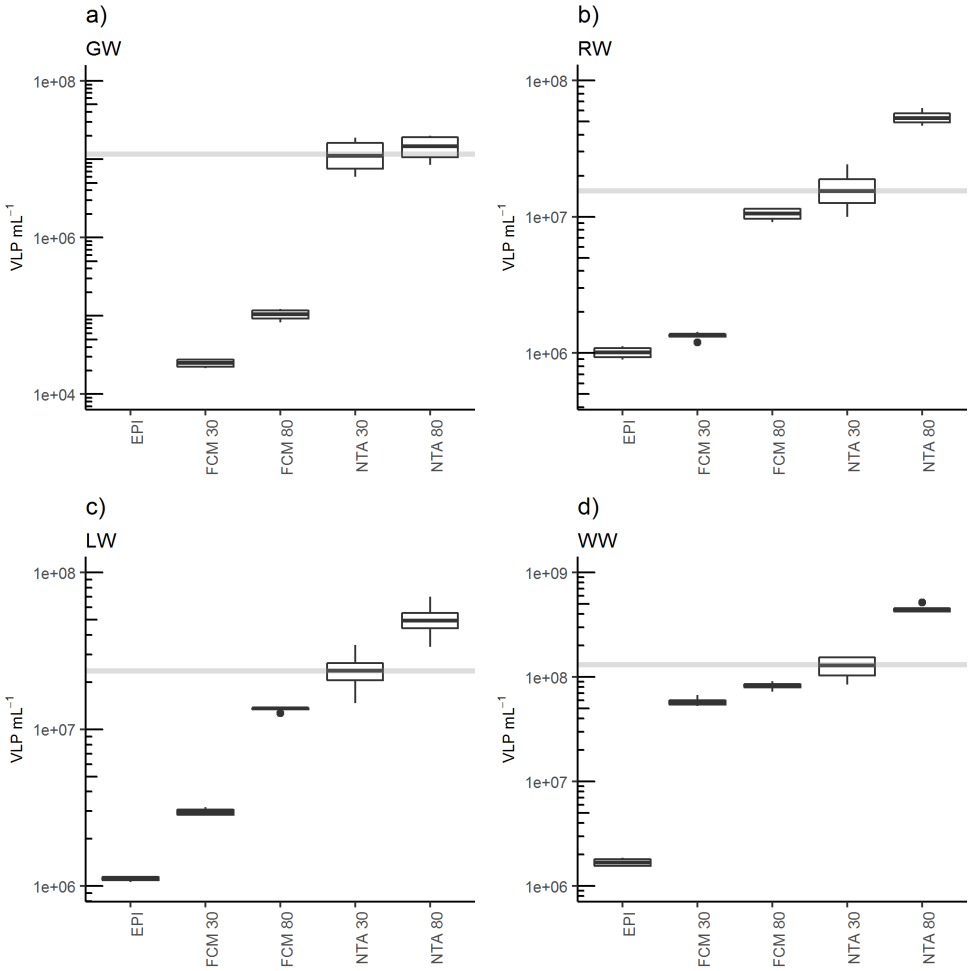

Figure 3-4: Quantified abundances of viral particles mL^{-1} in water. a: Groundwater; b: river water; c: lake water; d: wastewater. Grey line indicates the median particle concentration measured using NTA30.

3.1.4 Experimental results III: Mixed environmental sample spiked with phage T4

The mixed environmental sample has been prepared according to the previous measurements in order to reach an approximate concentration of 1×10^8 VLP mL^{-1}. To this sample, different concentrations of phage T4 (quantified by qPCR) have been added (1×10^8, 5×10^8 and 1×10^9 VLP mL^{-1}). These samples were only quantified with NTA and FCM in combination with the two different staining procedures (30 °C and 80 °C). The mixed water sample without artificially added phage particles is expected to have around 1.1×10^8 VLP mL^{-1} (**Figure 3-5 a**). Both, FCM30 and FCM80 underestimated the viral particle concentration by 47.4- and 12.8-fold, respectively. NTA80, however, overestimated the viral concentration by 6.7-fold, whereas NTA30 underestimated the expected viral concentration with 1.3-fold only slightly. A similar pattern could be observed for the mixed sample with 1×10^8 T4 particles mL^{-1} added (**Figure 3-5 b**). FCM measurements underestimated the virus concentration by 38.9- (FCM30) and 11.8-fold

(FCM80). NTA80 quantified 5.9-fold more viral particles and NTA30 resulted with a 2.6-fold lower concentration to the closet titer estimation. **Figure 3-5 c** represents the measurements of the mixed sample spiked with additional 5 × 10^8 T4 particles mL^{-1}. High deviations from the expected concentration of 6.1 × 10^8 VLP mL^{-1} could again be observed for both FCM measurements. NTA30 slightly underestimated the concentration (2.0-fold) whereas NTA80 overestimated the particle concentration by 1.6-fold. With a starting concentration of 1 × 10^9 VLP mL^{-1}, only NTA30 resulted in the closest estimation of the particle concentration with a slight overestimation of 1.3-fold (**Figure 3-5 d**).

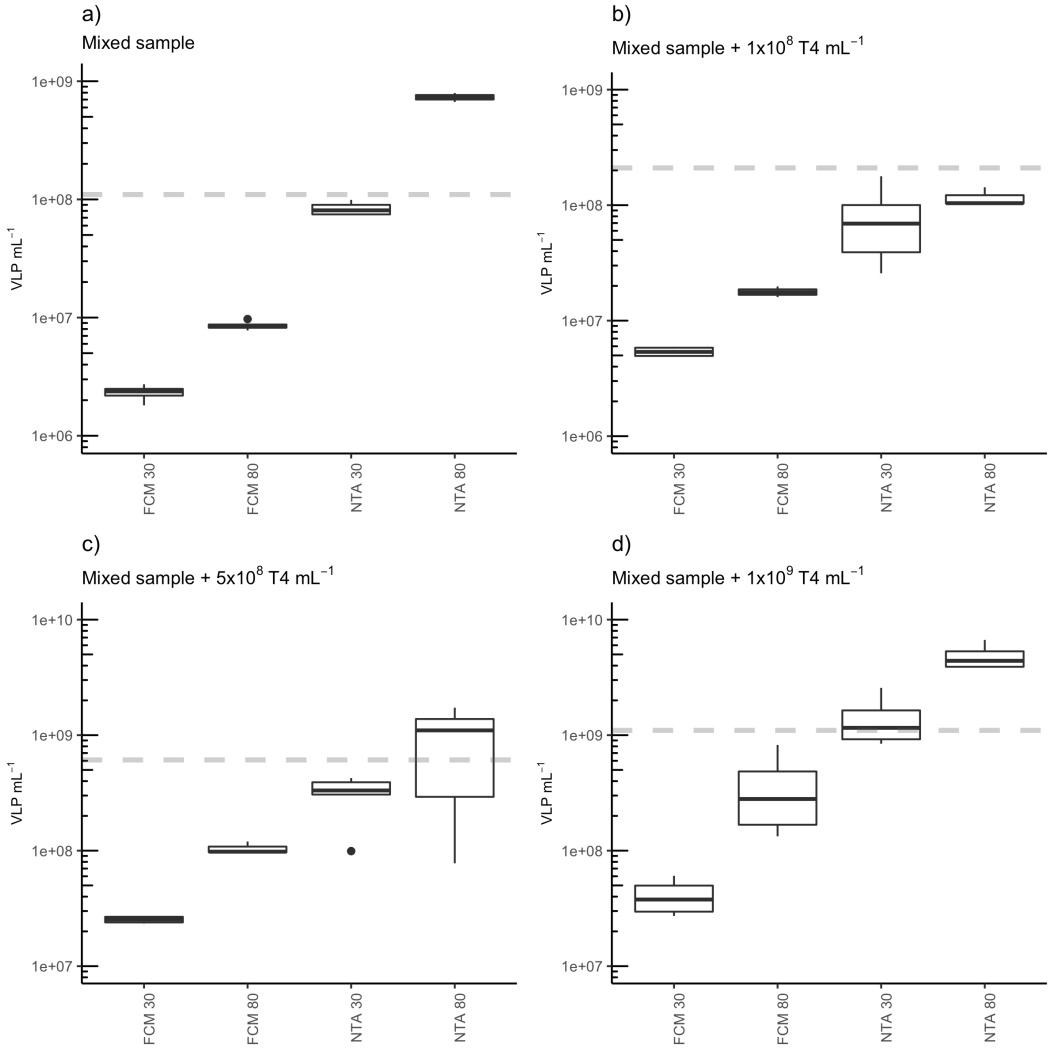

Figure 3-5: Enumeration of viral particles in mixed water samples spiked with different phage T4 concentrations. a: mixed water; b: mixed water spiked with 1 × 10^8 T4 mL^{-1}; c: mixed water spiked with 5 × 10^8 T4 mL^{-1}; d: mixed water spiked with 1 × 10^9 T4 mL^{-1}. Grey dashed lines indicate the expected total virus concentration for each sample.

3.1.5 Discussion

Evaluating the methods. For the method comparison, viral isolates that feature different size and genome characteristics were chosen. Five different methods were used for quantification. Traditional methods such as PA quantify viral particles that are able to infect and lyse a particular type of host cell; once the correct host has been determined, particular viruses can be detected with this technique. On the other hand, qPCR amplifies certain gene sequences, requiring a genome sequence of the targeted virus or viral family to be identified. As both infectious and non-infectious particles are similarly detected by qPCR, particle concentration is expected to be higher for this method than for PA. Indeed, this was the case for all viral isolates as PA results diverged by approximately 80 % from the qPCR results.

Laser-based methods, such as epifluorescence microscopy, flow cytometry or nanoparticle-tracking analysis, require a certain staining procedure in order to separate biotic particles (that is, particles containing genetic material) from abiotic noise for a reliable and accurate enumeration. Particularly for complex environmental samples, NTA unstained measurements resulted in an overestimation of the phage titers characterized by a broad variance (data not shown). Thus, nucleic acid- or protein-specific dyes are essential, as without staining, non-viral particles are included in enumerations.

The importance of an optimized staining procedure became apparent during the application of two different staining protocols (1 hr at 30 °C or 10 min at 80 °C), as NTA captures not only fluorescence, but also information on particle sizes based on their Brownian motion. Particularly with the viral isolates, treatment at 80 °C resulted in an altered size distribution of the viral particles that did not reflect the actual particle sizes (**Figure 3-2**). This became especially apparent for the very small phages MS2 and ΦX174, as NTA80 was not able to record any particles with an actual size of 30 nm. For ΦX174, no particle concentration could be determined at all, as only particles greater than 500 nm were identified, indicating an increased tendency of particle aggregation upon exposure to high temperature. As confirmation, TEM images of MS2 and T7 viruses, incubated for 10 min at 80 °C or untreated, were taken. Although singular MS2 particles appeared smaller when incubated at 80 °C (29.20 ± 7.18 nm) than when untreated (34.78 ± 8.23 nm), they did show a tendency to form aggregates (**Figure 3-6 b**). For phage T7, this aggregation was less apparent, but particles lost their distinct icosahedral shape upon incubation at 80 °C (**Figure 3-6 d**). Consequently, as staining temperatures affect the size, shape, and agglomeration tendency of viral particles, an optimal staining procedure has to be developed and evaluated *prior to* measurements.

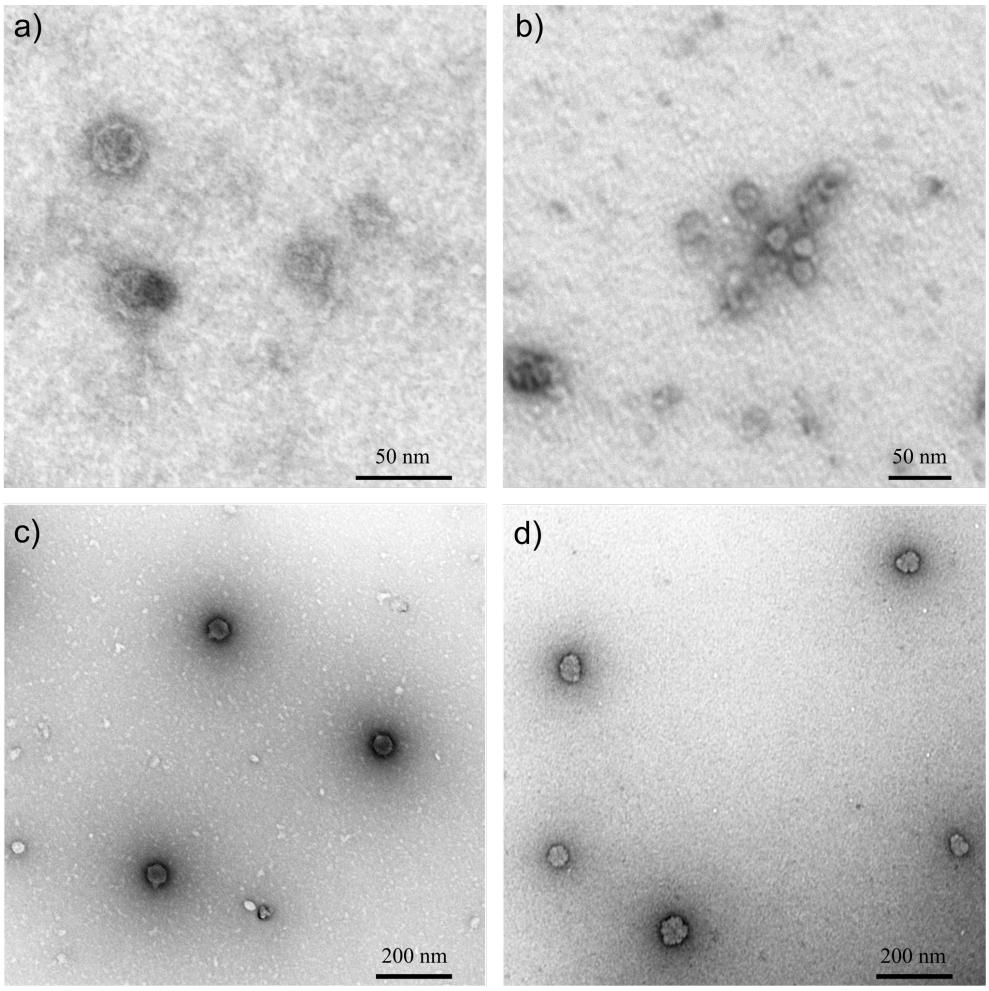

Figure 3-6: TEM picture of phages MS2 and T7 with 80 °C treatment or without. Upper panel: Phage MS2 with a scale bar of 50 nm, a: untreated and b: incubated at 80 °C for 10 min. Lower panel: Phage T7 with a scale bar of 100 nm, c: untreated and d: incubated at 80 °C for 10 min.

Optimal concentration range. Another important parameter crucial for reliable measurements is the optimal concentration range of a sample. For groundwater, both FCM30 and FCM80 gave concentrations between 10^4 and 10^5 VLP mL^{-1}, which is in the range of previously ascertained groundwater samples obtained with FCM in combination with a SYBR green I staining [278]. Paradoxically, for the groundwater samples measured in this study, all NTA measurements (independent of the staining procedure) gave concentrations of around 10^7 VLP mL^{-1}. This discrepancy between FCM and NTA could be because the optimal concentration required by NTA lies between 10^7 and 10^8 mL^{-1} (**Table 3-1**). For the calculation of particle concentration, the volume in the measuring chamber is extrapolated. In case of very low particle amounts, a high random error appears, especially when no syringe pump is used. Additionally, the signal-to-noise-ratio turns to be unfavorable when measuring in this minimum range. Consequently, NTA is incapable to accurately quantify a sample if its concentration is much less than the minimal

required concentration of around 10^7 VLP mL^{-1},. Thus, an application of NTA on an oligotrophic groundwater is unfeasible without prior enrichment.

However, varying optimal concentrations were required for the different instruments. Optimal concentrations for FCM quantification vary with the complexity of samples. Clonal isolates are generally featured with lower background signals, thus virus concentrations around 10^6 particles mL^{-1} to 10^7 particles mL^{-1} are optimal. For the highly variable environmental samples, lower virus concentrations (10^4 VLP mL^{-1}) were needed, as the background noise is then diluted, too. For NTA, these differences could be observed as well, although not as pronounced. Viral isolates need a final concentration of 10^8 VLP mL^{-1} for medium-sized viral particles (e.g., phages T4 or T7) or 10^9 VLP mL^{-1} for smaller particles (e.g., phages MS2 or ΦX174). Environmental samples need a minimal concentration of 10^7 VLP mL^{-1} for optimal results. For PA, samples were diluted to result in a countable plaque formation in the range of 20–200 PFU per plate. However, this number may be different between phage isolates as the plaque diameter also varies individually. Lower concentrations on the other hand may lead to pronounced variations between replicates. qPCR is theoretically capable to detect one gene copy per reaction volume. Thus, its sensitivity is more restricted to the efficiency of DNA or RNA extraction and cDNA synthesis, than to the limitations of the quantification method. For EPI, concentrations of 10^7 particles mL^{-1} are generally necessary in order to being countable. A total magnification of 1000 is however not sufficient for a reasonable enumeration of very small viruses (e.g., phages MS2 or ΦX174), although the amount of added dye was doubled for the EPI sample preparation compared to FCM or NTA, indicating that this increment does not influence particle visibility.

Besides the low viral concentrations, the laser-based methods also had their difficulties with tiny viral particles. Viruses that are characterized by small capsid diameters such as MS2 or ΦX174 (27 and 30 nm) are often featured as well with minor genome sizes and indeed, their genomes were only 4–5 kbp. Laser-based methods rely on the combination of sufficient dye molecules in order to return visible signals, which is often impossible in such small genomes. For EPI measurements, the excited fluorescence that derived from these extremely small genomes was weak and transient, thus no photo could be taken. It is therefore questionable weather EPI is capable to quantify such small genomes. Meanwhile NTA and FCM have their issues with such small particles, too, as both measurements of ΦX174 and MS2 resulted in concentrations similar to PA results (**Figure 3-1**). This similarity indicates that both NTA and FCM underestimate the actual particle concentrations. Based on this ineffectiveness in quantifying tiny virus particles, it

can be assumed that none of these methods are able to quantify small particles in an environmental sample accurately. SYBR gold, a dsDNA dye, is widely used for the staining of environmental samples in order to enumerate viral particles in their entirety (8). While it is still questionable whether ssDNA or ssRNA genomes (MS2 and ΦX174) are properly stained as well, the accuracy of these quantification techniques was not sufficient. Similarities have been observed with viruses less than 40 nm in diameter using SYBR green I [279]. For the assessment of these virus-types, more specific nucleic acid dyes should be evaluated in further studies.

An exact quantification of viral particles in a given sample is essential for many applications. Presently, there is no universal approach that is suitable for all types of samples, as the method depends on the scope of the application. Thus, if the exact amount of infectious viral particles must be determined, PA might be the method of choice. In other contexts, where the overall concentration of virus particles is needed, other methods like qPCR (for genetically elucidated viruses) or NTA (for unknown or composite samples) may be more suitable.

However, qPCR remains the gold standard for accurate quantification of particles that contain known genomic material. Thus, in the present study, viral isolates were quantified, and the results obtained using other methods were compared to those of qPCR in order to evaluate the accuracy and effectiveness of these methods. A high conformance for viral particles with an average particle diameter greater than 30 nm could be confirmed with the NTA30 method. The most reliable method for viral particles with an average particle diameter greater than 30 nm was confirmed as NTA30. For environmental samples, available methods for counting an unspecific virus are scarce. Neither qPCR nor PA are applicable, as their mode of operation is invalid for these composite samples, unless a specific virus with known host or genomic composition is to be quantified in the mixed sample. Comparisons among the environmental water samples and their respective NTA30 results showed similar outcomes for most methods. Notably, NTA80, NTA unstained, and EPI gave over- or underestimations. The evaluation of the quantification of a mixed water sample with an expected titer of 1.1×10^8 VLP mL^{-1} and different concentrations of phage T4 (ranging from 1×10^8 to 1×10^9 VLP mL^{-1}) added artificially to this sample, confirmed also the underestimations of the viral titer by FCM30 and FCM80 (**Figure 3-5**). NTA80 generally overpredicted the viral concentration. Assuming an optimal particle concentration, NTA together with 1 h staining at 30°C was confirmed as a reliable quantification technique for environmental samples on the condition that a minimum particle concentration of 10^7 VLP mL^{-1} is reached.

Table 3-1: Specifications, advantages and disadvantages of the applied virus quantification techniques.

	Plaque assay	**Epifluorescence microscopy**	**Flow cytometry**	**Nanoparticle-tracking analysis**	**Quantitative real-time PCR**
Size limitation	N/A	> 200 nm	0.5–40 µm	10–2000 nm	N/A
Measurable features	Active/lytic viral particles	Total viral particles	Total viral particles	Total viral particles	Specific gene abundance
Optimal concentration	40–400 PFU mL^{-1}	10^7–10^8 VLP mL^{-1}	10^6–10^7 VLP mL^{-1}	10^7–10^9 VLP mL^{-1}	10^6–10^8 VLP mL^{-1}
Time requirement per sample	Minimum of 24 h	Around 2 hr	Around 30 min	Around 15 min	Around 4 hr
Advantages	Measures infective particles, low consumable costs	Low operating and consumable costs, fast results, visible control	Low operating and consumable costs, fast results	Low operating and consumable costs, direct particle visualization	Good reproducibility, accurate quantification of specific genes
Disadvantages	Many dilution steps needed, poor reproducibility, result not immediately available, cultivable host needed	High initial costs for equipment, DNA-bound non-viral particles may be counted as well	High initial costs for equipment, DNA-bound non-viral particles may be counted as well	High initial costs for equipment	Phage-specific primers needed, DNA extraction needed (no direct quantification possible), high costs

Implications for viral abundance in water. The number of the global viral population in seawater has been estimated as 4.1×10^{30} VLP [22]. This value was based on epifluorescence microscopic counting using Yo-Pro1 dye. Clasen and colleagues quantified the viral population in freshwater and obtained a concentration of 9.50×10^{9} VLP L^{-1} using the same method and dye [280]. Assuming a global freshwater volume of 9.01×10^{16} L (including lakes and rivers), the viral freshwater population can be calculated as 8.56×10^{26} VLP [281]. However, in this study the inaccuracy especially by EPI as well as difficulties in quantifying very small viral particles could be observed. One important consideration regarding these significant underestimations is the chemical properties of the fluorescent dyes that applied in aforementioned and the present study. Yo-Pro1, SYBR gold, and SYBR green are dyes that preferentially stain dsDNA, thus RNA viruses or ssDNA viruses are only stained weakly or not at all. As Steward and colleagues showed earlier, only one-third of viruses in seawater are dsDNA viruses, whereas up to 63 % are RNA viruses [282]. With this high proportion of particles that are beyond the scope of conventional methods, it is reasonable to assume that more than half of the particles are not captured using EPI in combination with these dyes. Previous speculated values of the total viruses in a given environment, which are based on epifluorescence counting, have to be reconsidered as they likely lead to underestimations of global virus abundance.

3.2 Characterization of bacteria – phage interactions: Phages of *P. aeruginosa*

3.2.1 Description of the experiment

Virus isolation. The phage isolation was conducted using two *Pseudomonas aeruginosa* strains: PAO1, which represents the wildtype, and a strain isolated from clinical specimen, denoted as CI. Three different sources of samples that presumably contained phages of *P. aeruginosa* were used: 14 bronchoalveolar lavage (BAL) samples, which derived from patients with a differing chronic obstructive pulmonary disease (COPD) severity, 32 sputum samples deriving from the same context and four wastewater samples that were taken from the incoming wastewater (i), from the activated sludge water (ii) as well as sludge phase (iii) and the completely treated and purified water (iv). All samples were 0.22 µm filtered *prior to* use, except for the sputum samples, which were too viscous to being easily filtered. These samples were mixed with 2 mL sterile phage buffer, vigorously vortexed and centrifuged at 4000 × g at 4 °C for 40 min. The supernatant was then 0.22 µm filtered. In order to enrich the samples with phages of *P. aeruginosa*, a co-incubation was performed with all samples (2.3.3). Each sample was mixed with an equal volume of 2x LB medium and inoculated with approximately 10^5 CFU of the respective bacterial host. After an overnight incubation at 37 °C and 170 rpm, samples were again 0.22 µm filtered and a spot assay was performed three times per sample, in order to test for the presence of lytic phages (2.3.3.3). Of all samples, only one BAL sample and the wastewater income sample showed a cleared area in *P. aeruginosa* PAO1 lawn, whereas only the wastewater income resulted in a lawn in *P. aeruginosa* CI (**Figure 3-7**).

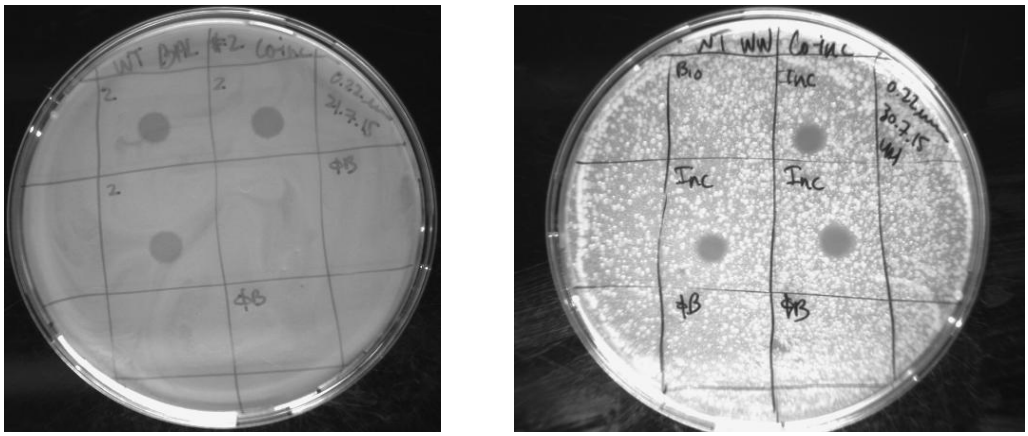

Figure 3-7: Spot assay result of *P. aeruginosa* PAO1. Positive results are indicated by a cleared area in the bacterial lawn, caused by the presence of lytic phages. Left: positive result for BAL sample (#2). Right: positive result for wastewater income sample.

Following that, five purification rounds starting with a plaque assay were conducted with the positive samples (2.3.3.4). From each sample, 30 well isolated plaques were picked and stored in sterile phage buffer. The PA was repeated for each of the 30 picked plaques and for each of the plates, five plaques were then picked. For the second round of purification, only one of the five picked plaques was chosen and a PA was performed, again resulting in 5 picked plaques. If the PA was not successful with the chosen picked plaque, it was repeated with the second of the five picked plaque, and so on. This was repeated until the fifth repetition. Only then, a clonal isolation of a phage could be assumed. Finally, high titer lysates were produced according to (2.3.4.1). Virus concentrations (plaque forming units, PFU mL^{-1}) were determined through PA (2.3.7.1). The isolates were further characterized concerning the optimal conditions for infection.

Optimal temperature. The optimal temperature for an infection was tested by performing a PA (2.3.7.1) and incubating the plates at different temperatures (4, 12, 22, 37, and 42 °C) for up to three weeks.

Infectivity at 36 °C or 40 °C. An additional experiment that aimed to monitor the infectivity of one isolate (BAL 5) over time at 36 °C or 40 °C was conducted. With this experiment the antibacterial activity of lytic phages under the conditions of a bacterial infection in a human setting (often accompanied by risen body temperature) should be simulated. The volume of 100 µL phage isolate BAL 5 was pipetted into each well of a 96-well plate, which was then sealed and incubated at 36 °C or 40 °C for a total time of two weeks. After one, three, seven days or two weeks the volume of 24 wells was taken out and the phage concentration estimated using PA (2.3.7.1) and FCM (2.3.7.2).

Optimal pH. The optimal pH conditions were screened by adjusting the pH of the soft agar (2.2.6) with HCl or NaOH to a pH of 4, 5, 6, 7, 8, 9, or 10.

Host range. The host range was tested with a PA using different hosts (*P. putida* IsoF, *P. putida* F117, and the clinical strain of *P. aeruginosa*).

VBR. The temporal population dynamics of the bacterial host and its phages was monitored with an inoculation at different virus-to-bacteria ratios (VBRs of 0.05, 0.1, 0.5, 1, 10 and 50). For this purpose, an aliquot of the bacterial stock was inoculated in 1× LB to an OD between 0.2 and 0.4. According to the growth curve generated from plate counts of *P. aeruginosa* at several time intervals, the equivalent cell number was calculated using the equation $y = 4.0 * 10^7 x + 5.0 * 10^7$. 100 µL of the bacterial inoculum was the pipetted to each well of a 96-well plate and the respective amount of phages was added, according to the desired VBR. The OD at 570 nm was measured every hour (t=1–t=7) for 7 hours and again at t=18, t=20, and t=24. The phage samples

Inc 9, BAL 2, and 3 were not inoculated for VBR 50 and BAL 1 was not for VBR 10 and 50, as the concentrations of the lysate preparations were too low.

Effect on biofilms. Besides the ability to reduce planktonic cells, also the activity against cells organized in a biofilm was monitored. Cells that reached the exponential phase were grown in microtiter well plates without agitation for a certain amount of time and subsequently, phages were added with a VBR of 0.1, 1 or 10. The incubation was pursued for a varying amount of time, in order to see short-term and long-term effects that the presence of phages have on the biofilms. The amount of viruses added to the system was related to the initial bacterial concentration added to each well. A microtiter dish assay was then performed with each plate (2.3.2). As the staining was only possible for a whole plate, a timeseries could only be achieved through temporally delayed inoculation of the wells. Pre-grown bacteria were in between stored at 4 °C.

PCR. Subsequently, isolates were prepared for DNA extraction. 35 mL of each lysate was concentrated using either Amicon Ultra 15 Centrifugal Filter Units (2.3.6.3) or $FeCl_3$ precipitation (2.3.6.2) to a final volume of 3 mL. DNA was then extracted according to 2.3.9.1. For a genetic characterization, PCRs targeting g20, g23 and DNApol (2.3.10.1) were conducted.

Digestion. The restriction profile of the isolated viral DNA was studied using AluI, HhaI, NdeI and EcoRI restriction enzymes (2.3.10.4).

Metagenomic sequencing. Further, an equal mixture of the viral isolates was prepared for Illumina sequencing. DNA samples were shipped to BGI (Genom, Shenzhen, China), where the library preparation and Illumina HiSeq sequencing was performed. Phage DNA was pooled equimolar. The contigs were assembled after a quality check using Newbler v2.7.

3.2.2 Experimental results I: Virus isolation

After completion of the purification steps, 13 lytic phages were isolated from the BAL sample and 17 phages were isolated from the wastewater sample that were able to infect *P. aeruginosa* PAO1. The phage IDs of successful isolates are listed in **Table 3-2** . On the contrary, the phages infecting the clinical *P. aeruginosa* strain could not be purified any further after the 4th purification as no plaques were detected anymore in none of the samples. From the sputum samples, no lytic activity could be detected.

Table 3-2: Sample IDs of phage isolates after the 5th round of purification.

Phage IDs	Source
Inc 1, 2, 3, 5, 6, 9, 10, 12, 13, 15, 16, 17, 21, 23, 24, 26, 33	Wastewater income
BAL 1, 2, 3, 4, 5, 8, 9, 11, 12, 13, 15, 16, 20	BAL

The concentration of the active phage particles ranged between 10^9 and 10^{11} PFU mL^{-1}. However, concentrations of Inc 9 and BAL 1–3 were approximately one to two orders of magnitude lower. Concentrations of the lysates can be found in **Table 6-1** (supplementary material). The size of the BAL phage plaques in the bacterial lawn were a little smaller compared to the plaques formed by the wastewater samples. Additionally, a larger halo has formed around the BAL phage isolates.

3.2.3 Experimental results II: Isolates characterization

Optimal temperature. Upon incubation at 4 °C, no bacterial growth could be detected, therefore no statement of viral infectivity at such a low temperature could be made. However, at 12 °C bacterial growth was detectable but no plaques were visible, even after a long incubation period. Phages were generally less successful in infecting their host at 22 °C compared to 37 °C (**Figure 3-8**). Depending on the isolates different efficiencies in infecting at 42 °C compared to 37 °C rates could be noted (**Table 6-2**, supplementary material). Only the two isolates BAL 1 and BAL 2 showed the same PFU concentration at both temperatures (indicated by grey filling in **Table 6-2**, supplementary material). For the phages BAL 2, 4, 8, 15, 20, and Inc 1–3, 9, 10, 12, 15–17, and 26, the optimal temperature was 37 °C, as incubation at a higher temperature reduced the number of lytic phages on the plates (indicated by light green filling in **Table 6-2**, supplementary material). For the phages BAL 5, 9, 11–13, 16, and Inc 5, 6, 13, 21, 23, 24, and 33, the higher temperature was preferred as for more particles an infection was successful (indicated by light blue filling in **Table 6-2**, supplementary material).

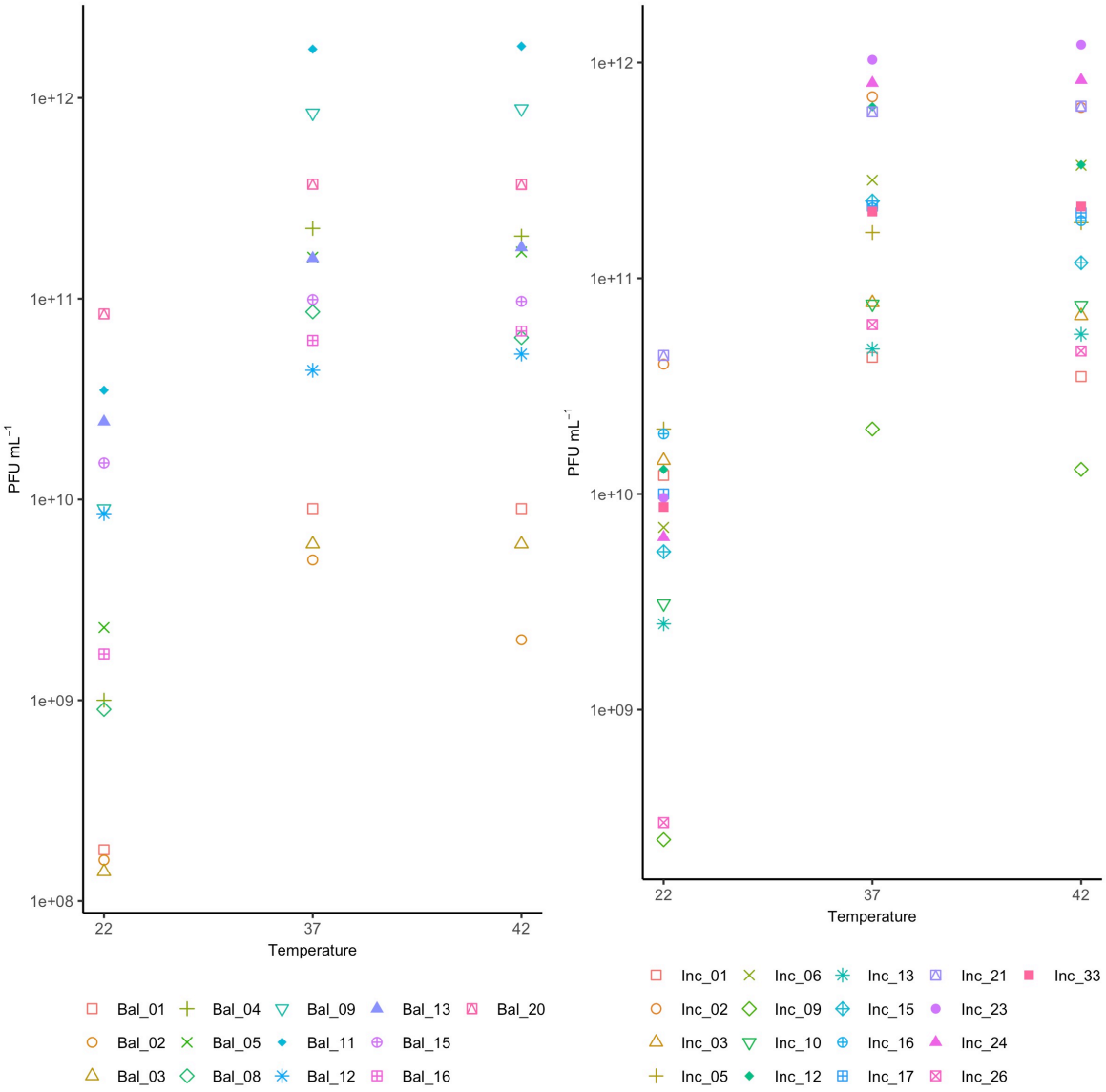

Figure 3-8: Average concentration (PFU mL^{-1}) of viral isolates upon incubation at different temperatures. Left panel: viral isolates generated from the BAL sample. Right panel: viral isolates generated from the wastewater income sample.

Infectivity at 36 °C or 40 °C. For this small experiment phage BAL 5 was incubated at 36 °C or 40 °C for up to two weeks and concentration was measured using plaque assay (PA) and flow cytometry (FCM). **Figure 3-9** summarizes the quantification results of BAL 5, grouped by temperature. Generally, FCM resulted in higher particle concentrations than PA. Short term incubation for one day did not affect the infectivity of the phages as no significant difference between 36 °C and 40 °C was observable with PA measurements using the Student's t-test ($p > 0.05$). For flow cytometry the Student's t-test showed significant differences between the temperatures across all days. Infectivity upon incubation at 36 °C increased only moderately

over time, whereas a clear gain up to two log units could be observed upon 40 °C incubation. Quantification with FCM resulted in lower concentration upon incubation at a higher temperature for the first three days compared to titers at 40 °C. After one week higher concentrations were measured at 40 °C incubation temperature.

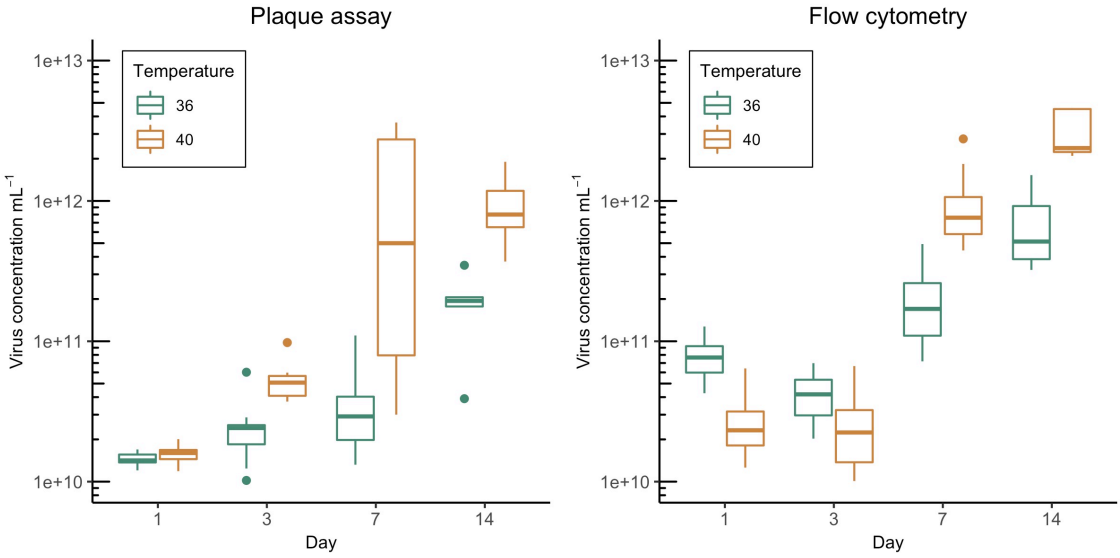

Figure 3-9: Phage BAL 5 concentration quantified with plaque assay (left panel) and flow cytometry (right panel). Green: Viral concentration upon incubation at 36 °C. Yellow: Viral concentration upon incubation at 40 °C.

Optimal pH. The incubation at different acidic and alkaline levels had also different effects on the phage isolates. Some phages had missing titer information for two or more pH values. As consequence, the isolates Inc 9 (values for pH 4, 8, and 10 are missing), Inc 10 (values for pH 4, 8, 9, and 10 are missing) and Inc 26 (values for pH 4 and 7 are missing) were not included for further analysis. For phages Inc 13 and BAL 6, 11, and 12 no concentration was determined at pH 4 and for the isolate Inc 12 values for pH 10 are missing. Generally, four different trends could be observed. An overview of phages grouped according to their pH response provides **Table 6-3** (supplementary material). In 23.08 % of the BAL isolates and 42.86 % of the Inc isolates the pH had no strong influence on the infectivity rate (**Figure 3-10,** upper left picture). 35.71 % of Inc phages and 38.46 % of BAL phages had their optimum at a pH of 7 (**Figure 3-10**, lower left picture). Their pH optimum at 6 had 42.86 % of the Inc isolates and 38.46 % of the BAL isolates (**Figure 3-10**, upper right picture). A general increase in titers at higher pH and consequently a tendency of preferring more alkaline environments showed 35.71 % of Inc isolates and 23.08 % of BAL isolates (**Figure 3-10**, lower right picture). Here, also a strong reduction in viral numbers at a pH of 4 could be observed.

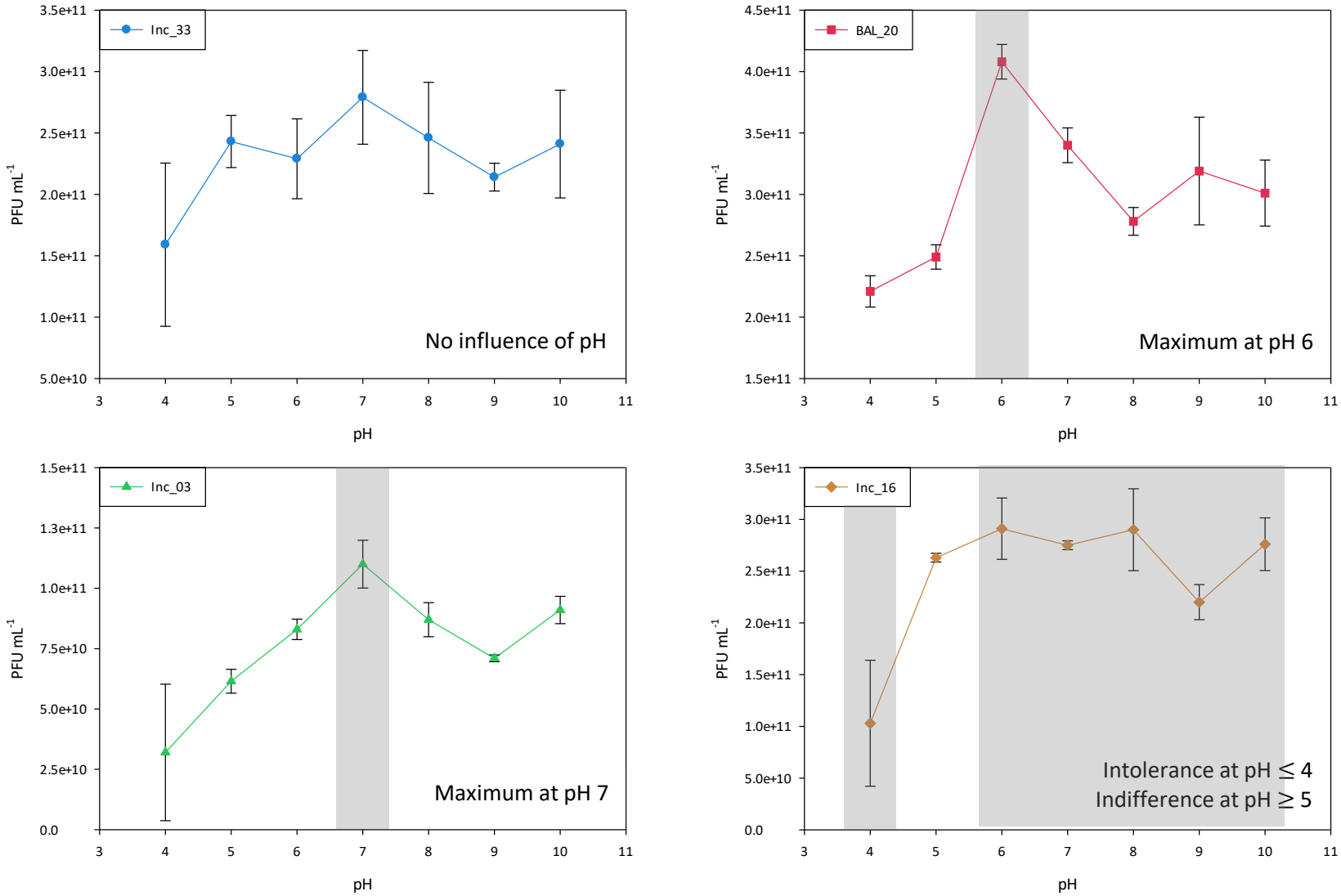

Figure 3-10: Four different behaviors the phage isolated showed upon incubation at different pH values. Other isolates showed a similar behavior as the depicted phages according to their grouping (Table 6-3, supplementary material).

Some of the isolates shared features of two different groups (**Figure 3-11**). For example, phages Inc 3, BAL 15, and BAL 16 showed a maximal reproducibility rate at pH 7 but also generally preferred higher pH values, or isolates Inc 3, 21, and 33 and BAL 4, had their preference at pH 7, however their response to the different pH was more or less invariant.

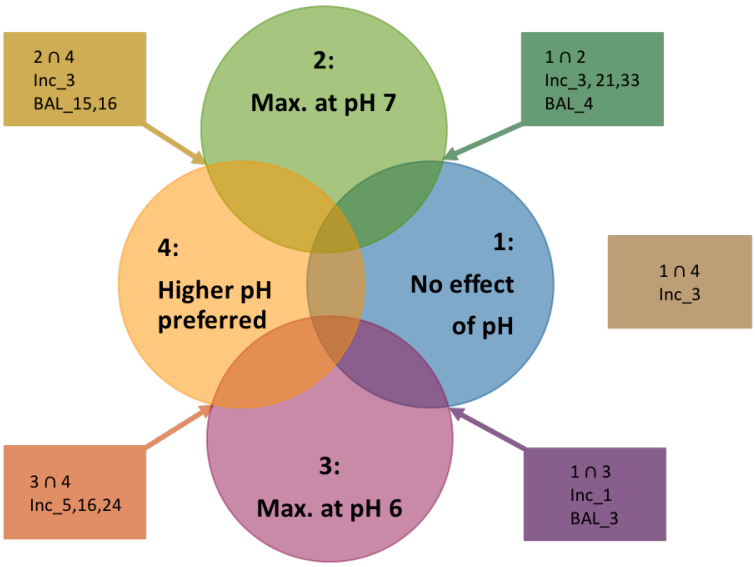

Figure 3-11: Venn diagram showing similarities between different trends in pH variations. Numbers indicate the four different groups as indicated in the picture.

Generally, at very low pH values of 4, the bacterial growth was relatively unstable and the phages were either not able to reproduce or infections occurred only at low numbers. Additionally, plaques were more turbid and smaller at the pH values 4 and 5. Most of the phage isolates (more than 76 %) had the highest reproduction rate at a more neutral pH range between 6 and 7 (Inc isolates: 78.57 %, BAL isolates: 76.92 %) (**Table 6-3**, supplementary material).

Host range. The host range of the isolates was determined with the strains *P. putida* IsoF and F117, *P. fluorescence* and *P. aeruginosa* CI. None of the phage isolates was able to infect any of the tested bacteria, indicating a high specificity of the isolates.

VBR. The cell density of *P. aeruginosa* PAO1 was monitored after inoculation with individual phage isolates at different VBR. According to the provoked increases in bacterial OD values, the phage isolates can be differentiated into five different groups. In group 1, the addition of phages at a low VBR ratio (0.05 and 0.1) showed initially a higher bacterial growth, or, in other words, less virus-induced lysis could be observed (**Figure 3-12**). Here, the OD increased slowly, but constantly. Higher VBR ratios reduced the bacterial OD more, but the increase after 7 hr was much stronger compared to the lower VBR incubations and even reached the level of the

bacterial control. The isolates Inc 10, 26 and 33, and BAL 1, 5 and 12 could be grouped herein. The isolates BAL 8, 13 and 15 were classified into group 2. They showed a behavior similar to before with the slow but steady increase in OD at low VBRs and the initial reduction of the OD at higher VBR ratios and strong increase after some hours; however a decline in OD between 7–20 hr for a very low VBR could be observed (**Figure 3-13**). In group 3, only small differences in the OD development between the different VBRs was detected (**Figure 3-14**). All OD values increased constantly, with a steeper augment at higher VBRs compared to lower VBRs. The viruses BAL 2 and BAL 4 belong to this group. Members of the group 4, including the phages BAL 3, 20, as well as Inc 1, 5, and 16, showed similar tendencies in the OD as groups 1 and 2. Lower VBRs (0.05 and 0.1) initially showed a higher OD value that increased constantly. However, between 7–18 hr, a drop in bacterial concentration could be denoted (**Figure 3-15**). Again, higher VBR resulted in a stronger reduction of the OD in the beginning but also a stronger increase afterwards. Most of the viral isolates (BAL 4 and 9 and Inc 2, 3, 6, 17, 21, 23, and 24) were combined in group 5 (**Figure 3-16**). This group is similar to group 4, with the difference that only the lowest VBR 0.05 showed this drop in OD.

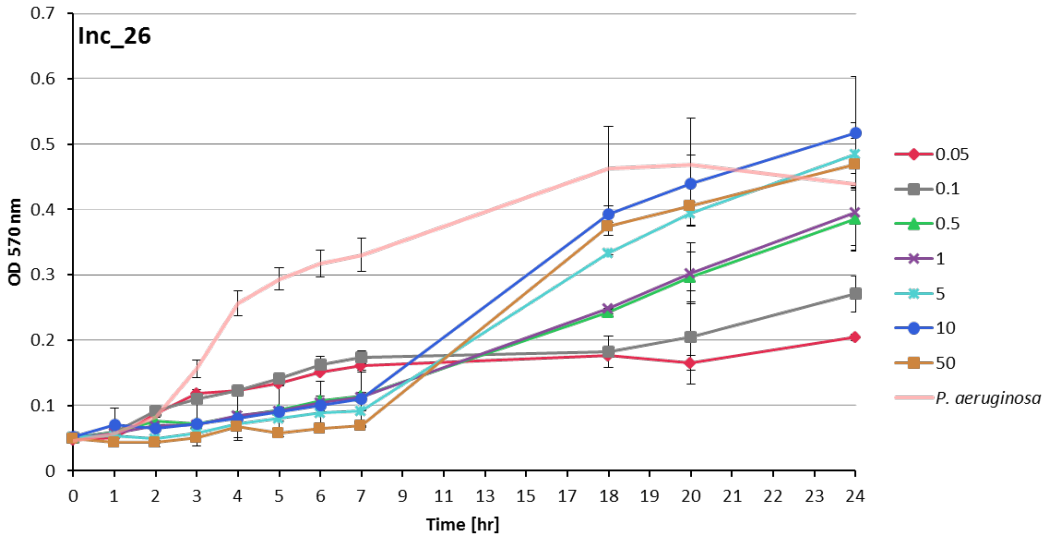

Figure 3-12: OD 570 nm measured over time with phage Inc 26 added to the *P. aeruginosa* PAO1 culture. This graph shows exemplarily the behavior for group 1 phages.

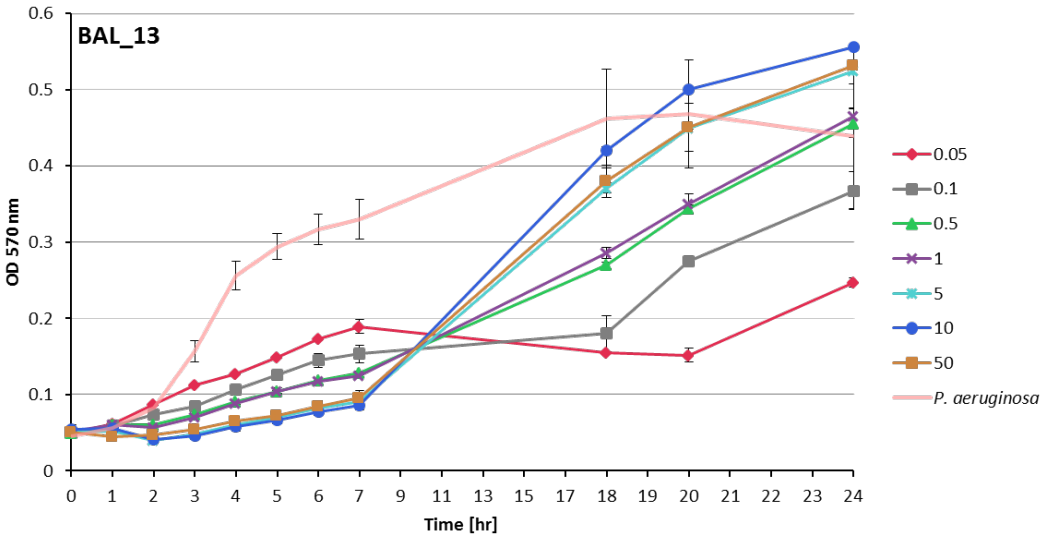

Figure 3-13: OD 570 nm measured over time with phage BAL 13 added to the *P. aeruginosa* PAO1 culture. This graph shows exemplarily the behavior for group 2 phages.

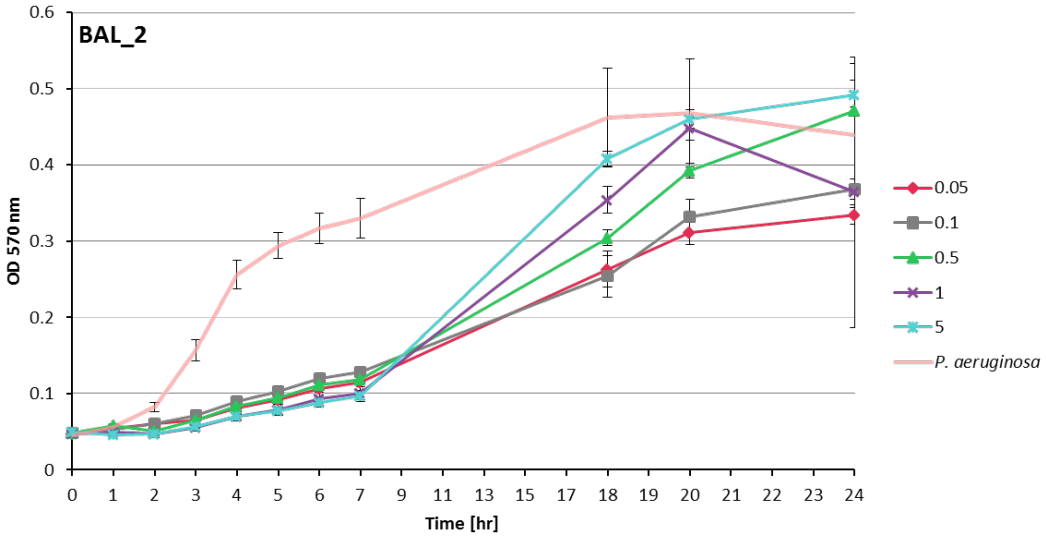

Figure 3-14: OD 570 nm measured over time with phage BAL 2 added to the *P. aeruginosa* PAO1 culture. This graph shows exemplarily the behavior for group 3 phages.

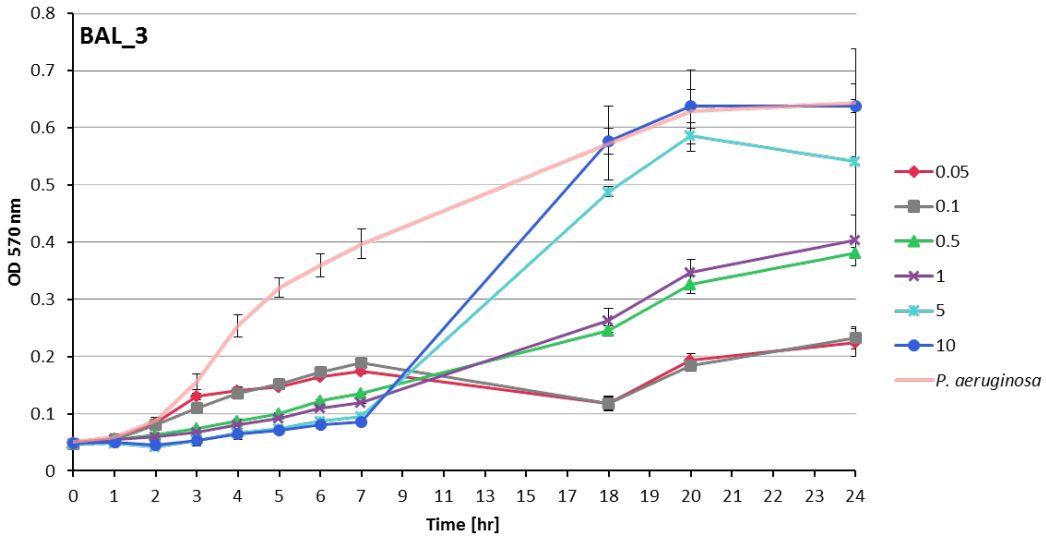

Figure 3-15: OD 570 nm measured over time with phage BAL 3 added to the *P. aeruginosa* PAO1 culture. This graph shows exemplarily the behavior for group 4 phages.

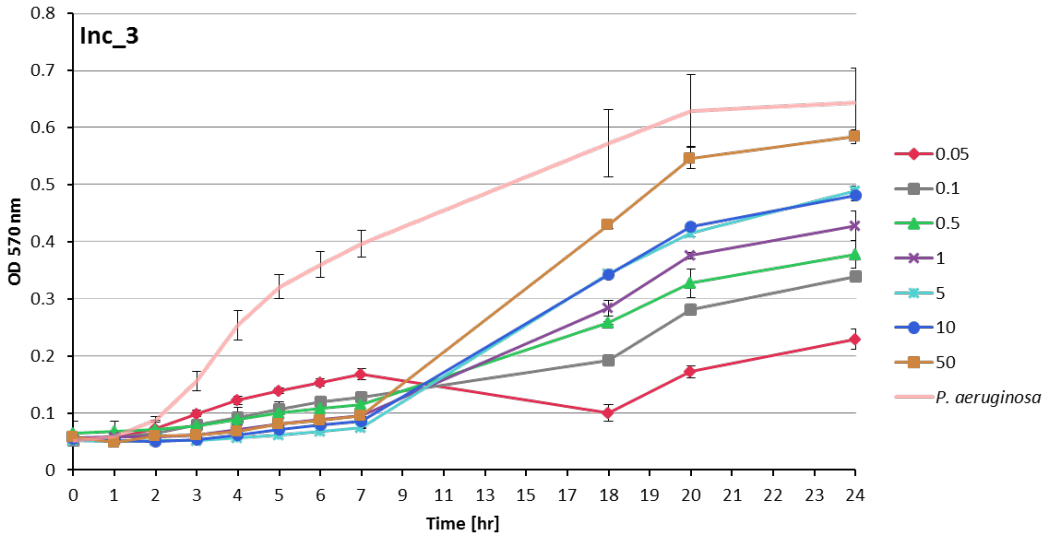

Figure 3-16: OD 570 nm measured over time with phage Inc 3 added to the *P. aeruginosa* PAO1 culture. This graph shows exemplarily the behavior for group 5 phages.

Generally it could be observed that most of the incubations showed a steep increase of the OD between 18 and 20 hr. The addition of phages to the bacteria led at low VBRs to a smaller reduction in OD values. However, OD values also did not increase very strongly afterwards. The higher the VBR, the more reduction in bacterial cell density could be observed, albeit this was accompanied by a strong increase in OD afterwards. High VBRs reached more or less the control OD values, whereas for lower VBRs this could not be observed.

Effect on biofilms. A number of different experiments investigated the effect the isolates had on *P. aeruginosa* grown in a biofilm. **Figure 3-17** depicts the biofilm formation of *P. aeruginosa* in minimal medium over time, without the presence of phages. The low and more or less invariant optical density along the initial time span (up to 10–14 hr) indicated no pronounced biofilm formation. Only upon longer incubation times an increase in the optical density could be observed, which means that after 14 hr, cells were organized in a biofilm.

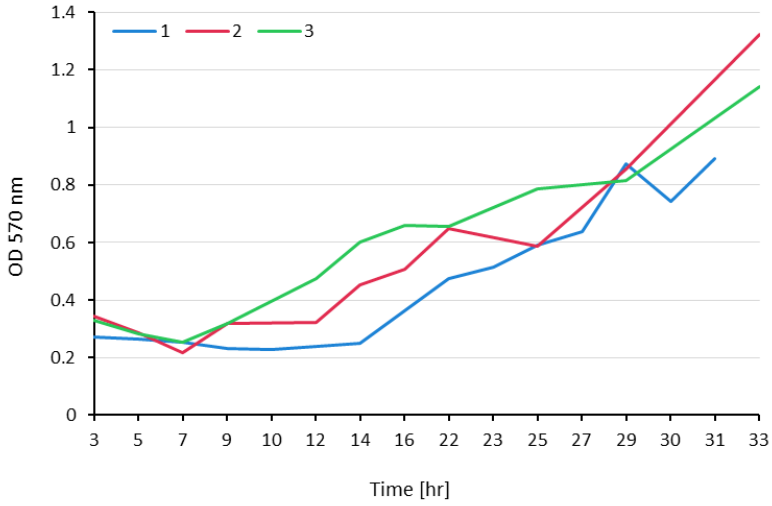

Figure 3-17: Biofilm formation of *P. aeruginosa* in three different preparations.

In a first attempt, bacteria were incubated for 2 to 25 hr *prior to* the addition of 4.00×10^9 PFU of the respective phage isolate. The viruses were added 1 hr before the staining occurred. Here, no difference to the bacterial control could be observed (data not shown). This implies that the duration of the co-incubation was not sufficient to cause any visible effects on the formed biofilms. As a next step, the co-incubation time was extended for up to 8 hr. In this experiment, the formation time of the biofilm was varied between 2.5 and 27 hr with a subsequent co-incubation time of the viruses with the biofilm ranging from 2–8 hr. A co-incubation for 8 hr together with a 21 hr old biofilm resulted for phages BAL 1–3 in higher OD values, indicating an increased formation of biofilm compared to the bacterial control (Student's t-test $p < 0.05$) (**Figure 3-18**, left figure). A longer incubation time of the bacteria for 23 hr together with a co-incubation of 6 hr resulted only for BAL 1 in a significant difference compared to other incubations. This indicates that here, phage isolates were not able to reduce the aggregated bacteria, but rather induce the formation of more biofilm. For BAL 4 and 5 no effect at all on the *P. aeruginosa* biofilm could be detected. Also longer biofilm incubation times of 25 and 27 hr together with 4 or 2 hr of virus co-incubation did not result in a notable reduction of the bacteria

for all tested phages. Interestingly, a short pre-growth time of 2.5 hr followed by 6 hr of virus co-incubation significantly increased the measured OD, indicating an enhanced formation of biofilm (**Figure 3-18**, right figure). Longer bacterial incubation times with shorter virus co-incubation times did not result in any significant difference between the bacterial control. The duration of the presence of viral particles is therefore more important, than the time the bacteria have for the formation of a biofilm, as only long co-incubation times of 8–6 hr resulted in a significant increase in the bacterial population for some phages (BAL 1–3). This could especially be observed in **Figure 3-18** (right figure) as here the longer duration of the presence of phages resulted even with the short biofilm formation time of 2.5 hr (a span, at which no biofilm has been formed yet, according to the growth curve in **Figure 3-17**) in an increase of the OD, indicating a strong expansion of the biofilm.

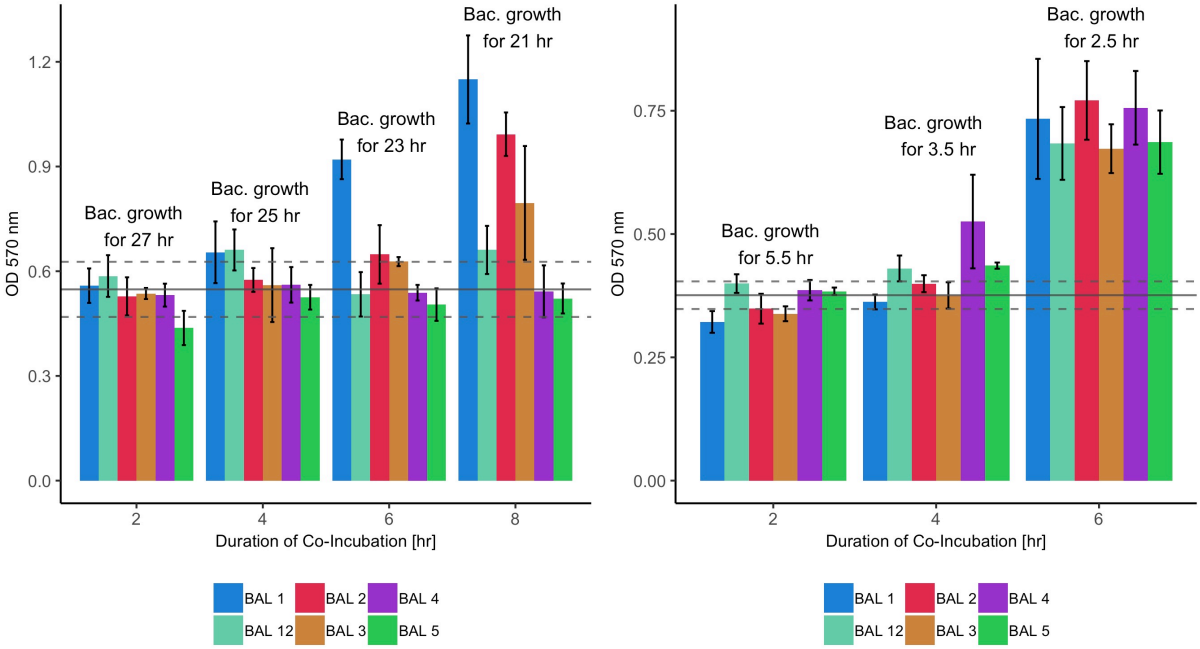

Figure 3-18: Biofilm formation in the presence of phages. Left panel: Bacteria were incubated 21–27 hr before 0.1 VBR phages were added. As staining occurred at the same time, variations in the duration of the co-incubation occurred. In total, an incubation was conducted for 29 hr. Right panel: Bacteria were incubated 2.5–5.5 hr before 0.1 VBR phages were added. In total, the incubation lasted for 7.5 hr. Horizontal gray lines: Average bacterial growth (solid line) without presence of phages with standard deviations (dashed lines).

Next, the effect different VBR have on a biofilm was determined. Bacteria were initially incubated for 28 hr before different VBR (0.1, 1 and 10) were added and co-incubated for another 17 hr. All optical densities were significantly elevated compared to the bacterial control

($p < 0.05$) (**Figure 3-19**). A significant difference was only observed for BAL 5 between the VBR of 0.1 and 1, for BAL 8 between the VBR of 0.1 and 10 and BAL 9 between the VBR 1 and 10 ($p < 0.05$). For all other phages and VBR, the amount of added viruses did not result in any detectable difference.

Consequently, only long co-incubation times of phages and bacteria resulted in significant increases in the measured OD values. The ratio of the added viruses to the bacteria did not have any considerable effect on the bacterial population, similar to a long growth time of the biofilm *prior to* the addition of phages.

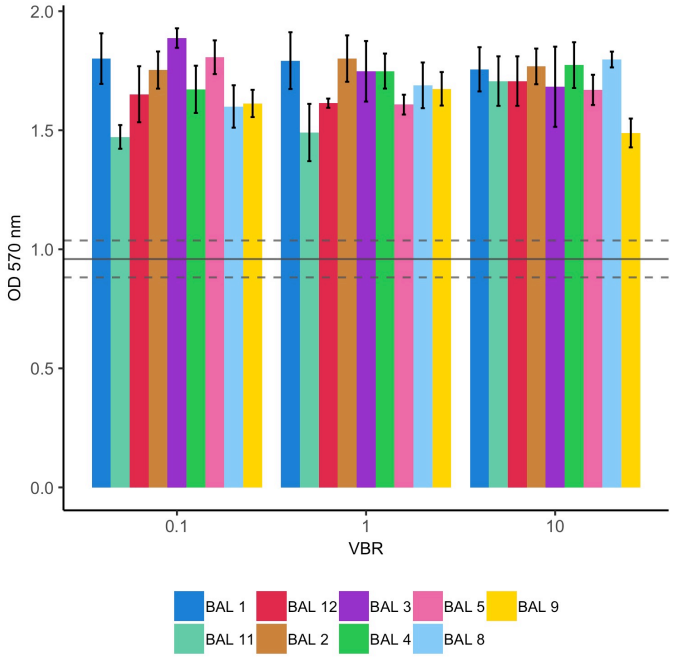

Figure 3-19: Biofilm formation in the presence of phages at different VBR. Bacteria were incubated for 28 hr *prior to* the addition of different VBR of phage isolates. These were then co-incubated for 17 hr before the staining was conducted. Horizontal gray lines: Average bacterial growth (solid line) without presence of phages with standard deviations (dashed lines). Significant difference (Student's t-test) for the phages BAL 5 between VBR 0.1 and 1 ($p < 0.05$), BAL 8 between VBR 0.1 and 10 ($p < 0.05$) and BAL 9 between VBR 1 and 10 ($p < 0.05$) was observed.

PCR. After extraction of DNA several PCRs targeting genes specific for different viral families were conducted. The primer pair g20 amplifies the 600 bp long portal-vertex-capsid protein gene of cyanomyoviruses (T7-like phages) [232]. None of the isolates were successfully amplified using g20 primers. Similar result was achieved by PCR with DNApol primers. These primers amplify the polymerase homologue (T7-like) [235], but here as well, no amplification of the isolates occurred. The last tested primer was g23, which amplifies the major capsid protein gene

g23 of *Myoviridae* (T4-like phages) [233]. The product ranges between 450 bp to 650 bp. Here, most of the viral isolates were amplified, although the fragment size was with ca. 350 bp smaller than expected (**Figure 3-20**). Only for isolates BAL 1–3, the g23 PCR resulted in no bands. For Inc 5 and 6, only a weak band could be detected, which was mostly overlaid by primer-dimers.

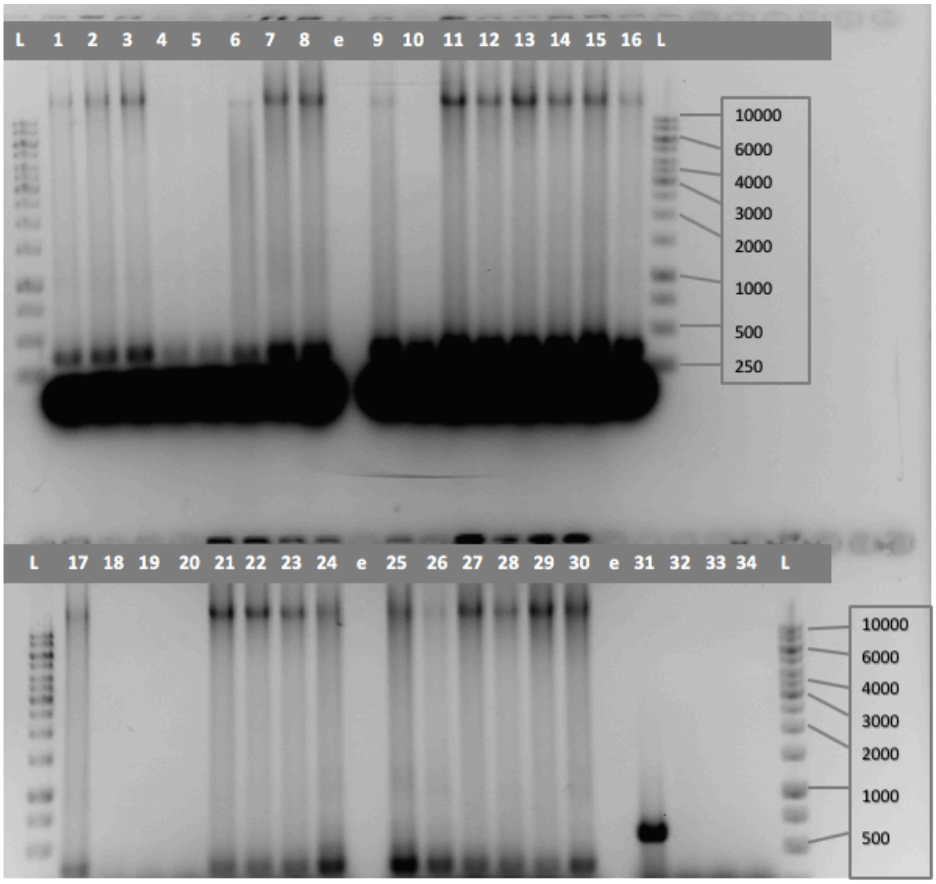

Figure 3-20: Result of g23 PCR. Abbreviations: L: 1 kb ladder, fragment sizes are given on the right. e: empty lane. Lanes 1–17: Inc 1–3, 5, 6, 9, 10, 12, 13, 15–17, 21, 23, 24, 26, 33. Lanes 18–30: BAL 1–5, 8, 9, 11–13, 15, 16, 20. Lane 31: T4 DNA. Lane 32: T7 DNA. Lanes 33 and 34: negative control.

As most of the bands were similar in size, the genetic difference of the viral isolates was presumably not very pronounced. As these primers, although degenerated and thus allowing more variability in the recognized sequences, were covering only a small proportion of a genome, the genetic diversity was further characterized by restriction enzyme digestion.

Digestion. The viral DNA was digested with the enzymes AluI, HhaI, NdeI, and EcoRI to generate restriction fragment length polymorphisms. No digestion was visible using the enzyme NdeI. EcoRI (**Figure 3-21**), AluI and HhaI (both results not shown) resulted in a fragment pattern; however, there were no differences in the patterns between the samples, indicating a certain

genetic similarity of the isolates. The DNA of the phages BAL 1–3 and Inc 6 was not digested with EcoRI. As T4 and T7 DNA was not digested as well, the concentration of the DNA was in all likelihood not high enough, as all enzymes were chosen according to their capability to digest T4 and T7 phage DNA.

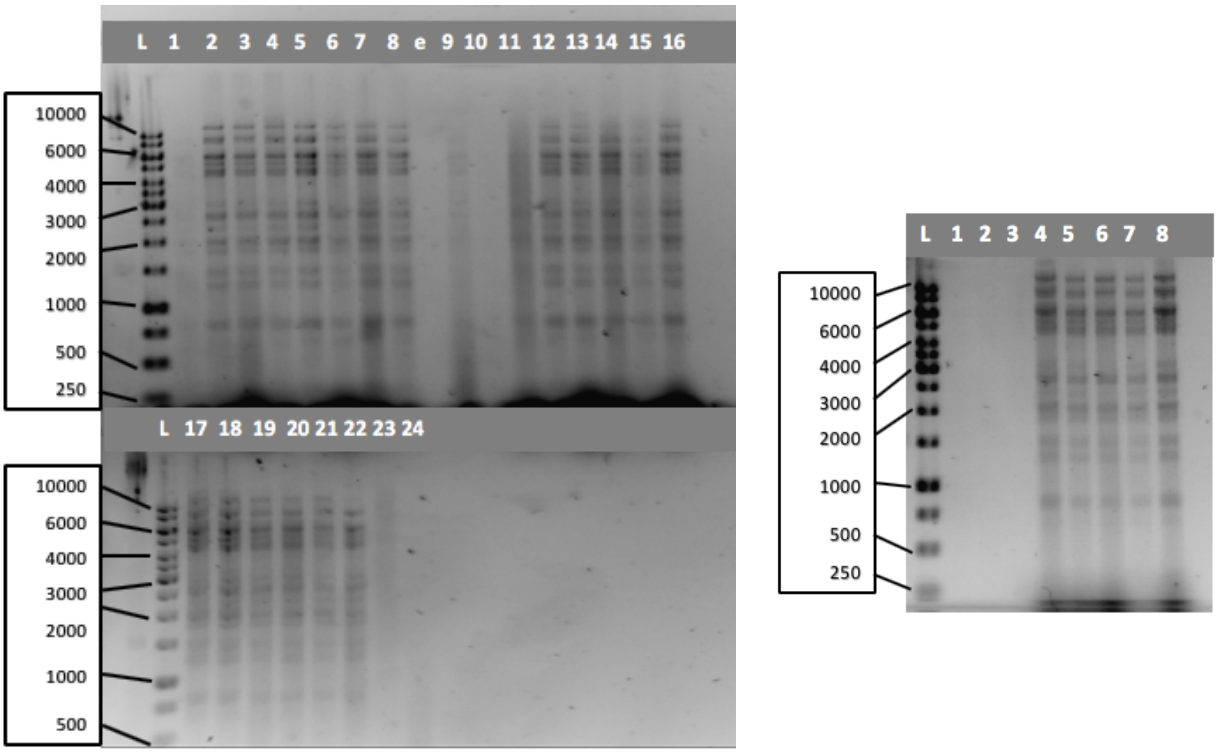

Figure 3-21: Digestion with EcoRI. Abbreviations: L: 1 kb ladder, fragment sizes are given on the left. e: empty lane. Left picture: Lanes 1–5: BAL 12, 13, 15, 16, 20. Lanes 6–22: Inc 1–3, 5, 6, 9, 10, 12, 13, 15–17, 21, 23, 24, 26, 33. Lane 23: T4. Lane 24: T7. Right picture: Lanes 1–8: BAL 1–5, 8, 9, 11.

Metagenomic sequencing. With the enzymatic digestion, first doubts in the genetic diversity of the different isolates appeared. Therefore, metagenomic sequencing was performed in order to get better insights into the genomic composition of the isolates. The contigs were assembled using the Newbler c2.7 software package. Surprisingly, the assembly resulted in only one phage genome with the size of 66 kbp. In order to exclude the possibility of a disproportional amplification of just one isolate, a primer pair was designed with the NCBI primer-BLAST online tool [250] to amplify only a part of the genome and to repeat the sequencing for only this fraction of the genome. The primer pair targets the gep5 protein, which showed 18 % similarity to gp20 and resulted in a fragment length of 407 bp. Additionally, a modified reverse primer with a substitution at position 16 from G to AC was used (gep5_rev_16G>AC) to amplify the

same fragment (**Figure 3-22**). From the sequencing result, this position could not exactly be determined.

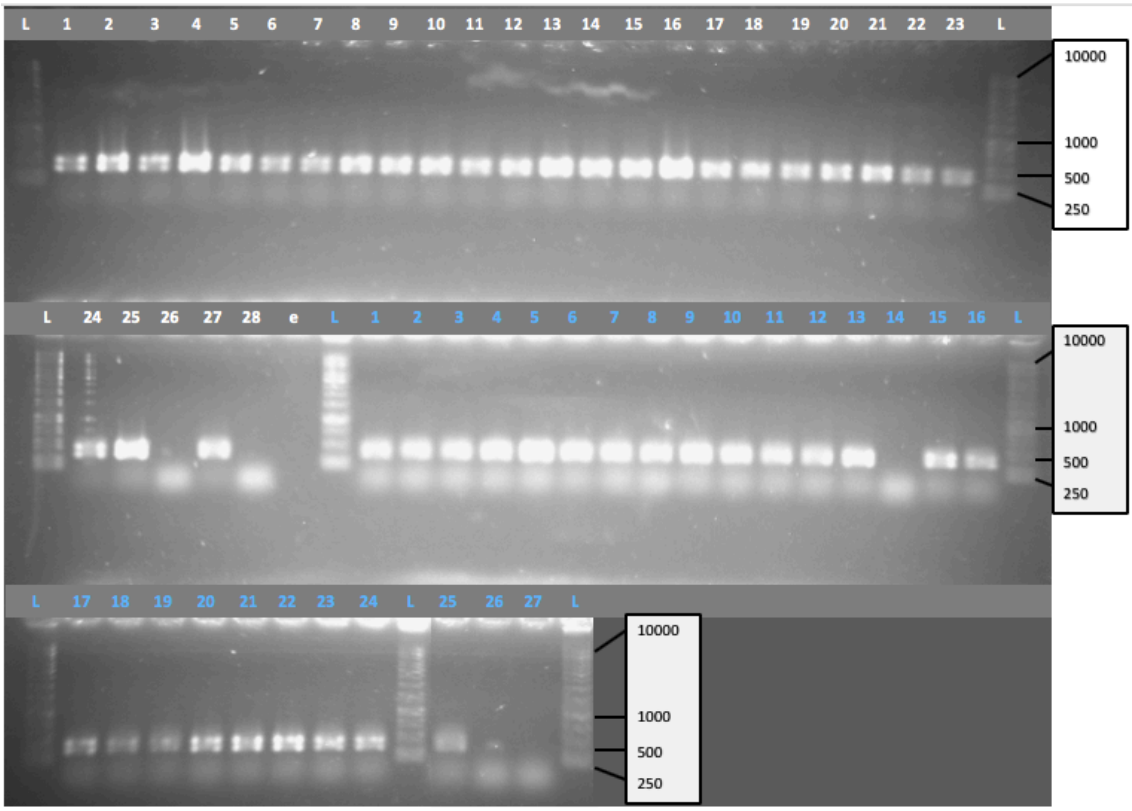

Figure 3-22: Result of gep5 PCR. Abbreviations: L: 1 kb ladder, fragment sizes are given on the right. e: empty lane. White labels: primer gep5_rev. Blue labels: primer gep5_rev_16G>AC. Lanes 1–24: BAL 4, 5, 8, 9, 12, 13, 15, 16, 20, Inc 1–3, 9–11, 13, 15–17, 21, 23, 24, 26, 33. Lane 25: positive control. Lanes 26 and 28: negative control. Lane 27 (white): BAL 9. Lane 27 (blue): negative control.

The following PCR mixes were purified (2.3.10.2) and sent out for sequencing to Eurofins company (**Table 6-4**, supplementary material). Results were aligned using MAFFT multiple sequence alignment tool (https://www.ebi.ac.uk/Tools/msa/mafft/). By visualizing the aligned sequences using Jalview (v 2.10.5), mostly no difference in the sequences could be detected (**Figure 6-1**, supplementary material).

As next step, the sequencing was repeated with a different primer pair amplifying a longer sequence (916 bp). In order to capture small differences, PCRs were performed using Phusion High Fidelity Polymerase. Only phage isolates BAL 4, 5, 8, 9, 11–13, 15, 20 and Inc 2, 3, 15, 21, 23, 24, and 26 were chosen for sequencing as here, the PCRs resulted in a single band. For phages Inc 9, 10, 13, 16, 17, 33 and BAL 16, a second band appeared around 550 bp, consequently they were not included. PCR products were again purified (2.3.10.2) and sent out

to Eurofins for sequencing. However, alignment with MAFFT and visualization with Jalview did not account for any differences, again.

3.2.4 Discussion

P. aeruginosa is an opportunistic bacterium ubiquitously present in various biotic and abiotic habitats [221]. The successful isolation of phages from sewage water of a wastewater treatment plant is therefore not surprising. *P. aeruginosa* is a problematic nosocomial pathogen deteriorating the situation of many patients suffering from chronic diseases, such as COPD or cystic fibrosis. In general, viral and bacterial pathogens are not only accelerating the progression of COPD, but also indirectly damaging the tissue of the lungs. However, the dominant species change with increasing disease progress and severity. *Streptococcus pneumoniae* is for example more prevalent in mild COPD, whereas in severe clinical courses of COPD *P. aeruginosa* can be found more often [283,284].

Contrary to the expectations, from 16 BAL samples that were taken from patients suffering from mild to severe COPD, only one sample was tested positively for the presence of phages of *P. aeruginosa*. Besides, phages could only be isolated for the wildtype strain (PAO1), but not for the clinical isolate of *P. aeruginosa*. Incubations of the sputum samples did not result in any isolated phages. The dense structure probably impeded the access of viruses in the samples. In order to tackle this issue, chemical or mechanical liquefaction might be used in future. Precaution has to be taken regarding the damaging of viral particle through mucolytic agents such as dithiothreitol or N-acetyl-L-cysteine [285,286]. These substances act by cleaving disulphide bonds, thus the protein capsid of a virus might be affected as well. Also mechanical treatments, such as bead-beating or sonication might render the particle inactive [287]. Hence, these methods have to be evaluated with care for their applicability on the isolation of active phage particles. The optimal temperature for infection was for all isolated phages between 36–42 °C (**Figure 3-8**). As their host prefers a temperature of 37 °C for optimal propagation, this result was expected [288]. The maintenance of infectivity also over a longer period of time allows for a therapeutic application of the phages (**Figure 3-9**). Lower temperatures influence the bacterial growth negatively, therefore the viral infectivity could not be estimated using plaque assay. The same was true for the incubation under extreme pH values (**Figure 3-10**). Very acidic environments were not well tolerated as here, bacterial growth was affected negatively. Besides, standard deviations were very high, indicating that either the bacteria were impaired in their growth and result in inconsistencies, or the viruses were affected and some of the clonal

isolates were more sensitive than others. Most isolates had their optimum at neutral or slightly acidic pH value. However, for some phages the pH did not play a major role for their infectivity. Generally, an alkaline environment was tolerated more than the very acidic environment at pH 4. The isolates themselves were very specific, as even bacteria of the same genus were not infected.

The selective pressure phages impose on a bacterial population could be well demonstrated with an incubation of phages and bacteria under different VBR. The presence of very high viral titers increases the selective pressure on bacteria. Here, fast development of resistance is beneficial and the associated fitness costs are minor, compared to the high risk of being infected by these lytic phages. This development could be observed in the initial lower concentration of the bacterial host due to the virus-induced cell lysis at high virus-to-bacteria ratios (e.g. in **Figure 3-16** for VBRs 50, 10 and 5). With progressing incubation time, the numbers of bacteria increased and even surmounted the control numbers (**Figure 3-13**). Here, the bacteria obviously acquired resistance against the applied phage isolate very soon. Remaining susceptible cells were still lysed by the phages, thus contributing to the pool of nutrients in the preparations. This might also be the reason for the higher density in these settings compared to the bacterial control. For very low VBR, the selective pressure on the bacteria is comparably low, therefore only a smaller amount of bacterial cells were lysed. As consequence, no anti-phage defense mechanisms evolved. Bacteria stayed fully susceptible and their cell density increased slowly over time (**Figure 3-15** for VBRs 0.05 and 0.1). However, it seems that for some co-incubations bacteria start to develop some resistance over time, as here the cell density increased stronger (**Figure 3-14** for VBRs 0.05 and 0.1). In those cases, the VBR shifted towards a higher ratio as phages have killed more bacteria, leading to increased viral numbers in the preparations. With increasing VBR also the selective pressure increased and thus promoted the development of a resistant bacterial subpopulation.

The lytic activity of the isolates could however not be proven for cells grown in biofilms. Presumably, the viral isolates did not have the ability to access the bacteria protected by an EPS layer. As these viruses were isolated based on their capability to lyse planktonic cells, the lack of EPS-degrading enzymes is therefore not that implausible. Some of the isolates (BAL 1–3) were not just incapable of hydrolyzing the protective layer, their presence even enhanced the formation or growth of the biofilms (**Figure 3-18**, left picture). This trend could also be observed with very young biofilms. According to the growth curve of the *P. aeruginosa* biofilm, only after about 16 hr an increase in the OD, respectively an increase of the biofilm could be observed

(**Figure 3-17**). The addition of phages to biofilms that were only grown for few hours, led to a strong increase in biofilm compared to the control without phages added (**Figure 3-18**, right picture). On the other hand, a long growth time of the biofilm in combination with only a very short presence of phages did not result in any differences compared to the control. Also variations in the VBR did not have any pronounced effect. Only if biofilms were exposed to phages long enough, an effect, albeit positive for the bacteria, could be observed. Consequently, these isolates are not suitable at all for the treatment of *P. aeruginosa* infections or the decontamination of surfaces, as in those cases the bacteria are mostly organized in biofilms.

Viruses are very diverse in their genetic composition and no universal genetic marker that spans all or at least most viruses, could be identified yet. It is therefore very surprising that the viruses isolated here show a great similarity in their genetic composition, as it became apparent during the restriction enzyme digestions. Of the tested four enzymes only NdeI was not able to find its cutting sites in the viral DNA. EcoRI, HhaI and AluI were able to digest the DNA, however the band pattern was similar in all samples. Only BAL 1–3 and Inc 5–6 were not digested with EcoRI (**Figure 3-21**). As for these samples, the concentrating of viral particles *prior to* DNA extraction was accomplished by $FeCl_3$ precipitation, this lack of bands might refer more to a low DNA concentration as a result of this method, than to an absence of EcoRI restriction sites. It seems likely that either the iron or the EDTA (from the EDTA-ascorbate buffer used for resolving the viral particles from the iron) was not removed entirely during the DNA extraction and now acts inhibitory on the restriction enzyme.

As for the application of different degenerative primers, only g23 which targets the major capsid protein gene of T4-like phages resulted in a weak amplification, with most of the primers forming primer-dimers (**Figure 3-20**). The fragments were with approximately 400 bp relatively small in size. Similar to the restriction digestions, no band was visible for BAL 1–3 and Inc 5–6. Purification of the g23 DNA fragments in order to sequence this fragment was performed (2.3.10.2), however, sequencing of the fragment with Eurofins sequencing service was repeatedly not successful. Viral DNA was therefore prepared for metagenomic sequencing. Previous genetic analyses indicated already a great similarity between the isolates. The assembly of the sequenced contigs confirmed this similarity. In fact, the DNA mixture of phages could be assembled to only one phage genome. To rule out any unequal amplifications due to different DNA concentrations in the sequenced mixture, a primer pair was designed based on the metagenomic sequence, which amplifies a 407 bp long fragment. Purified PCR products were again sent to Eurofins for sequencing. As neither of the sequences showed any variability, a

second primer pair, spanning over a longer sequence (916 bp) was designed. This time, the PCR was performed using the Phusion High Fidelity Polymerase, as this enzyme shows a better proof-reading function. Also this longer fragment did not account for any differences in the amplified region. The question, whether the genomes of the different isolates were indeed very similar or whether a contamination during the isolation occurred and only one phage was actually isolated in the end could not be conclusively clarified. The genomic sequence of the isolated phages resembled the sequence of phage vB_PaeM_CEB_DP1 by 98 %, which was originally isolated from hospital sewage [289]. The same research group has also shown the general high genetic similarity of their isolate compared to other *P. aeruginosa* phages from the same genus *Pbunalikevirus*: 95.6 % identity with phage LMA2, 94.3 % identity with phage KPP12 and 93.1 % identity with phage vB_PaeM_PAO1_Ab27 [289].

3.3 Viral impact on microbial communication

This chapter has been submitted to the journal *Royal Society Open Science* and is currently under review:

Ghorai, A., **Feichtmayer, J.**, Pérez-Velázquez, J., Rothballer, M., Kuttler, C., Griebler, C., Deng, L. & Hense, B. A. Do lytic bacteriophages interact with quorum sensing in *Pseudomonas putida*? Modelling evaluation of batch experiments. Submitted.

3.3.1 Description of the experiment

Prior to this experiment, lytic phages were isolated from the income water from a wastewater treatment plant targeting *Pseudomonas putida* IsoF, similar to the description in 3.2.

For each experimental setup, 150 µL of a frozen stock aliquot of *P. putida* IsoF was inoculated in 150 mL ABC medium (2.2.3) and incubated at 30 °C with constant agitation at 200 rpm. A mixture of five different viral isolates was then added at different time points to the system. These time points were chosen according to the bacterial cell density and the activity status of the QS system. The concentration of the added phage mixture was adapted to the bacterial cell density (confirmed by optical density measurements at 570 nm) at the moment of addition. A virus-to-bacteria ratio of 10, mimicking natural ratios in aquatic habitats, was chosen [5]. Four different conditions were selected: (i) In setting A, phages were added after 6 hr of bacterial incubation. At this time, the QS system was still inactive with an HSL concentration below the critical threshold of around 100 nM [265]. (ii) For setting B, phages were added after 10 hr. Here, the bacterial cell density has reached the threshold density and the QS system started to be activated, but was still not fully induced, yet. (iii) For the third setting (C), phages were added after 14 hr of incubation to a fully active QS environment. (iv) Setting D denotes the control, where no phages were added to the system. Samples were taken every 2–3 hr to measure bacterial cell density at 570 nm using the Victor2 Microplate Reader, phage titers (by flow cytometry, 2.3.7.2) and concentrations of HSL and HS, the degradation product of HSL (2.3.13). Each condition was tested in biological duplicates and every measurement was conducted in technical duplicates, HSL and HS quantifications were measured in triplicates. A conversion factor for the translation of OD values to their relating cell numbers was established by flow cytometric cell counts and simultaneous OD measurements of a *P. putida* IsoF culture in ABC medium over time [290].

3.3.2 Experimental results

Figure 3-23 A shows the control values of an undisturbed system (setting D). The graph resembled a typical growth curve, from lag to log phase, followed by an exponential and a stationary phase. Related to the bacterial growth was the curve progression of the HSL concentration. It slowly increased with increasing cell density, and with exceeding a threshold concentration, HSL augmented exponentially. This is a result of the positive feedback loop, which was initiated once the quorum was reached. After some hours, a decline in HSL concentration could be observed, which correlated with an increase in its degradation product HS. This correlation pointed towards a contribution of the QS-dependent HSL degradation mechanism. The addition of the phage mixture after 6 hr of incubation only delayed the bacterial growth and the HSL/HS production (**Figure 3-23 B**). Bacteria reached the exponential phase some hours later compared to the control with only a slightly reduced maximum cell concentration. The virus-induced bacterial cell lysis affected a certain susceptible subpopulation. However, resistant subpopulations were either already present in the system or have developed upon the predatory pressure. HSL concentrations showed a delayed increase as well, but reached a comparable maximum concentration as the undisturbed control. However, HS concentrations were much lower compared to the control. The increase of HS was much flatter and also the maximal concentration was halved. This is already an indication that the quorum sensing system is affect by the presence of phages to some extent. The addition of phages to a just activated QS system aggravated this effect on the QS even more (**Figure 3-23 C**). In setting C, the bacterial cell growth was again delayed, but finally reached similar concentrations compared to the control, although more time was needed. However, with addition of the phages, the HSL concentration collapsed. With time, HSL increases again, but it did not reach the required threshold concentration for QS activation anymore, although cell densities raised above the threshold concentration. As a consequence of the low HSL concentration, the HS concentration was also pending around zero. The effect of the phages on the QS system was even more pronounced, when they were added to a fully activated QS system (**Figure 3-23 D**). The general course of the bacterial cell density resembled more the control. The addition of the phages took place at a time, when the bacterial numbers were high enough, so that the presence of the phages manipulated the bacterial hosts to a lower extent than in the settings before. Nonetheless, the maximum concentration of approximately 3.0×10^{11} cells L^{-1} was not reached anymore. Here, the addition of the phages led to a collapse of the HSL concentration as well, from which no recovery could be achieved. Again, HS concentration was pending around zero.

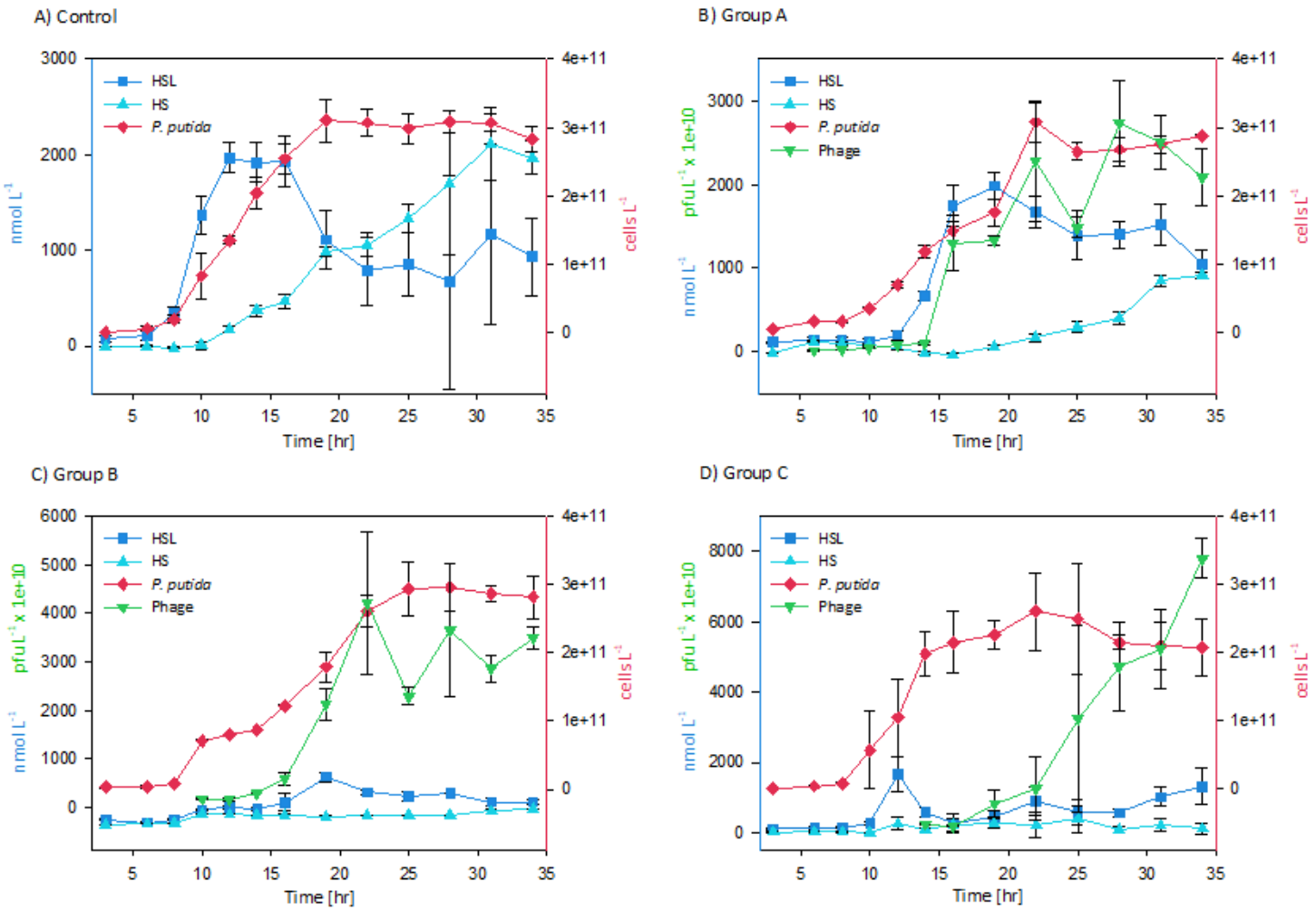

Figure 3-23: Average concentrations with standard deviations. Dark blue: HSL concentration [nmol L^{-1}]. Light blue: HS concentration [nmol L^{-1}]. Red: *P. putida* IsoF concentration [nmol L^{-1}]. Green: phage particles [pfu $mL^{-1} \times 10^{10}$]. A: control setting. B: Group A: Phages were added after 6 hr. C: Group B: Phages were added after 10 hr. D: Group C: Phages were added after 14 hr.

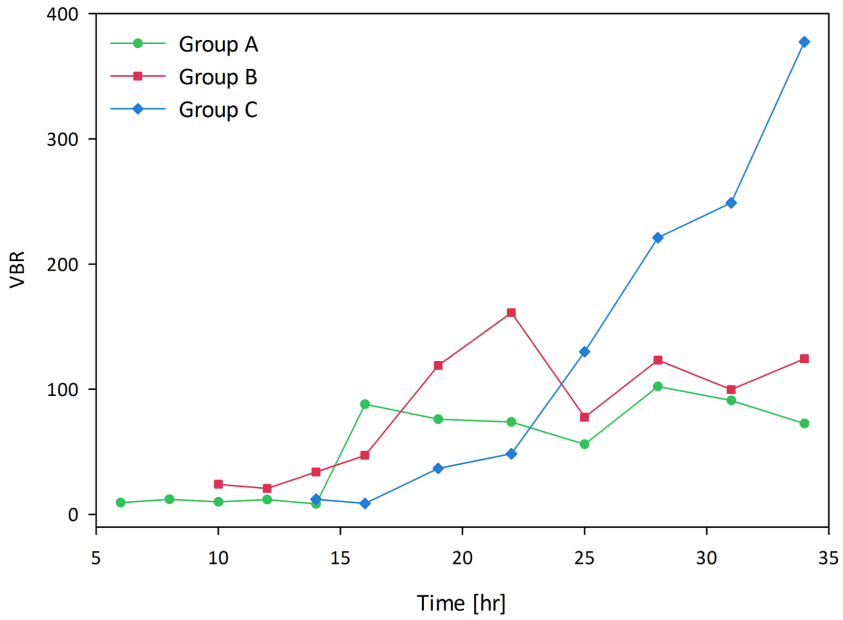

Figure 3-24: Calculated virus-to-bacteria ratios (VBR) for the setting A, B and C. Green: Group A (phages were added after 6 hr). Red: Group B (phages were added after 10 hr). Blue: Group C (phages were added after 14 hr).

By taking also the viral titer into account, the importance of the addition time point and thus the status of the QS system becomes clear (**Figure 3-24**). When phages were added after 6 hr, their influence was minor on the complete setting, as only the increase in the bacterial concentrations was slightly delayed. According to the group D data (**Figure 3-23 A**), a HSL concentration of 1.5–2.0 mmol L^{-1} defines the threshold beyond which the QS system is activated. Assuming now a similar concentration for Group A, the time of a QS activation can be scheduled between 10 and 15 hr. From the addition of the phages at 6–14 hr of incubation, VBRs remained constant (**Figure 3-24**). Between 14 and 16 hr, a remarkable increase in virus titer could be observed, embodied by a high VBR. After that, however, the VBR declined again, indicating some reinforced anti-phage defense, rendering less bacteria susceptible. After 25 hr, the degradation of HSL is in full swing and the QS system is gradually deactivated. This was reflected by a strong increase in phage titer. Nonetheless, after 28 hr of bacterial incubation, viral titers decreased again, which can be explained by a reduced growth of the stationary phase bacteria, providing less metabolic active cells for the viruses to infect and replicate. In the case of a lacking activation of the QS system, a steady increase of the VBR could be observed. For group B an exponential increase until 22 hr could be observed, followed by fluctuations in the VBR. However, the strong decrease after 22 hr might be an outlier measurement of the virus

titer. After 22 hr, the bacteria reached the stationary phase, thus explaining the decline in the VBR. In group C, the VBR increased moderately until 22 hr, only to then ascend exponentially, and even reaching the stationary phase did not lead to a decline as it could be observed for groups A and B. Summing up, the specific moment of the appearance of lytic phages in a *P. putida* population does indeed have an effect on the bacteria. A previously developed comprehensive mathematical model of the QS system of *P. putida* [263,269] was adapted and further improved in order to simulate the interaction with lytic phages.

3.3.3 Model predictions and data fitting

Hypothesis 1. Regarding the model testing hypothesis 1, that is there is no influence of the presence of phages on the QS system, results are plotted in **Figure 3-25**. Fitted parameter values are listed in **Table 6-5** (supplementary material). For the fitting, the control group D was used to determine the parameters, except those concerning the phages. Those were fitted using group A data. All parameters except for the growth rate of the resistant bacteria were kept in an expected range according to values previously found for *P. putida* [263,265] with some variations due to small differences in the experimental setting. As here it was assumed that the QS is not interfering with the development of phage resistance, the phages would always infect the most abundant group of bacteria, which is the non-resistant bacteria. After the first rounds of replication of the phages in the non-resistant bacteria, suitable hosts get less abundant, finally resulting in a co-existence between phages and bacteria.

Bacterial population dynamics can be predicted by the model in the case of group D and group A, but as soon as phages were added at a time of on-going (10 hr, group B) or completed (14 hr, group C) activation of the QS system, experimental data behave different than the model predicts. Likewise, phage titers and HSL concentrations cannot be predicted using this model. Hence, it was not possible to find a parameter fit, which was able to adequatly describe all data sets of the experiment at once using this basic model. These findings suggested that hypothesis 1 is not applicable and that some alternative or additional mechanisms must have a relevant influence on the dynamics.

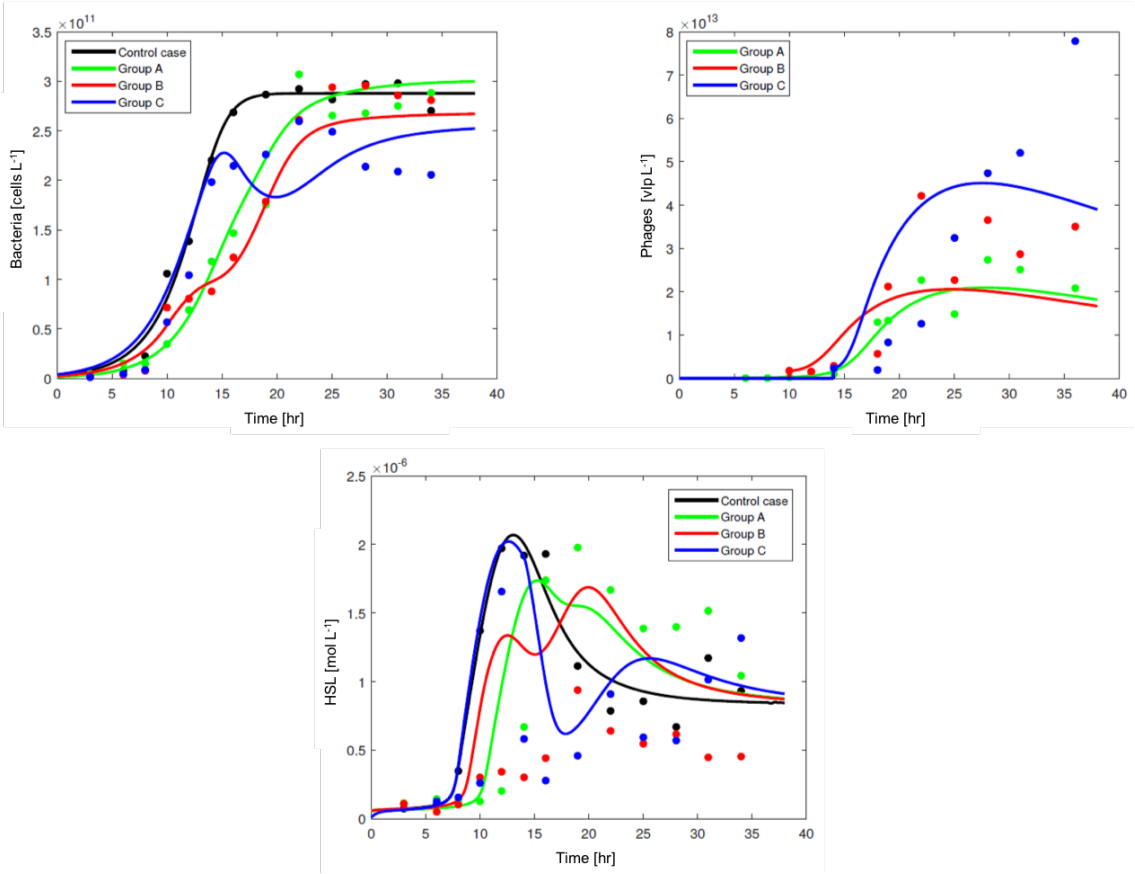

Figure 3-25: Modeling results for hypothesis 1. Dynamics after fitting of bacterial densities, phage titers and HSL concentrations in the basic model, assuming no influence of phages on the QS system. Dots represent experimental data. Solid lines reflect the corresponding model predictions. Black: control group D. Green: group A. Red: group: B. Blue: group C.

Hypothesis 2. This hypothesis is based on the idea that QS is a bacterial stress response with phages considered as stressors. As a consequence, the presence of phages might influence the strength of the QS activity via an altered HSL production rate. Consequently, the parameter values for the HSL production (α and β) changed according to the presence or absence of phages in the system. These parameters were fitted after the phage addition together with the phage dynamics parameters (ρ, δ, γ_t and c) for all three experimental settings (groups A, B and C) at once, while all other parameters were kept unmodified. As **Figure 3-26** shows, predictions of the bacterial and viral populations were not affected by the changes applied for implementing hypothesis 2. However, a better fit for HSL concentration predictions for setting A could be obtained. An optimal fit suggested a much lower basic HSL production rate α, with a sightly upregulated Ppur:HSL regulated production rate β, as can be seen in **Table 2-9**. However, especially at later time points, the basic HSL production rate became very low, and thus was hard to determine accurately. Besides the better fit for group A, data for the groups B and C

were still not predicted satisfactory enough, especially with regard to the late increase in phage titer observed in group C.

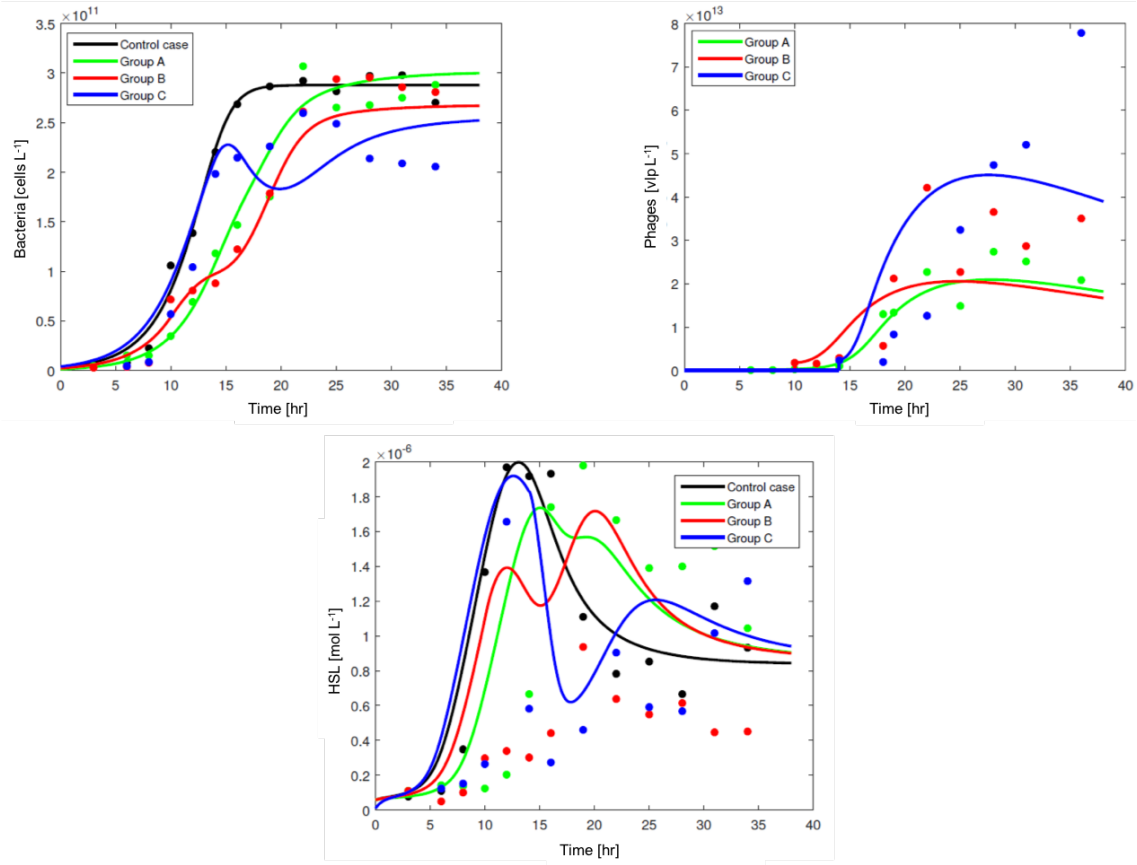

Figure 3-26: Modeling results for hypothesis 2. Dynamics after fitting of bacterial densities, phage titers and HSL concentrations in the basic model, assuming an influence of phages on the HSL production. Dots represent experimental data. Solid lines reflect the corresponding model predictions. Black: control group D. Green: group A. Red: group: B. Blue: group C.

Hypothesis 3. As a next step, a more direct interaction between the presence of phages and the production rate of the HSL receptor PpuR was assumed. As a consequence, the intracellular level of PpuR changed with presence of phages, which is expressed by changes in R_C. During the fitting process, R_C was increased by a factor of 3.5, which improved the congruency of the HSL predictions with the data (**Figure 3-27**). Nonetheless, the matching was not sufficient enough, although the tendency was better represented with only the specific values not matching. Also bacterial density predictions were Still, phage populations were only poorly predicted using this model adaption, with again only group A matching to the experimental data. improved across all groups.

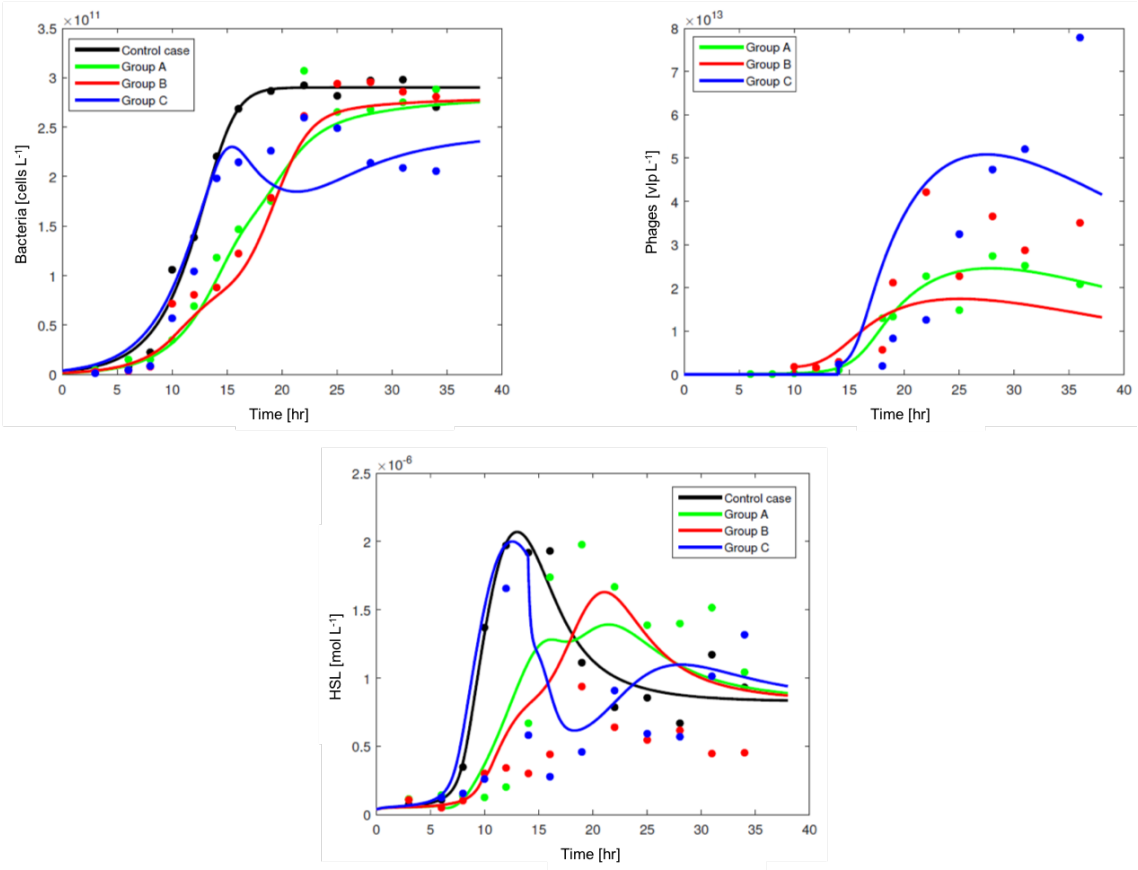

Figure 3-27: Modeling results for hypothesis 3. Dynamics after fitting of bacterial densities, phage titers and HSL concentrations in the basic model, assuming an influence of phages on the PpuR production. Dots represent experimental data. Solid lines reflect the corresponding model predictions. Black: control group D. Green: group A. Red: group: B. Blue: group C.

Hypothesis 4. The development of a bacterial population may be influenced by the specific protection strategy against phages and the associated fitness costs. Thus, changes in the proportions of the distinct bacterial sub-populations (resistant or non-resistant) may be of relevance. This hypothesis 4 is based on the assumption that, in addition to other QS-induced behaviors, the bacteria become more resistant against phage attacks compared to QS inactive cells. For the implementation, the parameter values were adapted and a new parameter describing the bacterial resistance (ψ) was introduced (supplementary material, **Table 6-6**). Now, the models were able to better reproduce the experimental findings for bacteria and phage dynamics compared to the previous models (**Figure 3-28**). Nonetheless, improvements of the HSL fitting especially with settings B and C have to be made, as here, although the models

were able to predict the correct trend, predicted and measured concentrations still lack congruency.

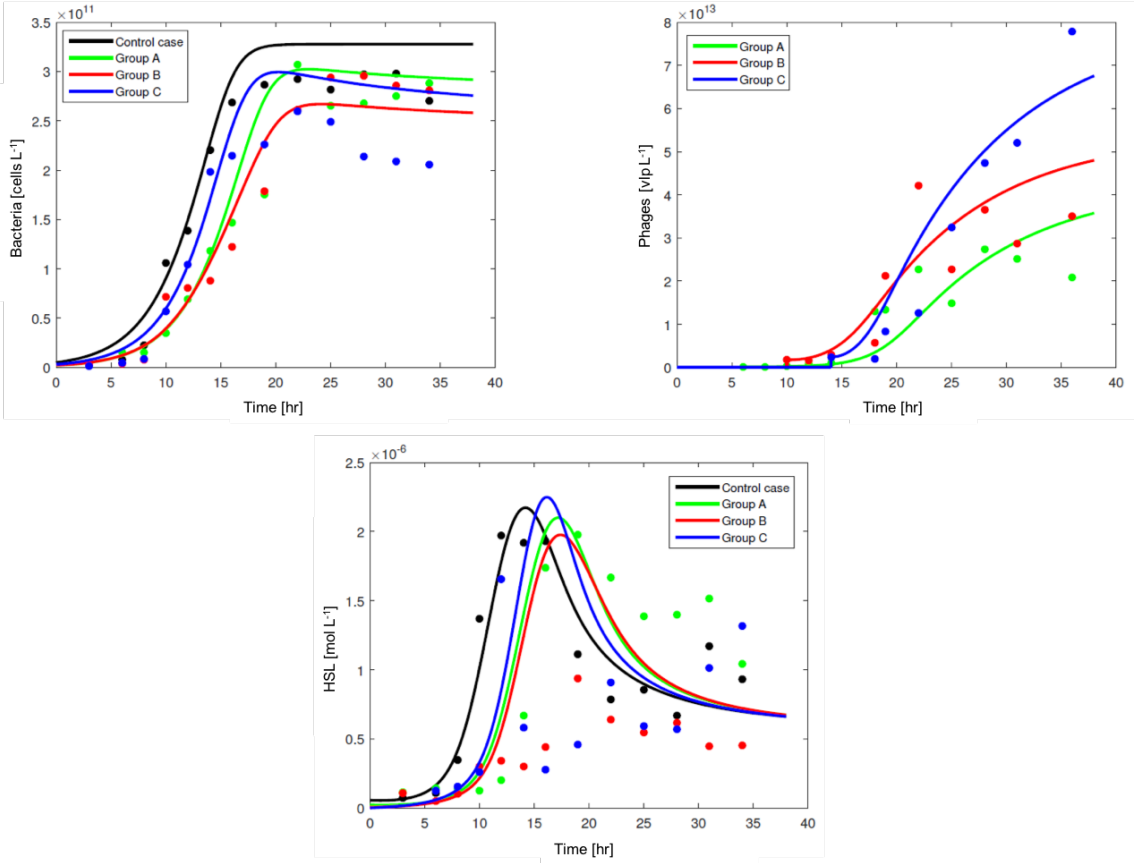

Figure 3-28: Modeling results for hypothesis 4. Dynamics after fitting of bacterial densities, phage titers and HSL concentrations in the model, assuming a QS-driven switch of resistance against phages. Dots represent experimental data. Solid lines reflect the corresponding model predictions. Black: control group D. Green: group A. Red: group: B. Blue: group C.

3.3.4 Discussion

The model strain *P. putida* utilizes a variety of acylated homoserine lactones, including oxo-C10-HSL in its QS system. However, compared to other bacteria, this strain has a rather simple QS system, the *ppu*, which is well understood and described by basic mathematical models [263,269]. By choosing this strain, additional effects that are caused by an interaction between *P. putida* and its lytic phages could be evaluated. Phages were added at a ratio typically for aquatic habitats [5], so that all findings can be related more to natural environments rather than only to laboratory conditions. By adding a mixture of lytic phages at different points in time, a rapid development of bacterial resistance shall be avoided and the bacterial behavior at different QS states (from inactive to active) could be tracked down.

From a general perspective, bacterial and viral populations behaved as expected in all four experimental settings. Upon the addition of the phage mixture, bacterial growth was initially retained for some hours by the lytic activity of the phages, but recovered finally. The later the addition of the phages took place, the more profound effects on the HSL concentration could be observed. Interestingly, the addition of phages to a fully activated QS system immediately led to a strong decrease of the HSL concentration. Although it recovered after some time, HS concentrations did not increase, suggesting that the QS system was not activated despite of a sufficient extracellular HSL concentration (and therefore also cell density). Moreover, degradation of the HSL molecule to HS by the QS-dependent lactonase [263,265,269], could not be observed anymore when phages appear at this later stage of bacterial growth with an activated QS system. This indicated, that the decline of the HSL concentrations was rather due to a reduction in the production rate than due to an enhanced degradation through the lactonase. By examining the development of bacteria populations and HSL or HS concentrations, respectively, it became evident that the time point of the phage addition played an important role. At an early time, with a still inactive QS system, it seemed not to be affected at all during the further course of incubation. After a slight delay in growth, bacterial numbers reached the threshold concentration, ultimately resulting in the QS-dependent degradation of the HSL molecule through the lactonase activity. In a nutshell, the differences in the concentration measurements between the control group D and the early phage addition to a QS-inactive system were only marginal. When phages appeared in the system when the QS was fully active (as in group C), HSL signal imploded immediately. Despite constantly high cell numbers, HSL concentrations increased only slowly over time, yet without any considerable increase in its degradation product HS. There are different explanations that may lead to this observation. HSL was either not produced anymore in the bacterial cells or it was not able to move outside the cell. This would indicate that the phages interacted with or inhibited somehow the transport. As a consequence, the QS was either more or less inactive as no lactonase activity has been observed or, alternatively, HSL was not available for the lactonase to degrade, which would mean that indeed, the QS was active but just the lactonase was lacking a substrate. The gradual increase of the HSL concentration at a later time might be explained by the intracellular presence of HSL molecules, which were released upon phage-induced cell lysis. However, if the lactonase was active, this would subsequently have led to an increase in HS, which did not happen. It could be therefore assumed that the QS system was most likely not active after 20 to 25 hr. Interesting in this setup was the fact that the VBR continuously increased over time, indicating less efficient or less employed phage defense mechanisms (**Figure 3-24**). On the contrary, upon the addition of phages after 10 hr, when the QS system was about to being activated, neither HSL nor HS

could be detected in quantities anymore. It is difficult to say, whether the activation of the QS system was abrogated, as with no detectable HSL, also no degradation to HS by the lactonase could take place. On the other hand, diffusion of HSL molecules might be impeded, so that no extracellular HSL could be detected, but intracellularly available HSL could nonetheless initiate the QS.

In order to better evaluate the relationship between phages, bacteria and the bacterial QS system, mathematical models have been employed. Four different hypotheses that might explain the bacterial response to phage predation and the correlation with the bacterial QS system were tested based on the experimentally generated data. Hypothesis 1 employed the basic *P. putida*-QS model. It considered the simultaneous presence of resistant and susceptible bacteria, but ignored any contribution of QS to a transient bacterial phage resistance. In hypotheses 2 and 3, the basic model was modified by taking additionally possible influences of phages on the QS-dynamics into account, either linked to an increased HSL production (hypothesis 2) or PpuR expression (hypothesis 3). In hypothesis 4, a QS-driven switch of resistance was assumed. In order to evaluate these hypotheses in a systematic and quantitative way, several mathematical models were adopted accordingly. The basic assumptions about the dynamics of growth, bacteria-phage interactions and QS dynamics were directly implemented into an established ODE model which was then gradually further developed.

From literature, it is known that sub-populations of bacteria are already in a resistant mode, even before phages appear in a system [291,292]. This helps to understand why some bacteria could deal with phage attacks better than others, even though they were living under the same condition. This information was picked up in hypothesis 1, which combined most accepted basic assumptions, such as bacterial growth being proportional to the available nutrients, phage infection occurring by law of mass action, initial presence of some resistant bacteria in the system or HSL degradation by QS-dependent lactonase. It was important to consider a resistant subpopulation *ab initio*, as it explained the bacterial growth after phage addition. From the low or lacking congruency of the model predictions with the experimental data, hypothesis 1 was not able to explain the relationships between phages, bacteria and the bacterial QS system (**Figure 3-25**). As here no contribution of the QS system to a phage defense was hypothesized, some contribution of QS cannot be questioned. QS can be seen as a kind of stress reaction of the bacteria towards changes in their environment. These changes may be provoked by lack of nutrients or the presence of competing bacterial species [293]. In a broader sense, also phages can be seen as a form of external stress. This idea was taken up in hypothesis 2, although without

focusing on refined details of the mechanisms behind. Here, a direct relationship between the presence of phages and an increased production rate of HSL molecules was assumed. However, accordance of predictions with experimental data was again very poor, leading to the rejection of hypothesis 2 (**Figure 3-26**). Therefore, bacterial defense is not advanced by an increased production of autoinducing molecules. With hypothesis 3, the concept of phages acting as bacterial stressors was further developed including the idea that the presence of phages may influence the expression rate of the QS receptor PpuR [140,141,294,295]. Although improvements in the HSL prediction could be achieved, still the assumptions made in this hypothesis were not sufficient enough to explain the observed dynamic behavior of phages (**Figure 3-27**). Consequently, the presence of phages did not induce an enhanced expression of the HSL receptor protein.

The importance of the addition time point of the phages has already been evaluated with the experimental data. This direct influence of the QS system on the bacterial resistance against a phage attack however, needed to be considered in a more elaborated modeling approach. For investigating hypothesis 4, the classical and more basic assumption of always having a (more) resistant subpopulation, was expanded with the idea of an additional transient resistance obtained by the activation of QS [296]. As a consequence, this led to four bacterial subpopulations (susceptible, *ab initio* or QS-acquired resistant and infected bacteria). Moreover, also the observation that the addition of phages after 14 hr, i.e. after the typical QS activation had taken place, had a lower impact on the bacterial dynamics than an earlier phage addition was taken into account for this model. The QS-governed resistance was assumed to occur through a switch, which depends on a certain HSL threshold concentration of around 100 nM [265]. With these assumptions and the generation of a small non-resistant subpopulation of bacteria that was allowed to stay alive during the model simulation, the model could reproduce the observed late increase of phage concentration in the setting C much better (**Figure 3-28**).

In the bacterial universe, QS is a measure to initiate a collective behavioral change upon an adversely changing environment. Concomitantly, genetic expression patterns are modified upon sensing certain amounts of bacterial-produced chemical signaling molecules. QS governs for example the expression of virulence factors, sporulation, antibiotic biosynthesis, bioluminescence, swarming or biofilm formation [297]. Besides, there is increasing evidence, that QS is also involved in phage defense, which could be verified for *E. coli*, *V. anguillarum* or *P. aeruginosa* [140–142]. Especially when it comes to phage defense, from a host perspective, initiating and maintaining the expression and activity of these mechanisms is accompanied by

fitness costs [298]. Thus, linking the risk of an infection with expression of countermeasures seems a beneficial strategy. From this experiment it could be concluded that QS in *P. putida* IsoF is not only responsible for the biofilm formation [230,231], but it also contributes to an enhanced bacterial resistance. However, neither the HSL production rate is influenced, nor is the PpuR expression rate. The exact mechanism by which QS triggers bacterial resistance thus remains concealed.

3.4 Virome assessment in the lung

Parts of this chapter (experiment I) has been published in the journal *Frontiers in Microbiology*:

Elbehery, A. H. A., **Feichtmayer, J.**, Singh, D., Griebler, C. & Deng, L. The Human Virome Protein Cluster Database (HVPC): A Human Viral Metagenomic Database for Diversity and Function Annotation. *Front. Microbiol.* **9,** 1110 (2018).

3.4.1 Description of experiment I: Human lung virome sequencing

The recruitment of patients and non-COPD controls was undertaken over a 3-year period (February 2009 to March 2012) for clinical examinations, computed tomography and lung function analysis. For assessing the viral composition in the lungs of patients and healthy controls, only BAL samples were used. The lavage was performed in the upper left lobe with a total volume of 150 mL sterile, pyrogen-free 37 °C saline [299]. In total 19 BAL samples from healthy controls (8 samples) or COPD patients with differing disease severity (11 samples) were processed. Between 3–4 mL of each BAL sample was 0.22 µm filtered and DNase I treated in order to exclude contamination with prokaryotic or eukaryotic cell mass and DNA (2.3.8). Viral DNA extraction was conducted afterward according to 2.3.9.1. A 16S rRNA PCR was done to check on the purity of viral samples and confirm freedom from bacterial contamination using the universal primer Ba27 fwd and Ba907 rev (2.3.10.1). As 454 pyrosequencing requires 3–5 µg of DNA for library preparation, but the average yield per sample was around 20 ng, an amplification step was required. Therefore, the linker amplification method was performed according to 2.3.11. Finally, of the 19 samples, only three could be extracted and amplified successfully. The 454 pyrosequencing was performed on the GS FLX+ instrument following the provided manuals. Only one of four lanes was used for the BAL samples with all three samples barcoded individually and pooled equally. The quality of the reads was controlled (2.3.12.1) and the remaining reads were assembled (2.3.12.2). The functional annotation and cross-comparison of the BAL samples was conducted as described in (2.3.12.3) by functionally annotating the BAL ORFs through alignment to the human virome protein cluster (HVPC) blast database. The HVPC database has been constructed in order to improve the functional annotation and characterization of human-derived viromes [300]. The database was built from 244 human virome datasets from 13 previously published studies in addition to one unpublished lung virome from NCBI's sequence read archive (SRA) from six different body sites. In total, more than 86 million high quality sequence reads, constituting more than 12 terabases were used to

build the HVPC database. To show the usefulness of the HVPC database for the analysis of human virome sequencing data, the three BAL viromes (one healthy control, one moderate and one severe COPD) were characterized therewith. Additionally, the taxonomy (2.3.12.4) and the presence of virome-borne virulence factors (2.3.12.5) was determined.

3.4.2 Results of experiment I

Functional annotation. In order to show the applicability of the HVPC, ORFs called from three BAL samples collected from one healthy individual and two COPD patients (moderate and severe) were aligned to the HVPC database for functional annotation. On average, 64 % of BAL sequences could be aligned to HVPC and almost all of them could be functionally annotated (**Table 3-4**). In contrast, around 9 % of sequences could be aligned to protein-coding sequences from RefSeq and non-RefSeq full genome DNA viruses in NCBI. Strikingly, only 10 % of these sequences could be functionally annotated, because most proteins were hypothetical or of unknown function. The annotation and classification of ORFs into SEED categories allowed the clustering of healthy and moderate COPD BAL samples together (**Figure 3-29**). Most identified SEED categories cluster appeared at a very low concentration. More frequently observed categories were membrane transport and carbohydrate metabolism, which appeared highest in the healthy sample and Co-factors, cell wall and capsule and amino acids and derivatives, which appeared highest in the sever COPD sample. DNA metabolism was higher in the COPD samples compared to the healthy sample. Regardless of the annotation, the healthy control and the moderate COPD samples showed higher similarity in terms of the number of shared HVPC clusters (**Figure 3-30**).

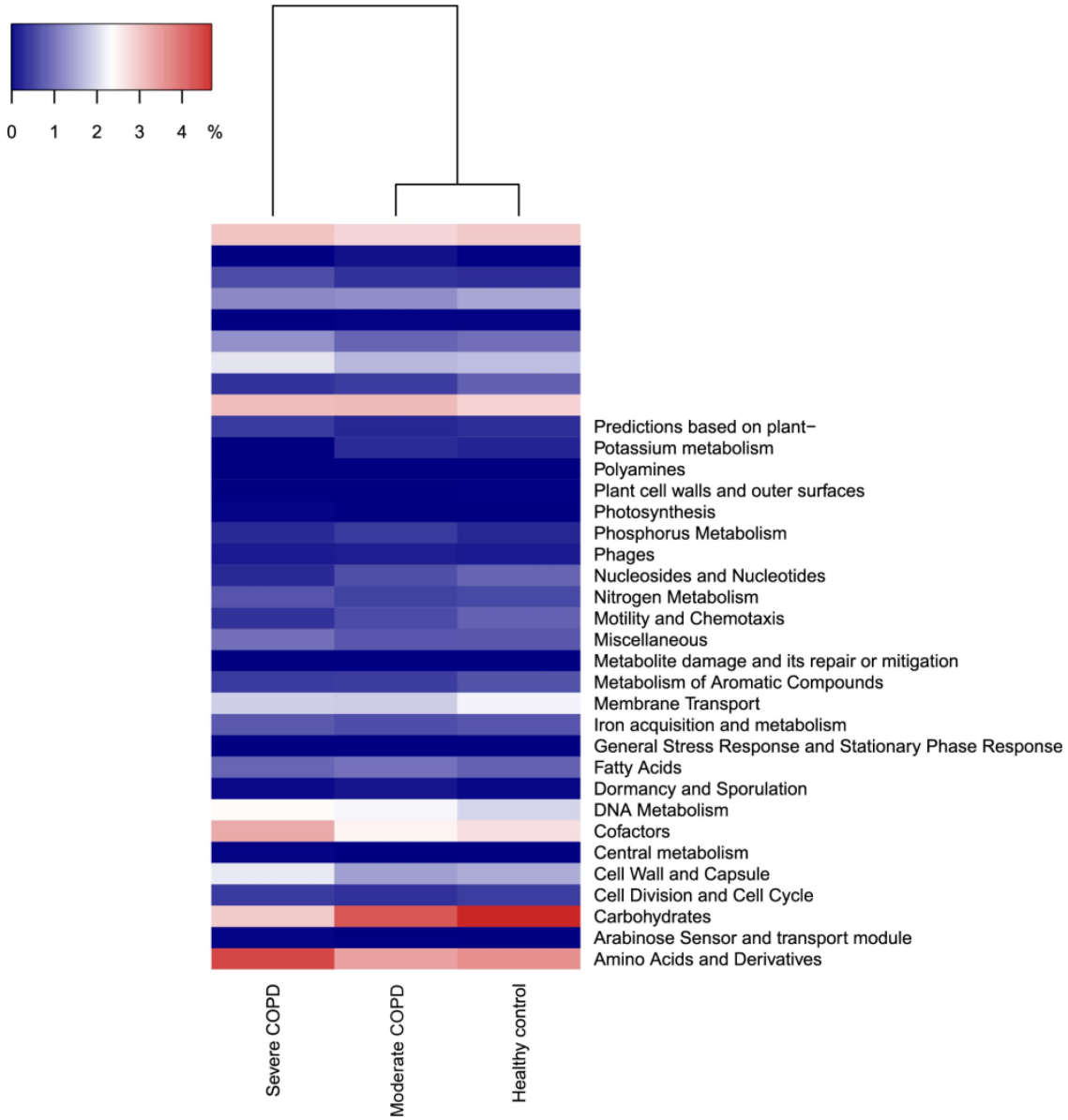

Figure 3-29: Dendrogram showing the clustering of the three BAL samples. The clustering is based on the abundance of identified SEED categories. COPD, chronic obstructive pulmonary disease. The figure was generated in R v3.4.0 [261], using heatmap3 v1.1.1 [301].

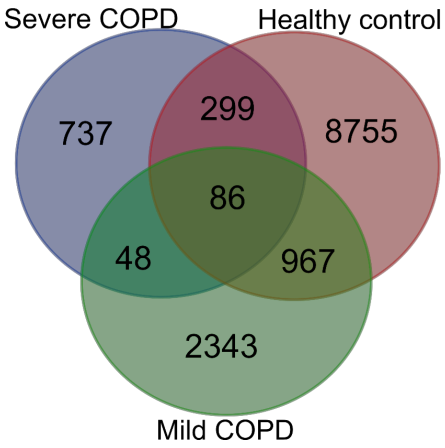

Figure 3-30: Venn diagram showing the number of shared HVPC clusters between the three BAL samples.

Likewise, comparative analysis of the three viromes in a reference-independent way using crAss, showed that the healthy control and the moderate COPD samples had more similarity to one another. Generally, the cross-assembly was made out of 1111 contigs (**Figure 3-31**). Only 32 contigs were shared between the three BAL samples (dots lying in the middle of the triangle plot). Contigs shared only between pairs of samples (represented by dots lying on the edges between each pair in the triangular plot) were as follows: 198 contigs shared between the healthy control and the moderate COPD, 68 shared between the healthy control and the severe COPD and only 18 shared between the moderate COPD and the severe COPD. The remaining contigs (represented by dots at the triangle vertices) were unique for each sample: 559 contigs for the healthy control, 229 for the moderate COPD and 15 for the severe COPD.

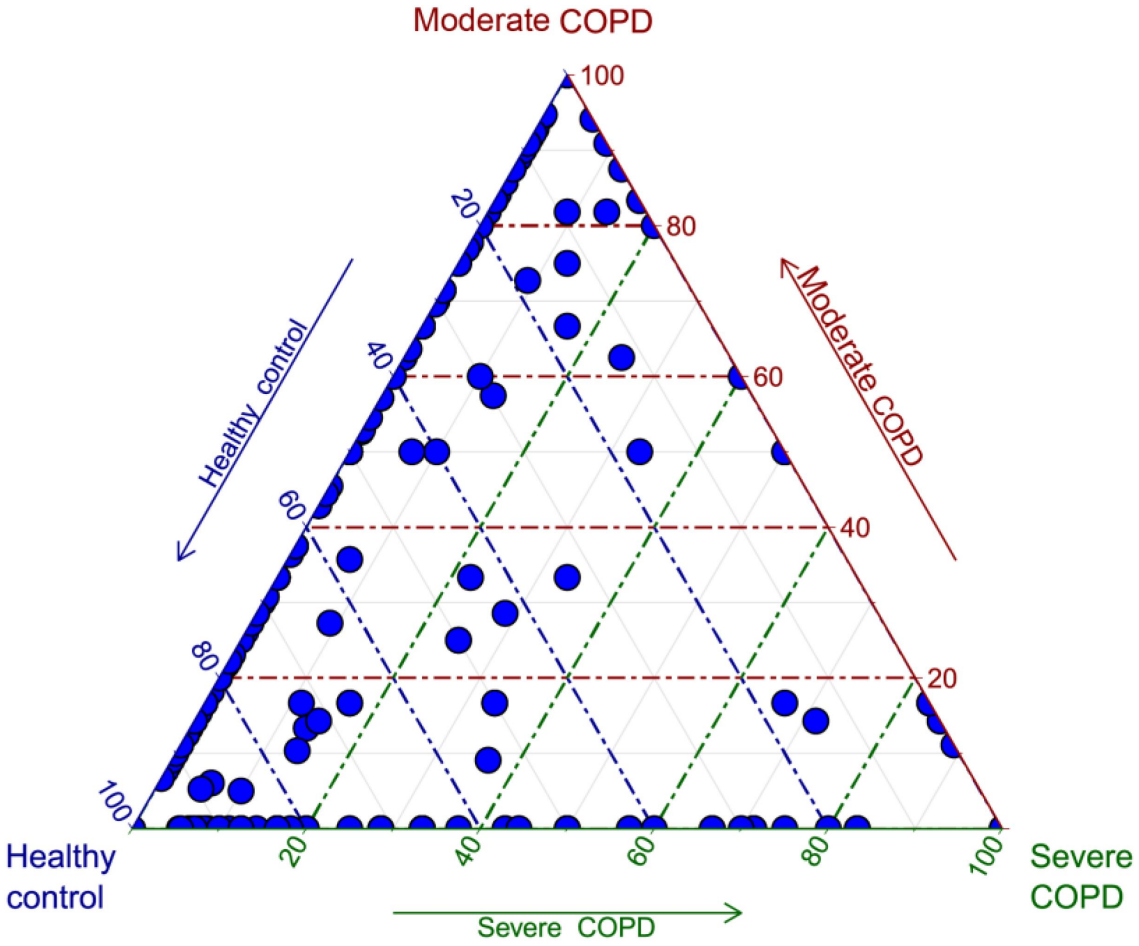

Figure 3-31: Trigonal plot showing, for each cross-assembled contig, the percentage of contributing reads from each of the three BAL samples. Each contig is represented by a small blue circle. The plot was generated in R v3.4.0 [261], using ggtern v2.2.1 [302].

Taxonomic classification. Approximately 90 % of sequences in the three BAL samples could not be assigned to any known viral lineage. For identified sequences, the most abundant viral family was *Myoviridae* followed by *Siphoviridae*, *Phycodnaviridae* and *Podoviridae* (**Figure 3-32**). The remaining viral families had abundances of less than or equal to 0.05 %. Both prokaryotic and eukaryotic DNA viruses could be identified. Concerning prokaryotic viruses, the abundance of phages was variable between samples, yet *Bacillus virus G* was the most abundant amongst all samples (supplementary material, **Figure 6-2**). Besides, also few archaeal viruses e.g., *Halovirus HGTV-1* and *Natrialba phage PhiCh1* could be detected. Notably, the abundance of certain phages, whose hosts are common in COPD such as *Pseudomonas*, *Moraxella* or *Streptococcus*, was found to be generally higher in COPD samples compared to the healthy control (**Table 3-3**). The abundance of eukaryotic viruses was also variable (supplementary material, **Figure 6-3**) with

Megavirus chilensis being the most abundant in the healthy control and the moderate COPD samples, while for the severe COPD sample, the most abundant eukaryotic virus was *Paramecium bursaria Chlorella virus A1*. Again, the abundance profiles of common eukaryotic and prokaryotic viruses allowed the clustering of healthy control and moderate COPD samples together (supplementary material, **Figure 6-2** and **Figure 6-3**). Noteworthy, some viral species (67 for moderate COPD and 24 for severe COPD) could be found only in COPD samples and not in the healthy control (supplementary material, **Table 6-7**). This flexible virome showed higher richness for the moderate COPD compared to the severe COPD sample.

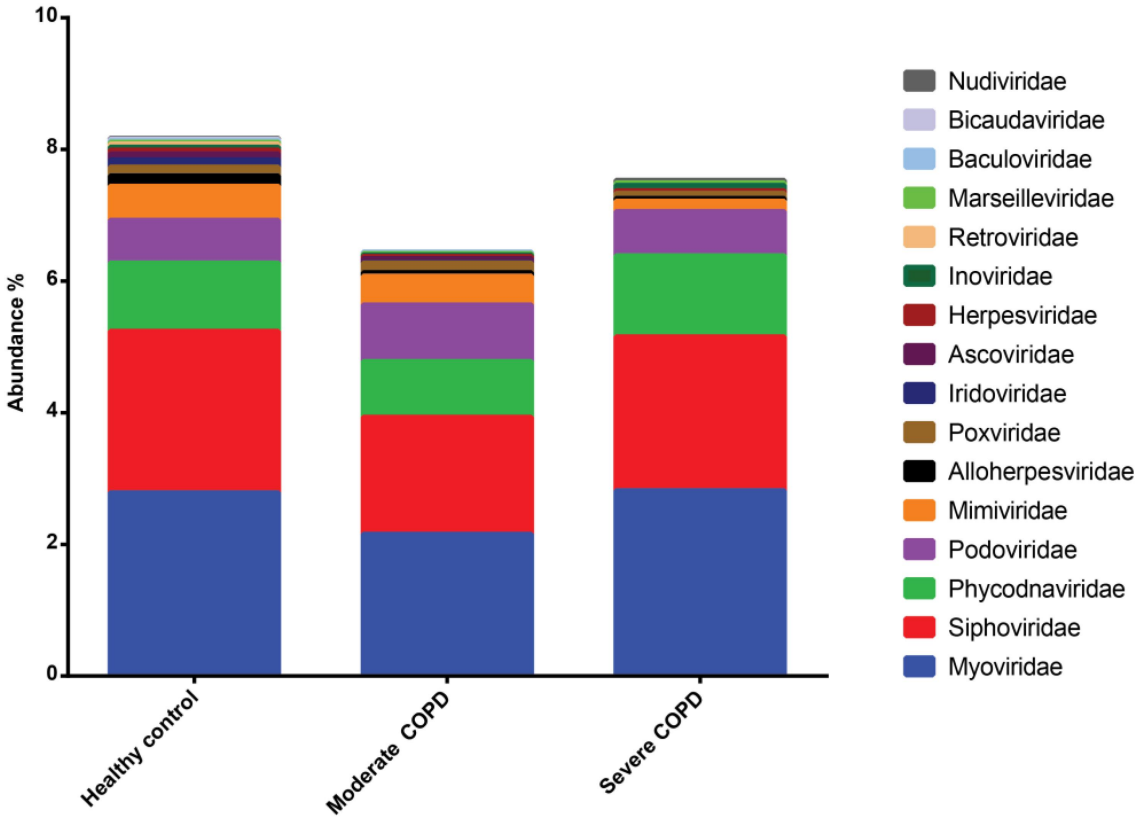

Figure 3-32: Abundance of viral families identified in BAL samples. Families with abundances less than 0.01 % in all samples were removed.

Table 3-3: Abundance of selected phages whose hosts are commonly found in COPD.

Virus*	Healthy Control	Moderate COPD	Severe COPD
Bordetella phages	nd	0.07 %	0.04%
Human alphaherpesvirus 1	nd	nd	0.04%
Moraxella phages	0.15 %	0.12 %	0.32 %
Pseudomonas phages	0.29 %	0.40 %	0.36 %
Stenotrophomonas phages	0.02 %	0.03 %	0.08 %
Streptococcus phages	0.15 %	0.39 %	0.40 %
*: All viruses infecting the same host. nd: not detected.			

Diversity. Diversity was assessed on both, the functional and the taxonomic level. Functional diversity was determined in an annotation-independent way, based on the number of different HVPC clusters to which BAL sequences could be assigned to in each sample, irrespective whether a cluster could be functionally annotated or not. None of the samples reached rarefaction (**Figure 3-33**), but generally it could be observed that functional diversity was highest in the healthy control sample and lowest in the severe COPD (**Table 3-5**). The same was noticed for taxonomic diversity, where samples could not reach rarefaction as well (**Figure 3-34**), nevertheless diversity was highest in the case of the healthy control sample, followed by the moderate COPD and the severe COPD samples, respectively (**Table 3-5**).

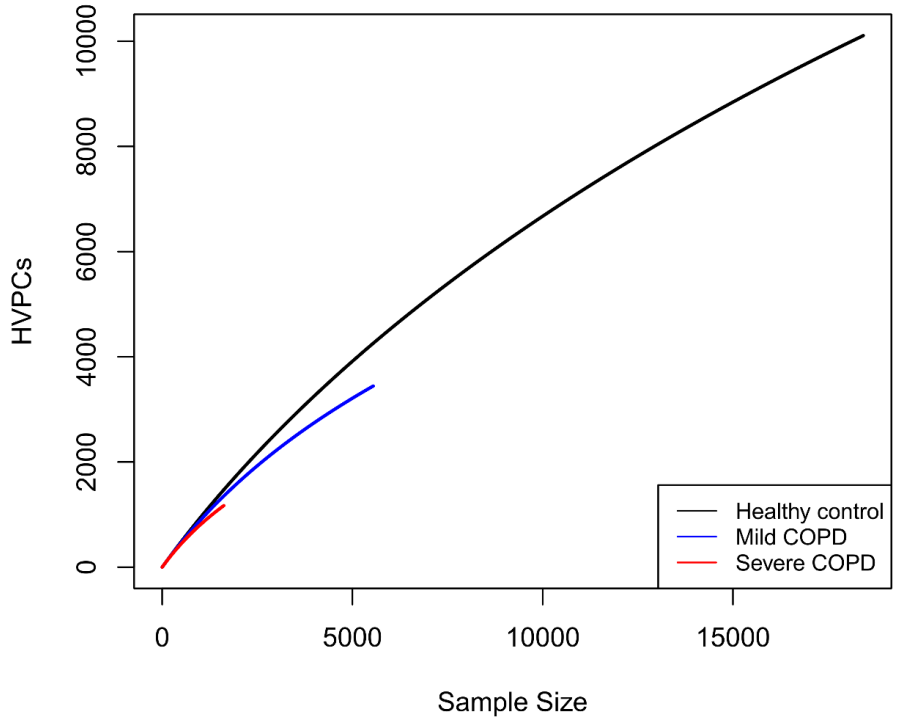

Figure 3-33: Rarefaction curves of HVPC hits versus sample size.

It is based on random subsampling and a step size of 50 sequences.

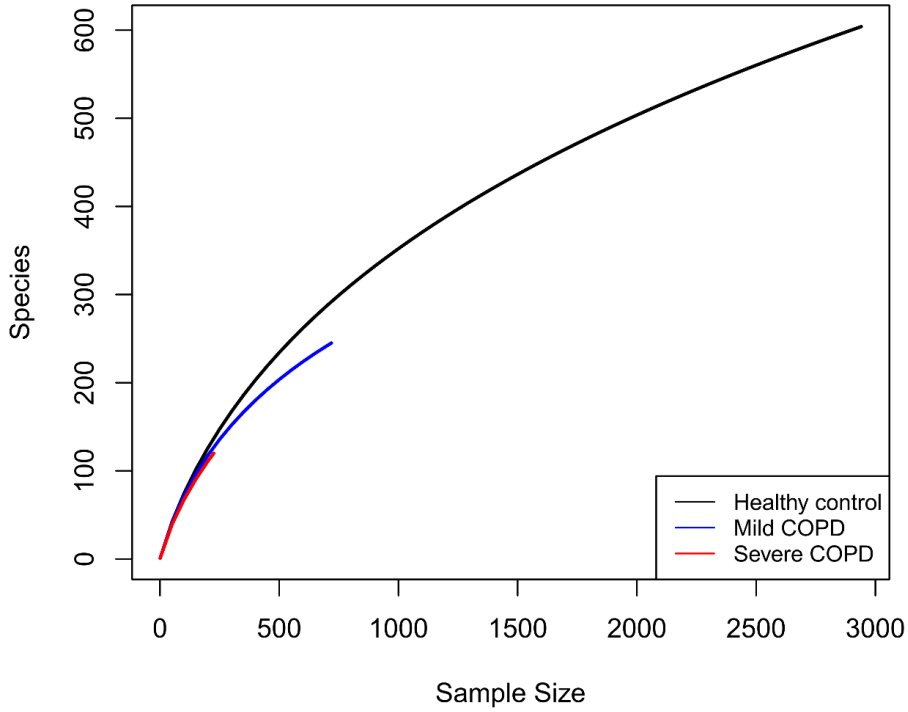

Figure 3-34: Rarefaction curves of number of species versus sample size.

It is based on random subsampling and a step size of 50 sequences.

Table 3-4: Comparison of functional annotation using HVPC versus RefSeq and non-RefSeq DNA viruses.

	#Sequences	#Sequences aligned to HVPC	% aligned	Functionally annotated	% annotated	#Sequences aligned to RefSeq and non-RefSeq DNA viruses	% aligned	Functionally annotated	% annotated
Healthy control	27669	18425	66.6	18212	65.8	2941	10.6	318	1.1
Moderate COPD	8956	5546	61.9	5541	61.9	719	8	61	0.7
Severe COPD	2522	1619	64.2	1604	63.6	226	9	21	0.8

Table 3-5: Taxonomic and functional diversity of the three BAL samples.

	Taxonomic diversity				Functional diversity			
Sample	Shannon	Inverse Simpson	Fisher's α	Species richness	Shannon	Inverse Simpson	Fisher's α	Species richness
Healthy control	5.48	97.23	230.32	604.00	8.94	5206.20	9180.23	10107.00
Moderate COPD	5.00	84.29	131.02	245.00	7.96	2255.322	3879.90	3444.00
Severe COPD	4.42	52.12	103.81	120.00	6.94	871.69	1893.53	1170.00

Virome-borne virulence factors. Besides the functional annotation of the identified viromes in the BAL samples, the possibility that the studied viromes harbor potential bacterial virulence factors was evaluated as well. Therefore, BAL sequences were aligned to polypeptides in the core Virulence Factor Database. Expectedly, the severe COPD virome sample had the highest relative abundance of bacterial virulence factors followed by the moderate and the non-COPD samples, respectively (**Figure 3-35**). Comparison of the means of relative abundances after 10000 rounds of random subsampling showed statistical significance through ANOVA ($p < 0.0001$). Besides, all sets of pairs showed statistically significant difference from each other ($p < 0.0001$). In all samples, the most represented virulence factors had resemblance to those of *Pseudomonas aeruginosa* e.g., components of xcp, type IV, and type VI secretion systems, pyoverdine biosynthesis proteins and components of alginate biosynthesis and O-acetylation (which are involved in the biofilm formation) (supplementary material, **Table 6-8**). The virome of the severe COPD patient showed with 85.71 % the highest abundance of virulence factors assigned to *Pseudomonas aeruginosa* PAO1 (**Table 3-6**). For moderate COPD, 71.79 % of the identified virulence factors were assigned to *P. aeruginosa*, whereas for the healthy patient it was 68.97 %. Strikingly, in the healthy patient, the virulence factors derived from a broader spectrum of bacteria with very low contributions (< 2 %) of *Corynebacterium diphteriae*, *Listeria monocytogenes* or *Bordetella pertrussis*, for example. Virulence factors of *Burkholderia pseudomallei* and *Listeria monocytogenes* were with 17.95 % and 5.13 %, respectively, very abundant in the moderate COPD patient, whereas virulence factors of *Salmonella enterica* and *Legionella pneumophila* were both with 7.14 % present in the virome of the severe COPD patient.

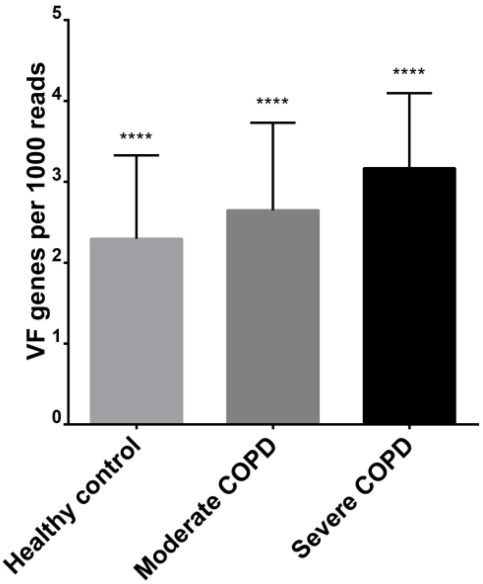

Figure 3-35: Relative abundance of virulence factors in each of the three BAL viromes. **** denote statistical significant difference with a p-value of less than 0.0001.

Table 3-6: Abundance of virulence factors of the respective bacteria found in the BAL samples. This table summarizes Table 6-8 (supplementary material) and shows the percentage of identified virulence factor for each bacterial species with an identity > 75 %.

Virulence factors deriving species	Healthy control	Moderate COPD	Severe COPD
Pseudomonas aeruginosa	68.97 %	71.79 %	85.71 %
Corynebacterium diphteriae	1.15 %		
Salmonella enterica	2.30 %		7.14 %
Burkholderia pseudomallei	8.05 %	17.95 %	
Legionella pneumophila	5.75 %		7.14 %
Yersinia enterococcolitica	2.30 %		
Mycobacterium tuberculosis	1.15 %		
Listeria monocytogenes	1.15 %	5.13 %	
Neisseria meningitidis	1.15 %		
Escherichia coli		2.56 %	
Bordetella pertrussis	1.15 %	2.56 %	
Heliobacter pylori	4.60 %		
Brucella melitensis	1.15 %		

3.4.3 Discussion of experiment I

Despite the growing interest in the recent years, studying viromes remains a challenging endeavor due to several reasons, including the scarcity of viral genomic material compared to microbial and human nucleic acid fraction, the small genome sizes of viruses or their low abundance in some cases, just to name some [303]. In a microbial community only 2–5 % of the total DNA is generally of viral origin [159,160]. Additionally, no conserved gene regions applicable for all viral types have been identified so far. Many viruses even have not been characterized yet and thus are not included in viral databases [304]. These facts impede straightforward contig assemblages as well as functional annotation of viral genomes and metagenomes. The aim of this study was the application of the human virome protein cluster (HVPC), a database which was built out of hundreds of virome datasets from six different body sites in order to facilitate and improve the functional annotation and characterization of human viromes. Out of the 19 processed BAL samples, only three could be successfully sequenced. Fortunately, those samples represented samples from a healthy control, a moderate and a severe COPD patient.

The use of the HVPC allowed a 70-fold increase in the annotation level compared to the case with only limited to information from full genome DNA viruses [300]. Even in the absence of annotation information from the clusters, alignment to the HVPC can still be informative, as it can give an indication about the diversity of the aligned samples. For the BAL samples, although they did not reach rarefaction, all diversity indices inferred from alignment to the HVPC point to a diversity that was highest in the healthy control sample and was reduced in the COPD samples according to case severity. This pattern coincides with that obtained from the taxonomic diversity analysis. Indeed, this disease-linked dysbiosis is common for the normal microbiota in many diseases [305]. The diversity of the lung virome was similarly reported to be greatly reduced in the highly diseased lobes of an explanted lung from a late-stage CF patient [168]. Besides, by utilizing the HVPC, it became apparent, that the healthy control and moderate COPD viromes were more similar to each other than to the severe COPD virome. This similarity was shown in both annotation-dependent and -independent ways. Specifically, annotations for each virome grouped into SEED categories allowed the clustering of the healthy control and moderate COPD viromes together. In addition, the number of HVPC hit clusters shared between the healthy control and moderate COPD viromes again showed higher similarity. This pattern was also confirmed by cross-assembly in a reference-independent way and by taxonomy results, which allowed the clustering of the healthy and moderate COPD pair together, based on shared prokaryotic and eukaryotic viruses.

On the taxonomic level, the majority of virome sequences usually fail to be assigned to a certain taxonomy [188,306], and the BAL viromes in this study were not an exception. Nevertheless, information content from known sequences might still allow better understanding of COPD disease progression. It became apparent that there is a core lung virome that shows different dynamics with progressive disease severity. Indeed, it was previously shown that the respiratory tract possesses a core virome for both prokaryotic and eukaryotic viruses [188]. Some of core eukaryotic viruses Willner and colleagues have reported have also been detected in the three BAL viromes e.g., *Acanthamoeba polyphaga mimivirus*, *Ectocarpus siliculosus virus* 1 and *Paramecium bursaria Chlorella virus* [188]. These eukaryotic viruses generally belong to *Phycodnaviridae* and *Mimiviridae*, which usually infect marine or freshwater algae [307] and amoeba [308], respectively. This observation could support the proposed environmental influence on the lung virome [188]. Indeed, a mimivirus was previously isolated from a pneumonia patient [309]. This virus showed sequence similarity to *Megavirus chilensis*, which was the most abundant eukaryotic virus in the healthy control and the moderate COPD samples. The isolation of this virus from a pneumonia patient does not necessarily mean pathogenicity and any claim of pathogenicity still warrants further study. In contrast, the prokaryotic viruses identified by Willner and colleagues showed no similarity to those identified in the three BAL samples [188]. This disagreement could be attributed in part to the differences in databases, especially for the prokaryotic viruses, because the authors used a custom database of only 510 phage genomes. Another explanation could be environmental differences, as evidently the inhaled air influences the composition of lung viromes and microbiomes [188,310]. On the other hand, COPD samples contained some viruses that were not shared with the healthy control. This flexible virome had higher species richness in the moderate COPD, an observation that confirms the progressive dysbiosis that accompanies disease development. In fact, some viruses that are directly associated with COPD and its exacerbation e.g., *human alphaherpesvirus 1* (also known as *herpes simplex virus 1*) [311] or whose hosts are commonly isolated from COPD patients e.g., *Bordetella*, *Moraxella*, *Pseudomonas Stenotrophomonas* and *Streptococcus* [284,312–314] have been found to be of higher abundance or exclusively present in COPD samples (**Table 3-3**). Further analysis showed that BAL viromes could harbor potential bacterial virulence factors. The abundance of these factors increases with increasing COPD disease severity (**Figure 3-35**). Truly, phages, which constitute the major fraction of most viromes do play a crucial role in the horizontal gene transfer of bacterial genes. Actually, the expression and dissemination of many bacterial toxins and virulence factors rely on phages (reviewed in [315]). It remains, however, arguable whether the presence of, for example, antibiotic resistance genes in the viral genomes is already an indication for a reduction of bacterial susceptibility to those antibiotics. Up to now,

experimental evidences fail to confirm that these detected genes actually confer resistance [316].

3.4.4 Description of experiment II: Refining optimal sample processing

As only three of initially 19 BAL samples could be successfully sequenced and the subsequent analysis of the contigs was rather difficult due to a the high proportion of contamination with human and bacterial DNA, the applied sample preparation had to be re-evaluated. Particular attention has been paid to the purification of the viral samples. Additionally to the filtration step with 0.22 µm, viruses were separated from human and bacterial cells and debris using CsCl gradient ultracentrifugation (2.3.5.2), which promises a higher purity of the isolated viral particles. In order to fit into the SW40Ti rotor and the used ultracentrifugal tubes, the sample volume had to be reduced after the first DNase I treatment and a concentrating step was applied. Two methods were compared regarding their efficiency: PEG and $FeCl_3$ precipitation (2.3.6.2). In this test, also the possibility to omit the virus:iron-pellet-dissolving step with the addition of EDTA-ascorbate buffer was tested. This test was conducted with 5 mL T4 and T7 phage stock solution. Both viruses were concentrated using PEG (2.3.6.1) or $FeCl_3$ precipitation (2.3.6.2) with eluting the virus:iron pellet either in 110 µL EDTA-ascorbate buffer or in 110 µL 1× TE buffer. DNA was afterwards extracted according to (2.3.9.2).

Independently, two DNA extraction methods were evaluated as well: the Promega Wizard kit (as described in 2.3.9.1), which was used for the previous DNA extraction in 3.4.1, and a modification of the AMPure beads DNA clean-up according to 2.3.9.2. For this test 0.1 and 0.5 mL of the virus stocks T4, T7 and ΦX174 were DNase I treated (2.3.8) and further concentrated with PEG (2.3.6.1) to a volume of 110 µL, as it is required by the AMPure beads DNA extraction method. The PEG protocol was slightly modified, as samples were centrifuged at a higher speed (10000 × g) for 30 min and the pellet was dissolved in 100 µL phage buffer (2.2.7).

The efficiency of the DNase I treatment has been evaluated applying different concentrations of the enzyme (0.1 U, 1 U and 2 U) on 200 µL of 0.22 µm filtered *E.coli* 5695 in the stationary phase (according to 2.3.8 with the respective enzyme concentrations). Copy numbers of 16S rRNA were afterwards enumerated using qPCR and the primers Ba519/Ba907 (2.3.10.8).

In an attempt to reduce the human and bacterial contamination in human-derived samples and to assess the contamination level after each step of sample treatment, a human fecal sample was spiked with T4 phage and processed until pure viral DNA was achieved. Levels of human and bacterial DNA were monitored after each step with qPCR. 50 g of freshly collected human feces was dissolved in 1 L phage buffer and incubated at 4 °C overnight with constant agitation.

On the next day, the sample was centrifuged at 14000 × g at 4 °C for 5 min and finally 0.22 µm filtered. Viral particles in the sample were quantified with FCM (2.3.7.2). Phage T4 was added to this filtrate in the same order of magnitude as the already present viruses (1.23×10^{10} VLP mL^{-1}). Subsamples from this mixture were taken for qPCR quantification and stored at –20 °C (200 µL non-filtered sample, 200 µL 0.22 µm filtered with subsequent DNA extraction [2.3.9.2]). In order to remove specifically human DNA, the MolYsis kit basic 5 was applied according to the manufacturer's protocol on 5 mL of the prepared sample (200 µL sample was taken afterwards and stored at –20 °C). The entire volume of 5 mL was then further purified using CsCl gradient ultracentrifugation (2.3.5.2). For comparison, 5 mL of the untreated T4-spiked fecal sample was loaded as well. From each of the density fractions (viruses: ρ = 1.4–1.5, bacteria: ρ > 1.5 and waste: ρ < 1.4) 200 µL samples were taken and cleaned-up in order to remove the CsCl (2.3.5.2). With the virus containing fraction, a DNase I treatment was performed (2.3.8). A subsample of 50 µL was again drawn and kept at –20 °C, but, as no DNA extraction was performed on this subsample, the DNase was inactivated trough incubation at 70 °C for 10 min instead of the EDTA addition. The remaining sample was treated as described in the DNase protocol (2.3.8). $FeCl_3$ was then used to reduce the sample volume after the ultracentrifugation to 110 µL (2.3.6.2) and subsequently, the DNA was extracted (2.3.9.2). For all of the subsamples as well as the extracted DNA from the initial sample and the purified virus containing sample, qPCR was performed to quantify the human DNA (using the primer GAPDH_1 fwd and rev), bacterial DNA (using the 16S rRNA primer Ba519 fwd and Ba907 rev) and viral DNA (using the primer T4 fwd and T4 rev).

3.4.5 Results of experiment II

From the sequencing data analysis of the previous section, it became apparent that first, the DNA extraction method is not efficient enough as only three out of 19 samples could be successfully extracted and amplified and second, the contamination with human and bacterial DNA highly reduced the number of viral reads that have been sequenced. Thus, there is the need for an alternative sample preparation procedure, which increases the success-rate of DNA extraction and reduces the level of non-viral contamination. In a first step, two methods for the reduction of the sample volume have been evaluated. This step is needed now, as CsCl gradient ultracentrifugation will be applied as a viral particle separation step and the maximal sample volume that can be loaded is 5 mL. In the previous section, sample volumes in the range of 4 mL were used. However, this volume was apparently too low to result in sufficient amounts of DNA. Consequently, bigger human sample volumes should be used in future, which then require a reduction in the volume. In addition, DNase treatment should be included as well to reduce the amount of free (contaminating human or bacterial) DNA in the sample after filtration. The PEG

precipitation method was compared to the chemical flocculation method using $FeCl_3$ for their capability of reducing a sample volume without losing its viral particles. As the dissolving EDTA-ascorbate buffer has to be prepared freshly on the day of usage, the possibility of omitting this step by "dissolving" the pellet only in 1× TE buffer was additionally evaluated. **Figure 3-36** summarizes the DNA concentrations isolated after concentrating five mL of the respective virus isolate. For both viruses, although T7 stock was relatively low in particle concentration, thus resulting also in low DNA concentrations, the $FeCl_3$ precipitation (with EDTA-ascorbate buffer) was the most efficient method. PEG precipitation achieved relatively low amounts of DNA, indicating that this method is not suitable for the enrichment of low concentrated viral samples, as too many particles are lost with this procedure. Despite higher concentration compared to PEG, dissolving the virus:iron pellet in 1× TE buffer is not advisable.

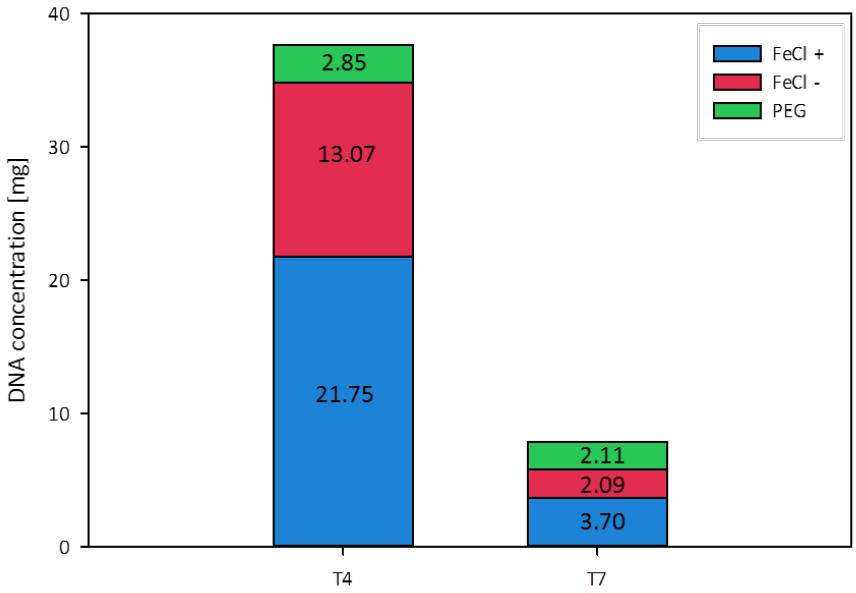

Figure 3-36: T4 and T7 concentrated with PEG or $FeCl_3$. DNA concentration has been calculated for the whole volume which has been concentrated. Green: PEG. Red: $FeCl_3$ precipitation with dissolving the pellet only in 1× TE buffer (FeCl -). Blue: $FeCl_3$ precipitation with dissolving the pellet according to the protocol in EDTA-ascorbate buffer (FeCl +).

As the DNA quality resulting from an extraction with the Promega Wizard kit was relatively bad and the number of successfully extracted samples was also quite low (3.4.2), an alternative DNA extraction method was evaluated. **Figure 3-37** shows the relative amount of extracted DNA from either 0.1 mL or 0.5 mL starting volume and **Table 3-7** lists the absolute DNA concentrations in ng μL^{-1}. Generally, the AMPure beads method resulted in a higher amount of DNA compared to the Promega Wizard kit. For ΦX174, the Promega Wizard kit was not able to extract any DNA at

all. Especially for lower concentrated viral samples and ssDNA viruses, the AMPure beads extraction method seemed to be more efficient.

Table 3-7: Concentration of viral DNA extracted with two different methods.

Phage	Initial volume	ng µL^{-1}	
		Promega	AMPure
T4	0.1 mL	5.2135	8.1825
	0.5 mL	5.6615	26.85
T7	0.1 mL	8.073	16.5275
	0.5 mL	37.7	102.2
ΦX174	0.1 mL	NA	0.4358
	0.5 mL	NA	10.51

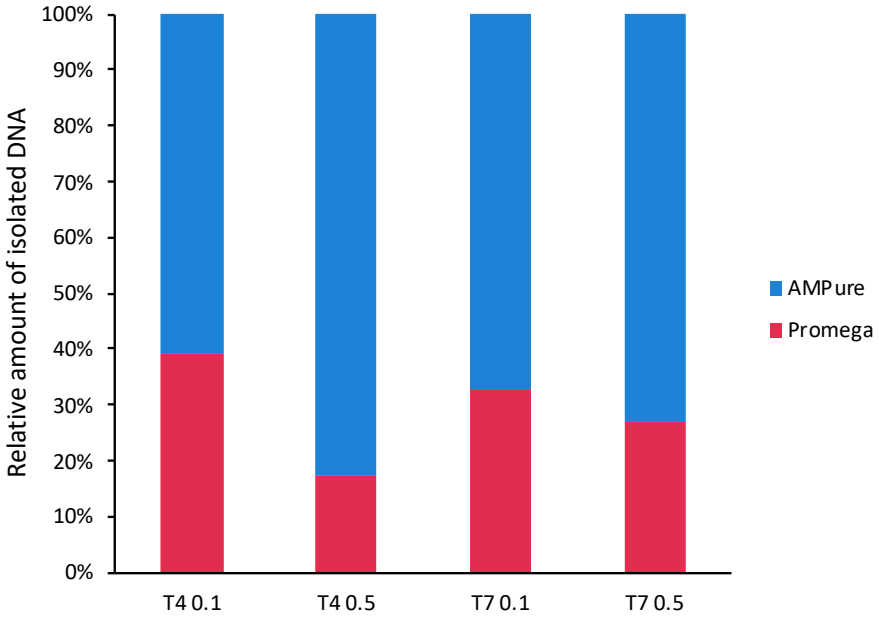

Figure 3-37: Relative comparison between DNA extraction methods. Blue: AMPure beads extraction. Red: Promega Wizard kit. 0.1 and 0.5 indicate the starting volume of the phages T4 and T7, which was extracted.

DNase I was very efficient in degrading free DNA. Independent of the applied enzyme concentration, no bacterial DNA could be detected with qPCR after each digestion anymore. It seemed therefore unlikely, that the contaminating bacterial or human DNA derived from an inefficient Dnase treatment.

Depleting a sample from human and bacterial DNA and solely extracting viral DNA is crucial, when viral metagenomes are about to being studied. Oftentimes, with every purification step, also the viral load is reduced. Especially with lower sample volumes, this might be very problematic. **Figure 3-38** shows the amount of bacterial 16S gene copies and the respective amount of isolated T4 DNA after each step of the applied viral purification procedure. Apparently, free bacterial DNA could be detected in all samples. Filtration successfully removed bacterial cells, thus the load of the bacterial DNA after DNA extraction was 180-fold lower in the filtered sample (1f) compared to the unfiltered one (1u). The application of the MolYsis kit removed also a certain amount of free bacterial DNA (2f, 2u) and, after the ultracentrifugation, the bacterial DNA in the viral fraction (2ph) was approximately 6-fold lower compared to only ultracentrifugation (3ph). In both approaches, the Dnase I treatment removed any free bacterial DNA (2dn and 3dn). Nonetheless, after extracting the DNA from both samples, a considerable amount of bacterial DNA could be detected in both treatments, although approximately 4-fold less in the approach with the additional MolYsis kit treatment. As it could be observed for the viral DNA, this stronger reduction in the bacterial DNA was also accompanied by a greater loss of viral particles. With the additional step of the MolYsis kit, approximately 4-times less T4 DNA could be extracted (2ex) compared to the approach with only ultracentrifugation (3ex). In those samples, where only the free DNA was quantified, no viral DNA could be detected.

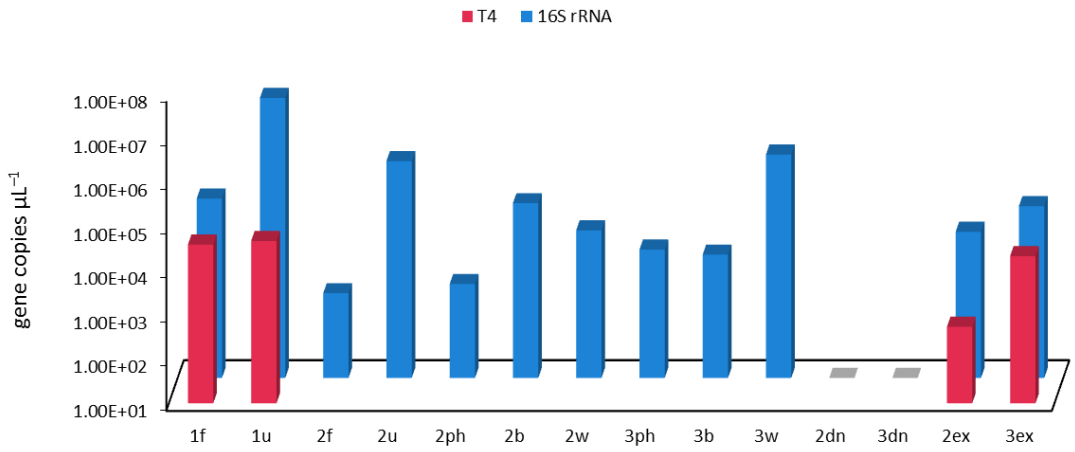

Figure 3-38: Free bacterial DNA and extracted T4 DNA during each step of purification. 1f: DNA extraction from 0.22 µm filtered sample. 1u: DNA extraction from unfiltered sample. 2f: sample after MolYsis kit treatment (0.22 µm filtered sample). 2u: sample after MolYsis kit treatment (unfiltered sample). 2ph: MolYsis kit + UZ samples, ρ = 1.5–1.4 (phage-fraction). 2b: MolYsis kit + UZ samples, ρ > 1.5 (bacterial fraction). 2w: MolYsis kit + UZ samples, ρ < 1.4 (waste fraction). 3ph: UZ only samples, ρ = 1.5–1.4. 3b: UZ only samples, ρ > 1.5. 3w: UZ only samples, ρ < 1.4. 2dn, 3dn: after Dnase treatment from MolYsis kit + UZ or UZ only phage fraction. 2ex, 3ex: DNA extraction from MolYsis kit + UZ or UZ only phage fraction.

As the DNA in all of the 5 mL has been extracted, a direct comparison between the initial T4 concentration and the concentration after the purification can only be drawn, if the concentrations refer to the whole five mL sample volume, which is the case in **Figure 3-39**. The difference between the unfiltered and filtered sample without treatment is neglectable. During the virus particle purification procedure with only the ultracentrifugation, approximately 90-fold less viral DNA could be isolated compared to the initial sample. With the additional step of MolYsis kit, even less particles could be isolated (3.67×10^3 -fold less gene copies).

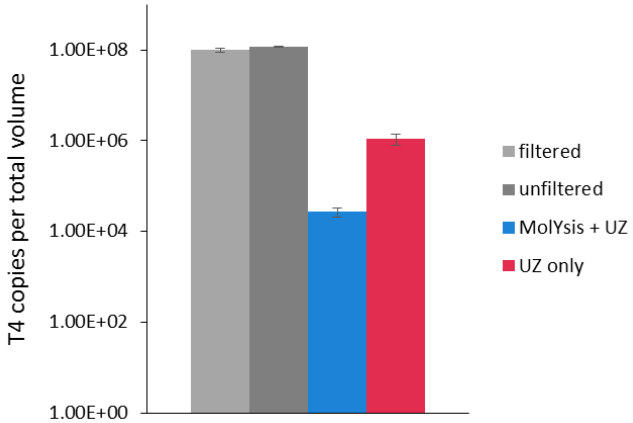

Figure 3-39: Total abundance of T4 gene copies. Grey: DNA extracted from untreated fecal-phage-mix. Light: 0.22 µm filtered. Dark: unfiltered sample. Blue: DNA extracted after purification process with MolYsis kit treatment and UZ. Red: DNA extracted after purification process with only UZ.

Unfortunately, in none of the samples, neither treated nor untreated, any human DNA could be identified. The designed primers target a region in the human glyceraldehyde 3-phosphate dehydrogenase gene, which is widely used as a reference gene in order to normalize qPCR results. Hence, it was assumed, that it would be a suitable marker for the presence of human DNA contamination. As the designed primers *per se* worked upon testing them on freshly isolated DNA from a human saliva sample, the constant thawing and freezing of the samples presumably reduced the possibility of a successful gene amplification.

3.4.6 Discussion of experiment II

For metagenomic sequencing, pure DNA material without the presence of any other contaminating DNA is crucial for a successful downstream analysis. This is especially true for the genetic analysis of viral DNA isolated from complex environment, such as human-derived samples. As the proportion of viral DNA compared to bacterial or human DNA is with 2–5 % relatively low [159,160,317], insufficient separation of viral DNA leads to an excess of bacterial or human DNA in the extract. As consequence, essential space, needed for the sequencing of viral DNA is lost, as bacterial and human DNA is sequenced instead. This became also apparent during the analysis of the three sequenced BAL samples from section 3.4.2. The procedure of generating viral DNA from a sample plays therefore a crucial role for the metagenomic analysis of viruses or viromes. The procedural method of already published virome studies is however inconsistent. In some studies, viral particles are isolated using two filtration steps (0.45 and 0.22 µm), followed by a lysozyme, chloroform and Dnase treatment *prior to* DNA extraction [318]. Most commonly, samples are repeatedly filtered and applied on a cesium chloride density gradient, with the viral fraction treated with Dnase *prior to* DNA extraction [160,319] or added

for further purification on Amicon YM100 protein columns, followed by Dnase treatment and DNA extraction [164,320–322]. Oftentimes, PEG is used to concentrate viral particles and reduce larger sample volumes. This method is, however, accompanied by a relative high loss of viral particles as could be seen in this thesis (**Figure 3-36)**. Precipitating the viruses with $FeCl_3$ is a more efficient alternative. Also the method of DNA extraction has to be chosen carefully. Especially with lower concentrated samples, efficiency matters. The Promega Wizard kit has shown to be not suitable for the extraction of DNA from low concentrated samples. An advantage using the AMPure beads is, besides the higher output of DNA, also the extraction of ssDNA (**Figure 3-37)**. The procedure of the generation of preferably pure viral particles from a contaminant-rich human sample was evaluated next. Here, samples were filtered twice with 0.22 µm, followed by CsCl gradient centrifugation, Dnase I treatment and DNA extraction. In order to remove specifically human DNA, some sub-samples were additionally treated with the MolYsis kit *prior to* the CsCl gradient centrifugation. Although the bacterial DNA was completely removed after the Dnase step, it could still be detected in the viral DNA extracts. The contamination with bacterial DNA in the extract was lower in those subsamples, which underwent an additional treatment with the MolYsis kit, however, approximately 4-fold less viral DNA could be extracted compared to the untreated subsamples. The incomplete removal of bacterial DNA together with considerable the loss of viral particles (from 10^8 to 10^4 copies, **Figure 3-39**) from unfiltered original sample to extracted MolYsis treated sample, makes the additional usage of this kit arguable. Generally, obtaining a higher purity of the sample is always also accompanied by a stronger loss of viral particles. To date, one has to deliberate about whether a higher degree of sample purity, accepting also a higher loss of viral particles, or whether a minor loss with a higher proportion of contaminating DNA is preferred. In this case, the downstream data analysis has supposedly to be adapted, including a greater attention to data filtration. In order to compensate for the loss of viral particles upon any purification, an increased sample volume might be processed. In this case the yield in viral reads might finally be increased, as a higher proportion of viral particles can be extracted. With higher sample volumes, also a more restrictive purification protocol can be applied, as here the loss of viral particles might be not substantial.

4 CONCLUSIONS AND OUTLOOK

4.1 Further perspectives I: Virus quantification techniques in the spotlight

Having reliable quantification techniques at hand is essential for studying viruses in various environments. Besides gaining an increased ecological understanding, also the potential application of phages as therapeutic agents can be better evaluated with knowledge of accurate viral numbers. However, low viral concentration and scarcity of precise virus-specific enumeration methods are common problems when working with environmental samples. During the broad comparison of five different viral quantification methods and two different staining procedures conducted in this thesis, the nanoparticle-tracking analysis in combination with a virus staining at a lower temperature was identified as the most reliable technique to date, especially for the unspecific enumeration of viral particles in environmental samples. Interestingly, the widespread staining procedure conducted at 80 °C seemed to be inappropriate, as this treatment resulted in an increased formation of viral aggregates. Nanoparticle tracking analysis had, however, its limitation when quantifying low concentrated and complex environmental samples as well as very small viral particles, such as the phages MS2 and ΦX174. Besides, qPCR or PA remain the most reliable quantification methods available for pure viral isolates or if specific viruses shall be enumerated in a sample. Strikingly, none of the tested methods was able to satisfactorily enumerate viral particles in all the different sample types. Consequently, no single method that can be applied for the quantification of viruses, independent of the sample type, particle concentration or size, or impurities could be identified in this comparison. Certain determining factors regarding the particle concentration and size influence the results thus have to be considered when applying a certain quantification technique. Besides, also the purpose of the quantification has to be taken into account when choosing the right quantification technique for a certain type of sample. Unspecific detection methods, such as flow cytometry or nanoparticle-tracking analysis, might benefit from an additional purification step in order to remove free DNA or bacterial cell debris that remains after the filtration step. One has to be aware that with every additional step, however, also viral particles will get lost, thus potentially falsify the enumeration.

4.2 Further perspectives II: Phages of *Pseudomonas aeruginosa*

The excessive use of broad-spectrum antibiotics has accelerated the emergence of multidrug resistant bacteria, which are as a consequence very difficult to control. One of these very problematic bacteria is the opportunistic *Pseudomonas aeruginosa*, which is a leading cause of mortality, particularly in immunocompromised patients [223,224].
This study investigated the potential of using specific lytic phages to control *P. aeruginosa*. The viruses were isolated from different sources, from treated and untreated wastewater to human lavage and sputum samples and their interactions with *P. aeruginosa* under different environmental conditions regarding temperature and pH, as well as various predation pressures were characterized. Although a differing response of the phages to external stress (such as pH or temperature) could be observed, the genetic analysis could not confirm any difference in the genetic composition, which pointed either towards a contamination during the isolation process or towards a generally great genetic similarity between the isolates as could be shown by Pires and colleagues, whose Pseudomonas aeruginosa phage isolates showed a great similarity of more than 93% to other *Pbunalikevirus* [289]. Despite this high genetic similarity between the viral isolates, they still might express different features. For bacteria, however, it has been shown that, although HGT may induce only small genetic variations, it finally leads to considerable differences in the physiological behavior of closely related bacterial strains [323]. Therefore, a high similarity in the phage genomes does not necessarily point towards a similar physiology.

From a general perspective, it could be observed that, in the moment phages appeared at very high concentrations in a bacterial population, the chances that bacteria develop resistance at least to some extent is very high. For some of the phage isolates identified in this thesis, low virus-to-bacteria rates did not lead to a strong increase of the bacterial numbers, however, bacterial densities did also not decline. The question remains, whether natural phage isolates can be used to completely clear a bacterial infection without giving rise to progeny cells that have turned non-susceptible. Previous mathematical simulations showed, that indeed, bacterial infections can only be cleared using phages when the immune system is involved [210,211]. Phages alone are not able to clear infections. For the phages isolated in this thesis, an increased biofilm formation of the bacteria upon the addition of phages could be observed. If this scenario happens in a patient, the application of phages would cause more problems than benefits.

Therefore, the phages suitability and possible unwanted effects they might cause have to be evaluated carefully.
However, the high percental resemblance of the genetic sequence of the isolates with an already published and described phage isolate [289], together with the inability of the isolates to clear or at least reduce bacteria organized in a biofilm, renders the isolates unattractive for further inquiries. In addition, the fast development of bacterial resistance, which could be observed during the conducted experiments, in combination with the laborious generation of viral isolates, also question a potential broad application of these phages for the pathogen control.

Instead of using phages as exclusive antimicrobial treatment, a combination of antibiotics or other antimicrobial substances (e.g. bacteriocins) with, potentially also genetically engineered phages might be an alternative. For example the organization of *P. aeruginosa* in biofilms is controlled by a cell density dependent secretion of 3-oxo-C12-HSL and C4-HSL, in other words quorum sensing. Substances, such as azithromycin reduce not only cell-to-cell signal production and by that reduce also the production of extracellular virulence factors, but most importantly they interfere with the formation of biofilm at different levels [324]. Combining lytic phages with quorum sensing-interfering compounds might lead to a stronger reduction of bacterial cells and might also reduce the colonialization of surfaces by adhering cells. As the bacterial organization in biofilms is also one resistance strategy to avoid predation by phages [77], phages find, once they get inside a biofilm, mostly susceptible bacteria in great quantities [170]. In this context, also the induction of temperate phages would be more beneficial, as this would result in a degradation of the biofilms from within [325]. The combination of biofilm deteriorating agents together with the administration of lytic phages, or the disturbance of lysogenic bacteria, which are organized in a biofilm, seems to be promising targets for further researches.

4.3 Further perspectives III: Viral impact on microbial communication

Additional information, which derive not only from descriptive interaction between phages and their host, can be gained through the inclusion of mathematical models. Using models allows not only to identify trends, they may also result in specific parameters that allow a prediction of behavior under certain conditions. In this chapter, a modelling approach was used to investigate, whether quorum sensing (QS) is involved in the anti-phage defense of *Pseudomonas putida*. Generally, *P. putida* utilizes QS for switching into an attached lifestyle (QS-induced biofilm formation) [230,231]. For some bacteria, however, QS regulates the anti-phage defense strategy. In *Vibrio anguillarum* and *Escherichia coli*, surface receptors used for phage adsorption are downregulated upon certain cell densities, therefore bacteria are turned fully resistant [140,141]. *P. aeruginosa* and *Serratia* sp. even have their CRISPR-Cas system activated by QS [142,143]. These previous studies showed, however, that the interplay between a host, its quorum sensing system and phages might be very complex. In *Vibrio anguillarum* for example, two different anti-phage strategies are active, depending on the bacterial cell density. At a low abundance, enhanced biofilm formation protects cells from phage infection. At high cell densities, QS mediates the downregulation of the surface receptor OmpK, which is crucial for the phage attachment to the cell membrane [140].

The focus of this study was on identifying the most probable interactive processes behind the experimental observations in an explorative manner. Consequently, the structures of the models were kept as simple as possible. However, although the results provided strong evidence that bacterial anti-phage resistance in *P. putida* is apparently controlled by QS, the applied model was not able to fully reproduce the experimental data. As it could be proven by confuting the formulated hypotheses, QS does somehow interfere with the anti-phage defense (hypothesis 1), but neither is the HSL production affected (hypothesis 2), nor is the intracellular HSL receptor (PpuR) expression augmented (hypothesis 3). Hypothesis 4 achieved, a better congruency with the experimental data, hence the assumption, that bacteria turned more resistant against phages due to the activation of the QS system seemed likely. Still, some further aspects, which were not yet considered when constructing the model of hypothesis 4 would be needed to be taken into account for further amelioration. One process that has not been fully considered, concerns the activation of the lactonase. It is known that the production and activation of the lactonase is regulated by the *ppu* system with a delay of 1–2 hr, hence leading to a delayed negative feedback loop [263,265,269]. For the mathematical modelling, this would

require a delay differential equation. Fitting to this delay differential equation system would need more extensive numerical and computational efforts, exceeding the original scope of this study. Likewise, the latency period, i.e. the time interval from a new infection of a bacterial cell until the burst and spread of new phage progeny, has not been considered as well. Including this effect in detail would lead to a state-dependent delay, as the metabolism of the bacterial cell depends on nutrient availability. This in particular concerned the replication of the lytic phages in the setting C experiment, where phages were added 14 hr after the onset of bacterial growth. Apart from this varying latency period, the mean burst size might be non-constant and dependent on the growth phase of the bacterial host (see e.g. [267]). These possible effects have to be addressed in future experiments and modelling approaches. The reason for these deficiencies in fitting may be grounded in missing processes that were not incorporated in the model, thus rendering the model too superficial and not capable to fully reproduce the experimental data.

Besides the phage defense mechanisms that have been incorporated in the mathematical model, there are further strategies bacteria can follow to avoid or at least minimize the risk for phage infection (1.3.1). Generally, anti-phage resistance might develop rather quickly after only few cycles of replication [326]. One strategy is based on preventing phage adsorption to the cell surface by an increased production of extracellular polymers, often accompanied by an organization in biofilms or by the downregulation of surface receptors crucial for phage attachment and infection. For *P. putida*, it is known that QS triggers the structural organization in biofilms [231]. As all the experiments conducted in this study were batch tests incubated under constant agitation, the formation of a stable biofilm was hampered. Thus, this phage defense strategy could not be evaluated in this study. A QS-dependent downregulation of the surface receptor OmpK could be shown for *V. anguillarum*, resulting in a lowered infection rate by the phage KVP40 [140]. For this experiment, five different lytic phages, isolated from wastewater samples with *P. putida* as host *prior to* this experiment were used in combination. Deciphering, whether the downregulation of certain surface receptors is responsible for resistance would have required as a first step the identification of the receptors involved in phage attachment and in a second step the generation of bacterial knock-out mutants of those receptors. This work might be considered in future experiments. A further well known phage defense strategy is the prevention of a collapse of the bacterial population by an induced suicide of few infected clonal cells [76]. However, it is unlikely that these abortive infection systems played a role here, as in all experimental settings phage replication has been taken place, resulting in high viral titers. Another mechanism that provides protection against phage

infection is the CRISPR-Cas system. Viral nucleic acid is specifically recognized by the CRISPR spacer content and degraded by the Cas enzymatic apparatus [84]. Here as well, based on the experimental setting, it cannot be proven whether this mechanism was involved or responsible for the observed bacterial phage resistance.

With regard to the increasing and fast development of (multiple) antibiotic resistant pathogenic bacteria, the call for alternative therapeutics is high. Phage therapy represents one of these developments that regained interest [327]. However, as it has been shown for some bacteria, QS may reduce the viral infection success [140,141]. By applying QS inhibitors, also known as quorum quenching, the bacterium might be turned even more susceptible towards its phages [142] and indeed, these alternative treatment strategies gain more and more attention [226–229]. However, for these ideas becoming reality, a fundamental understanding of the underlying mechanisms is crucial, not only with regard to individual isolates in a one strain population, but also in multispecies settings and under different environmental conditions [19]. Thus, there is a strong interest in better understanding the mechanisms that control both, QS and phage dynamics, and especially their interplay, to optimize potential treatment strategies and to avoid the development of additional resistance against therapeutic phages. By combining experimental findings with explorative modelling, this study heads in the direction towards a better understanding of the dynamic and highly non-linear interplay.

4.4 Further perspectives IV: Virome assessment in the lung

The virome of the human gut has been extensively studies in the past, however, only few studies covering the virome of the human lung exist. Mostly, these studies are linked to a certain chronic disease of the lung, such as CF. General capture of the virome present in a healthy lung has so far not been undertaken.

In this last chapter, the analysis of human lavage samples from COPD patients but also healthy individuals was conducted. The evaluation of the influence commensal viruses and bacteria have on human health can ideally be implemented using metagenomic analysis of suitable samples, that allows a preferably broad view on the community compositions in the light of different medical conditions. From the poor sequencing output, the problems when isolating viral DNA from human samples became apparent as well as the importance of careful sample preparation and an optimal purification procedure. The output of the genetic material arising from viruses isolated from complex, human-derived samples might be very low in concentration and of insufficient quality. High background signals of bacterial and human DNA hampers the success rate of sequenced viral reads. From the evaluated methods to increase the success rate of the viral DNA extraction, it became apparent that DNA quality and particle quantity are negatively correlated. In order to obtain pure viral DNA, protocols have to be further optimized as the restrictive purification protocols, which will increase the quality of the viral DNA are also accompanied by high losses of viral particles during the purification process. Bigger sample volumes of several deciliters might overcome these issues as here, the impact of the particle reduction will be less problematic. Further, suitable samples should be well described in order to facilitate the evaluation of inter-personal variations with respect to the identification of disease-specific alterations in the virome. Another challenge when analyzing human-based virome data is the coverage of the existing databases. The number of already identified viruses is relatively low; therefore a great proportion of the sequenced virome remains unknown. The human virome protein cluster was built specifically based on previously sequenced human-derived virome studies. Utilizing this HVPC database facilitates the analysis of virome sequencing data, as additional information on a functional level can be gained, which helps to circumvent the lack of knowledge of identified viruses prevalent in available databases.

The sequencing of the three BAL viromes gave a first insight into viral communities of COPD patients and confirmed through the presence of certain viruses a certain state of dysbiosis in the lung, which could be linked to disease progression. As hypothesized, a core virome could be

found in all samples, independent of their disease state. Further, a flexible virome could be identified, which is more related to the health status. The severe COPD virome showed a distinct composition, which was different compared to the healthy virome. Interestingly, the virome in the moderate COPD sample was more similar to the healthy virome than to the severe COPD virome. With disease progression, viruses of *Pseudomonas* or *Streptococcus* were found more frequently in the severe COPD sample, compared to the healthy control. Nonetheless, the analysis of these few samples can only give some indications and trends, which have to be further evaluated with the processing of more, well characterized samples.

Further studies could for example tackle the over-time changes in the healthy virome. For the gut virome it has been shown that it remains relatively stable over time and that a change in diet also affects the composition of the virome [160]. An extensive data set of virome compositions from healthy individuals augments also the validity of data from diseased individuals. Monitoring the virome composition from an acute infection of the lung during the infection and after a recovery has been taken place may give a hint on the stability and resilience of the pulmonary system, especially if antibiotics were administered. Also a comparison between different pulmonary diseases and/or progression states or the influence oral diseases have on the pulmonary virome has might be of interest. It is believed that the oral microbiome is the main source for the bacterial community in the lungs [328]. Moreover, it is expected to find some of the microbial communities shared between the gut and the lungs, since the ingested microbes have the ability to access both sites and microbes from the gut can enter the respiratory tract through aspiration [329]. In this context, the influence of a short-term or long-term administration of antibiotics on the microbial composition of the lung and by that also on the virome, should be evaluated. Besides, also the influence antibiotics prescribed to treat non-pulmonary infections have on the virome would be worth to assess. In all of the described settings, the large group of temperate phages, as present in the human gut virome [330], has not been included in the analysis as for that, also the microbiome has to be analyzed during the sequencing process. Gaining knowledge of the potential influence of the viral gene transfer on the disease progression, augmentation of bacterial virulence and antibiotic resistance is indispensable. Possible experimental validations could be the co-incubation of viruses, which genetically harbor genes conferring resistance against a specific antibiotic together with susceptible bacteria, or the co-incubation of different bacteria that harbor no temperate phage or at least lack the ability to be resistant against certain antibiotics with bacteria that harbor a resistance-conferring temperate phage.

4.5 Closing statement

In this thesis, the interactions between phages and their hosts were examined in details, using a variety of different approaches. The ultimate goal was to deepen our understanding of the roles bacteriophages have in complex ecosystem. Only then, phages can be actively used, either for the control of pathogenic bacteria as in the setting of a phage therapy or for the targeted enhancement of the microbiota, to give some examples. Otherwise, the administration of phages in order to lyse specific bacteria might not improve but even worsen the patient's situation as it has been observed in this thesis with the increase of *P. aeruginosa* biofilm formation upon presence of phages. In these terms, an in-depth knowledge of a certain phage-host system is inevitable, as only then the too ineffective single phage treatments can be efficiently complemented by additional measures, such as quorum quenching.

A chronically diseased organ, such as a lung with the background of COPD can also be seen as a complex ecosystem. Here, the microbiota changes upon disease progression and certain imbalances between pathogenic or opportunistic and commensal bacteria appear. Having a closer look at this viral composition and comparing it to the composition in non or less diseased lungs will help to better understand how the bacterial community adapts to an altered environment and to what extent phages contribute to their adaptation. Ultimately, this will support the understanding how chronic diseases such as COPD develop and progress, and how this affects the patients prognosis.

5 REFERENCES

1. Modrow, S., Falke, D., Truyen, U. & Schätzl, H. Viren: Definition, Aufbau, Einteilung. in *Molekulare Virologie* 13–21 (Spektrum Akademischer Verlag, 2010).
2. Claverie, J.-M. & Abergel, C. Mimiviridae: An Expanding Family of Highly Diverse Large dsDNA Viruses Infecting a Wide Phylogenetic Range of Aquatic Eukaryotes. *Viruses* **10,** 506 (2018).
3. Raoult, D. *et al.* The 1.2-megabase genome sequence of Mimivirus. *Science (80-.).* (2004). doi:10.1126/science.1101485
4. Whitman, W. B., Coleman, D. C. & Wiebe, W. J. Prokaryotes: The unseen majority. *Proc. Natl. Acad. Sci.* **95,** 6578–6583 (1998).
5. Weinbauer, M. G. Ecology of prokaryotic viruses. *Fems Microbiol. Rev.* **28,** 127–181 (2004).
6. Ackermann, H.-W. Tailed Bacteriophages: The Order *Caudovirales*. *Adv. Virus Res.* **51,** 135–201 (1999).
7. Fuhrman, J. A. Marine viruses and their biogeochemical and ecological effects. *Nature* **399,** 541–548 (1999).
8. Williamson, K. E., Radosevich, M. & Wommack, K. E. Abundance and diversity of virus in six Delaware soils. *Appl. Environ. Microbiol.* **71,** 3119–3125 (2005).
9. Pan, D., Nolan, J., Williams, K. H., Robbins, M. J. & Weber, K. A. Abundance and distribution of microbial cells and viruses in an alluvial aquifer. *Front. Microbiol.* **8,** 1–11 (2017).
10. Bergh, O., Borsheim, K. Y., Bratbak, G. & Heldal, M. High abundance of viruses found in aquatic environments. *Nature* **340,** 467–468 (1989).
11. Muhling, M. *et al.* Genetic diversity of marine Synechococcus and co-occurring cyanophage communities: evidence for viral control of phytoplankton. *Env. Microbiol* **7,** 499–508 (2005).
12. Waterbury, J. B. & Valois, F. W. Resistance to co-occurring phages enables marine Synechococcus communities to coexist with cyanophages abundant in seawater. *Appl. Environ. Microbiol.* **59,** 3393–3399 (1993).
13. Fortier, L.-C. & Sekulovic, O. Importance of prophages to evolution and virulence of bacterial pathogens. *Virulence* **4,** 354–365 (2013).
14. Clokie, M. R., Millard, A. D., Letarov, A. V & Heaphy, S. Phages in nature. *Bacteriophage* **1,** 31–45 (2011).
15. Bratbak, G., Thingstad, F. & Heldal, M. Viruses and the microbial loop. *Microb Ecol* **28,**

209–221 (1994).

16. Los, M. & Wegrzyn, G. Pseudolysogeny. *Adv. Virus Res.* **82,** 339–349 (2012).
17. Abedon, S. T. Phages, ecology, evolution. in *Bacteriophage ecology : population growth, evolution, and impact of bacterial viruses* (ed. Abedon, S. T.) 508 (Cambridge University Press, 2008).
18. Rice, C. M. Flaviviridae: The Viruses and Their Replication. in *Fields Virology* (eds. Fields, B. N., Knipe, D. M. & Howlay, P. M.) 931–950 (Lippincott-Raven, 1996). doi:10.1016/0038-092X(88)90131-4
19. Feichtmayer, J., Deng, L. & Griebler, C. Antagonistic microbial interactions: Contributions and potential applications for controlling pathogens in the aquatic systems. *Front. Microbiol.* **8,** (2017).
20. Wichels, A. *et al.* Bacteriophage diversity in the North Sea. *Appl. Environ. Microbiol.* **64,** 4128–4133 (1998).
21. Suttle, C. A. & Chan, A. M. Dynamics and distribution of cyanophages and their effect on marine Synechococcus spp. *Appl. Environ. Microbiol.* **424,** 1047–1051 (1994).
22. Suttle, C. A. Viruses in the sea. *Nature* **437,** 356–361 (2005).
23. Edwards, R. a & Rohwer, F. Viral metagenomics. *Nat Rev Microbiol* **3,** 504–510 (2005).
24. Breitbart, M. & Rohwer, F. Here a virus, there a virus, everywhere the same virus? *Trends Microbiol.* **13,** 278–284 (2005).
25. Wommack, K. E. & Colwell, R. R. Virioplankton: Viruses in Aquatic Ecosystems. *Microbiol. Mol. Biol. Rev.* **64,** 69–114 (2000).
26. Fuhrman, J. A., Noble, R. T., Fuhrmann, J. A. & Nobel, R. Viruses and protists cause similar bacterial mortality in coastal seawater. *Limnol Ocean.* **40,** 1236–1242 (1995).
27. Marti, E., Variatza, E. & Balcazar, J. L. The role of aquatic ecosystems as reservoirs of antibiotic resistance. *Trends Microbiol* **22,** 36–41 (2014).
28. Clemente, J. C., Ursell, L. K., Parfrey, L. W. & Knight, R. The impact of the gut microbiota on human health: an integrative view. *Cell* **148,** 1258–1270 (2012).
29. Bratbak, G., Heldal, M., Thingstad, T. F. & Tuomi, P. Dynamics of virus abundance in coastal seawater. *FEMS Microbiol Ecol* **19,** 263–269 (1996).
30. Hennes, K. P., Suttle, C. A. & Chan, A. M. Fluorescently Labeled Virus Probes Show that Natural Virus Populations Can Control the Structure of Marine Microbial Communities. *Appl Env. Microbiol* **61,** 3623–3627 (1995).
31. Wilhelm, S. W. & Suttle, C. A. Viruses and Nutrient Cycles the aquatic food webs. **49,** 781–788 (1999).
32. Cottrell, M. T. & Suttle, C. A. Dynamics of lytic virus infecting the photosynthetic marine

picoflagellate Micromonas pusilla. *Limnol. Oceanogr.* **40,** 730–739 (1995).

33. Middelboe, M., Jørgensen, N. O. G. & Kroer, N. Effects of viruses on nutrient turnover and growth efficiency of noninfected marine bacterioplankton. *Appl. Environ. Microbiol.* **62,** 1991–1997 (1996).
34. Gobler, C. J., Hutchins, D. A., Fisher, N. S., Cosper, E. M. & Sañudo-Wilhelmy, S. A. Release and bioavailability of C, N, P, Se, and Fe following viral lysis of a marine chrysophyte. *Limnol. Oceanogr.* **42,** 1492–1504 (1997).
35. Fuhrman, J. A. Bacterioplankton roles in cycling of organic matter: The microbial food web. in *Primary Productivity and Biogeochemical Cycles in the Sea* (eds. Falkowski, P. & Woodhead, A.) 361–384 (Plenum Pres, 1992).
36. Proctor, L. M. & Fuhrmann, J. A. Roles of viral infection in organic particle flux. *Mar Ecol Prog Ser* **69,** 133–142 (1991).
37. Weinbauer, M. G., Höfle, M. G. & Hofle, M. G. Significance of Viral Lysis and Flagellate Grazing as Factors Controlling Bacterioplankton Production in a Eutrophic Lake. *Appl Env. Microbiol* **64,** 431–438 (1998).
38. Stanley, M., Cronan, J. & Freifelder, D. *Microbial Genetics*. (Jones and Bartlett Publishers Inc., 1987).
39. Stopar, D., Černe, A., Žigman, M., Poljšak-Prijatelj, M. & Turk, V. Viral abundance and a high proportion of lysogens suggest that viruses are important members of the microbial community in the Gulf of Trieste. *Microb. Ecol.* **47,** 1–8 (2004).
40. Jiang, S. C., Kellogg, C. A. & Paul, J. H. Characterization of marine temperate phage-host systems isolated from Mamala Bay, Oahu, Hawaii. *Appl. Environ. Microbiol.* **64,** 535–542 (1998).
41. Jiang, S. C. & Paul, J. H. Seasonal and diel abundance of viruses and occurrence of lysogeny/bacteriocinogeny in the marine environment. *Mar. Ecol. Prog. Ser.* **104,** 163–172 (1994).
42. Jiang, S. C. & Paul, J. H. Gene transfer by transduction in the marine environment. *Appl Env. Microbiol* **64,** 2780–2787 (1998).
43. Brüssow, H. *et al.* Phages and the Evolution of Bacterial Pathogens: from Genomic Rearrangements to Lysogenic Conversion. *Microbiol. Mol. Biol. Rev.* **68,** 560–602 (2004).
44. Casjens, S. Prophages and bacterial genomics: what have we learned so far? *Mol Microbiol* **49,** 277–300 (2003).
45. Banks, D., Beres, S. & Musser, J. The fundamental contribution of phages to GAS evolution, genome diversification and strain emergence. *Trends Microbiol* **10,** 515–521 (2002).

46. Canchaya, C., Fournous, G. & Brüssow, H. The impact of prophages on bacterial chromosomes. *Mol Microbiol* **53,** 9–18 (2004).

47. Rohwer, F. & Thurber, R. V. Viruses manipulate the marine environment. *Nature* **459,** 207–212 (2009).

48. Tinsley, C. R., Bille, E. & Nassif, X. Bacteriophages and pathogenicity: more than just providing a toxin? *Microbes Infect* **8,** 1365–1371 (2006).

49. Sullivan, M. B., Coleman, M. L., Weigele, P., Rohwer, F. & Chisholm, S. W. Three Prochlorococcus cyanophage genomes: signature features and ecological interpretations. *PLoS Biol* **3,** e44 (2005).

50. Eklund, M., Poysky, F., Reed, S. & Smith, C. Bacteriophage and the toxigenicity of *Clostridium botulinum* type C. *Science* **172,** 480–482 (1971).

51. Waldor, M. K. & Mekalanos, J. J. Lysogenic conversion by a filamentous phage encoding cholera toxin. *Science* **272,** 1910–1914 (1996).

52. Freeman, V. J. Studies on the virulence of bacteriophage-infected strains of *Corynebacterium diphtheriae*. *J. Bacteriol.* **61,** 675–688 (1951).

53. Ohnishi, M., Kurokawa, K. & Hayashi, T. Diversification of *Escherichia coli* genomes: are bacteriophages the major contributors? *Trends Microbiol* **9,** 481–485 (2001).

54. Mead, P. & Griffin, P. *Escherichia coli* O157:H7. *Lancet* **352,** 1207–1212 (1998).

55. Aziz, R. *et al.* Mosaic prophages with horizontally acquired genes account for the emergence and diversification of the globally disseminated M1T1 clone of *Streptococcus pyogenes*. *J Bacteriol* **187,** 3311–3318 (2005).

56. Cleary, P., LaPenta, D., Vessela, R., Lam, H. & Cue, D. A globally disseminated M1 subclone of group A streptococci differs from other subclones by 70 kilobases of prophage DNA and capacity for high-frequency intracellular invasion. *Infect Immun* **66,** 5592–5597 (1998).

57. Cooke, F. *et al.* Prophage sequences defining hot spots of genome variation in *Salmonella enterica* serovar Typhimurium can be used to discriminate between field isolates. *J Clin Microbiol* **45,** 2590–2598 (2007).

58. Hermans, A. P. H. M., Abee, T., Zwietering, M. H. & Aarts, H. J. M. Identification of novel *Salmonella enterica* serovar typhimurium DT104-specific prophage and nonprophage chromosomal sequences among serovar typhimurium isolates by genomic subtractive hybridization. *Appl. Environ. Microbiol.* **71,** 4979–4985 (2005).

59. Thomson, N. *et al.* The role of prophage-like elements in the diversity of *Salmonella enterica* serovars. *J Mol Biol* **339,** 279–300 (2004).

60. Figueroa-Bossi, N., Uzzau, S., Maloriol, D. & Bossi, L. Variable assortment of prophages

provides a transferable repertoire of pathogenic determinants in Salmonella. *Mol Microbiol* **39,** 260–271 (2001).

61. Rahimi, F., Bouzari, M., Katouli, M. & Pourshafie, M. Prophage and antibiotic resistance profiles of methicillin-resistant *Staphylococcus aureus* strains in Iran. *Arch Virol* **157,** 1807–1811 (2012).
62. Goerke, C. *et al.* Diversity of prophages in dominant Staphylococcus aureus clonal lineages. *J Bacteriol* **191,** 3462–3468 (2009).
63. Bae, T., Baba, T., Hiramatsu, K. & Schneewind, O. Prophages of *Staphylococcus aureus* Newman and their contribution to virulence. *Mol Microbiol* **62,** 1035–1047 (2006).
64. Boyd, E. Bacteriophage-encoded bacterial virulence factors and phage-pathogenicity island interactions. *Adv Virus Res* **82,** 91–118 (2012).
65. Yokoyama, K. *et al.* Complete nucleotide sequence of the prophage VT1-Sakai carrying the Shiga toxin 1 genes of the enterohemorrhagic *Escherichia coli* O157:H7 strain derived from the Sakai outbreak. *Gene* **258,** 127–139 (2000).
66. Makino, K. *et al.* Complete nucleotide sequence of the prophage VT2-Sakai carrying the verotoxin 2 genes of the enterohemorrhagic *Escherichia coli* O157:H7 derived from the Sakai outbreak. *Genes Genet Syst* **74,** 227–239 (1999).
67. Wagner, P. L. *et al.* Bacteriophage control of Shiga toxin 1 production and release by *Escherichia coli*. *Mol Microbiol* **44,** 957–970 (2002).
68. Kimmitt, P., Harwood, C. & Barer, M. Induction of type 2 Shiga toxin synthesis in *Escherichia coli* O157 by 4-quinolones. *Lancet* **353,** 1588–1589 (1999).
69. Zhang, X. *et al.* Quinolone antibiotics induce Shiga toxin-encoding bacteriophages, toxin produc- tion, and death in mice. *J Infect Dis* **181,** 664–670 (2000).
70. Clokie, M. R. J. *et al.* Transcription of a 'photosynthetic' T4-type phage during infection of a marine cyanobacterium. *Environ. Microbiol.* **8,** 827–835 (2006).
71. Bailey, S., Clokie, M. R. J., Millard, A. & Mann, N. H. Cyanophage infection and photoinhibition in marine cyanobacteria. *Res. Microbiol.* **155,** 720–725 (2004).
72. Lindell, D., Jaffe, J. D., Johnson, Z. I., Church, G. M. & Chisholm, S. W. Photosynthesis genes in marine viruses yield proteins during host infection. *Nature* **438,** 86–9 (2005).
73. Lindell, D. *et al.* Transfer of photosynthesis genes to and from Prochlorococcus viruses. *Proc Natl Acad Sci U S A* **101,** 11013–11018 (2004).
74. Wang, X. *et al.* Cryptic prophages help bacteria cope with adverse environments. *Nat Commun* **1,** 147 (2010).
75. Modi, S. R., Lee, H. H., Spina, C. S. & Collins, J. J. Antibiotic treatment expands the resistance reservoir and ecological network of the phage metagenome. *Nature* **499,** 219–

222 (2013).

76. Labrie, S. J., Samson, J. E. & Moineau, S. Bacteriophage resistance mechanisms. *Nat. Rev. Microbiol.* **8,** 317–327 (2010).
77. Scholl, D., Adhya, S. & Merril, C. Escherichia coli K1's capsule is a barrier to bacteriophage T7. *Appl Env. Microbiol* **71,** 4872–4874 (2005).
78. Manning, A. & Kuehn, M. Contribution of bacterial outer membrane vesicles to innate bacterial defense. *BMC Microbiol* **11,** 258 (2011).
79. Seed, K. D. Battling Phages: How Bacteria Defend against Viral Attack. *PLoS Pathog.* **11,** e1004847 (2015).
80. Koonin, E. V, Makarova, K. S. & Wolf, Y. I. Evolutionary Genomics of Defense Systems in Archaea and Bacteria. *Annu. Rev. Microbiol.* **71,** 233–261 (2017).
81. Tock, M. R. & Dryden, D. T. F. The biology of restriction and anti-restriction. *Curr. Opin. Microbiol.* **8,** 466–472 (2005).
82. Williams, R. Restriction endonucleases: classification, properties, and applications. *Mol Biotechnol* **23,** 225–243 (2003).
83. Eckstein, F. Phosphorothioation of DNA in bacteria. *Nat Chem Biol* **3,** 689–690 (2007).
84. Barrangou, R. *et al.* CRISPR Provides Acquired Resistance Against Viruses in Prokaryotes. *Science* **315,** 1709–1712 (2007).
85. Stern, A. & Sorek, R. The phage-host arms-race : Shaping the evolution of microbes. *Bioessays* **33,** 43–51 (2011).
86. Marrafini, L. & Sontheimer, E. Self versus non-self versus dis- crimination during CRISPR RNA-directed immunity. *Nature* **463,** 568–572 (2010).
87. Deveau, H., Gerueau, J. & Moineau, S. CRISPR/CAS system and its role in phage-bacteria interactions. *Ann Rev Microbiol* **64,** 475–493 (2010).
88. Samson, J. E., Magadán, A. H., Sabri, M. & Moineau, S. Revenge of the phages: defeating bacterial defences. *Nat. Rev. Microbiol.* **11,** 675–87 (2013).
89. Snyder, L. Phage-exclusion enzymes: a bonanza of biochemical and cell biology reagents? *Mol Microbiol* **15,** 415–420 (1995).
90. Chopin, M., Chopin, A. & Bidnenko, E. Phage abortive infection in lactococci: variations on a theme. *Curr Opin Microbiol* **8,** 473–479 (2005).
91. Hendrix, R., Smith, M., Burns, R., Ford, M. & Hatfull, G. Evolutionary relationships among diverse bacteriophages and prophages: all the world's a phage. *Proc Natl Acad Sci USA* **96,** 2192–2197 (1999).
92. Lu, M. & Henning, U. Superinfection exclusion by T-even-type coliphages. *Trends Microbiol* **2,** 137–139 (1994).

93. Van Valen, L. A new evolutionary law. *Evol Theor* **1,** 1–30 (1973).

94. Meyer, J. R. *et al.* Repeatability and contingency in the evolution of a key innovation in phage lambda. *Science* **335,** 428–432 (2012).

95. Liu, M. *et al.* Reverse transcriptase-mediated tropism switching in Bordetella bacteriophage. *Science* **295,** 2091–2094 (2002).

96. Cornelissen, A. *et al.* Identification of EPS-degrading activity within the tail spikes of the novel Pseudomonas putida phage AF. *Virology* **434,** 251–256 (2012).

97. Glonti, T., Chanishvili, N. & Taylor, P. W. Bacteriophage-derived enzyme that depolymerizes the alginic acid capsule associated with cystic fibrosis isolates of Pseudomonas aeruginosa. *J. Appl. Microbiol.* **108,** 695–702 (2010).

98. Paterson, S. *et al.* Antagonistic coevolution accelerates molecular evolution. *Nature* **464,** 275–278 (2010).

99. Scanlan, P. D., Hall, A. R., Lopez-Pascua, L. D. C. & Buckling, A. Genetic basis of infectivity evolution in a bacteriophage. *Mol. Ecol.* **20,** 981–989 (2011).

100. Bickle, T. A. & Kruger, D. H. Biology of DNA restriction. *Microbiol Rev* **57,** 434–450 (1993).

101. Warren, R. A. Modified bases in bacteriophage DNAs. *Annu. Rev. Microbiol.* **34,** 137–158 (1980).

102. Kruger, D. H. & Bickle, T. A. Bacteriophage survival: multiple mechanisms for avoiding the deoxyribonucleic acid restriction systems of their hosts. *Microbiol. Rev.* **47,** 345–360 (1983).

103. Iida, S., Streiff, M. B., Bickle, T. A. & Arber, W. Two DNA antirestriction systems of bacteriophage P1, darA, and darB: characterization of darA-phages. *Virology* **157,** 156–166 (1987).

104. Walkinshaw, M. D. *et al.* Structure of Ocr from bacteriophage T7, a protein that mimics b-form DNA. *Mol. Cell* **9,** 187–194 (2002).

105. Atanasiu, C., Su, T. J., Sturrock, S. S. & Dryden, D. T. Interaction of the ocr gene 0.3 protein of bacteriophage T7 with EcoKI restriction/modification enzyme. *Nucleic Acids Res.* **30,** 3936–3944 (2002).

106. Deveau, H. *et al.* Phage response to CRISPR-encoded resistance in Streptococcus thermophilus. *J. Bacteriol.* **190,** 1390–1400 (2008).

107. Bondy-Denomy, J., Pawluk, A., Maxwell, K. L. & Davidson, A. R. Bacteriophage genes that inactivate the CRISPR/Cas bacterial immune system. *Nature* **493,** 429–432 (2013).

108. Seed, K. D., Lazinski, D. W., Calderwood, S. B. & Camilli, A. A bacteriophage encodes its own CRISPR/Cas adaptive response to evade host innate immunity. *Nature* **494,** 489–491 (2013).

109. Villion, M. & Moineau, S. Phages hijack a host's defence. *Nature* **494,** 433–434 (2013).

110. Sberro, H. *et al.* Discovery of functional toxin/antitoxin systems in bacteria by shotgun cloning. *Mol. Cell* **50,** 136–148 (2013).

111. Otsuka, Y. & Yonesaki, T. Dmd of bacteriophage T4 functions as an antitoxin against Escherichia coli LsoA and RnlA toxins. *Mol. Microbiol.* **83,** 669–681 (2012).

112. Short, F. L., Blower, T. R. & Salmond, G. P. C. A promiscuous antitoxin of bacteriophage T4 ensures successful viral replication. *Mol. Microbiol.* **83,** 665–668 (2012).

113. Hoskisson, P. & Smith, M. Hypervariation and phase variation in the bacteriophage 'resistome'. *Curr Opin Microbiol* **10,** 396–400 (2007).

114. Orlowski, J. & Bujnicki, J. M. Structural and evolutionary classification of Type II restriction enzymes based on theoretical and experimental analyses. *Nucleic Acids Res.* **36,** 3552–3569 (2008).

115. Haft, D. H., Selengut, J., Mongodin, E. F. & Nelson, K. E. A guild of 45 CRISPR-associated (Cas) protein families and multiple CRISPR/cas subtypes exist in prokaryotic genomes. *PLoS Comput. Biol.* **1,** 474–483 (2005).

116. Kunin, V., Sorek, R. & Hugenholtz, P. Evolutionary conservation of sequence and secondary structures in CRISPR repeats. *Genome Biol.* **8,** R61 (2007).

117. Sharp, P., Kelleher, J., Daniel, A., Cowan, G. & Murray, N. Roles of selection and recombination in the evolution of type I restriction-modification systems in enterobacteria. *Proc Natl Acad Sci USA* **89,** 9836–9840 (1992).

118. Murray, N., Daniel, A., Cowan, G. & Sharp, P. Conservation of motifs within the unusually variable polypeptide sequences of type I restriction and modification enzymes. *Mol Microbiol* **9,** 133–134 (1993).

119. Zheng, Y., Roberts, R. & Kasif, S. Identification of genes with fast-evolving regions in microbial genomes. *Nucleic Acids Res* **32,** 6347–6357 (2004).

120. Suttle, C. A. Marine viruses - major players in the global ecosystem. *Nat Rev Micro* **5,** 801–812 (2007).

121. Comeau, A. & Krisch, H. War is peace - dispatches from the bacterial and phage killing fields. *Curr Opin Microbiol* **8,** 488–494 (2005).

122. Buckling, A. & Brockhurst, M. Bacteria–virus coevolution. *Adv Exp Med Biol* **751,** 347–370 (2012).

123. Bono, L. M., Gensel, C. L., Pfennig, D. W. & Burch, C. L. Competition and the origins of novelty: experimental evolution of niche-width expansion in a virus. *Biol Lett* **9,** 20120616 (2013).

124. Weinbauer, M. G. & Rassoulzadegan, F. Are viruses driving microbial diversification and

diversity? *Environ. Microbiol.* **6,** 1–11 (2004).

125. Rodriguez-Valera, F. *et al.* Explaining microbial population genomics through phage predation. *Nat. Rev. Microbiol.* **7,** 828–836 (2009).
126. Avrani, S., Wurtzel, O., Sharon, I., Sorek, R. & Lindell, D. Genomic island variability facilitates Prochlorococcus-virus coexistence. *Nature* **474,** 604–608 (2011).
127. Chatterjee, S. & Rothenberg, E. Interaction of Bacteriophage λ with Its E. coli Receptor, LamB. *Viruses* **4,** 3162–3178 (2012).
128. Naito, T., Kusano, K. & Kobayashi, I. Selfish behavior of restriction-modification systems. *Science* **267,** 897–899 (1995).
129. Stern, A., Keren, L., Wurtzel, O., Amitai, G. & Sorek, R. Self-targeting by CRISPR: gene regulation or autoimmunity? *Trends Genet.* **26,** (2010).
130. Papenfort, K. & Bassler, B. L. Quorum sensing signal–response systems in Gram-negative bacteria. *Nat. Rev. Microbiol.* **14,** 576 (2016).
131. Williams, P., Winzer, K., Chan, W. C. & Camara, M. Look who's talking: communication and quorum sensing in the bacterial world. *Philos. Trans. R. Soc. B Biol. Sci.* **362,** 1119–1134 (2007).
132. Fuqua, W. C., Winans, S. C. & Greenberg, E. P. Quorum sensing in bacteria: The LuxR-LuxI family of cell density- responsive transcriptional regulators. *J. Bacteriol.* **176,** 269–275 (1994).
133. Winzer, K., Hardie, K. R. & Williams, P. Bacterial cell-to-cell communication: Sorry, can't talk now - Gone to lunch! *Current Opinion in Microbiology* (2002). doi:10.1016/S1369-5274(02)00304-1
134. Atkinson, S., Camara, M. & Williams, P. N-acylhomoserine lactones, quorum sensing and biofilm development in Gram- negative bacteria. in *The biofilm mode of life. Mechanisms and adaptations* (eds. Kjellberg, S. & Givskov, M.) 55–122 (Horizon Bioscience, 2007).
135. Horng, Y. T. *et al.* The LuxR family protein SpnR functions as a negative regulator of N-acylhomoserine lactone-dependent quorum sensing in Serratia marcescens. *Mol. Microbiol.* **45,** 1655–1671 (2002).
136. Van der Meer, J. R. *et al.* Characterization of the Lactococcus lactis nisin A operon genes nisP, encoding a subtilisin-like serine protease involved in precursor processing, and nisR, encoding a regulatory protein involved in nisin biosynthesis. *J. Bacteriol.* **174,** 2053–2058 (1993).
137. McDowell, P. *et al.* Structure, activity and evolution of the group I thiolactone peptide quorum-sensing system of Staphylococcus aureus. *Mol. Microbiol.* **41,** 503–512 (2001).
138. Ansaldi, M., Marolt, D., Stebe, T., Mandic-Mulec, I. & Dubnau, D. Specific activation of

the Bacillus quorum-sensing systems by isoprenylated pheromone variants. *Mol Microbiol* **44,** 1561–1573 (2002).

139. Okada, M. *et al.* Structure of the Bacillus subtilis quorum-sensing peptide pheromone ComX. *Nat Chem Biol* **1,** 23–24 (2005).
140. Tan, D., Svenningsen, S. Lo & Middelboe, M. Quorum Sensing Determines the Choice of Antiphage Defense Strategy in Vibrio anguillarum. *MBio* **6,** e00627 (2015).
141. Høyland-Kroghsbo, N. M., Mærkedahl, R. B. & Svenningsen, S. Lo. A quorum-sensing-induced bacteriophage defense mechanism. *MBio* **4,** 1–8 (2013).
142. Høyland-Kroghsbo, N. M. *et al.* Quorum sensing controls the *Pseudomonas aeruginosa* CRISPR-Cas adaptive immune system. *Proc. Natl. Acad. Sci.* **114,** 131–135 (2017).
143. Patterson, A. G. *et al.* Quorum Sensing Controls Adaptive Immunity through the Regulation of Multiple CRISPR-Cas Systems. *Mol. Cell* **64,** 1102–1108 (2016).
144. Baughman, R. P., Thorpe, J. E., Staneck, J., Rashkin, M. & Frame, P. T. Use of the protected specimen brush in patients with endotracheal or tracheostomy tubes. *Chest* **91,** 233–236 (1987).
145. Beck, J. M. *et al.* The microbiome of the lung. *Transl Res* **160,** 258–266 (2012).
146. Thorpe, J. E., Baughman, R. P., Frame, P. T., Wesseler, T. A. & Staneck, J. L. Bronchoalveolar lavage for diagnosing acute bacterial pneumonia. *J Infect Dis* **155,** 855–861 (1987).
147. Turnbaugh, P. J. *et al.* The human microbiome project. *Nature* **449,** 804–10 (2007).
148. Round, J. L. & Mazmanian, S. K. The gut microbiota shapes intestinal immune responses during health and disease. *Nat Rev Immunol* **9,** 313–323 (2009).
149. Haiser, H. J. & Turnbaugh, P. J. Is it time for a metagenomic basis of therapeutics? *Science (80-.).* **336,** 1253–1255 (2012).
150. Hilty, M. *et al.* Disordered microbial communities in asthmatic airways. *PLoS One* **5,** e8578 (2010).
151. Erb-Downward, J. R. *et al.* Analysis of the lung microbiome in the 'healthy' smoker and in COPD. *PLoS One* **6,** e16384 (2011).
152. Sze, M. A. *et al.* The lung tissue microbiome in chronic obstructive pulmonary disease. *Am J Respir Crit Care Med* **185,** 1073–1080 (2012).
153. van der Gast, C. J. *et al.* Partitioning core and satellite taxa from within cystic fibrosis lung bacterial communities. *ISME J* **5,** 780–791 (2011).
154. Ley, R. E., Turnbaugh, P. J., Klein, S. & Gordon, J. I. Microbial ecology: human gut microbes associated with obesity. *Nature* **444,** 1022–1023 (2006).
155. Huffnagle, G. B. The microbiota and allergies/asthma. *PLoS Pathog* **6,** e1000549 (2010).

156. Ursell, L. K. *et al.* The intestinal metabolome: An intersection between microbiota and host. *Gastroenterology* **146,** 1470–1476 (2014).

157. Le Chatelier, E. *et al.* Richness of human gut microbiome correlates with metabolic markers. *Nature* **500,** 541–546 (2013).

158. Virgin, H. W. The virome in mammalian physiology and disease. *Cell* **157,** 142–150 (2014).

159. Reyes, A. *et al.* Viruses in the faecal microbiota of monozygotic twins and their mothers. *Nature* **466,** 334–338 (2010).

160. Minot, S. *et al.* The human gut virome: Inter-individual variation and dynamic response to diet. *Genome Res.* **21,** 1616–1625 (2011).

161. Barr, J. J. *et al.* Bacteriophage adhering to mucus provide a non-host-derived immunity. *Proc Natl Acad Sci U S A* **110,** 10771–10776 (2013).

162. Minot, S. *et al.* Rapid evolution of the human gut virome. *Proc Natl Acad Sci U S A* **110,** 12450–12455 (2013).

163. Kapusinszky, B., Minor, P. & Delwart, E. Nearly constant shedding of diverse enteric viruses by two healthy infants. *J. Clin. Microbiol.* **50,** 3427–3434 (2012).

164. Pride, D. T. *et al.* Evidence of a robust resident bacteriophage population revealed through analysis of the human salivary virome. *ISME J* **6,** 915–926 (2012).

165. Foulongne, V. *et al.* Human skin microbiota: high diversity of DNA viruses identified on the human skin by high throughput sequencing. *PLoS One* **7,** e38499 (2012).

166. Lim, Y. W. *et al.* Clinical insights from metagenomic analysis of sputum samples from patients with cystic fibrosis. *J Clin Microbiol* **52,** 425–437 (2014).

167. Willner, D. & Furlan, M. Deciphering the role of phage in the cystic fibrosis airway. *Virulence* **1,** 309–313 (2010).

168. Willner, D. *et al.* Case studies of the spatial heterogeneity of DNA viruses in the cystic fibrosis lung. *Am J Respir Cell Mol Biol* **46,** 127–131 (2012).

169. De Paepe, M., Leclerc, M., Tinsley, C. R. & Petit, M.-A. M.-A. Bacteriophages: an underestimated role in human and animal health? *Front Cell Infect Microbiol* **4,** 39 (2014).

170. Wiggins, B. A. & Alexander, M. Minimum bacterial density for bacteriophage replication: implications for significance of bacteriophages in natural ecosystems. *Appl. Environ. Microbiol.* **49,** 19–23 (1985).

171. Reyes, A., Wu, M., McNulty, N. P., Rohwer, F. L. & Gordon, J. I. Gnotobiotic mouse model of phage-bacterial host dynamics in the human gut. *Proc Natl Acad Sci U S A* **110,** 20236–20241 (2013).

172. Parsons, R. J., Breitbart, M., Lomas, M. W. & Carlson, C. A. Ocean time-series reveals recurring seasonal patterns of virioplankton dynamics in the northwestern Sargasso Sea.

ISME J. **6,** 273–284 (2012).

173. Golomidova, A., Kulikov, E., Isaeva, A., Manykin, A. & Letarov, A. The diversity of coliphages and coliforms in horse feces reveals a complex pattern of ecological interactions. *Appl. Environ. Microbiol.* **73,** 5975–5981 (2007).
174. Allen, H. K. *et al.* Antibiotics in feed induce prophages in swine fecal microbiomes. *MBio* **2,** e00260–e00211 (2011).
175. Boyd, E. F., Carpenter, M. R. & Chowdhury, N. Mobile effector proteins on phage genomes. *Bacteriophage* **2,** 139–148 (2012).
176. Verma, N. K., Brandt, J. M., Verma, D. J. & Lindberg, A. A. Molecular characterization of the O-acetyl transferase gene of converting bacteriophage SF6 that adds group antigen 6 to *Shigella flexneri*. *Mol Microbiol* **5,** 71–75 (1991).
177. Holmes, R. K. & Barksdale, L. Genetic analysis of tox+ and tox- bacteriophages of *Corynebacterium diphtheriae*. *J Virol* **3,** 586–598 (1969).
178. Tyler, J. S. *et al.* Prophage induction is enhanced and required for renal disease and lethality in an EHEC mouse model. *PLoS Pathog* **9,** e1003236 (2013).
179. Tobe, T. *et al.* An extensive repertoire of type III secretion effectors in *Escherichia coli* O157 and the role of lambdoid phages in their dissemination. *Proc Natl Acad Sci U S A* **103,** 14941–14946 (2006).
180. Harper, D. *et al.* Bacteriophages and Biofilms. *Antibiotics* **3,** 270 (2014).
181. Mills, S. *et al.* Movers and shakers: Influence of bacteriophages in shaping the mammalian gut microbiota. *Gut Microbes* **4,** 4–16 (2013).
182. Levin, B. R. & Bull, J. J. Population and evolutionary dynamics of phage therapy. *Nat Rev Microbiol* **2,** 166–173 (2004).
183. Pavlova, S. I. & Tao, L. Induction of vaginal Lactobacillus phages by the cigarette smoke chemical benzo[a]pyrene diol epoxide. *Mutat. Res. - Genet. Toxicol. Environ. Mutagen.* **466,** 57–62 (2000).
184. Wang, J., Gao, Y. & Zhao, F. Phage-bacteria interaction network in human oral microbiome. *Env. Microbiol* n/a-n/a (2015). doi:10.1111/1462-2920.12923
185. Preus, H. R., Olsen, I. & Gjermo, P. Bacteriophage infection--a possible mechanism for increased virulence of bacteria associated with rapidly destructive periodontitis. *Acta Odontol Scand* **45,** 49–54 (1987).
186. Palmer, K. L., Mashburn, L. M., Singh, P. K. & Whiteley, M. Cystic fibrosis sputum supports growth and cues key aspects of Pseudomonas aeruginosa physiology. *J Bacteriol* **187,** 5267–5277 (2005).
187. Harrison, F. Microbial ecology of the cystic fibrosis lung. *Microbiology* **153,** 917–923

(2007).

188. Willner, D. *et al.* Metagenomic analysis of respiratory tract DNA viral communities in cystic fibrosis and non-cystic fibrosis individuals. *PLoS One* **4,** e7370 (2009).

189. Hunter, P. The secret garden's gardeners. Research increasingly appreciates the crucial role of gut viruses for human health and disease. *EMBO Rep* **14,** 683–685 (2013).

190. Hamzeh-Mivehroud, M., Mahmoudpour, A., Rezazadeh, H. & Dastmalchi, S. Non-specific translocation of peptide-displaying bacteriophage particles across the gastrointestinal barrier. *Eur. J. Pharm. Biopharm.* **70,** 577–581 (2008).

191. Duerr, D. M., White, S. J. & Schluesener, H. J. Identification of peptide sequences that induce the transport ofphage across the gastrointestinalmucosal barrier. *J. Virol. Methods* **116,** 177–180 (2004).

192. Cario, E. Microbiota and innate immunity in intestinal inflammation and neoplasia. *Curr. Opin. Gastroenterol.* **29,** 85–91 (2013).

193. Hanahan, D & Weinberg, R. A. Hallmarks ofcancer: the next generation. *Cell* **144,** 646–674 (2011).

194. Delwart, E. A roadmap to the human virome. *PLoS Pathog* **9,** e1003146 (2013).

195. Scarpellini, E. *et al.* The human gut microbiota and virome: potential therapeutic implications. *Dig. Liver Dis.* **47,** 6–11 (2015).

196. Matsuzaki, S. *et al.* Bacteriophage therapy: A revitalized therapy against bacterial infectious diseases. *J. Infect. Chemother.* **11,** 211–219 (2005).

197. Pires, D., Sillankorva, S., Faustino, A. & Azeredo, J. Use of newly isolated phages for control of Pseudomonas aeruginosa PAO1 and ATCC 10145 biofilms. *Res. Microbiol.* **162,** 798–806 (2011).

198. Nakai, T. & Park, S. C. Bacteriophage therapy of infectious diseases in aquaculture. *Research in Microbiology* **153,** 13–18 (2002).

199. Goodridge, L. D. & Bisha, B. Phage-based biocontrol strategies to reduce foodborne pathogens in foods. *Bacteriophage* **1,** 130–137 (2011).

200. Balogh, B., Jones, J. B., Iriarte, F. B. & Momol, M. T. Phage therapy for plant disease control. *Curr Pharm Biotechnol* **11,** 48–57 (2010).

201. McCoy, M. Microphage staph test wins FDA approval. *Chem Eng News* **89,** 17 (2011).

202. Hagens, S. & Loessner, M. Application of bacteriophages for detection and control of foodborne pathogens. *Appl Microbiol Biotechnol* **76,** 513–519 (2007).

203. Lu, T. K. & Collins, J. J. Dispersing biofilms with engineered enzymatic bacteriophage. *Proc. Natl. Acad. Sci. U. S. A.* **104,** 11197–202 (2007).

204. Fischetti, V. A. Bacteriophage endolysins: A novel anti-infective to control Gram-positive

pathogens. *Int J Med Microbiol* **300,** 357–362 (2010).

205. Keary, R. *et al.* Bacteriophages and their endolysins for control of pathogenic bacteria. in *Microbial pathogens and strategies for combating them: science, technology and education Vol 2* (ed. Méndez-Vilas, A.) 1028–1040 (Formatex Research Center, 2013).
206. Wright, A., Hawkins, C. H., Änggard, E. E. & Harper, D. R. A controlled clinical trial of a therapeutic bacteriophage preparation in chronic otitis due to antibiotic-resistant Pseudomonas aeruginosa; A preliminary report of efficacy. *Clin. Otolaryngol.* **34,** 349–357 (2009).
207. Rhoads, D. D. *et al.* Bacteriophage therapy of venous leg ulcers in humans: results of a phase I safety trial. *Jounal Wound Care* **18,** 237–238 (2009).
208. Lu, T. K. & Koeris, M. S. The next generation of bacteriophage therapy. *Current Opinion in Microbiology* **14,** 524–531 (2011).
209. Krut, O. & Bekeredjian-Ding, I. Contribution of the Immune Response to Phage Therapy. *J. Immunol.* **200,** 3037–3044 (2018).
210. Leung, J. C. Y. & Weitz, J. S. Modeling the synergistic elimination of bacteria by phage and the innate immune system. *J. Theor. Biol.* **429,** 241–252 (2017).
211. Roach, D. R. *et al.* Synergy between the Host Immune System and Bacteriophage Is Essential for Successful Phage Therapy against an Acute Respiratory Pathogen. *Cell Host Microbe* **22,** 38–47.e4 (2017).
212. Dabrowska, K. *et al.* Immunogenicity Studies of Proteins Forming the T4 Phage Head Surface. *J. Virol.* **88,** 12551–12557 (2014).
213. Grütz, G. New insights into the molecular mechanism of interleukin-10-mediated immunosuppression. *J. Leukoc. Biol.* **77,** 3–15 (2005).
214. Górski, A. *et al.* The potential of phage therapy in sepsis. *Front. Immunol.* **8,** 1783 (2017).
215. Höglund, S. Electron microscopic investigations of the interaction between the T2-phage and its IgG-and IgM-antibodies. *Virology* **32,** 662–677 (1967).
216. Kucharewicz-Krukowska, A. & Slopek, S. Immunogenic effect of bacteriophage in patients subjected to phage therapy. *Arch Immunol Ther Exp* **35,** 553–561 (1987).
217. Suttle, C. A. & Fuhrman, J. A. Enumeration of virus particles in aquatic or sediment samples by epifluorescence microscopy. *Man. Aquat. Viral Ecol.* **15,** 145–153 (2010).
218. Brussaard, C. P. D. Optimization of Procedures for Counting Viruses by Flow Cytometry. *Appl. Environ. Microbiol.* **70,** 1506–1513 (2004).
219. Jacquet, S. & Bratbak, G. Effects of ultraviolet radiation on marine virus-phytoplankton interactions. *FEMS Microbiol. Ecol.* **44,** 279–289 (2003).
220. Filipe, V., Hawe, A. & Jiskoot, W. Critical evaluation of nanoparticle tracking analysis

(NTA) by NanoSight for the measurement of nanoparticles and protein aggregates. *Pharm. Res.* **27,** 796–810 (2010).

221. Ringen, L. & Drake, C. A study of the incidence of Pseudomonas aeruginosa from various natural sources. *J Bacteriol* **64,** 841–845 (1952).
222. Green, S. K., Schroth, M. N., Cho, J. J., Kominos, S. K. & Vitanza-jack, V. B. Agricultural plants and soil as a reservoir for Pseudomonas aeruginosa. *Appl. Microbiol.* **28,** 987–991 (1974).
223. Driscoll, J. A., Brody, S. L. & Kollef, M. H. The epidemiology, pathogenesis and treatment of Pseudomonas aeruginosa infections. *Drugs* **67,** 351–368 (2007).
224. Drenkard, E. Antimicrobial resistance of Pseudomonas aeruginosa biofilms. *Microbes Infect.* **5,** 1213–1219 (2003).
225. Mah, T. F. & O'Toole, G. A. Mechanisms of biofilm resistance to antimicrobial agents. *Trends Microbiol* **9,** (2001).
226. Hentzer, M. *et al.* Attenuation of Pseudomonas aeruginosa virulence by quorum sensing inhibitors. *EMBO J.* **22,** 3803–3815 (2003).
227. Bjarnsholt, T. *et al.* Pseudomonas aeruginosa tolerance to tobramycin, hydrogen peroxide and polymorphonuclear leukocytes is quorum-sensing dependent. *Microbiology* **151,** 373–383 (2005).
228. Sulakvelidze, A., Alavidze, Z., Morris Jr, J. G., Morris, J. G. & Morris Jr, J. G. Bacteriophage Therapy. *Antimicrob. Agents Chemother.* **45,** 649–659 (2001).
229. Sharma, M. Lytic bacteriophages: Potential interventions against enteric bacterial pathogens on produce. *Bacteriophage* **3,** e25518 (2013).
230. Arevalo-Ferro, C., Reil, G., Görg, A., Eberl, L. & Riedel, K. Biofilm formation of Pseudomonas putida IsoF: the role of quorum sensing as assessed by proteomics. *Syst. Appl. Microbiol.* **28,** 87–114 (2005).
231. Steidle, A. *et al.* Visualization of N-Acylhomoserine Lactone-Mediated Cell-Cell Communication between Bacteria Colonizing the Tomato Rhizosphere. *Appl. Environ. Microbiol.* **67,** 5761–5770 (2001).
232. Sullivan, M. B. *et al.* Portal protein diversity and phage ecology. *Env. Microbiol* **10,** 2810–2823 (2008).
233. Filee, J., Tetart, F., Suttle, C. A. & Krisch, H. M. Marine T4-type bacteriophages, a ubiquitous component of the dark matter of the biosphere. *Proc Natl Acad Sci U S A* **102,** 12471–12476 (2005).
234. Lau C., P. & Spencer H., J. An efficient synthetic primer for the M13 cloning dideoxy sequencing system. *Biosci. Rep.* **2,** 687–696 (1982).

235. Sullivan, M. B. *et al.* Prevalence and evolution of core photosystem II genes in marine cyanobacterial viruses and their hosts. *PLoS Biol* **4,** e234 (2006).

236. Lane J., D. 16S/23S rRNA sequencing. in *Nucleic acid techniques in bacterial systematics* (eds. Stackebrandt, E. & Goodfellow, M.) 115–175 (John Wiley and Sons, 1991).

237. Turner, S., Pryer, K. M. M., Miao, V. P. W. P. W. & Palmer, J. D. D. Investigating deep phylogenetic relationships among cyanobacteria and plastids by small subunit rRNA sequence analysis. in *Journal of Eukaryotic Microbiology* **46,** 327–338 (1999).

238. Gerriets, J. E., Greiner, T. C. & Gebhart, C. L. Implementation of a T4 Extraction Control for Molecular Assays of Cerebrospinal Fluid and Stool Specimens. *J Mol Diagn* **10,** 28–32 (2008).

239. Hegedüs, M. *et al.* Validation of phage T7 biological dosimeter by quantitative polymerase chain reaction using short and long segments of phage T7 DNA. *Photochem Photobiol* **78,** 213–219 (2003).

240. Dreier, J., Stormer, M. & Kleesiek, K. Use of bacteriophage MS2 as an internal control in viral reverse transcription-PCR assays. *J Clin Microbiol* **43,** 4551–4557 (2005).

241. Verreault, D. *et al.* Comparison of Polycarbonate and Polytetrafluoroethylene Filters for Sampling of Airborne Bacteriophages. *Aerosol Sci. Technol.* **44,** 197–201 (2010).

242. Duhaime, M. B., Deng, L., Poulos, B. T. & Sullivan, M. B. Towards quantitative metagenomics of wild viruses and other ultra-low concentration DNA samples: a rigorous assessment and optimization of the linker amplification method. *Env. Microbiol* **14,** 2526–2537 (2012).

243. Clark, D. J. & Maaløe, O. DNA replication and division cycle in Escherichia coli. *J Mol Biol* **23,** 99–103 (1967).

244. John, S. G. *et al.* A simple and efficient method for concentration of ocean viruses by chemical flocculation. *Environ. Microbiol. Rep.* **3,** 195–202 (2011).

245. O'Toole, G. A. Microtiter Dish Biofilm Formation Assay. *J. Vis. Exp.* 2437 (2011). doi:10.3791/2437

246. Hurwitz, B. L., Deng, L., Poulos, B. T. & Sullivan, M. B. Evaluation of methods to concentrate and purify ocean virus communities through comparative, replicated metagenomics. *Env. Microbiol* **15,** 1428–1440 (2013).

247. Patel, A. *et al.* Virus and prokaryote enumeration from planktonic aquatic environments by epifluorescence microscopy with SYBR Green I. *Nat. Protoc.* **2,** 269–276 (2007).

248. Rachel, R. *et al. Analysis of the ultrastructure of archaea by electron microscopy*. *Methods in Cell Biology* **96,** (2010).

249. Henn, M. R. *et al.* Analysis of high-throughput sequencing and annotation strategies for

phage genomes. *PLoS One* **5,** e9083 (2010).

250. Zhang, Z., Schwartz, S., Wagner, L. & Miller, W. A Greedy Algorithm for Aligning DNA Sequences. *J. Comput. Biol.* **7,** 203–214 (2000).
251. Schmieder, R., Lim, Y. W., Rohwer, F. & Edwards, R. TagCleaner: Identification and removal of tag sequences from genomic and metagenomic datasets. *BMC Bioinformatics* **11,** 341 (2010).
252. Lindgreen, S. *et al.* AdapterRemoval: easy cleaning of next generation sequencing reads. *BMC Res. Notes* **5,** 337 (2012).
253. Schmieder, R. & Edwards, R. Quality control and preprocessing of metagenomic datasets. *Bioinformatics* **27,** 863–864 (2011).
254. Schmieder, R. & Edwards, R. Fast identification and removal of sequence contamination from genomic and metagenomic datasets. *PLoS One* **6:e17288,** (2011).
255. Li, D., Liu, C. M., Luo, R., Sadakane, K. & Lam, T. W. MEGAHIT: An ultra-fast single-node solution for large and complex metagenomics assembly via succinct de Bruijn graph. *Bioinformatics* **31,** 1674–1676 (2015).
256. Hyatt, D. *et al.* Prodigal: Prokaryotic gene recognition and translation initiation site identification. *BMC Bioinformatics* **11,** 119 (2010).
257. Li, W., Jaroszewski, L. & Godzik, A. Clustering of highly homologous sequences to reduce the size of large protein databases. *Bioinformatics* **17,** 282–283 (2001).
258. Altschul, S. F., Gish, W., Miller, W., Myers, E. W. & Lipman, D. J. Basic local alignment search tool. *J Mol Biol* **215,** 403–410 (1990).
259. Grazziotin, A. L., Koonin, E. V. & Kristensen, D. M. Prokaryotic Virus Orthologous Groups (pVOGs): A resource for comparative genomics and protein family annotation. *Nucleic Acids Res.* **45,** D491–D498 (2017).
260. Dutilh, B. E. *et al.* Reference-independent comparative metagenomics using cross-assembly: CrAss. *Bioinformatics* **28,** 3225–3231 (2012).
261. R Core Team. R: A Language and Environment for Statistical Computing [Online]. Vienna: R Foundation for Statistical Computing. (2017).
262. Oksanen, J. *et al.* Vegan: Community Ecology Package. (2017).
263. Buddrus-Schiemann, K. *et al.* Analysis of N-acylhomoserine lactone dynamics in continuous cultures of Pseudomonas putida IsoF by use of ELISA and UHPLC/qTOF-MS-derived measurements and mathematical models. *Anal. Bioanal. Chem.* **406,** 6373–6383 (2014).
264. Chen, X. *et al.* Development and characterization of rat monoclonal antibodies for N-acylated homoserine lactones. *Anal. Bioanal. Chem.* **398,** 2655–2667 (2010).

265. Fekete, A. *et al.* Dynamic regulation of N-acyl-homoserine lactone production and degradation in *Pseudomonas putida* IsoF. *FEMS Microbiol. Ecol.* **72,** 22–34 (2010).

266. Englmann, M. *et al.* The hydrolysis of unsubstituted N-acylhomoserine lactones to their homoserine metabolites: analytical approaches using ultra performance liquid chromatography. *J Chromatogr A* **1160,** 184–193 (2007).

267. Schrader, H. S. *et al.* Bacteriophage infection and multiplication occur in Pseudomonas aeruginosa starved for 5 years. *Can. J. Microbiol.* **43,** 1157–63 (1997).

268. Kokjohn, T., Sayler, G. & Miller, R. Attachment and replication of Pseudomonas aeruginosa bacteriophages under conditions simulating aquatic environments. *J. Gen. Microbiol.* 661–666 (1991).

269. Barbarossa, M. & Kuttler, C. Mathematical Modeling of Bacteria Communication in Continuous Cultures. *Appl. Sci.* **6,** 149 (2016).

270. Dockery, J. & Keener, J. P. A Mathematical Model for Quorum Sensing in Pseudomonas aeruginosa. *Bull. Math. Biol.* **63,** 95–116 (2001).

271. Frederick, M. R., Kuttler, C., Hense, B. A. & Eberl, H. J. A mathematical model of quorum sensing regulated EPS production in biofilm communities. *Theor. Biol. Med. Model.* **8,** 8 (2011).

272. Emerenini, B. O., Hense, B. A., Kuttler, C. & Eberl, H. J. A mathematical model of quorum sensing induced biofilm detachment. *PLoS One* **10,** 1–25 (2015).

273. Guttman, B., Raya, R. & Kutter, E. Basic Phage Biology. in *Bacteriophages: Biology and Application* 29–66 (CRC Press, 2005).

274. Sanger, F. *et al.* The nucleotide sequence of bacteriophage phiX174. *J. Mol. Biol.* **125,** 225–246 (1978).

275. Wickham, H. ggplot2: Elegant Graphics for Data Analysis. (2016).

276. Baptiste, A. gridExtra: Miscellaneous Functions for 'Grid' Graphics. R package version 2.0.0. (2015).

277. Fox, J. & Weisberg, S. An {R} Companion to Applied Regression. (2011).

278. Roudnew, B. *et al.* Bacterial and Virus-Like Particle Abundances in Purged and Unpurged Groundwater Depth Profiles. *Ground Water Monit. Remediat.* **32,** 72–77 (2012).

279. Yoshida, T. *et al.* Isolation and Characterization of a Cyanophage Infecting the Toxic Cyanobacterium Microcystis aeruginosa Isolation and Characterization of a Cyanophage Infecting the Toxic Cyanobacterium Microcystis aeruginosa. *Appl. Environ. Microbiol.* **72,** 1239–1247 (2006).

280. Clasen, J. L., Brigden, S. M., Payet, J. P. & Suttle, C. A. Evidence that viral abundance across oceans and lakes is driven by different biological factors. *Freshw. Biol.* **53,** 1090–1100

(2008).

281. Shiklomanov, I. A. Appraisal and Assessment of world water resources. *Water Int.* **25,** 11–32 (2000).

282. Steward, G., Montiel, J. & Azam, F. Genome size distributions indicate variability and similarities among marine viral assemblages from diverse environments. *Limnol Ocean.* **45,** 1697–1706 (2000).

283. Miravitlles, M. *et al.* Relationship between bacterial flora in sputum and functional impairment in patients with acute exacerbations of COPD. Study Group of Bacterial Infection in COPD. *Chest* **116,** 40–46 (1999).

284. Murphy, T. F. *et al.* Pseudomonas aeruginosa in chronic obstructive pulmonary disease. *Am J Respir Crit Care Med* **177,** 853–860 (2008).

285. Nielsen, H., Hvidt, S., Sheils, C. A. & Janmey, P. A. Elastic contributions dominate the viscoelastic properties of sputum from cystic fibrosis patients. *Biophys. Chem.* **112,** 193–200 (2004).

286. Rancourt, R. C. *et al.* Thioredoxin liquefies and decreases the viscoelasticity of cystic fibrosis sputum. *Am. J. Physiol. Lung Cell. Mol. Physiol.* **286,** L931–L938 (2004).

287. Baxter, C. G., Jones, A. M., Webb, K. & Denning, D. W. Homogenisation of cystic fibrosis sputum by sonication - An essential step for Aspergillus PCR. *J. Microbiol. Methods* **85,** 75–81 (2011).

288. LaBauve, A. E. & Wargo, M. J. Growth and laboratory maintenance of Pseudomonas aeruginosa. in *Curr Protoc Microbiol* 6E 1 (2012).

289. Pires, D. P., Sillankorva, S., Kropinski, A. M., Lu, T. K. & Azeredo, J. Complete Genome Sequence of Pseudomonas aeruginosa Phage vB_PaeM_CEB_DP1. *Genome Announc.* **3,** e00918-15 (2015).

290. Bayer, A., Drexel, R., Weber, N. & Griebler, C. Quantification of aquatic sediment prokaryotes-A multiple-steps optimization testing sands from pristine and contaminated aquifers. *Limnologica* **56,** 6–13 (2016).

291. Carey-Smith, G. V., Billington, C., Cornelius, A. J., Hudson, J. A. & Heinemann, J. A. Isolation and characterization of bacteriophages infecting Salmonella spp. *FEMS Microbiol. Lett.* **258,** 182–186 (2006).

292. Fischer, C. R., Yoichi, M., Unno, H. & Tanji, Y. The coexistence of Escherichia coli serotype O157:H7 and its specific bacteriophage in continuous culture. *FEMS Microbiol. Lett.* **241,** 171–177 (2004).

293. Hense, B. A., Müller, J., Kuttler, C. & Hartmann, A. Spatial heterogeneity of autoinducer regulation systems. *Sensors* **12,** 4156–4171 (2012).

294. Longo, F. *et al.* A New Transcriptional Repressor of the Pseudomonas aeruginosa Quorum Sensing Receptor Gene lasR. *PLoS One* **8,** e69554 (2013).

295. Li, R. *et al.* Type I CRISPR-Cas targets endogenous genes and regulates virulence to evade mammalian host immunity. *Cell Res.* **26,** 1273–1287 (2016).

296. Moreau, P., Diggle, S. P. & Friman, V. P. Bacterial cell-to-cell signaling promotes the evolution of resistance to parasitic bacteriophages. *Ecol. Evol.* **7,** 1936–1941 (2017).

297. Venturi, V. Regulation of quorum sensing in Pseudomonas. *FEMS Microbiol. Rev.* **30,** 274–291 (2006).

298. Szmelcman, S. & Hofnung, M. Maltose transport in Escherichia coli K-12: involvement of the bacteriophage lambda receptor. *J. Bacteriol.* **124,** 112–8 (1975).

299. Ziegler-Heitbrock, L. *et al.* The EvA study: aims and strategy. *Eur Respir J* **40,** 823–829 (2012).

300. Elbehery, A. H. A., Feichtmayer, J., Singh, D., Griebler, C. & Deng, L. The Human Virome Protein Cluster Database (HVPC): A Human Viral Metagenomic Database for Diversity and Function Annotation. *Front. Microbiol.* **9,** 1110 (2018).

301. Zhao, S., Guo, Y., Sheng, Q. & Shyr, Y. Heatmap3: An Improved Heatmap Package [Online]. (2015).

302. Hamilton, N. ggtern: An Extension to 'ggplot2', for the Creation of Ternary Diagrams [Online]. (2017).

303. Wylie, K. M., Weinstock, G. M. & Storch, G. A. Emerging View of the Human Virome. *Transl Res* **160,** 283–290 (2012).

304. Woolhouse, M. E. J. *et al.* Temporal trends in the discovery of human viruses. *Proc. R. Soc. B-Biological Sci.* **275,** 2111–2115 (2008).

305. Belizário, J. E. & Napolitano, M. Human microbiomes and their roles in dysbiosis, common diseases, and novel therapeutic approaches. *Front. Microbiol.* **6,** 1050 (2015).

306. Hurwitz, B. L. & Sullivan, M. B. The Pacific ocean virome (POV): a marine viral metagenomic dataset and associated protein clusters for quantitative viral ecology. *PLoS One* **8:e57355,** (2013).

307. Wilson, W. H., Van Etten, J. L. & Allen, M. J. The phycodnaviridae: the story of how tiny giants rule the world. *Curr. Top. Microbiol. Immunol* **328,** 1–42 (2009).

308. Aherfi, S., Colson, P., La Scola, B. & Raoult, D. Giant viruses of amoebas: an update. *Front. Microbiol.* **7,** 349 (2016).

309. Saadi, H. *et al.* First Isolation of Mimivirus in a patient with pneumonia. *Clin. Infect. Dis.* **57,** e127-134 (2013).

310. Li, N. *et al.* Exposure to ambient particulate matter alters the microbial composition and

induces immune changes in rat lung. *Respir. Res.* **18,** 143 (2017).

311. McManus, T. *et al.* Herpes simplex virus and mortality in COPD. *Am. J. Respir. Crit. Care Med.* **179,** A5348 (2009).
312. Brooke, J. S. Stenotrophomonas maltophilia: an emerging global opportunistic pathogen. *Clin. Microbiol. Rev.* **25,** 2–41 (2012).
313. King, P. T., Macdonald, M. & Bardin, P. G. Bacteria in COPD; their potential role and treatment. *Transl. Respir. Med.* **1,** 13 (2013).
314. Hashemi, S. H., Nadi, E., Hajilooi, M., Seif-Rabiei, M.-A. & Samaei, A. High seroprevalence of Bordetella pertussis in patients with chronic obstructive pulmonary disease: a case-control study. *Tanaffos* **14,** 172–176 (2015).
315. Penadés, J. R., Chen, J., Quiles-Puchalt, N., Carpena, N. & Novick, R. P. Bacteriophage-mediated spread of bacterial virulence genes. *Curr. Opin. Microbiol.* **23,** 171–178 (2015).
316. Enault, F. *et al.* Phages rarely encode antibiotic resistance genes: a cautionary tale for virome analyses. *ISME J.* **11,** 237–247 (2017).
317. Qin, J. *et al.* A human gut microbial gene catalogue established by metagenomic sequencing. *Nature* **464,** 59–65 (2010).
318. Reyes, A. *et al.* Gut DNA viromes of Malawian twins discordant for severe acute malnutrition. *Proc. Natl. Acad. Sci.* **112,** 201514285 (2015).
319. Kim, M. S., Park, E. J., Roh, S. W. & Bae, J. W. Diversity and abundance of single-stranded DNA viruses in human feces. *Appl Env. Microbiol* **77,** 8062–8070 (2011).
320. Santiago-Rodriguez, T. M., Ly, M., Bonilla, N. & Pride, D. T. The human urine virome in association with urinary tract infections. *Front. Microbiol.* **6,** 14 (2015).
321. Abeles, S. R. *et al.* Human oral viruses are personal, persistent and gender-consistent. *ISME J* **8,** 1753–1767 (2014).
322. Abeles, S. R., Ly, M., Santiago-Rodriguez, T. M. & Pride, D. T. Effects of Long Term Antibiotic Therapy on Human Oral and Fecal Viromes. *PLoS One* **10,** e0134941 (2015).
323. Wiedenbeck, J. & Cohan, F. M. Origins of bacterial diversity through horizontal genetic transfer and adaptation to new ecological niches. *FEMS Microbiol. Rev.* **35,** 957–976 (2011).
324. Favre-Bonté, S., Köhler, T. & Van Delden, C. Biofilm formation by Pseudomonas aeruginosa: Role of the C4-HSL cell-to-cell signal and inhibition by azithromycin. *J. Antimicrob. Chemother.* **52,** 598–604 (2003).
325. Hughes, K. A., Sutherland, I. W., Jones, M. V. & Rutherford, D. Biofilm susceptibility to bacteriophage attack: The role of phage-borne polysaccharide depolymerase. *Microbiology* **144,** 3039–3047 (1998).

326. Moons, P., Faster, D. & Aertsen, A. Lysogenic Conversion and Phage Resistance Development in Phage Exposed Escherichia coli Biofilms. *Viruses* **5,** 150–161 (2013).

327. Kutateladze, M., March, I., Young, R. & Reardon, S. Phage therapy gets revitalized. *Nature* **510,** 15–16 (2014).

328. Dickson, R. P. & Huffnagle, G. B. The lung microbiome: new principles for respiratory bacteriology in health and disease. *PLoS Pathog* **11,** e1004923 (2015).

329. Budden, K. F. *et al.* Emerging pathogenic links between microbiota and the gut-lung axis. *Nat Rev Microbiol* **15,** 55–63 (2017).

330. Manrique, P., Dills, M. & Young, M. The Human Gut Phage Community and Its Implications for Health and Disease. *Viruses* **9,** 141 (2017).

6 SUPPLEMENTARY MATERIAL

6.1 Supplementary material for 3.2

Table 6-1: Concentrations of phage isolates of *P. aeruginosa* PAO1 determined by plaque assay.

Phage ID	PFU mL^{-1}
Inc_01	2.00×10^{10}
Inc_02	1.60×10^{11}
Inc_03	2.95×10^{10}
Inc_05	1.03×10^{11}
Inc_06	2.85×10^{11}
Inc_09	4.00×10^{9}
Inc_10	3.90×10^{10}
Inc_12	1.35×10^{11}
Inc_13	1.00×10^{10}
Inc_15	3.90×10^{10}
Inc_16	1.96×10^{11}
Inc_17	1.50×10^{11}
Inc_21	8.35×10^{10}
Inc_23	2.30×10^{10}
Inc_24	2.10×10^{10}
Inc_26	1.70×10^{10}
Inc_33	5.70×10^{10}
BAL_01	1.72×10^{9}
BAL_02	1.51×10^{9}
BAL_03	2.01×10^{9}
BAL_04	1.05×10^{11}
BAL_05	5.80×10^{10}
BAL_08	2.59×10^{10}
BAL_09	1.56×10^{11}
BAL_11	1.45×10^{11}
BAL_12	2.80×10^{10}
BAL_13	7.80×10^{10}
BAL_15	4.08×10^{10}
BAL_16	3.80×10^{10}
BAL_20	2.61×10^{11}

Table 6-2: Average number of PFU mL^{-1} upon incubation at different temperatures. Colored areas represent comparisons between phage titers at 37 °C and 42 °C. Grey color indicates no difference. Light green color indicates a lower concentration at 42 °C. Light blue color indicates a higher concentration at 42 °C.

	22 °C		37 °C		42 °C	
	mean PFU mL^{-1}	**sd**	**mean PFU mL^{-1}**	**sd**	**mean PFU mL^{-1}**	**sd**
BAL_01	1.80×10^{8}	5.66×10^{7}	9.00×10^{9}	1.41×10^{9}	9.00×10^{9}	1.41×10^{9}
BAL_02	1.60×10^{8}	5.66×10^{7}	5.00×10^{9}	1.41×10^{9}	2.00×10^{9}	0
BAL_03	1.40×10^{8}	5.66×10^{7}	6.00×10^{9}	2.83×10^{9}	6.00×10^{9}	2.83×10^{9}
BAL_04	1.00×10^{9}	1.41×10^{9}	2.24×10^{11}	1.41×10^{10}	2.05×10^{11}	2.12×10^{10}
BAL_05	2.30×10^{9}	7.07×10^{8}	1.61×10^{11}	1.56×10^{10}	1.71×10^{11}	1.84×10^{10}
BAL_08	9.00×10^{8}	1.41×10^{8}	8.60×10^{10}	0	6.40×10^{10}	3.11×10^{10}
BAL_09	9.00×10^{9}	1.41×10^{9}	8.41×10^{11}	1.41×10^{9}	8.83×10^{11}	2.40×10^{10}
BAL_11	3.50×10^{10}	2.12×10^{10}	1.75×10^{12}	6.51×10^{10}	1.81×10^{12}	1.56×10^{10}
BAL_12	8.50×10^{9}	1.84×10^{9}	4.40×10^{10}	2.26×10^{10}	5.30×10^{10}	4.24×10^{9}
BAL_13	2.44×10^{10}	1.98×10^{9}	1.59×10^{11}	1.41×10^{9}	1.80×10^{11}	3.96×10^{10}
BAL_15	1.52×10^{10}	1.13×10^{9}	9.90×10^{10}	7.07×10^{9}	9.70×10^{10}	1.27×10^{10}
BAL_16	1.70×10^{9}	1.41×10^{8}	6.20×10^{10}	5.66×10^{9}	6.90×10^{10}	1.84×10^{10}
BAL_20	8.40×10^{10}	1.41×10^{10}	3.72×10^{11}	3.39×10^{10}	3.71×10^{11}	4.38×10^{10}
Inc_01	1.22×10^{10}	1.98×10^{9}	4.30×10^{10}	9.90×10^{9}	3.50×10^{10}	7.07×10^{9}
Inc_02	4.00×10^{10}	2.83×10^{9}	6.94×10^{11}	3.68×10^{10}	6.19×10^{11}	5.80×10^{10}
Inc_03	1.43×10^{10}	6.65×10^{9}	7.70×10^{10}	7.07×10^{9}	6.70×10^{10}	1.84×10^{10}
Inc_05	2.00×10^{10}	5.66×10^{9}	1.63×10^{11}	4.24×10^{9}	1.81×10^{11}	4.24×10^{9}
Inc_06	7.00×10^{9}	1.41×10^{9}	2.85×10^{11}	1.97×10^{11}	3.34×10^{11}	2.52×10^{11}
Inc_09	2.50×10^{8}	1.56×10^{8}	2.00×10^{10}	2.83×10^{9}	1.30×10^{10}	1.41×10^{9}
Inc_10	3.10×10^{9}	9.90×10^{8}	7.60×10^{10}	1.41×10^{10}	7.50×10^{10}	7.07×10^{9}
Inc_12	1.30×10^{10}	1.41×10^{9}	6.24×10^{11}	1.56×10^{11}	3.36×10^{11}	2.83×10^{9}
Inc_13	2.50×10^{9}	1.41×10^{8}	4.70×10^{10}	4.24×10^{9}	5.50×10^{10}	9.90×10^{9}
Inc_15	5.40×10^{9}	1.98×10^{9}	2.28×10^{11}	1.67×10^{11}	1.18×10^{11}	4.53×10^{10}
Inc_16	1.90×10^{10}	7.07×10^{9}	2.12×10^{11}	1.10×10^{11}	1.85×10^{11}	6.93×10^{10}
Inc_17	1.00E+10	5.66E+09	2.16E+11	0.00E+00	2.01E+11	1.56E+10
Inc_21	4.39E+10	7.78E+09	5.90E+11	1.70E+10	6.28E+11	4.24E+10
Inc_23	9.60E+09	5.66E+08	1.03E+12	5.23E+10	1.21E+12	4.24E+10
Inc_24	6.30E+09	2.12E+09	8.03E+11	1.41E+09	8.29E+11	4.38E+10
Inc_26	3.00E+08	1.41E+08	6.10E+10	4.24E+09	4.60E+10	1.98E+10
Inc_33	8.70E+09	7.07E+08	2.04E+11	1.13E+10	2.15E+11	4.24E+09

Table 6-3: Phage isolates grouped according to their behavior at different pH values.

No effect of pH on infectivity	Maximal infectivity at pH 7	Maximal infectivity at pH 6	higher pH values preferred
Inc_1	Inc_3	Inc_1	Inc_3
Inc_3	Inc_12	Inc_2	Inc_5
Inc_17	Inc_13	Inc_5	Inc_15
Inc_21	Inc_21	Inc_6	Inc_16
Inc_23	Inc_33	Inc_16	Inc_24
Inc_33		Inc_24	
6/14 = 42.86 %	5/14 = 35.71 %	6/14 = 42.86 %	5/14 = 35.71 %
BAL_2	BAL_4	BAL_3	BAL_9
BAL_3	BAL_5	BAL_8	BAL_15
BAL_4	BAL_9	BAL_11	BAL_16
	BAL_15	BAL_13	
	BAL_16	BAL_20	
3/13 = 23.08 %	5/13 = 38.46 %	5/13 = 38.46 %	3/13 = 23.08 %
	Inc: 11/14 = 78.57 %; BAL: 10/13 = 76.92 %		

Table 6-4: Phage isolates sent out for sequencing with the respective reverse primer used for PCR.

Phage ID	Rev. primer used for PCR
BAL 4	gep5_rev_16G>AC
BAL 5	gep5_rev_16G>AC
BAL 8	gep5_rev_16G>AC
BAL 9	gep5_rev_16G>AC
BAL 12	gep5_rev_16G>AC
BAL 13	gep5_rev_16G>AC
BAL 15	gep5_rev_16G>AC
BAL 16	gep5_rev_16G>AC
BAL 20	gep5_rev_16G>AC
Inc 1	gep5_rev_16G>AC
Inc 2	gep5_rev_16G>AC
Inc 3	gep5_rev_16G>AC
Inc 9	gep5_rev_16G>AC
Inc 10	gep5_rev_16G>AC
Inc 11	gep5_rev_16G>AC
Inc 13	gep5_rev_16G>AC
Inc 15	gep5_rev_16G>AC

Inc 16	gep5_rev_16G>AC
Inc 17	gep5_rev_16G>AC
Inc 21	gep5_rev_16G>AC
Inc 23	gep5_rev_16G>AC
Inc 24	gep5_rev_16G>AC
Inc 26	gep5_rev_16G>AC
Inc 33	gep5_rev_16G>AC
BAL 4_Rv	gep5_rev
BAL 5_Rv	gep5_rev
BAL 8_Rv	gep5_rev
BAL 9_Rv	gep5_rev
pos.	gep5_rev_16G>AC
neg.	gep5_rev_16G>AC

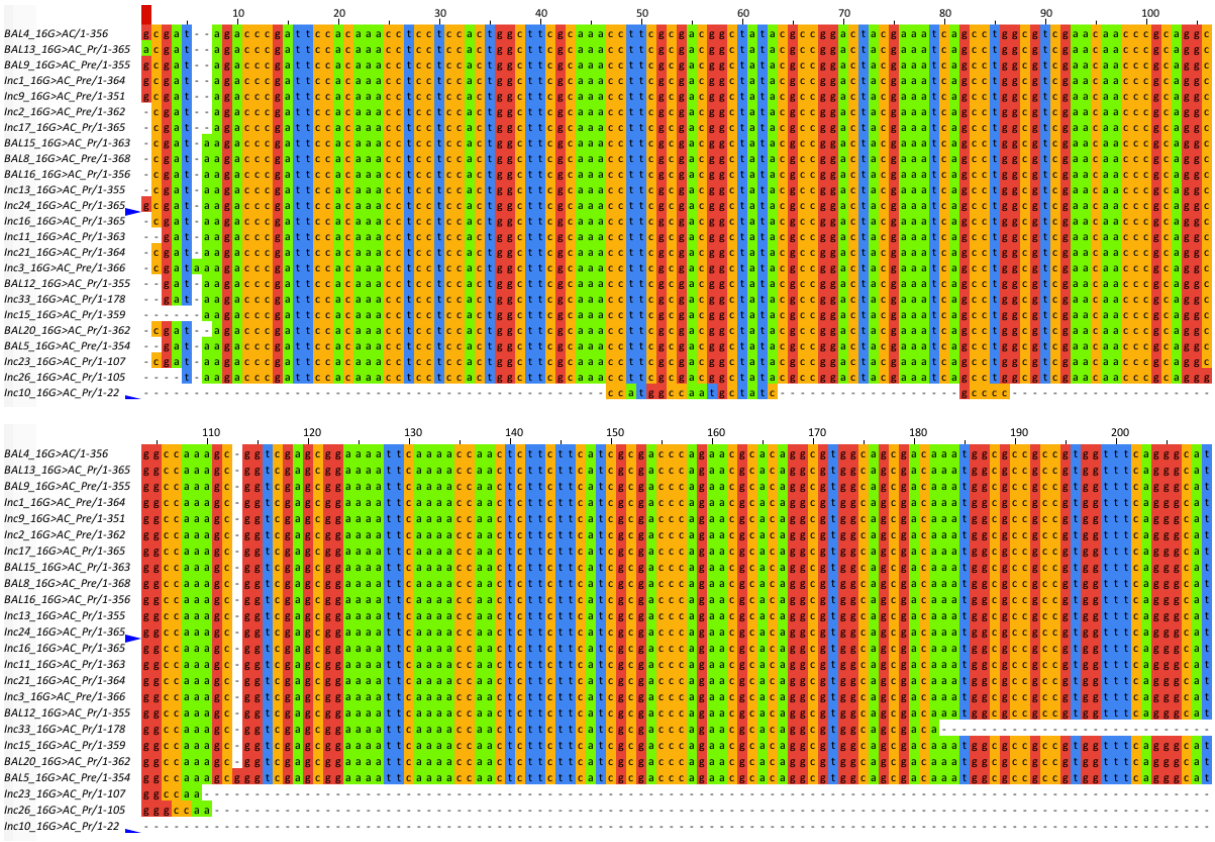

Figure 6-1: Alignment of gep5 sequencing result. The alignment was performed using the MAFFT multiple sequence alignment tool. Visualization occurred with Jalview software (v 2.10.5). This alignment contains only the sequences of the reverse primer gep5_rev_16G>AC.

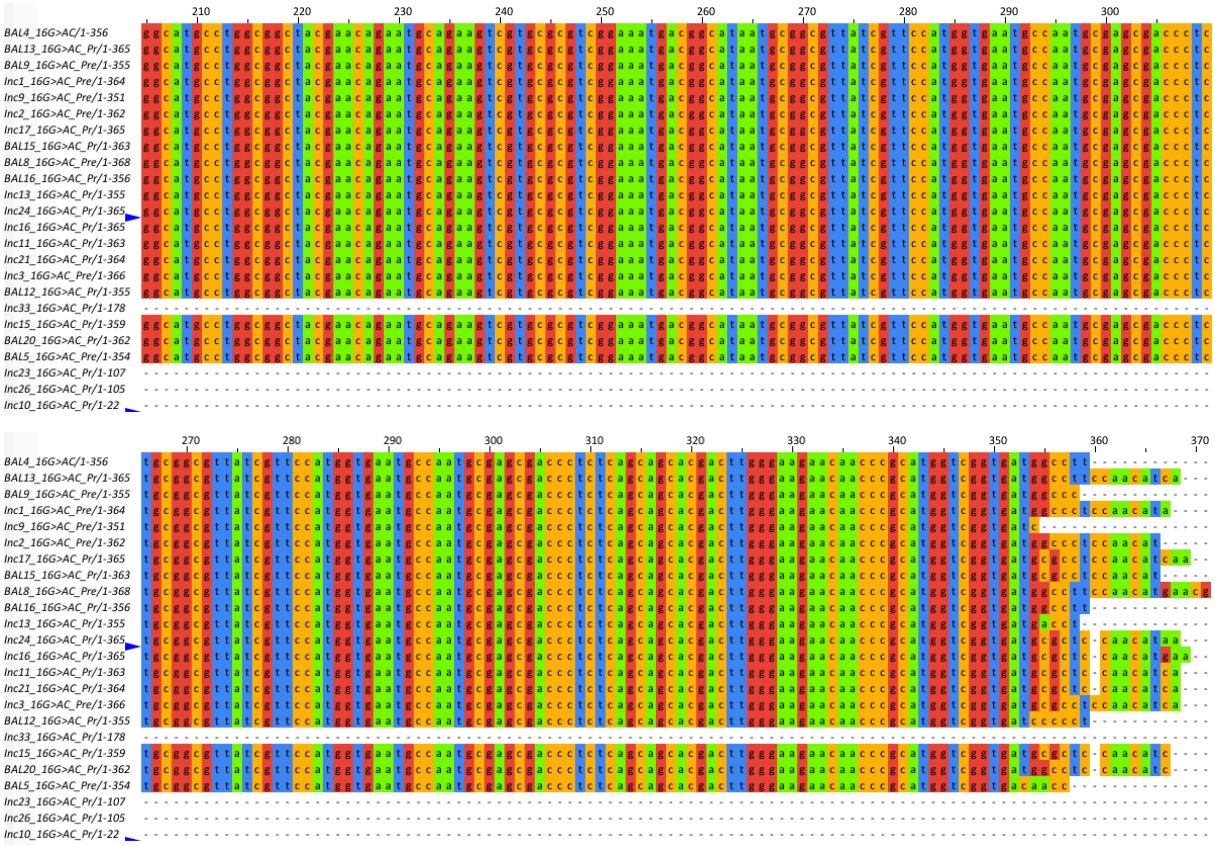

Figure 6-1 (continued): Alignment of gep5 sequencing result. The alignment was performed using the MAFFT multiple sequence alignment tool. Visualization occurred with Jalview software (v 2.10.5). This alignment contains only the sequences of the reverse primer gep5_rev_16G>AC.

6.2 Supplementary material for 3.3

Table 6-5: Denotation of the parameters describing the basic model. The respective values were fitted to the control group D and, where necessary, also to group A.

Parameters	Meaning and units	Fitted value
α_{Nut}	Max. growth rate of non-resistant bacteria (h^{-1})	0.54
α_{Nutr}	Max. growth rate of resistant bacteria (h^{-1})	0.89
γ_{Nut}	Nutrient consumption rate by bacteria (L cells^{-1} h^{-1})	2.30×10^{-6}
K_m	Nutrient concentration for half-max. bacterial growth	0.73
R_{recy}	Proportion of recycling (L cells^{-1})	4.10×10^{-6}
γ_t	Infection rate of non-resist. Bacteria by phages (L cells^{-1} h^{-1})	1.60×10^{-10}
γ_{tt}	Infection rate of resistant bacteria by phages (L cells^{-1} h^{-1})	5.70×10^{-16}
δ	Phage-induced death rate of infected bacteria (h^{-1})	0.19
d	Infected cells natural death rate (h^{-1})	7.30×10^{-6}
ρ	Amplification factor of phages	$3.10\ 10^{2}$
c	Virus inactivation rate (h^{-1})	$2.60\ 10^{-2}$
n	Hill coefficient (dimensionless)	7.00
α	Basic production rate of HSL (mol cells^{-1} h^{-1})	8.00×10^{-19}
β	PpuR:HSL regulated production rate of HSL (mol cells^{-1} h^{-1})	1.50×10^{-17}
γ_A	Abiotic HSL degradation rate (h^{-1})	$3.10\ 10^{-2}$
K_e	HSL degradation rate by lactonase (L mol^{-1} h^{-1})	4.30×10^{-7}
C_1	Threshold value of PpuR:HSL concentration for pos. feedback in QS (mol L^{-1})	8.30×10^{-8}
α_c	PpuR:HSL binding rate (L mol^{-1} h^{-1})	3.80×10^{4}
γ_c	PpuR:HSL degradation rate (h^{-1})	1.60
R_c	Total PpuR concentration in the cells (mol L^{-1})	3.60×10^{-5}
α_L	Lactonase activation/production rate (mol cells^{-1} h^{-1})	8.50×10^{-6}
γ_L	Lactonase degradation rate (h^{-1})	0.19

Table 6-6: Denotation of the parameters describing the advanced model. The respective values describing hypothesis 4 were fitted to the control group D and, where necessary, also to group A.

Parameters	Meaning and units	Fitted value
α_{Nut}	Max. growth rate of non-resistant bacteria (h^{-1})	0.45
α_{Nutr}	Max. growth rate of resistant bacteria (h^{-1})	0.42
γ_{Nut}	Nutrient consumption rate by bacteria (L $cells^{-1}$ h^{-1})	1.30×10^{-9}
K_m	Nutrient concentration for half-max. bacterial growth	0.45
R_{recy}	Proportion of recycling (L $cells^{-1}$)	1.20×10^{-9}
γ_t	Infection rate of non-resist. Bacteria by phages (L $cells^{-1}$ h^{-1})	4.50×10^{-11}
γ_{tt}	Infection rate of resistant bacteria by phages (L $cells^{-1}$ h^{-1})	3.20×10^{-14}
ψ_1	Rate at which cells loose resistance (L mol^{-1} h^{-1})	1.40×10^{-3}
ψ_2	Switch rate from non-resistant to resistant state (L mol^{-1} h^{-1})	0.18
δ	Phage-induced death rate of infected bacteria (h^{-1})	0.08
d	Infected cells natural death rate (h^{-1})	7.30×10^{-6}
ρ	Amplification factor of phages	1.20×10^{3}
c	Virus inactivation rate (h^{-1})	$8.20\ 10^{-3}$
n	Hill coefficient (dimensionless)	2.70
α	Basic production rate of HSL (mol $cells^{-1}$ h^{-1})	1.20×10^{-18}
β	PpuR:HSL regulated production rate of HSL (mol $cells^{-1}$ h^{-1})	1.30×10^{-17}
K_e	HSL degradation rate by lactonase (L mol^{-1} h^{-1})	1.07×10^{-7}
C_1	Threshold value of PpuR:HSL concentration for pos. feedback in QS (mol L^{-1})	1.50×10^{-7}
α_c	PpuR:HSL binding rate (L mol^{-1} h^{-1})	4.20×10^{3}
γ_c	PpuR:HSL degradation rate (h^{-1})	2.20×10^{-5}
R_c	Total PpuR concentration in the cells (mol L^{-1})	3.40×10^{-5}
α_L	Lactonase activation/production rate (mol $cells^{-1}$ h^{-1})	7.40×10^{-6}
γ_L	Lactonase degradation rate (h^{-1})	0.10

Equation 6-1: Formulas describing the basic model.

$$\frac{dN}{dt} = -\frac{\gamma_{Nut}(B_N + B_R + B_I)N}{K_m + N} + R_{recy}(d+\delta)B_I \quad (1.1a)$$

$$\frac{dB_N}{dt} = \frac{\alpha_{Nut}B_N N}{K_m + N} - \gamma_t P B_N \quad (1.1b)$$

$$\frac{dB_R}{dt} = \frac{\alpha_{Nutr}B_R N}{K_m + N} - \gamma_{tt} P B_R \quad (1.1c)$$

$$\frac{dB_I}{dt} = \gamma_t P B_N + \gamma_{tt} P B_R - (d+\delta)B_I \quad (1.1d)$$

$$\frac{dP}{dt} = \rho\delta B_I - \gamma_t P B_N - \gamma_{tt} P B_R - cP \quad (1.1e)$$

$$\frac{dA}{dt} = \left(\alpha + \beta\frac{R_A^n}{C_1^n + R_A^n}\right)(B_N + B_R) - \alpha_c(R_c - R_A)A - K_e A L + \gamma_c R_A - \gamma_A A \quad (1.1f)$$

$$\frac{dR_A}{dt} = \alpha_c(R_c - R_A)A - \gamma_c R_A \quad (1.1g)$$

$$\frac{dL}{dt} = \alpha_L(B_N + B_R)\frac{R_A^n}{C_1^{n_2} + R_A^n} - \gamma_L L. \quad (1.1h)$$

Equation 6-2: Formulas describing the advanced model for hypothesis 4.

$$\frac{dN}{dt} = -\frac{\gamma_{Nut}(B_N + B_{R_1} + B_{R_2} + B_I)N}{K_m + N} + R_{recy}(d+\delta)B_I \quad (1.2a)$$

$$\frac{dB_N}{dt} = \frac{\alpha_{Nut}B_N N}{K_m + N} - \gamma_t P B_N - \psi_2 B_N\frac{R_A^n}{C_1^n + R_A^n} + \psi_1 B_{R_1}\frac{C1^n}{C_1^n + R_A^n} \quad (1.2b)$$

$$\frac{dB_{R_1}}{dt} = \frac{\alpha_{Nutr}B_{R_1} N}{K_m + N} - \gamma_{tt} P B_{R_1} + \psi_2 B_N\frac{R_A^n}{C_1^n + Ra^n} - \psi_1 B_{R_1}\frac{C1^n}{C_1^n + R_A^n} \quad (1.2c)$$

$$\frac{dB_{R_2}}{dt} = \frac{\alpha_{Nutr}B_{R_2} N}{K_m + N} \quad (1.2d)$$

$$\frac{dB_I}{dt} = \gamma_t P B_N + \gamma_{tt} P B_{R_1} - (d+\delta)B_I \quad (1.2e)$$

$$\frac{dP}{dt} = \rho\delta B_I - \gamma_t P B_N - \gamma_{tt} P B_{R_1} - cP \quad (1.2f)$$

$$\frac{dA}{dt} = \alpha B_N + (\alpha+\beta)B_{R_1} + (\alpha + \beta\frac{R_A^n}{C1^n + R_A^n})B_{R_2} - \alpha_c(R_c - R_A)A - K_e A L + \gamma_c R_A - \gamma_A A \quad (1.2g)$$

$$\frac{dR_A}{dt} = \alpha_c(R_c - R_A)A - \gamma_c R_A \quad (1.2h)$$

$$\frac{dL}{dt} = \alpha_L B_{R_2}\frac{R_A^n}{C_1^n + R_A^n} + \alpha_L B_{R_1} - \gamma_L L. \quad (1.2i)$$

6.3 Supplementary material for 3.4

Ethics statement:

The emphysema versus airway disease (EvA) study is an EU-funded project (# 200506) under the Seventh Framework Program (FP7). During visit one, candidates willing to participate have the opportunity to discuss all aspects and informed consent is obtained in line with the Declaration of Helsinki and based on approval by the local ethics committees and those samples analyzed by this manuscript were covered by ethics approval 08/H0402/19 (the NHS National Research Ethics Service, Nottingham, United Kingdom).

Table 6-7: The flexible virome of COPD samples.

Virus	Abundance	
	Moderate COPD	Severe COPD
Achromobacter virus JWX	0.01 %	
Acinetobacter phage Presley	0.01 %	
Amsacta moorei entomopoxvirus		0.04 %
Archaeal BJ1 virus	0.01 %	
Arthrobacter phage EdgarPoe	0.01 %	
Arthrobacter virus Trina	0.01 %	
Bacillus phage vB_BhaS-171	0.01 %	0.04 %
Bacillus virus 1	0.01 %	
Bacillus virus Bp8pC	0.02 %	
Bacillus virus Page	0.07 %	
Bacteriophage Lily		0.04 %
Bordetella virus BPP1	0.07 %	0.04 %
Burkholderia phage AH2	0.02 %	
Burkholderia virus KL1		0.04 %
Burkholderia virus phi52237		0.04 %
Burkholderia virus phiE122	0.02 %	
Burkholderia virus phiE255	0.03 %	0.04 %
Cellulophaga phage phi46:1	0.01 %	
Cellulophaga virus Cba172		0.04 %
Clostridium phage phiCD506	0.01 %	
Clostridium phage phiCT19406C		0.04 %
Cronobacter phage vB_CskP_GAP227	0.01 %	
Cyanophage KBS-S-2A	0.01 %	
Edwardsiella virus MSW3	0.02 %	
Enterobacteria phage GEC-3S	0.01 %	

Erwinia phage PhiEaH1	0.01 %	
Erysipelothrix phage SE-1	0.01 %	
Escherichia phage CICC 80001		0.04 %
Escherichia phage ECML-117	0.01 %	
Escherichia virus Cajan	0.01 %	
Gordonia phage BritBrat	0.01 %	
Gordonia phage GTE8	0.02 %	
Gordonia phage Jumbo	0.02 %	
Halovirus HVTV-1		0.04 %
Human alphaherpesvirus 1		0.04 %
Kurlavirus BKC-1	0.01 %	
Lactobacillus phage phiJB	0.01 %	
Lactococcus phage 949		0.08 %
Liberibacter phage SC2	0.03 %	
Macacine betaherpesvirus 3	0.03 %	
Mannheimia phage vB_MhM_3927AP2	0.02 %	
Marinitoga camini virus 1	0.02 %	
Mycobacterium phage Idleandcovert	0.01 %	
Mycobacterium phage MarQuardt	0.01 %	
Mycobacterium phage Milly		0.04 %
Mycobacterium phage Sheen		0.08 %
Mycobacterium virus Gaia	0.01 %	
Mycobacterium virus Soto	0.01 %	
Myxococcus phage Mx8	0.01 %	
Pectobacterium phage My1	0.01 %	
Pelagibacter phage HTVC011P	0.01 %	
Penguinpox virus	0.01 %	
Prochlorococcus phage P-RSM4		0.04 %
Prochlorococcus phage P-SSM4		0.04 %
Propionibacterium phage B3	0.03 %	
Pseudomonas phage B3		0.04 %
Pseudomonas phage O4	0.01 %	
Pseudomonas phage YH6	0.02 %	
Puniceispirillum phage HMO-2011	0.07 %	
Red seabream iridovirus	0.01 %	
Rhodobacter phage RcapMu		0.04 %
Salmonella phage Fels-1	0.01 %	
Salmonella phage IME207	0.01 %	
Salmonella phage ST160		0.04 %
Salmonella phage vB_SosS_Oslo	0.01 %	
Salmonella virus FelixO1	0.01 %	

Shigella phage SfIV	0.01 %	
Spodoptera frugiperda granulovirus	0.01 %	
Spodoptera frugiperda multiple nucleopolyhedrovirus	0.01 %	
Staphylococcus phage Stau2	0.01 %	
Staphylococcus virus SEP9	0.01 %	
Stenotrophomonas phage phiSMA7		0.08 %
Stenotrophomonas phage S1	0.01 %	
Streptococcus phage 315.6	0.01 %	
Streptococcus phage IPP67		0.04 %
Streptococcus phage JX01	0.01 %	
Streptomyces phage Godpower	0.01 %	
Streptomyces phage mu1/6		0.04 %
Streptomyces virus TP1604	0.03 %	
Tetrasphaera phage TJE1	0.02 %	
Tsukamurella phage TPA2	0.02 %	
Vibrio phage CHOED	0.02 %	
Vibrio phage ICP2	0.04 %	
Vibrio phage SIO-2	0.01 %	
Vibrio virus VFJ	0.02 %	
Xanthomonas phage CP1	0.01 %	
Yersinia phage phiA1122	0.02 %	
Yersinia phage phiR1-37		0.08 %
Grand Total	1.22 %	1.11 %

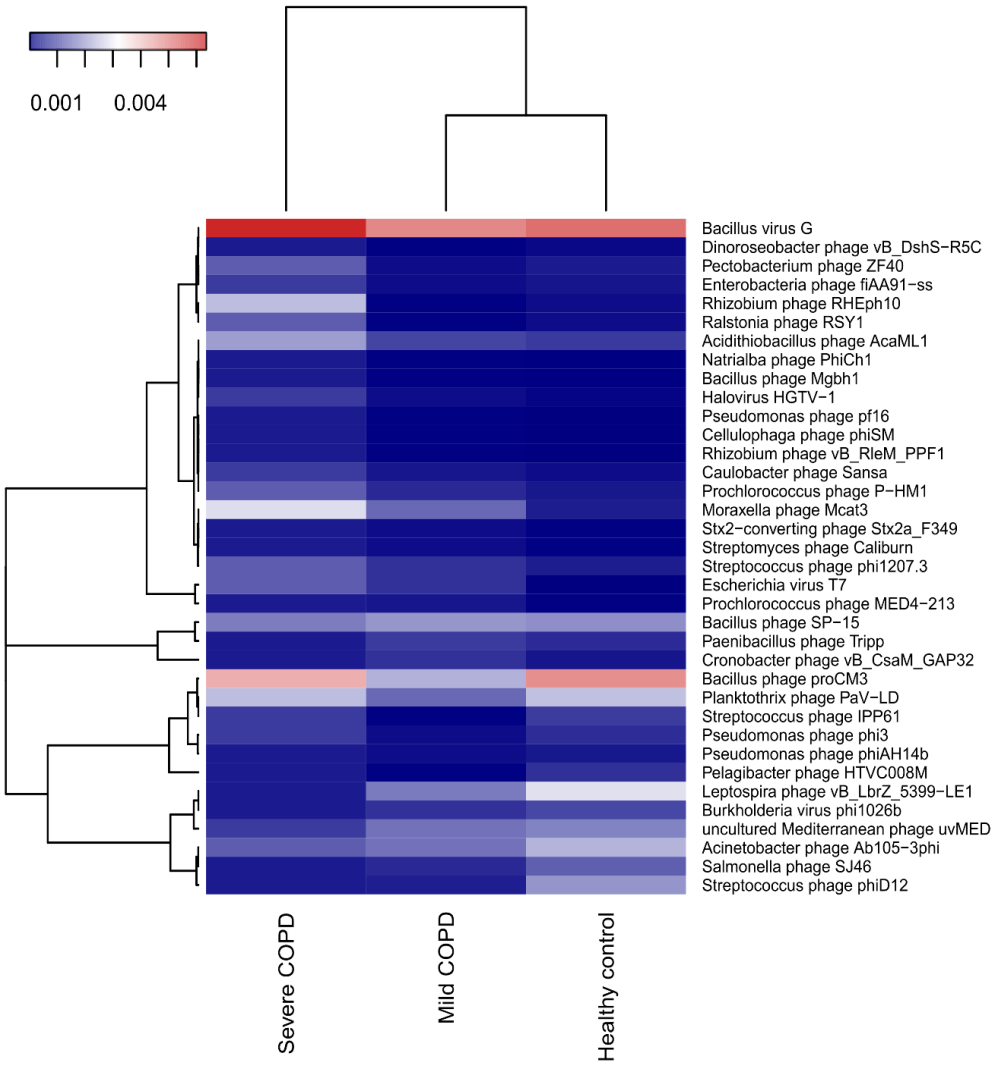

Figure 6-2: Heat map showing the relative abundance of 36 prokaryotic viruses shared between the three BAL samples.

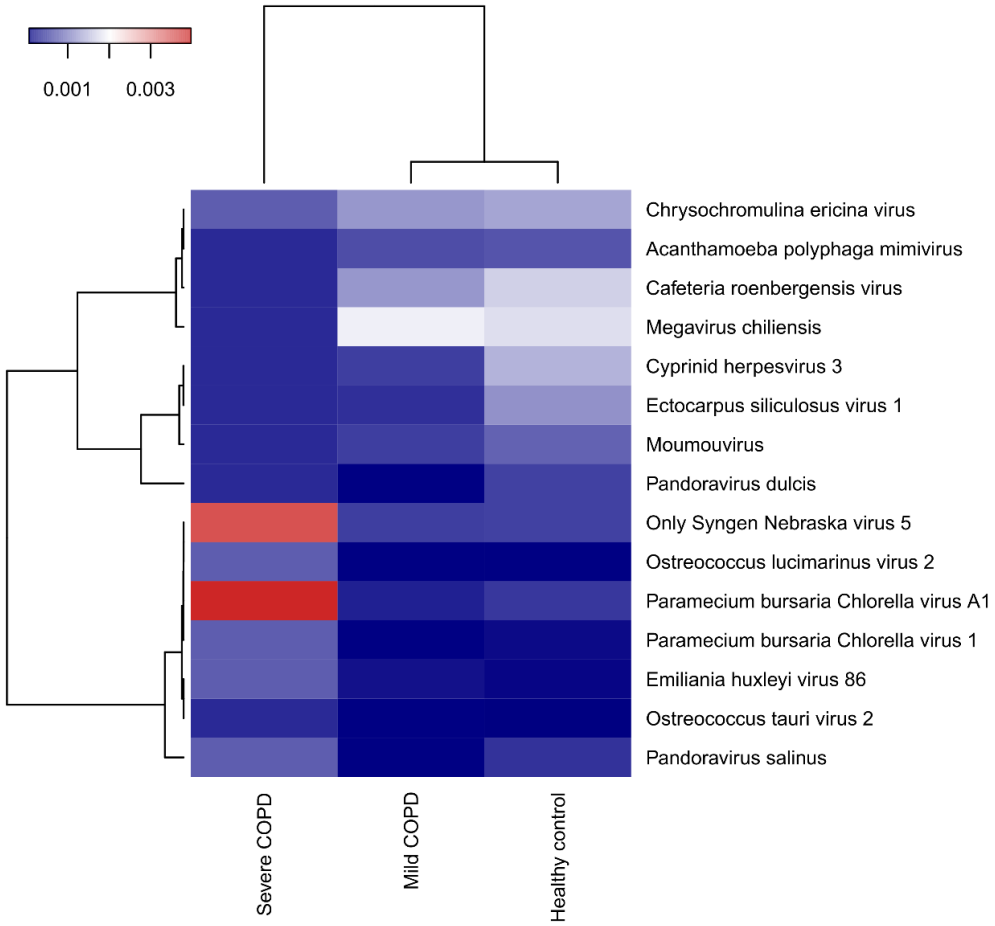

Figure 6-3: Heat map showing the relative abundance of 15 eukaryotic viruses shared between the three BAL samples.

Table 6-8: Blast results for BAL sequences vs the core virulence factors database which showed an identity > 75 %.

Healthy control		
% identity	e-value	Blast hits
93.55	5.00E-55	(algB) two-component response regulator AlgB [Alginate (VF0091)] [Pseudomonas aeruginosa PAO1]
93.1	1.00E-12	(pilJ) twitching motility protein PilJ [Type IV pili (VF0082)] [Pseudomonas aeruginosa PAO1]
92.77	9.00E-102	(pvdJ) pyoverdine biosynthesis protein PvdJ [pyoverdine (IA001)] [Pseudomonas aeruginosa PAO1]
92.59	6.00E-13	(fliF) flagellar M-ring protein FliF [Flagella (VF0273)] [Pseudomonas aeruginosa PAO1]
91.84	2.00E-08	(spaD) SpaD-type pili major subunit SpaD [Pili (VF0364)] [Corynebacterium diphtheriae NCTC 13129]
91.54	2.00E-82	(hsiB1/vipA) type VI secretion system tubule-forming protein VipA [I-I (VF0334)] [Pseudomonas aeruginosa PAO1]
90.21	3.00E-87	(algB) two-component response regulator AlgB [Alginate (VF0091)] [Pseudomonas aeruginosa PAO1]

89.53	6.00E-48	(fliP) flagellar biosynthetic protein FliP [Flagella (VF0273)] [Pseudomonas aeruginosa PAO1]
89.29	1.00E-64	(hsiG1) type VI secretion system hcp secretion island protein HsiG1 [HSI-I (VF0334)] [Pseudomonas aeruginosa PAO1]
88.89	8.00E-29	(pvdL) peptide synthase PvdL [pyoverdine (IA001)] [Pseudomonas aeruginosa PAO1]
88.52	6.00E-29	(algI) alginate o-acetyltransferase AlgI [Alginate (VF0091)] [Pseudomonas aeruginosa PAO1]
88.24	5.00E-36	(algB) two-component response regulator AlgB [Alginate (VF0091)] [Pseudomonas aeruginosa PAO1]
88.24	5.00E-36	(algB) two-component response regulator AlgB [Alginate (VF0091)] [Pseudomonas aeruginosa PAO1]
88.15	3.00E-79	(algB) two-component response regulator AlgB [Alginate (VF0091)] [Pseudomonas aeruginosa PAO1]
87.92	1.00E-74	(pvdL) peptide synthase PvdL [pyoverdine (IA001)] [Pseudomonas aeruginosa PAO1]
87.8	5.00E-37	(algI) alginate o-acetyltransferase AlgI [Alginate (VF0091)] [Pseudomonas aeruginosa PAO1]
87.61	5.00E-68	(flgG) flagellar basal-body rod protein FlgG [Flagella (VF0273)] [Pseudomonas aeruginosa PAO1]
87.39	4.00E-62	(algI) alginate o-acetyltransferase AlgI [Alginate (VF0091)] [Pseudomonas aeruginosa PAO1]
87.1	2.00E-44	(algI) alginate o-acetyltransferase AlgI [Alginate (VF0091)] [Pseudomonas aeruginosa PAO1]
86.96	7.00E-24	(waaF) heptosyltransferase I [LPS (VF0085)] [Pseudomonas aeruginosa PAO1]
86.67	2.00E-19	(hsiG1) type VI secretion system hcp secretion island protein HsiG1 [HSI-I (VF0334)] [Pseudomonas aeruginosa PAO1]
86.49	7.00E-59	(algI) alginate o-acetyltransferase AlgI [Alginate (VF0091)] [Pseudomonas aeruginosa PAO1]
86.36	5.00E-22	(waaF) heptosyltransferase I [LPS (VF0085)] [Pseudomonas aeruginosa PAO1]
86.13	7.00E-84	(flgG) flagellar basal-body rod protein FlgG [Flagella (VF0273)] [Pseudomonas aeruginosa PAO1]
85.37	1.00E-17	(hsiG1) type VI secretion system hcp secretion island protein HsiG1 [HSI-I (VF0334)] [Pseudomonas aeruginosa PAO1]
85	2.00E-83	(flgG) flagellar basal-body rod protein FlgG [Flagella (VF0273)] [Pseudomonas aeruginosa PAO1]
84.85	2.00E-14	(waaF) heptosyltransferase I [LPS (VF0085)] [Pseudomonas aeruginosa PAO1]
84.62	8.00E-69	(algR) alginate biosynthesis regulatory protein AlgR [Alginate (VF0091)] [Pseudomonas aeruginosa PAO1]
84.44	5.00E-45	(icmF1/tssM1) type VI secretion system protein IcmF1 [HSI-I (VF0334)] [Pseudomonas aeruginosa PAO1]
84.44	1.00E-19	(hsiG1) type VI secretion system hcp secretion island protein HsiG1 [HSI-I (VF0334)] [Pseudomonas aeruginosa PAO1]
83.56	1.00E-38	(manC) GDP-mannose pyrophosphorylase [Capsule I (VF0436)] [Burkholderia pseudomallei K96243]
83.33	2.00E-56	(katA) catalase/(hydro)peroxidase [KatAB (VF0168)] [Legionella pneumophila subsp. Pneumophila str. Philadelphia 1]
83.18	1.00E-55	(fliP) flagellar biosynthetic protein FliP [Flagella (VF0273)] [Pseudomonas aeruginosa PAO1]
82.98	1.00E-81	(mgtB) Mg2+ transport protein [MgtBC (VF0106)] [Salmonella enterica subsp. Enterica serovar Typhimurium str. LT2]
82.76	9.00E-63	(motA) flagellar motor protein MotA [Flagella (VF0430)] [Burkholderia pseudomallei K96243]

82.11	9.00E-70	(hsiG1) type VI secretion system hcp secretion island protein HsiG1 [HSI-I (VF0334)] [Pseudomonas aeruginosa PAO1]
81.48	2.00E-62	(algD) GDP-mannose 6-dehydrogenase AlgD [Alginate (VF0091)] [Pseudomonas aeruginosa PAO1]
81.48	6.00E-27	(algI) alginate o-acetyltransferase AlgI [Alginate (VF0091)] [Pseudomonas aeruginosa PAO1]
81.44	1.00E-55	(pvdA) L-ornithine N5-oxygenase PvdA [Pyoverdine (VF0094)] [Pseudomonas aeruginosa PAO1]
81.4	7.00E-24	(ureG) urease accessory protein (ureG) [Urease (VF0050)] [Helicobacter pylori 26695]
81.29	1.00E-80	(algW) AlgW protein [Alginate regulation (CVF523)] [Pseudomonas aeruginosa PAO1]
81.16	3.00E-32	(algG) outer membrane protein AlgE [Alginate (VF0091)] [Pseudomonas aeruginosa PAO1]
81.13	1.00E-46	(flgI) flagellar P-ring protein precursor FlgI [Flagella (VF0394)] [Yersinia enterocolitica subsp. Enterocolitica 8081]
81.08	2.00E-55	(icmF1/tssM1) type VI secretion system protein IcmF1 [HSI-I (VF0334)] [Pseudomonas aeruginosa PAO1]
80.9	1.00E-39	(irtA) Iron-regulated transporter IrtA [mycobactin (IA031)] [Mycobacterium tuberculosis H37Rv]
80.43	7.00E-09	(tlpA) membrane-bound chemoreceptor sensing arginine and bicarbonate [Pse5Ac7Ac (AI150)] [Helicobacter pylori 26695]
80	3.00E-36	(pvdI) peptide synthase [pyoverdine (IA001)] [Pseudomonas aeruginosa PAO1]
80	5.00E-34	(htpB) Hsp60, 60K heat shock protein HtpB [Hsp60 (VF0159)] [Legionella pneumophila subsp. Pneumophila str. Philadelphia 1]
79.44	6.00E-60	(hsiG1) type VI secretion system hcp secretion island protein HsiG1 [HSI-I (VF0334)] [Pseudomonas aeruginosa PAO1]
79.44	3.00E-58	(hsiG1) type VI secretion system hcp secretion island protein HsiG1 [HSI-I (VF0334)] [Pseudomonas aeruginosa PAO1]
79.44	2.00E-56	(hsiG1) type VI secretion system hcp secretion island protein HsiG1 [HSI-I (VF0334)] [Pseudomonas aeruginosa PAO1]
79.03	4.00E-37	(gmd) GDP-mannose 4,6-dehydratase [O-antigen (VF0392)] [Yersinia enterocolitica subsp. Enterocolitica 8081]
78.95	1.00E-50	(hsiC1/vipB) type VI secretion system tubule-forming protein VipB [I-I (VF0334)] [Pseudomonas aeruginosa PAO1]
78.95	8.00E-48	(clpC) endopeptidase Clp ATP-binding chain C [ClpC (VF0072)] [Listeria monocytogenes EGD-e]
78.82	3.00E-77	(clpV1) type VI secretion system AAA+ family ATPase [I-I (VF0334)] [Pseudomonas aeruginosa PAO1]
78.76	2.00E-58	(pvdL) peptide synthase PvdL [pyoverdine (IA001)] [Pseudomonas aeruginosa PAO1]
78.72	1.00E-28	(pilT2) twitching motility protein PilT [Type IV pili (CVF189)] [Neisseria meningitidis MC58]
78.71	1.00E-81	(flgH) flagellar L-ring protein precursor FlgH [Flagella (VF0273)] [Pseudomonas aeruginosa PAO1]
78.64	6.00E-56	(algG) outer membrane protein AlgE [Alginate (VF0091)] [Pseudomonas aeruginosa PAO1]
78.57	4.00E-09	(tlpC) membrane-bound chemoreceptor [Pse5Ac7Ac (AI150)] [Helicobacter pylori 26695]
78.57	4.00E-09	(tlpA) membrane-bound chemoreceptor sensing arginine and bicarbonate [Pse5Ac7Ac (AI150)] [Helicobacter pylori 26695]
78.57	1.00E-08	(mgtC) Mg2+ transport protein [MgtBC (VF0106)] [Salmonella enterica subsp. Enterica serovar Typhimurium str. LT2]
78.43	4.00E-21	(acpXL) acyl carrier protein [LPS (CVF383)] [Brucella melitensis bv. 1 str. 16M]

78.08	4.00E-75	(flgH) flagellar L-ring protein precursor FlgH [Flagella (VF0273)] [Pseudomonas aeruginosa PAO1]
78.02	2.00E-46	(bplB) probable acetyltransferase [LPS (VF0033)] [Bordetella pertussis Tohama I]
77.78	2.00E-17	(xcpR) general secretion pathway protein E [xcp secretion system (VF0084)] [Pseudomonas aeruginosa PAO1]
77.69	2.00E-65	(flgH) flagellar L-ring protein precursor FlgH [Flagella (VF0273)] [Pseudomonas aeruginosa PAO1]
77.44	7.00E-38	(htpB) Hsp60, 60K heat shock protein HtpB [Hsp60 (VF0159)] [Legionella pneumophila subsp. Pneumophila str. Philadelphia 1]
77.27	9.00E-57	(katA) catalase/(hydro)peroxidase [KatAB (VF0168)] [Legionella pneumophila subsp. Pneumophila str. Philadelphia 1]
77.27	2.00E-44	(pvdO) pyoverdine biosynthesis protein PvdO [pyoverdine (IA001)] [Pseudomonas aeruginosa PAO1]
77.14	5.00E-10	(pilM) type IV pilus inner membrane platform protein PilM [Type IV pili (VF0082)] [Pseudomonas aeruginosa PAO1]
77.08	2.00E-20	(manC) GDP-mannose pyrophosphorylase [Capsule I (VF0436)] [Burkholderia pseudomallei K96243]
77.08	2.00E-20	(manC) GDP-mannose pyrophosphorylase [Capsule I (VF0436)] [Burkholderia pseudomallei K96243]
77.05	1.00E-37	(tsr) methyl-accepting chemotaxis protein I [Flagella (VF0430)] [Burkholderia pseudomallei K96243]
76.99	2.00E-53	(pvdD) pyoverdine synthetase D [Pyoverdine (VF0094)] [Pseudomonas aeruginosa PAO1]
76.92	2.00E-15	(fliP) flagellar biosynthetic protein FliP [Flagella (VF0273)] [Pseudomonas aeruginosa PAO1]
76.92	2.00E-10	(tsr) methyl-accepting chemotaxis protein I [Flagella (VF0430)] [Burkholderia pseudomallei K96243]
76.81	2.00E-62	(pvdE) pyoverdine biosynthesis protein PvdE [Pyoverdine (VF0094)] [Pseudomonas aeruginosa PAO1]
76.62	6.00E-39	(katA) catalase/(hydro)peroxidase [KatAB (VF0168)] [Legionella pneumophila subsp. Pneumophila str. Philadelphia 1]
76.32	2.00E-16	(lspE) general secretion pathway protein E [lsp T2SS (VF0154)] [Legionella pneumophila subsp. Pneumophila str. Philadelphia 1]
76.24	3.00E-49	(cheB) chemotaxis-specific methylesterase [Flagella (VF0430)] [Burkholderia pseudomallei K96243]
76.22	5.00E-68	(pvdD) pyoverdine synthetase D [Pyoverdine (VF0094)] [Pseudomonas aeruginosa PAO1]
76	7.00E-44	(pvdL) peptide synthase PvdL [pyoverdine (IA001)] [Pseudomonas aeruginosa PAO1]
75.58	9.00E-35	(hcp1) type VI secretion system substrate Hcp1 [I-I (VF0334)] [Pseudomonas aeruginosa PAO1]
75.28	2.00E-46	(algA) phosphomannose isomerase / guanosine 5'-diphospho-D-mannose pyrophosphorylase [Alginate (VF0091)] [Pseudomonas aeruginosa PAO1]
75	1.00E-34	(fleQ) transcriptional regulator FleQ [Flagella (VF0273)] [Pseudomonas aeruginosa PAO1]
75	1.00E-18	(fleQ) transcriptional regulator FleQ [Flagella (VF0273)] [Pseudomonas aeruginosa PAO1]
Moderate COPD		
% identity	e-value	Blast hits
94.44	4.00E-17	(flgC) flagellar basal-body rod protein FlgC [Flagella (VF0273)] [Pseudomonas aeruginosa PAO1]
93.18	5.00E-23	(pilT) twitching motility protein PilT [Type IV pili (VF0082)] [Pseudomonas aeruginosa PAO1]
90.91	2.00E-78	(pvdJ) pyoverdine biosynthesis protein PvdJ [pyoverdine (IA001)] [Pseudomonas aeruginosa PAO1]

89.77	2.00E-43	(algU) alginate biosynthesis protein AlgZ/FimS [Alginate (VF0091)] [Pseudomonas aeruginosa PAO1]
86.67	3.00E-13	(clpV1) type VI secretion system AAA+ family ATPase [I-I (VF0334)] [Pseudomonas aeruginosa PAO1]
86.67	3.00E-13	(clpV1) type VI secretion system AAA+ family ATPase [I-I (VF0334)] [Pseudomonas aeruginosa PAO1]
85.19	3.00E-08	(bsaZ) YscU homolog, component of the inner membrane ring [Bsa T3SS (VF0428)] [Burkholderia pseudomallei K96243]
85.19	7.00E-09	(bsaZ) YscU homolog, component of the inner membrane ring [Bsa T3SS (VF0428)] [Burkholderia pseudomallei K96243]
85.19	3.00E-08	(bsaZ) YscU homolog, component of the inner membrane ring [Bsa T3SS (VF0428)] [Burkholderia pseudomallei K96243]
85.19	1.00E-08	(bsaZ) YscU homolog, component of the inner membrane ring [Bsa T3SS (VF0428)] [Burkholderia pseudomallei K96243]
85.19	4.00E-09	(bsaZ) YscU homolog, component of the inner membrane ring [Bsa T3SS (VF0428)] [Burkholderia pseudomallei K96243]
82.52	8.00E-79	(clpV1) type VI secretion system AAA+ family ATPase [I-I (VF0334)] [Pseudomonas aeruginosa PAO1]
81.82	3.00E-71	(clpV1) type VI secretion system AAA+ family ATPase [I-I (VF0334)] [Pseudomonas aeruginosa PAO1]
81.82	5.00E-29	(clpV1) type VI secretion system AAA+ family ATPase [I-I (VF0334)] [Pseudomonas aeruginosa PAO1]
81.48	2.00E-35	(icmF1/tssM1) type VI secretion system protein IcmF1 [HSI-I (VF0334)] [Pseudomonas aeruginosa PAO1]
81.13	4.00E-56	(pilT) twitching motility protein PilT [Type IV pili (VF0082)] [Pseudomonas aeruginosa PAO1]
81.08	2.00E-81	(clpV1) type VI secretion system AAA+ family ATPase [I-I (VF0334)] [Pseudomonas aeruginosa PAO1]
81.08	6.00E-14	(flhA) flagellar biosynthesis protein FlhA [Flagella (VF0273)] [Pseudomonas aeruginosa PAO1]
80	6.00E-10	(pvdA) L-ornithine N5-oxygenase PvdA [Pyoverdine (VF0094)] [Pseudomonas aeruginosa PAO1]
80	8.00E-10	(pvdA) L-ornithine N5-oxygenase PvdA [Pyoverdine (VF0094)] [Pseudomonas aeruginosa PAO1]
80	6.00E-10	(pvdA) L-ornithine N5-oxygenase PvdA [Pyoverdine (VF0094)] [Pseudomonas aeruginosa PAO1]
79.45	8.00E-35	(pilT) twitching motility protein PilT [Type IV pili (VF0082)] [Pseudomonas aeruginosa PAO1]
78.79	8.00E-11	(pvdA) L-ornithine N5-oxygenase PvdA [Pyoverdine (VF0094)] [Pseudomonas aeruginosa PAO1]
78.72	2.00E-50	(clpV1) type VI secretion system AAA+ family ATPase [I-I (VF0334)] [Pseudomonas aeruginosa PAO1]
78.46	8.00E-16	(fliP) flagellar biosynthetic protein FliP [Flagella (VF0273)] [Pseudomonas aeruginosa PAO1]
77.67	7.00E-52	(tagR) type IV secretion associated protein TagR, positively regulates PpkA [I-I (VF0334)] [Pseudomonas aeruginosa PAO1]
77.03	3.00E-34	(wcbR) capsular polysaccharide biosynthesis fatty acid synthase [Capsule I (VF0436)] [Burkholderia pseudomallei K96243]
76.92	2.00E-07	(hlyB) Hemolysin B [Hemolysin (VF0225)] [Escherichia coli CFT073]
76.47	5.00E-21	(clpC) endopeptidase Clp ATP-binding chain C [ClpC (VF0072)] [Listeria monocytogenes EGD-e]
76.32	5.00E-35	(tagR) type IV secretion associated protein TagR, positively regulates PpkA [I-I (VF0334)] [Pseudomonas aeruginosa PAO1]
76.16	7.00E-68	(pvdJ) pyoverdine biosynthesis protein PvdJ [pyoverdine (IA001)] [Pseudomonas aeruginosa PAO1]
76	9.00E-11	(tssH-5/clpV) Clp-type ATPase chaperone protein [T6SS-1 (VF0429)] [Burkholderia pseudomallei K96243]

75.86	1.00E-07	(tagT) type six secretion associated protein TagT, ATP-binding component of ABC transporter [I-I (VF0334)] [Pseudomonas aeruginosa PAO1]
75.76	5.00E-10	(pvdA) L-ornithine N5-oxygenase PvdA [Pyoverdine (VF0094)] [Pseudomonas aeruginosa PAO1]
75.47	2.00E-34	(tagR) type IV secretion associated protein TagR, positively regulates PpkA [I-I (VF0334)] [Pseudomonas aeruginosa PAO1]
75.44	5.00E-50	(aprA) alkaline metalloproteinase precursor [Alkaline protease (VF0090)] [Pseudomonas aeruginosa PAO1]
75.21	8.00E-64	(bplA) probable oxidoreductase [LPS (VF0033)] [Bordetella pertussis Tohama I]
75	8.00E-80	(pvdP) tyrosinase required for pyoverdine maturation [pyoverdine (IA001)] [Pseudomonas aeruginosa PAO1]
75	2.00E-19	(clpC) endopeptidase Clp ATP-binding chain C [ClpC (VF0072)] [Listeria monocytogenes EGD-e]
Severe COPD		
% identity	e-value	Blast hits
96.36	5.00E-75	(hsiC1/vipB) type VI secretion system tubule-forming protein VipB [I-I (VF0334)] [Pseudomonas aeruginosa PAO1]
92.31	1.00E-23	(pvdA) L-ornithine N5-oxygenase PvdA [Pyoverdine (VF0094)] [Pseudomonas aeruginosa PAO1]
87.78	3.00E-50	(algW) AlgW protein [Alginate regulation (CVF523)] [Pseudomonas aeruginosa PAO1]
86.67	3.00E-14	(mgtB) Mg2+ transport protein [MgtBC (VF0106)] [Salmonella enterica subsp. Enterica serovar Typhimurium str. LT2]
86.54	1.00E-25	(fliI) flagellum-specific ATP synthase FliI [Flagella (VF0273)] [Pseudomonas aeruginosa PAO1]
83.33	6.00E-21	(hcp1) type VI secretion system substrate Hcp1 [I-I (VF0334)] [Pseudomonas aeruginosa PAO1]
82.14	1.00E-39	(pvdL) peptide synthase PvdL [pyoverdine (IA001)] [Pseudomonas aeruginosa PAO1]
79.41	2.00E-10	(algC) phosphomannomutase AlgC [Alginate biosynthesis (CVF522)] [Pseudomonas aeruginosa PAO1]
79.38	2.00E-51	(pvdA) L-ornithine N5-oxygenase PvdA [Pyoverdine (VF0094)] [Pseudomonas aeruginosa PAO1]
78.79	1.00E-29	(fliI) flagellum-specific ATP synthase FliI [Flagella (VF0273)] [Pseudomonas aeruginosa PAO1]
77.27	3.00E-20	(hcp1) type VI secretion system substrate Hcp1 [I-I (VF0334)] [Pseudomonas aeruginosa PAO1]
75.86	3.00E-13	(ccmC) cytochrome c-type biogenesis protein CcmC, putative heme lyase for CcmE [CcmC (VF0292)] [Legionella pneumophila subsp. Pneumophila str. Philadelphia 1]
75	3.00E-40	(xcpR) general secretion pathway protein E [xcp secretion system (VF0084)] [Pseudomonas aeruginosa PAO1]
75	5.00E-34	(xcpR) general secretion pathway protein E [xcp secretion system (VF0084)] [Pseudomonas aeruginosa PAO1]

7 CLARIFICATIONS

Chapter 3.1: “Virus quantification techniques in the spotlight”.

The concept of the experiment was developed by Dr. Li Deng and the PhD candidate. The experiment was designed by Dr. Li Deng, PD Dr. Christian Griebler and the PhD candidate. Environmental samples were collected by PhD student. Sample preparation and staining, plaque assay, quantitative PCR, epifluorescence microscopy and nanoparticle-tracking analysis were performed by the PhD candidate, flow cytometry measurement were conducted by Nina Weber. TEM pictures were prepared and taken by Dr. Carolin Pickl and Prof. Dr. Andreas Klingl. Statistical analysis, evaluation and graphic analysis of the results was performed by the PhD candidate. PD Dr. Christian Griebler, Dr. Li Deng and the PhD candidate interpreted and discussed the results together. The draft for the manuscript was written by the PhD candidate independently, with the comments of PD Dr. Christian Griebler and Dr. Li Deng added afterwards. The manuscript will be submitted by the corresponding author Dr. Li Deng to the Journal *Frontiers in Microbiology*.

Chapter 3.2: “Characterization of bacteria-phage interactions: Phages of *P. aeruginosa*”.

The concept of the experiment was developed by Dr. Li Deng and the PhD candidate. The experiment was designed by the Phd candidate including consultations with Dr. Li Deng and PD Dr. Christian Griebler. The isolation of the different phages of *Pseudomonas aeruginosa* as well as the physiological characterization (optimal temperature, optimal pH, host range, virus-to-bacteria ratios, PCR and digestion) was conducted by Youl Han. Alexandra Matthes tested the infectivity at 36 °C and 40 °C. The biofilm experiments and the genetic analysis involving the sequencing of the isolates was performed by the PhD candidate. The metagenomic assembly was conducted by Dr. Ali Elbehery. The preparation and analysis of the commissioned sequencing of shorter DNA fragments was done by the PhD candidate. Statistical analysis, evaluation and graphic analysis of the results was performed by the PhD candidate. PD Dr. Christian Griebler, Dr. Li Deng and the PhD candidate interpreted and discussed the results together.

Chapter 3.3: “Viral impact on microbial communication”.

The concept of the experiment and the mathematical modeling was developed by Dr. Burkhard Hense, Dr. Abhijit Ghorai, PD Dr. Christian Griebler, Dr. Judith Perez-Velazquez, Dr. Michael Rothballer, Dr. Christina Kuttler, Dr. Li Deng and the PhD candidate. The experiment was designed by the Phd candidate, Dr. Li Deng, PD Dr. Christian Griebler and Dr. Michael Rothballer.

Isolation of phages of *Pseudomonas putida* was performed by Irina Kolpakova. The experiment was prepared and conducted by the PhD candidate. Bacterial and viral numbers were quantified by the PhD student. The quorum sensing molecules HSL and HS were enumerated by Dr. Michael Rothballer. Statistical analysis, evaluation and graphic analysis of the experimental results was performed by the PhD candidate. The development and fitting of the models was performed by Dr. Abhijit Ghorai and Dr. Christina Kuttler. The discussion and interpretation of the experimental results in the context of the modeling results were performed by Dr. Burkhard Hense, Dr. Abhijit Ghorai, PD Dr. Christian Griebler, Dr. Judith Perez-Velazquez, Dr. Christina Kuttler and the PhD candidate. The draft for the manuscript was written by the PhD candidate independently (all parts referring to the biological information in the introduction, results and discussion sections, description of the methodological part of the experiment). All descriptions regarding the modeling were written by Dr. Abhijit Ghorai and Dr. Christina Kuttler. The comments on the manuscript of PD Dr. Christian Griebler, Dr. Li Deng, Dr. Michael Rothballer and Dr. Judith Perez-Velazquez were incorporated afterwards. The manuscript has been submitted by the corresponding author Dr. Christina Kuttler to the Journal *Royal Society Open Science* with the review process still running.

Chapter 3.4: “Virome assessment in the lung: towards metagenomic sequencing of low concentrated viral DNA”.

The concept of the experiment was developed by PD Dr. Christian Griebler, Dr. Li Deng and the PhD candidate. The experiment was designed by Dr. Li Deng, PD Dr. Christian Griebler and the PhD candidate. Samples were provided by the EvA consortium represented by Dr. Loems Ziegler-Heitbrock and Dr. Dave Singh. The PhD candidate conducted the purification and isolation of viral particles and the successive DNA extraction. The library preparation for the 454 pyrosequencing was performed by Susanne Kublik. Loading of the sequencing plate and initiating the sequencing run was completed by Susanne Kublik and the PhD candidate. The metagenomic assembly and analysis of the reads were performed by Dr. Ali Elbehery. PD Dr. Christian Griebler, Dr. Li Deng, Dr. Ali Elbehery and the PhD candidate interpreted and discussed the results together. The draft for the manuscript was written by the Dr. Ali Elbehery and the PhD candidate, with the comments of PD Dr. Christian Griebler and Dr. Li Deng added afterwards. The manuscript has been published in the Journal *Frontiers in Microbiology* 9:1110, 29.05.2018, doi:10.3389/fmicb.2018.01110.

8 ACKNOWLEDGEMENTS

"Keine Schuld, ist dringender als die, Dank zu sagen"

Cicero

First of all, I would like to thank my supervisor PD Dr. Christian Griebler for his support in developing the main concept for this thesis, his optimism and cheerfulness, which always lifted up my spirits, his fantastic and speedy support for paper-writing, his input for improving the paper drafts and also his active involvement in the writing process.

Next, I would like my second supervisor Dr. Li Deng for her contributions and inputs for my experiments, her help during the experiments and the possibility to continue working after termination of my PhD contract in her group.

I want to thank my office-mates Aileen and Sviatlana for their constant help, scientific and emotional support, for compensating my frustration and annoyance and cheering me up! It was a great time I had with you girls!

I also want to thank Gabi, Nina and Helena for their constant support in the lab, their helping hands on solving problems and their time to introduce me to new instruments.

Next, I would like to thank my collaborators Dr. Burkhard Hense, Dr. Christina Kuttler, Dr. Abhijit Ghorai, Dr. Judith Perez-Velazquez and Dr. Michael Rothballer for their expertise and extensive discussions. Additionally, I want to thank Christina for her efforts on writing, improving and assembling our manuscript. I also would like to emphasize my gratitude Burkhard, with whom I had many fruitful discussions and who helped me a lot in understanding his field, the bacterial communication, better. He initialized this interdisciplinary project and influenced it a lot while working on it. Unfortunately, he passed away unexpectedly on February 28, 2017.

I would like to thank my colleague Dr. Ali Elbehery for his scientific impulses and his comments on my drafts.

I'm obliged to my Master students Alexandra Matthes, Youl Han and Irina Kolpakova for their motivation and their diligence.

One highlight during my thesis for which I'm more than grateful was our tabletop soccer lunchtime group: Aileen, Alex, Anne, Ben, Günter, Hubert, Jean, Marina, Niklas, Phillip, Ramona and Tina. This time generated so much team spirit, fun and motivation and kicked us out of our afternoon slump! Thank you so much for this phenomenal time!

I also would like to thank Lauren, for, amongst many other things, improving my English and eliminating my mistakes in my writings.

Of course, I would also like to thank all the unmentioned people from my institute, who helped to create such an enjoyable atmosphere and made my time here sublime.

Finally, I want to thank my partner and my family for their loving support, constant help and endurance of my moods! Without them I would not be where I am now!